THE UNIVERSITY *of* EDINBURGH

Simulating the carbon cycling of croplands - model development, diagnosis, and regional application through data assimilation

Oliver Sus

Thesis submitted in fulfilment of
the requirements for the degree of
Doctor of Philosophy
to the
University of Edinburgh — 2011

Declaration

I declare that this thesis has been composed solely by myself and that it has not been submitted, either in whole or in part, in any previous application for a degree. Except where otherwise acknowledged, the work presented is entirely my own.

Oliver Sus

December 2011

Abstract

In the year 2000, croplands covered about 12% of the Earth's ice-free land surface. Through cropland management, humankind momentarily appropriates about 25% of terrestrial ecosystem productivity. Not only are croplands a key element of human food supply, but also bear potential in increased carbon (C) uptake when best-practice land management approaches are adopted. A detailed assessment of the impact of land use on terrestrial ecosystems can be achieved by modelling, but the simulation of crop C cycling itself is a relatively new discipline. Observational data on crop net ecosystem exchange (NEE) are available only recently, and constitute an important tool for model development, diagnosis, and validation. Before crop functional types (CFT) had been introduced, however, large-scale biogeochemical models (BGCM) lacked crop-specific patterns of phenology, C allocation, and land management. As a consequence, the influence of cropland C cycling on biosphere-atmosphere C exchange seasonality and magnitude is currently poorly known. To date, no regional assessment of crop C cycling and yield formation exists that specifically accounts for spatially and temporally varying patterns of sowing dates within models.

In this thesis, I present such an assessment for the first time. In the first step (chapter 2), I built a crop C mass balance model (SPAc) that models crop development and C allocation as a response to ambient meteorological conditions. I compared model outputs against C flux and stock observations of six different sites in Europe, and found a high degree of agreement between simulated and measured fluxes ($R^2 = 0.83$). However, the model tended to overestimate leaf area index (LAI), and underestimate

final yield. In a model comparison study (chapter 3), I found in cooperation with further researchers that SPAc best reproduces observed fluxes of C and water (owed to the model's high temporal and process resolution), but is deficient due to a lack in simulating full crop rotations.

I then conducted a detailed diagnosis of SPAc through the assimilation of C fluxes and biometry with the Ensemble Kalman Filter (EnKF, chapter 4), and identified potential model weaknesses in C allocation fractions and plant hydraulics. Further, an overestimation of plant respiration and seasonal leaf thickness variability were evident. Temporal parameter variability as a response to C flux data assimilation (DA) is indicative of ecosystem processes that are resolved in NEE data but are not captured by a model's structure. Through DA, I gained important insights into model shortcomings in a quantitative way, and highlighted further needs for model improvement and future field studies.

Finally, I developed a framework allowing for spatio-temporally resolved simulation of cropland C fluxes under observational constraints on land management and canopy greenness (chapter 5). MODIS (Moderate Resolution Imaging Spectroradiometer) data were assimilated both variationally (for sowing date estimation) and sequentially (for improved model state estimation, using the EnKF) into SPAc. In doing so, I was able to accurately quantify the multiannual (2000-2006) regional C flux and biometry seasonality of maize-soybean crop rotations surrounding the Bondville Ameriflux eddy covariance (EC) site, averaged over 104 pixel locations within the wider area. Results show that MODIS-derived sowing dates and the assimilation of LAI data allow for highly accurate simulations of growing season C cycling at locations for which ground-truth sowing dates are not available. Through quantification of the spatial variability in biometry, NEE, and net biome productivity (NBP), I found that regional patterns of land management are important drivers of agricultural C cycling and major sources of uncertainty if not appropriately accounted for. Observing C cycling at one single field with its individual sowing pattern is not sufficient to constrain large-scale agroecosystem behaviour. Here, I developed a framework that enables modellers to accurately simulate current (i.e. last 10 years) C cycling of major agricultural regions and their contribution

to atmospheric CO_2 variability. Follow-up studies can provide crucial insights into testing and validating large-scale applications of biogeochemical models.

Acknowledgements

I want to thank everybody who supported or accompanied me during my PhD. Special thanks go to my friends in the Crew Attic, everybody I "enjoyed" lunch with in KB house, and the Rocka Juniors. I also want to thank people back in Spain and Germany, friends and family, who frequently visited Anna and me in Edinburgh and so provided some important distraction.

I want to thank Martin Wattenbach for his collaboration and help with the special issue papers. My co-supervisors Pete Smith and Stephen Sitch have always been helpful and available when questions arose. Most importantly, I want to thank Ruth Doherty and Mat Williams for their valuable support and suggestions, and proof reading of my over-long texts. Especially my primary supervisor, Mat, has always been available, provided help with model coding and programming, was open for discussion, and always had good advice at hand. Finally, I want to thank the Edinburgh School of Geosciences (Torrance Bequest studentship) and the Scottish Alliance for Geoscience, Environment and Society (SAGES) for financial support.

Last but not least, I want to thank Anna, who suffered with and through me in times of doubt. Pula, this is for you.

Contents

List of Tables

List of Figures

Glossary

C_{aresp}	autotrophic respiration pool C mass
C_{d}	dead foliar C mass
C_{f}	foliar C mass
C_{lab}	labile C mass
C_{lit}	litter C mass
C_{r}	fine root C mass
C_{SOM}	Soil Organic Matter C mass
C_{s}	stem C mass
AV	study area flux AVerage
AVHRR	Advanced Very High Resolution Radiometer
BGCM	BioGeoChemical Model
C	Carbon
CDL	Cropland Data Layer
CFT	Crop Functional Type
CMPDOY	Composite Day Of Year
d	day
DA	Data Assimilation
DGVM	Dynamic Global Vegetation Model
DM	Dry Matter
DOY	Day Of Year
DR	Developmental Rate
DS	Developmental Stage
E	Nash–Sutcliffe model Efficiency factor
EAI	Ear Area Index
EC	Eddy Covariance
EnKF	Ensemble Kalman Filter
EoS	End of Season
ETa	EvapoTranspiration
EVI	Enhanced Vegetation Index
fwd	forward (i.e. no DA) model run
GDD	Growing Degree Day
GPP	Gross Primary Productivity
GS	Growing Season
GSL	Growing Season Length
HANPP	Human Appropriation of Net Primary Productivity
LAI	Leaf Area Index
MODIS	Moderate Resolution Imaging Spectroradiometer

MS	Maize-Soybean crop rotation
MSCR	Maize-Soybean Crop Rotation, independent of crop type grown in particular year or field
N	Nitrogen
NASS	National Agricultural Statistics Service
NBP	Net Biome Productivity
NDVI	Normalized Difference Vegetation Index
NEE	Net Ecosystem Exchange
NPP	Net Primary Productivity
NRR	Normalized RMSE Ratio
OM	Organic Matter
PDF	Probability Density Function
R_a	autotrophic Respiration
R_e	ecosystem Respiration
R_h	heterotrophic Respiration
RDVI	Renormalized Difference Vegetation Index
RMSE	Root Mean Squared Error
RS	Remote Sensing
RUE	Radiation Use Efficiency
S	parameter Sensitivity index
SAI	Stem Area Index
SM	Soybean-Maize crop rotation
SOM	Soil Organic Matter
SoS	Start of Season
SV	State Variable
SVAT	Soil Vegetation Atmosphere Transfer model
ts	time step
USDA	U.S. Department of Agriculture
VD	Vernalization Day
VI	Vegetation Index
wb	winter barley
ww	winter wheat
y	year

Chapter 1

Introduction

1.1 The importance of agriculture in a global context

Agroecosystems (which are defined throughout this thesis as cropland ecosystems, excluding managed grasslands, Kucharik and Twine (2007)) are of major importance to humankind. They provide key ecosystem services, namely agricultural goods for human consumption, a potential for C sequestration in cropland soils (Smith, 2008; Luo *et al.*, 2010; West and Marland, 2002; Lal, 2004), and renewable energy resources in the form of biofuels (Foley *et al.*, 2005). At the same time, these agroecosystems are largely controlled by human management. Innovations in agriculture might have had a considerable influence on atmospheric CH_4 levels for at least the past 5000 years (Ruddiman, 2003), and the immense impact of humankind on Earth System structure and functioning now equals or exceeds many natural forces at the global scale (Crutzen and Steffen, 2003). Ruddiman (2003) argues that the cumulative impact of the discovery of agriculture and subsequent technological innovations on terrestrial biogeochemical cycles justify an advanced estimated onset of the Anthropocene era (originally defined by Crutzen and Steffen (2003) as the period during which industrial-era human activities have had a discernible impact on atmospheric greenhouse gas concentrations, starting around 1800 A.D.).

Through agricultural advancements, humankind created a new ecosystem by transforming about 30-50% of the world's land surface (Vitousek *et al.*, 1997), and pushed the Earth into a "no-analogue state" (Crutzen and Steffen, 2003). One single invention, the Haber-Bosch industrial process of synthetic atmospheric nitrogen (N) fixing for agricultural fertiliser production, is thought to have made human population explosion possible (a tenfold population rise during the past three centuries, and a fourfold increase in the 20th century, Crutzen and Steffen (2003)). Historic changes in agricultural production show clear links with climate variability and population growth (Zhang *et al.*, 2011; Lee *et al.*, 2008). In general, the carrying capacity of agroecosystems shrinks considerably in a deteriorating climate: cooling drives population collapses in cooler or warmer humid climate zones, whilst both cooling and warming correlate with observed population collapses in dry climate zones of the Northern Hemisphere (Zhang *et al.*, 2011). For example, Zhang *et al.* (2011) found indications for a cause-and-effect relationship between agricultural shrinkage caused by cooling since the late 16th century in Europe and a subsequent population collapse in the mid-17th century.

Lobell and Field (2007) expect that ∼30% of global yield variability is attributable to climate variables. However, this also shows that through the adoption of appropriate agricultural practices, farmers are largely able to respond to gradually changing environmental conditions for crop cultivation (Porter and Semenov, 2005). In the U.S., observations of maize and soybean sowing dates and developmental stages reveal a trend towards earlier sowing dates (about 10-12 days advancement from 1981 to 2005) and lengthening of the growing period (by ∼12 days), so that harvest dates remained relatively constant. These data are thought to reflect an adoption of longer season cultivars, which in turn is expected to explain ∼26% of the observed maize yield increases over this period (Sacks and Kucharik, 2011).

One key question for the 21st century is how future agricultural production will develop under expected trends of global climate warming. Future yield increases are expected to be brought about by increases in agricultural intensity, i.e. gains in cropland yield per area, and by further expansion of agricultural area predominantly in Latin America and sub-Saharan central Africa (Tilman *et al.*, 2001). These trends

will considerably increase the weight of land management on the sustainability of global ecosystem services. Haberl *et al.* (2007) estimate that humankind currently appropriates about a quarter of potential net primary productivity (NPP) available in global ecosystems (also referred to as human appropriation of NPP, or HANPP). Despite its comparably limited spatial extent (in 2000, ∼12% of the Earth's ice-free land surface was cropland, Ramankutty *et al.* (2008)), cropping alone accounts for ∼half of global HANPP (Haberl *et al.*, 2007). Thus, the dilemma of modern agriculture is that many land-use practices are absolutely essential for the survival of humankind, but the very same land-use practices are degrading ecosystems and their services we so heavily depend upon (Foley *et al.*, 2005). Given future global trends in population growth, warming, and food demand (which Tilman *et al.* (2001) expect to rise by 50% until 2050), human societies might soon be faced with the limits of the carrying capacity of agroecosystems on which their existence is founded. Today, global wheat stocks are declining and fell to a 30-year low in 2008 (Becker-Reshef *et al.*, 2010). Land management is a key element of past, present, and future survivability of human societies. Therefore, it is crucial to improve our understanding of the interplay between climate variables, land management, and agroecosystem services, functioning, and C cycling.

1.2 The C balance of croplands - key components and current estimates

Modern agriculture has a profound impact on global biogeochemical cycles (Denman *et al.*, 2007), and more specifically on terrestrial C cycling. The amount of synthetically fixed N applied as fertiliser in agriculture now surmounts the amount fixed naturally in all terrestrial ecosystems (120 Tg y^{-1} vs 90 Tg y^{-1}, Galloway *et al.* (2002, 2008)). Fossil fuel burning, agricultural management, deforestation, and animal husbandry have lead to a substantial increase in atmospheric CO_2 (>30%) and CH_4 (>100%) over the past two centuries (Crutzen and Steffen, 2003). In Europe, croplands are estimated to be the largest biospheric source of C to the atmosphere (0.3

Gt C y^{-1}, Janssens *et al.* (2005)). However, Lal (2004) expects that there is a considerable potential in restoring historic C loss due to soil cultivation (78 ± 12 Gt C, primarily caused by losses through mineralisation and erosion). 50% to 66% of these C losses might be reintegrated into cropland soils through a set of appropriate management practices (Lal, 2004), such as no-till farming (Hollinger *et al.*, 2004), manuring (Dawson and Smith, 2007), crop residue retention (van Groenigen *et al.*, 2011), cover crops, efficient irrigation, and soil restoration (Lal, 2004). Further, Lal (2004) expects that an increase of 1 ton of soil organic matter (SOM) C may increase crop yield by 20-40 kg ha^{-1} for wheat and by 10-20 kg ha^{-1} for maize. Thus, next to improving C sequestration potential, the aforementioned agricultural practices could also be seen as one of the tools for future yield increases.

Estimates of SOM C losses from cropland are (1) spatially variable, (2) highly dependent on methodology (stock taking or inventories vs. model estimates), (3) and prone to large uncertainties (West *et al.*, 2010). Global estimates of soil C remain uncertain, and literature values vary strongly (Bondeau *et al.*, 2007). In general, it is expected that the C content of extratropical soils decreases by 50% to 60% following the conversion from natural to agricultural ecosystems until reaching a new equilibrium state (Lal, 2004; Luo *et al.*, 2010), but estimates of the magnitude and sign of observed trends in SOM C vary considerably. In short, studies suggest that assessments of U.S. SOM C stock changes for the 1990s are reaching a consensus (i.e. gains in SOM C), as there is a high degree of consistency amongst corresponding studies (Ogle *et al.*, 2010). Chinese cropland soil C monitoring sites also indicate a mean increase of 25.5 Tg C y^{-1} between 1985 and 2006. This C sequestration rate is equivalent to offset ∼20% of total CO_2 emissions of China in 1994 (Pan *et al.*, 2010). In contrast to that, most observed and modelled trends indicate a decline in European cropland SOM C (Bellamy *et al.*, 2005; Dawson and Smith, 2007; Ciais *et al.*, 2010; Janssens *et al.*, 2005).

Overall, our current understanding of how land management practices affect agricultural yield and the net C balance is still limited (Smith *et al.*, 2010). However, with the onset of a global network of eddy covariance (EC) flux measurements (FLUXNET, Baldocchi *et al.* (2001), Figure 1.1), a new dataset is now available that provides

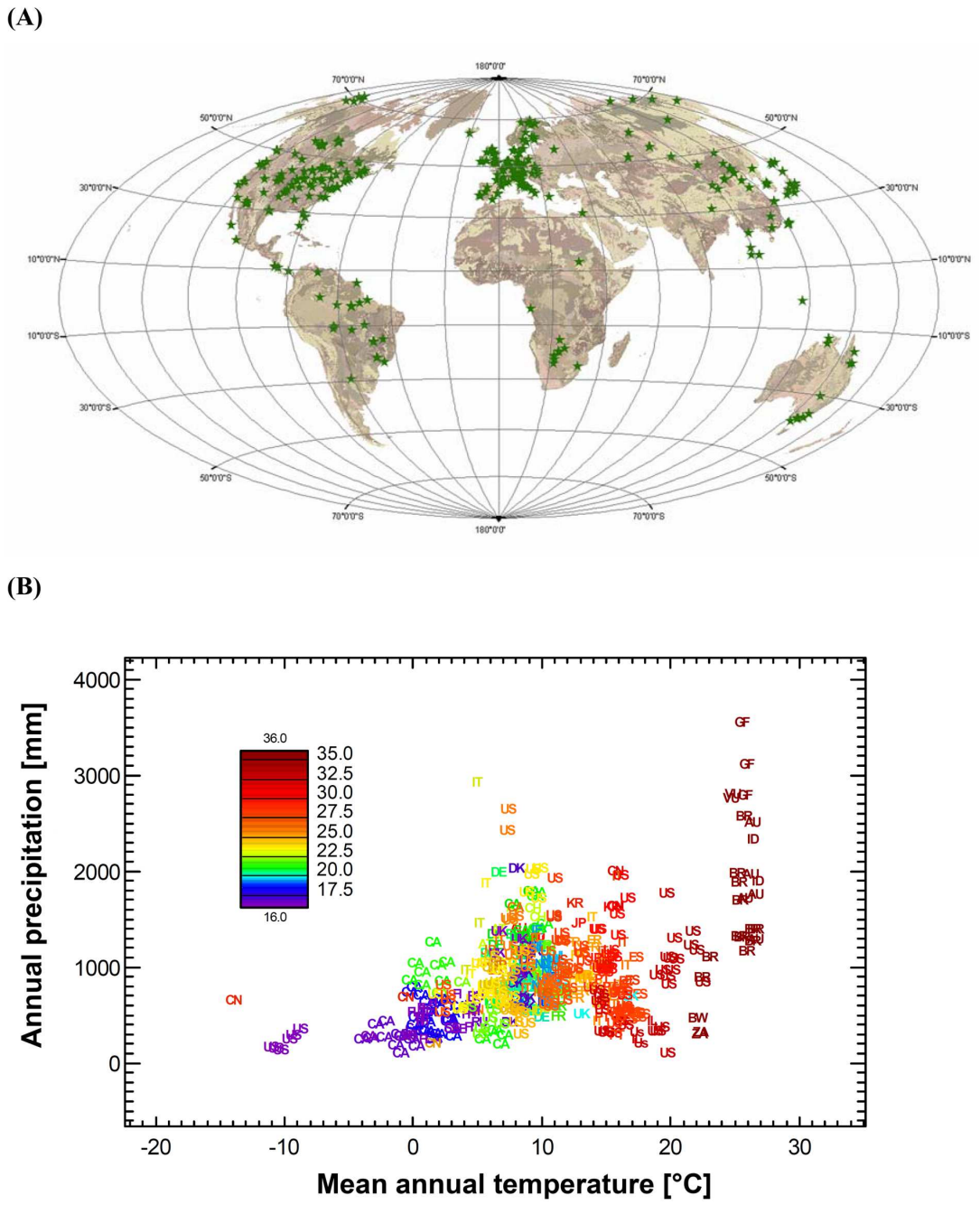

Figure 1.1: Distribution of sites that are present in the La-THuile 2007 FLUXNET database. (a) Geographical distribution, (b) in climate (annual temperature and precipitation) space. In (b) colours code annual potential shortwave radiation flux density [MJ m^{-2} day^{-1}] according to the legend. Letters are country codes. From Williams *et al.* (2009).

an independent source of information on cropland C cycling (Williams *et al.*, 2009). They "offer a non-intrusive means of studying canopy-scale gains and losses of C and water" (Baldocchi, 1994), providing the only direct observation of terrestrial NEE (Friend *et al.*, 2006). I will describe the key components of the cropland C budget (based on Smith *et al.* (2010), see also Figure 1.2) in the following:

Net ecosystem exchange (NEE, the only entity directly measured by EC) is the difference between total ecosystem respiration (R_e) and gross primary productivity (GPP, i.e. the gross uptake of CO_2 that is used in photosynthesis, Ciais *et al.* (2010)). An ecosystem is a sink of CO_2 (or C) if the sign of NEE is negative.

$$NEE = R_e - GPP \tag{1.1}$$

R_e in turn is represented by the sum of heterotrophic respiration (R_h, mineralization of litter and soil C pools by microbial activity) and autotrophic respiration (R_a). The sum of the belowground fractions of R_a and R_h is referred to as soil respiration.

$$R_e = R_a + R_h \tag{1.2}$$

About a third to a half of photo-assimilates from GPP are consumed by R_a for the synthesis of new plant tissues and the maintenance of living tissues (i.e. the sum of growth and maintenance respiration, Luyssaert *et al.* (2007)). The remaining fraction is referred to as net primary productivity (NPP).

$$NPP = GPP - R_a \tag{1.3}$$

To obtain the full C budget, non-CO_2 and non-respiratory gains and losses of C need to be accounted for. I adopted a simplified approach similar to Kutsch *et al.* (2010), ignoring "minor" terms of the fully integrated net biome production (NBP).

Accordingly, a so-called "lateral" flux of the C removed by harvest (H) needs to be integrated in NBP (Figure 1.2).

$$NBP = NEE + H \tag{1.4}$$

Flux measurements of NEE between the atmosphere and the biosphere are available for about 500 tower locations from ∼30 regional networks (FLUXNET, Figure 1.1). As the majority of flux stations has been erected above forests, measurements on agroecosystems are somewhat under represented. However, cropland NEE observations might be just as important, for they probably constitute a strong C source (Anthoni *et al.*, 2004). A range of studies on cropland NEE EC-fluxes has been published, assessing the C cycling of wheat (Anthoni *et al.*, 2004; Moureaux *et al.*, 2008; Suleau *et al.*, 2011; Gilmanov *et al.*, 2003; Aubinet *et al.*, 2009; Hoyaux *et al.*, 2008), barley (Adiku *et al.*, 2006; Prescher *et al.*, 2010; Soegaard *et al.*, 2003), maize (Suyker *et al.*, 2004; Vitale *et al.*, 2007), and maize-soybean rotations (Hollinger *et al.*, 2004; Verma *et al.*, 2005; Grant *et al.*, 2007; Suyker *et al.*, 2005). These four crop types are of major importance to global agricultural production and food security, ranking (in terms of total global area harvested, 2009) at number one (wheat), three (maize), four (soybean), and five (barley, FAOSTAT [Rome, Italy]: FAO, http://faostat.fao.org/).

In general, the NEE flux data published in the above studies suggest that most agroecosystems are a net sink of C. Growing season (GS, from sowing to harvest) C sink strength ranges between -730 to -273 gC m^{-2} GS^{-1} for wheat (Aubinet *et al.*, 2009; Gilmanov *et al.*, 2003; Moureaux *et al.*, 2008), ∼-590 gC m^{-2} GS^{-1} for maize, and ∼-140 gC m^{-2} GS^{-1} (soybean, Suyker *et al.* (2005)). When NEE fluxes are cumulated over a whole year (i.e. including fallow periods), the sink strength appears considerably reduced. Most maize agroecosystems are still C sinks (-576 to -397 gC m^{-2} y^{-1}, Hollinger *et al.* (2004); Verma *et al.* (2005); Grant *et al.* (2007), but +136 gC m^{-2} y^{-1} in Prescher *et al.* (2010)). Cumulative NEE of wheat moved closer to the sink-to-source crossover point (-245 to -66 gC m^{-2} y^{-1}, Anthoni *et al.* (2004); Prescher *et al.* (2010)), and barley (-21 gC m^{-2} y^{-1}, Prescher *et al.* (2010)) and

soybean (-33 to +18, Verma *et al.* (2005); Grant *et al.* (2007); Hollinger *et al.* (2004)) are estimated to be nearly C neutral. In general, cropland annual NEE is found by adding a large negative number (growing season NEE) and a large positive number (fallow season NEE, Soegaard *et al.* (2003)), and annual balances are confounded by residue decomposition of previously cultivated crops (Verma *et al.*, 2005). Some studies account for further "lateral" C fluxes, such as manure application, C outgassing from irrigation (Verma *et al.*, 2005) or soil water (Hollinger *et al.*, 2004), and seed C content (Aubinet *et al.*, 2009; Kutsch *et al.*, 2010), which are however often (except for manure, when applied) much smaller than H in Equation 1.4. These are not explicitly considered here. The NBP of the big majority of agroecosystems analysed indicates a net C source (i.e. a potential loss of soil C if EC-measurements are not systematically biased, Baker and Griffis (2005)), especially when measurement campaigns span full rotational successions (Kutsch *et al.*, 2010; Aubinet *et al.*, 2009; Baker and Griffis, 2005). For 5 crop rotations and 2 monoculture European agroecosystems, Kutsch *et al.* (2010) estimated an average NBP of 95 $\pm$ 87 gC m^{-2} y^{-1}, i.e. the analysed croplands are net C source even though large uncertainties remain. Published values vary considerably, caused by uncertainties in EC measurements and estimated harvested C mass, differences in rotational successions, study period length, management practices, climate variables, and soil conditions (Kutsch *et al.*, 2010).

1.3 The state of the art of agroecosystem modelling

As the results of EC measurement campaigns indicate, flux tower based assessments of the agroecosystem C budget are reflecting rather specific, localised field conditions, and cannot be easily upscaled (i.e. extrapolated in time and space) unless regional patterns in land management, soil conditions, and climatic variability are accounted for (Kutsch *et al.*, 2010). One way forward is using process-based models of terrestrial ecosystems, in the following referred to as biogeochemical models (BGCM, Figure 1.3), for predicting agricultural C cycling under known or hypothesized climates or land use patterns that are not or only partially covered by EC observations in the FLUXNET

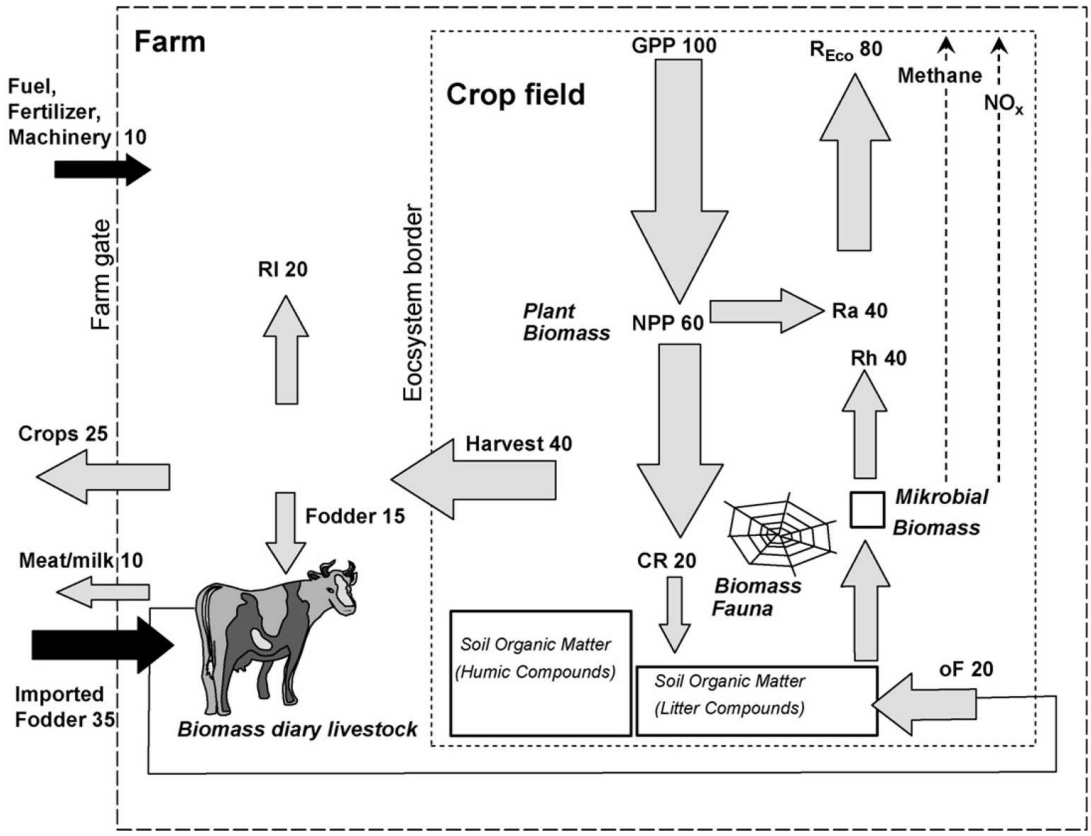

Figure 1.2: Schematic representation of the various components of the C balance of croplands, in percent. CR: crop residues. oF: organic fertilizer. R_l: Respiration of the lifestock at the farm. From Smith *et al.* (2010).

database (Grant *et al.*, 2007). BGCM are driven by simulated or site-observed environmental variables, and predict key components of an agroecosystem, such as developmental stage, C partitioning, leaf area index (LAI), biomass growth, plant or ecosystem respiration, and photosynthesis (Figure 1.3). Due to their richness in time, NEE measurements constitute an ideal dataset for agroecosystem model conception, calibration, and validation. Flux measurements are often combined with simultaneous observations of crop biometry, and so multiple constraints on cropland C budgeting and climate controls are available.

Traditionally, agronomists focused on yield simulations rather than intending to simulate the seasonal cycle of C fluxes and how these differ from unmanaged systems, which led to the emergence of a variety of so-called crop-growth models (Jamieson *et al.*, 1998; Keating *et al.*, 2003; Porter *et al.*, 1983; Stöckle *et al.*, 1994; van Laar *et al.*, 1997;

Williams *et al.*, 1989; Yang *et al.*, 2004). Until recently, land surface models lacked a crop-related plant functional type, and applied grassland-specific model structure and parameters as proxies (Osborne *et al.*, 2007). However, the lack of representing agroecosystem C cycling within four BGCMs was estimated to be a major source of uncertainty for modelling global C and water cycles (McGuire *et al.*, 2001). It has been recognised that BGCMs would generally greatly benefit from an improved representation of interannual phenological variability (Schwalm *et al.*, 2010), of which we still have rather little understanding (Stöckli *et al.*, 2008). Crop phenology is a key driver of the seasonality of agricultural biological dynamics, and affects fluctuations of atmospheric CO_2 on (inter-)annual scales (Moureaux *et al.*, 2008; Houghton, 1999). If the uncertainty in global applications of BGCMs is to be reduced, the short-lived developmental life cycle of agroecosystems has to be accounted for. This is achieved by simulating key processes related to crop phenology, such as seasonal C allocation shifts and timing and rate of canopy senescence (Kucharik and Twine, 2007). In addition, the spatial and temporal sequence of agricultural management largely determines cropland CO_2 emissions, our knowledge of which is still rather limited (Smith *et al.*, 2005b; Osborne *et al.*, 2010). The onset and length of growing periods of summer crops (e.g. maize and soybean) and crop yield are largely dependent on sowing date (Sacks and Kucharik, 2011; Brown and de Beurs, 2008), which is currently vaguely approximated within global applications of BGCMs. For the sake of simplicity, sowing dates are commonly set to a fixed value, or estimated as a function of local climate (Bondeau *et al.*, 2007; de Noblet-Ducoudré *et al.*, 2004). Several remote sensing studies have attempted to derive land management parameters from vegetation index (VI) time series (Karkee *et al.*, 2009; Ines and Honda, 2005; Brown and de Beurs, 2008; Doraiswamy *et al.*, 2004; Dente *et al.*, 2008), even though errors are still considerably large (at best 4-14 days).

1.3.1 Simulating development — a key component of crop modelling

In recent years, a number of crop C budget modelling studies emerged (Adiku *et al.*, 2006; Arora, 2003; Huang *et al.*, 2009a; Lokupitiya *et al.*, 2009; Wang *et al.*, 2005, 2007)

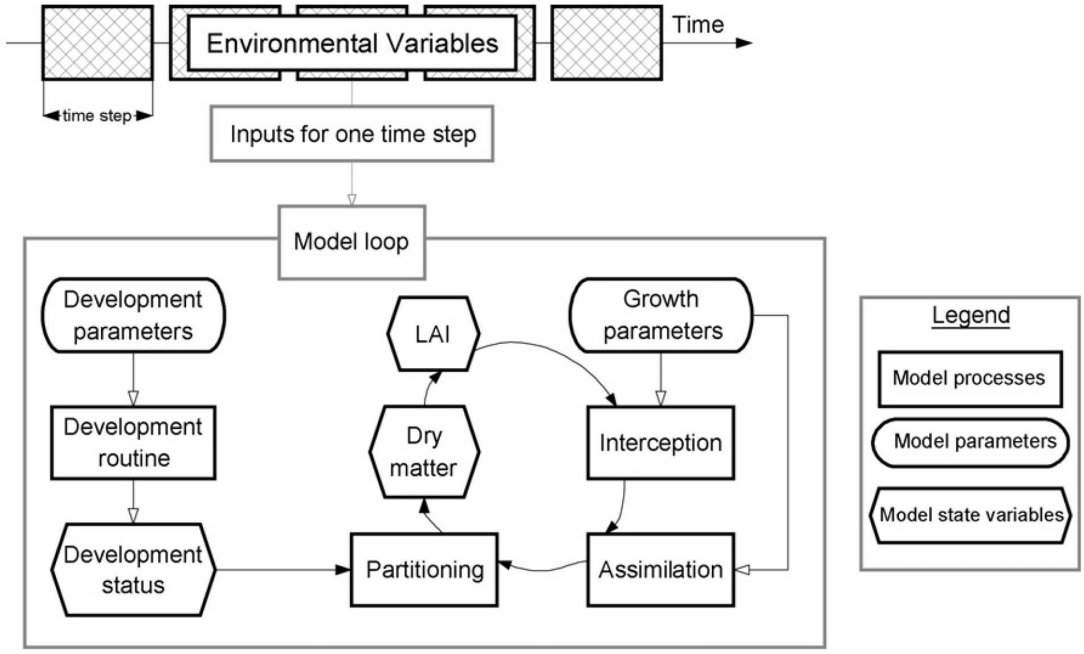

Figure 1.3: Simplified scheme of an agroecosystem. From Dorigo *et al.* (2007).

and global land surface models with crop representation are being developed and tested (Bondeau *et al.*, 2007; Kucharik and Twine, 2007; de Noblet-Ducoudré *et al.*, 2004). Despite of considerable improvements in simulated agroecosystem C cycling (especially when compared to previous grassland-proxy model performance, Bondeau *et al.* (2007); de Noblet-Ducoudré *et al.* (2004)), significant model weaknesses remain. The simulation of crop phenology is based on deterministic functions relating plant development to ambient environmental conditions, such as temperature and photoperiod (i.e. daylength). These developmental functions serve as surrogates for complex biochemical pathways (Setiyono *et al.*, 2007), and none of the BGCMs mentioned above apply a mechanistic approach of modelling crop phenology. The influence of phenology on the seasonality and magnitude of agroecosystem C assimilation is strongest (1) around the turnover point from vegetative to reproductive development (i.e. anthesis), when leaf and root growth begin to decrease significantly and are gradually replaced by stem and storage organ C allocation (Penning de Vries *et al.*, 1989), and (2) during canopy senescence, which is induced after anthesis and related to developmental rate (van Laar *et al.*, 1997). Taken together, both processes control the duration and rate of leaf growth and decline, and thus are strong constraints on the availability of

photosynthetically active biomass. Next to land management, crop development highly regulates cropland C fluxes (Kutsch *et al.*, 2010).

Whilst a mechanistic representation of phenology is highly desirable, no generalised (i.e. applicable to several crop types) process-based crop developmental model is known to the author that could be readily built into a BCGM. Instead, an advanced method of modelling crop phenology exists (Wang and Engel, 1998; Streck *et al.*, 2003) that is based on non-linear, rather than linear relationships to cumulative temperature (growing degree days, GDD), photoperiod, and vernalisation (the "acquisition or acceleration of the ability to flower by a chilling treatment", Chouard (1960)) as applied in all but one (Wang *et al.*, 2007) of the crop C budget models mentioned above. Moreover, no existing BGCM includes, for example, plant development, C remobilisation, and senescence, all within a full crop C budget. In some of the models, leaf area index is not directly linked to the agroecosystem C budget through a linear relationship with foliar C mass, but instead is either prescribed (Bondeau *et al.*, 2007; de Noblet-Ducoudré *et al.*, 2004) or constrained through a maximum LAI value (Kucharik and Twine, 2007; Huang *et al.*, 2009a). The appropriate handling of leaf senescence remains a key difficulty in current crop BGCMs (Suyker *et al.*, 2005; Kucharik and Twine, 2007).

1.3.2 Data assimilation as a tool for model diagnosis and upscaling

A promising way of diagnosing, calibrating, and upscaling an agroecosystem BCGM is the assimilation of temporally and/or spatially highly resolved observations of key model state variables, such as C flux data (e.g. EC-derived NEE, Williams *et al.* (2005), soil chamber respiration fluxes) or remote sensing (RS) data related to canopy variables (LAI, Demarty *et al.* (2007); Doraiswamy *et al.* (2004)), VI (Fang *et al.*, 2011), spectral reflectance (Quaife *et al.*, 2008), radar backscattering (de Wit and van Diepen, 2007; Dente *et al.*, 2008)). Data assimilation (DA) can be described as a set of techniques that aims for finding an optimal combination of observations and models, referred to as the "analysis" (Mathieu and O'Neill, 2008). Observational data can be

assimilated, amongst other methods (Williams *et al.*, 2009), variationally or sequentially (Dorigo *et al.* (2007), Figure 1.4). Applying the variational approach, a model is "calibrated" by adjusting parameters or initial states, so that simulated and observed state variables agree optimally. In sequential applications, the model state variables are continually "updated" whenever an observation is available. The underlying assumption is that state variables are predicted with higher accuracy at future time steps if observational constraints at the present time step are more closely met, keeping the model "on-track" (Dorigo *et al.*, 2007). DA is critically dependant on a realistic estimation of uncertainties within both observations and model state variables, as these are being used to weight both entities accordingly. This weighting procedure then provides a new estimate of model state variables and parameters contained in the model state vector, on which the DA analysis is performed. The overall success of DA lies in an unbiased model state prediction, which in turn is largely dependent on accurate parameter estimation (Moradkhani *et al.*, 2005).

The popularity of Ensemble Kalman Filter (EnKF) based DA for state estimation in the geosciences has increased in the past decade (Hu *et al.*, 2010; Moradkhani *et al.*, 2005). The EnKF has been applied in various studies, covering the subjects of hydrology, oceanography, meteorology, atmospheric transport models, and land surface modelling (Evensen, 2003). It is a sequential DA technique that uses an ensemble of model forecasts to resemble a large cloud of model states, from which probability density functions (PDF) and approximate estimates for moments of these PDFs can be derived (Evensen, 2003). More recently, the EnKF was also used in the context of C cycling of terrestrial ecosystems (Williams *et al.*, 2005) and crop modelling (de Wit and van Diepen, 2007). Williams *et al.* (2005) showed that a combination of observations and modelling yields a more precise estimate of C dynamics and further highlights areas of model improvement. The usual assumption that observed data has a primacy over model representation was complemented by the notion that neither of them perfectly describes a system. Instead, and this is the premise of DA, a combination of both data and model provides optimal results. DA is designed to find a model representation that is most consistent with observations (Williams *et al.*, 2005).

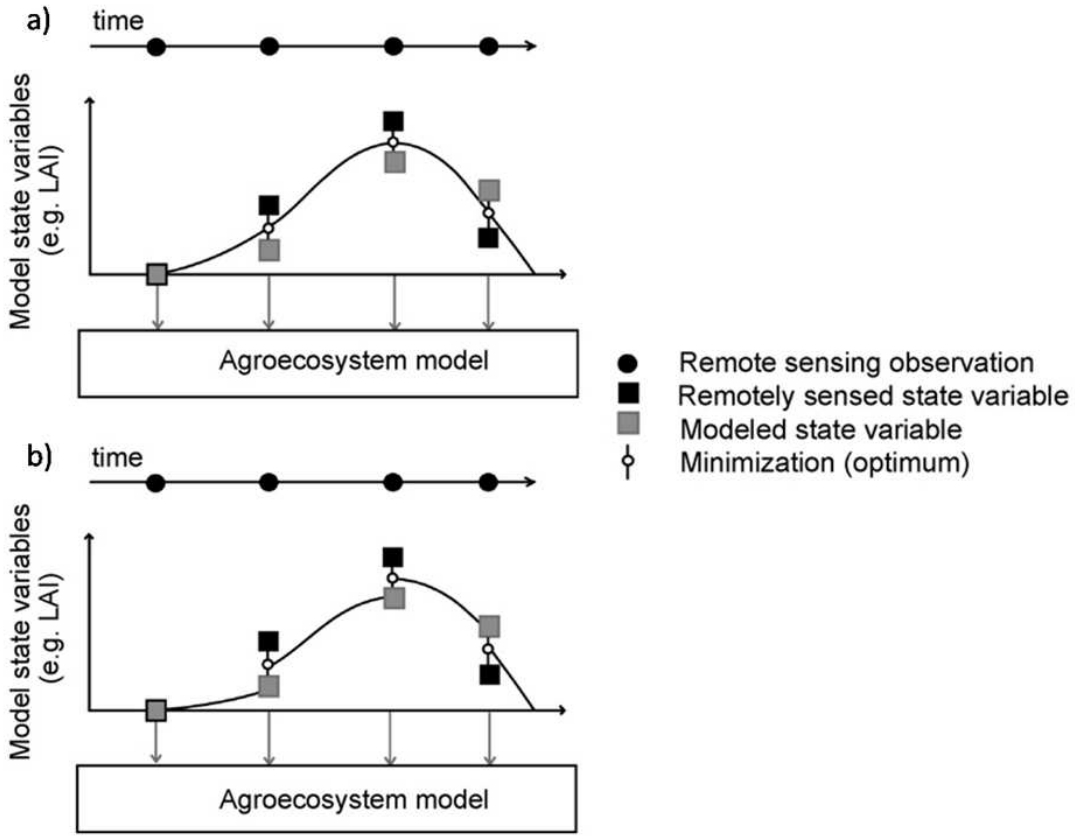

Figure 1.4: Schematic representation of different methods for the assimilation of remotely sensed model state variables in agroecosystem models: (a) "calibration", (b) "updating". From Dorigo *et al.* (2007).

Possibly, our best current estimate of regionalised agroecosystem C cycling can be achieved by driving BGCMs with maps of land management and crop development (which can be derived from RS VI time series), or through RS DA into a BGCM (Demarty *et al.*, 2007). It has long been shown that several major crop growth phases, such as emergence, canopy establishment, senescence, and maturity, are detectable from spectral reflectance data and simple VI, like the Normalized Difference Vegetation Index (NDVI, Tucker *et al.* (1979)). Weaknesses in model structure (limited process understanding of crop development, photosynthesis, and respiration; parameter uncertainty) and the lack of spatio-temporal land management information can, to some extent, be compensated for by information contained in VI time series of satellite sensors with appropriate pixel size and revisit capacity. Studies on RS DA are generally complicated by the trade-off between spatial and temporal resolution of

space-born remote sensors available (Moulin *et al.*, 1998). Agroecosystem canopies are comparably homogeneous within single field patches, beyond which cropping patterns produce a highly heterogeneous landscape picture. Today however, a decadal VI data set of 250 m pixel resolution and near-daily coverage is available from MODIS, which has been found highly suitable for providing crop type specific VI time series for field patch sizes of >25 ha (Doraiswamy *et al.*, 2004). There are a number of studies that applied RS DA for agroecosystem modelling (Brown and de Beurs, 2008; Dente *et al.*, 2008; Doraiswamy *et al.*, 2004; Launay and Guerif, 2005; Karkee *et al.*, 2009; Inoue and Olioso, 2006), but attempts to move from the level of individual land cover units to regional or continental scales are still relatively rare (Dorigo *et al.*, 2007).

Several important aspects of agroecosystem services are linked to cropland management and climate variables. Probably the major linking "medium" is crop phenology: it largely determines the seasonality of EC-derived NEE fluxes (Kutsch *et al.*, 2010), influences bio(geo)physical surface properties (e.g. through effects of crop residue on albedo and thermal insulation, which affects energy, water, and C balance, Kucharik and Twine (2007)), has yield implications through the choice of longer season cultivars adopted to local climate (Sacks and Kucharik, 2011) and effects on SOM C sequestration (Lal, 2004), is directly dependent on land management through sowing date cropping patterns, and can be derived from RS VI data time series (Tucker *et al.*, 1979).

1.4 Structure of the thesis

In this thesis, the initial step was the development of a crop C mass balance model that realistically simulates key crop processes that constrain agroecosystem response to ambient environmental conditions. Hereby I worked with the SPA model, a process-based ecosystem model which was originally developed for application to non-managed landscapes (Williams *et al.*, 1998). Accordingly, I modified model structure and parameterisation so that observations of cropland C exchange and biometry (as derived from the FLUXNET database) could be reproduced. The research rationale was

to develop a simplified modelling approach that embeds key processes and corresponding generic parameter values. This approach was built in the hindsight that future upscaling applications are feasible and provide realistic outputs. The model should be representative of spatio-temporal patterns in agroecosystem C cycling for major agricultural crops (wheat, barley (chapter 2, chapter 3, and chapter 4), maize, and soybean (chapter 5)). I developed and tested the resulting model, SPAc (SPA version 2, crop), with various FLUXNET datasets (i.e. meteorological driver data, initial soil conditions, C flux and stock data) for its accuracy in reproducing observed biometry and fluxes of C (chapter 2, chapter 4, chapter 5) and water (chapter 3). Further, a detailed sensitivity study was conducted to identify key parameters constraining model behaviour (chapter 2). A model-intercomparison study highlighted generic weaknesses in four different process-based agroecosystem C models, and discussed the models' representativity of modern agricultural practices (chapter 3). Data assimilation methodology was applied as a tool for model diagnosis (winter wheat at Klingenberg, Germany, chapter 4) and upscaling (soybean-maize no-till rotations at Bondville, U.S., chapter 5). The key research questions are outlined as follows.

In chapter 2, I proposed a generalised crop BGCM (i.e. SPAc) for application at various sites in Western Europe, and assessed whether a generic winter wheat/barley parameterisation is acceptable. I compared half-hourly simulated NEE fluxes and biometric data outputs against observations of fluxes and stocks of C at six FLUXNET sites. I also undertook a detailed sensitivity analysis to highlight critical model parameters constraining model performance, from which recommendations for future field studies can be derived. Key research questions were: does the newly embedded developmental module produce reliable simulations of crop phenology? Is a single parameterisation appropriate for SPAc applications at different European locations?

In cooperation with Wattenbach *et al.* (2010), we then used SPAc within a cross-site comparison study of four different crop C mass balance models (chapter 3). We compared the accuracy of models in predicting NEE, but also GPP, R_e, and evapotranspiration (ETa) against observations contained in the CarboEurope dataset, i.e. assessing four different main components of the cropland C cycle. We provided

answers to the following questions: are fluxes of C and water equally well reproduced? What are common key weaknesses in simulating observations? Based on these multiple constraints, we determined which models are most suitable for simulations of European crop (rotational) C cycling, and whether common model deficiencies can be identified.

Using the EnKF, I then assimilated C flux and stock data for one winter wheat growing season into SPAc for model diagnosis and parameter estimation (chapter 4). The overall research rationale was to diagnose key processes of a crop model through explicit consideration of independent, multiple constraints. External control of state estimation through assimilated measurements revealed model behaviour under realistic conditions, whilst confidence limits on simulated and observed data were explicitly respected for. The key research questions were: are key crop processes resolved in the time richness of NEE data? Are NEE data better simulated when model biometry meets observational constraints? I further estimated key model parameters and their uncertainty for prognostic applications, and derived recommendations of more detailed field studies. This study is the first combined assimilation of C fluxes and biometric data into an agroecosystem BGCM.

In a last step, SPAc was extended by two summer crop types (maize and soybean) for application in an upscaling study, in which 104 MODIS 250 m VI time series surrounding a flux tower site in Illinois (USA) were assimilated for an improved estimation of C flux seasonality and biometry (chapter 5). I explicitly accounted for spatially and temporally varying field-specific land management and crop developmental patterns. The two key research questions were: do MODIS VI data allow for accurately reproducing observed crop C fluxes at the point scale, when these data are assimilated into SPAc without prior knowledge or prescription of sowing dates? How large is the regional and interannual variability in simulated agroecosystem C fluxes and biometry due to land management? Within this study, I propose a model-DA-framework for accurate simulation of spatio-temporally resolved cropland C fluxes and biometry without a priori requirements on sowing dates, and possibly further land management practices.

Taken together, these research aims and key research questions establish the set of

overarching thesis goals and questions, as discussed in chapter 6. These are: (1) Can SPAc be regarded as a generalised agroecosystem BGCM, readily applicable to the Earth's major agricultural regions? What are persistent key weaknesses, limiting its regional applicability? (2) What key lessons could be learnt from DA-based model diagnosis? And finally (3), does MODIS DA provide insights into the C flux seasonality of regional agroecosystems? How crucial is land management in determining interannual variability in phenological parameters, such as growing season length (GSL) and start of season (SoS)?

Chapter 2

A linked carbon cycle and crop developmental model: description and evaluation against measurements of carbon fluxes and carbon stocks at several European agricultural sites

For this publication (Sus *et al.*, 2010), I developed the model (together with M. Williams) and undertook the simulations and data intercomparison. E. Céschia, P. Béziat, T. Grünwald, C. Bernhofer, W. Kutsch, W. Eugster, and N. Buchmann provided flux and biometric data. I wrote the paper with support from M. Williams and R. Doherty, and input from all other authors, and produced all Figures and Tables shown.

Abstract

Croplands are the largest biospheric source of carbon (C) to the atmosphere in Europe each year (∼0.3 GtC y^{-1}). Moreover, the biological dynamics of managed landscapes affect the fluctuations of atmospheric CO_2 levels on annual and inter-annual scales. The activity of croplands must therefore be included in efforts to quantify, understand and regulate the global C cycle. C flux data for croplands, existing mostly from ∼2003 onwards, provide an opportunity to better understand the timing and magnitude of C exchanges in croplands and can help to improve crop C modelling on various spatio-temporal scales. A crucial process to be considered for C budget modelling is crop development, to which the C allocation pattern and senescence and remobilisation processes are directly linked.

We developed, parameterised, and tested a new crop C mass balance model (SPAc), which included all major developmental stages (DS) and C remobilisation. Model results were compared against independent observations of C fluxes and biometric data for eight site years, at six European sites growing winter wheat and barley. We used a single parameterisation for all sites, varying only maximal carboxylation rate (V_{cmax}), maximal photosynthetic electron transport rate (J_{max}), and C per leaf area (C_{la}) between wheat and barley. The model effectively described the seasonal dynamics of net ecosystem exchange (NEE) through simulation of DS. We found high model reliability for predicting daily NEE fluxes (mean R^2 = 0.83, mean RMSE = 1.47 gC $m^{-2}d^{-1}$). Results for cumulative NEE from sowing to harvest were of lower quality (mean R^2 = 0.27). The model tended to overestimate leaf area index (LAI, 160% of observed), and underpredict final yield (71% of observed). The introduction of a dead leaf C pool considerably improved at-harvest estimates of total leaf C mass. Simulating the shift from green to brown above-ground biomass is of potential significance for solving the surface energy balance and for future remote sensing studies through an improved simulation of crop canopy optical properties. [1]

[1] Published as: Sus, O., Williams, M., Doherty, R. et al. (2010). A linked carbon cycle and crop developmental model: Description and evaluation against measurements of carbon fluxes and carbon stocks at several European agricultural sites. *Agriculture, Ecosystems & Environment*, **139**, 402 – 418.

2.1 Introduction

In 2000, about 12% of the Earth's ice-free land surface was cropland, with pasture accounting for a further 22% (Ramankutty *et al.*, 2008). These managed lands play a significant role in global biogeochemical cycles (Denman *et al.*, 2007). The global human appropriation of net primary production (the aggregate impact of land use on the biomass produced each year in ecosystems) has been estimated to amount to ∼25% (Haberl *et al.*, 2007), with a significant share of this ascribed to biomass removal during harvest (∼53%). Janssens *et al.* (2005) estimated croplands to be the largest biospheric source of C to the atmosphere in Europe each year (∼0.3 GtC y^{-1}, for Europe as far east as the Urals). The biological dynamics of managed landscapes affect the fluctuations of atmospheric CO_2 levels on annual and inter-annual scales (Moureaux *et al.*, 2008; Houghton, 1999). The activity of croplands must therefore be included in efforts to quantify, understand and regulate the global C cycle, for example through the United Nations Framework Convention on Climate Change.

Currently there is limited understanding of the interplay between land management and C cycling, and more specifically between management practices, agricultural yield and net C balance (Smith *et al.*, 2010). Studies on cropland C balance, linking both plant and soil C dynamics, have been rare. Agronomists have largely focused on measuring and modelling crop yields and their dependence on crop management and intervention, rather than the seasonal cycle of C fluxes and how these differ from unmanaged ("natural") systems. The observation, analysis and modelling of C fluxes since the 1990s, when it began in earnest, has largely focused on these unmanaged ecosystems. To date, only 30 out of the 251 sites contained within the FLUXNET La-Thuile data set are croplands (Williams *et al.*, 2009).

C flux data for croplands exist mostly from ∼2003 onwards (with a few earlier exceptions, e.g. the Ameriflux network provides cropland NEE data from 1997 onwards for their Bondville site). These data provide an opportunity to better understand the timing and magnitude of C exchanges in croplands and can help to improve crop C modelling on various spatio-temporal scales. However, land surface models have mostly

lacked crop-related plant functional types (PFT), and often the grassland PFT has been used as a proxy for crops (Osborne *et al.*, 2007). But now crop C budget modelling studies are taking into account eddy flux information (Adiku *et al.*, 2006; Arora, 2003; Huang *et al.*, 2009a; Lokupitiya *et al.*, 2009; Wang *et al.*, 2005, 2007), and global land surface models, which incorporate land management, are being developed and tested (such as LPJmL (Bondeau *et al.*, 2007), Agro-IBIS (Kucharik and Twine, 2007) and ORCHIDEE-STICS (de Noblet-Ducoudré *et al.*, 2004)). One of the major challenges in modelling crops is to simulate the complete spectrum of plant development, from seed to senescence. This spectrum is important because developmental stages represent shifts in C allocation and remobilisation patterns. Natural vegetation C models tend not to include such shifts, so significant changes to C models are required.

Both a realistic representation of the aforementioned crop developmental pattern and the consideration of soil C dynamics are required in order to effectively simulate C dynamics in croplands. Whilst physiological models exist for specific crops or cropping systems (Jamieson *et al.*, 1998; Keating *et al.*, 2003; Porter *et al.*, 1983; Stöckle *et al.*, 1994; van Laar *et al.*, 1997; Williams *et al.*, 1989; Yang *et al.*, 2004), no existing Dynamic Global Vegetation Model (DGVM) includes, for example, plant development, C remobilisation, and senescence, all within a full crop C budget. For all but one (Wang *et al.*, 2007) of the models mentioned above, crop development is based on a linear relationship to cumulative temperature (growing degree days, GDD), photoperiod, and vernalization. Furthermore, the models do not account for C remobilisation in the reproductive phase, nor do they contain a standing dead leaf C pool. Additionally, in some of the models, the evolution of potential leaf area index (LAI) is either prescribed (Bondeau *et al.*, 2007; de Noblet-Ducoudré *et al.*, 2004) or constrained through a maximum LAI value (Kucharik and Twine, 2007; Huang *et al.*, 2009a), or leaf senescence rate was set to a constant value (Adiku *et al.*, 2006).

In this paper we present a new model, which simulates the full crop C balance, and explicitly models all major developmental stages, including senescence, with justifiable non-linear relationships to temperature, photoperiod and vernalisation, as well as C remobilisation. Further, we evaluate the model outputs against independent

observations and thus determine model validity and weaknesses. Our objective here was to compare model results with both CO_2 flux data and time series of biomass harvests from a selection of six European cropland sites over multiple years. Out of the crop C budget models mentioned above, only SiBcrop (three sites, Lokupitiya *et al.* (2009)), LPJmL (three sites), and ORCHIDEE-STICS (two sites) have been compared to C flux data measured at several sites. We aimed to determine (1) how effectively the model described observed fluxes and C biomass changes as the crops developed, and (2) critical weaknesses in model formulation and parameterisations. One major advantage of using eddy covariance data is their temporal resolution, which allows predicted C exchanges to be evaluated over a range of time scales, weather conditions, and, particularly important in this case, crop developmental stages.

Our further objectives were to determine whether different crop types and European locations could be accommodated within a single model structure, with resulting predictions of C fluxes and biomass that differ from observations only within acceptable limits. We also undertook a detailed sensitivity analysis to identify which parameters controlled NEE and model error.

This study is novel in two ways. Firstly, the model includes a broadly applicable and advanced representation of crop development based on Penning de Vries *et al.* (1989), Wang and Engel (1998), and Streck *et al.* (2003), within a full C budget framework. Secondly, we have evaluated the model against multiple data sets with an explicit focus on parameter sensitivity. Hence we present our insights into both model weaknesses and requirements for field studies that can constrain critical parameters.

2.2 Data and Methods

2.2.1 Data and study sites

We compared modelled estimates of NEE against observations of NEE made over croplands by the eddy covariance method, derived from the CarboEurope database

(http://gaia.agraria.unitus.it/database/carboeuropeip/). We used gap-filled half-hourly level 4 data (Falge *et al.*, 2001; Reichstein *et al.*, 2005), so that an observation value existed for each model time-step (0.5 h) and each simulation day. The gap-filling procedure introduced empirically modelled estimates into the gaps within the data record. Consequently, the process modelling was compared to a mix of observations and empirical interpolations. As daily NEE values are aggregates of half-hourly observations, the percentage of gap-filled values used for estimating daily NEE was variable. Around 30% to 60% of half-hourly NEE values within a growing seasons overall record were flagged as gap-filled (Table 2.1). However, for each of the NEE data time series used in this study, the percentage of half-hourly values falling in the quality classes 0 (original value) or 1 (most reliable gap-filled) is >90%.

Table 2.1: List of study sites showing length of crop growing period (from sowing to harvest), the percentage of half hourly NEE data that were gap-filled, average temperature (av. temp.) and precipitation (precip.) during the growing period, and soil texture (Clay:Sand:Silt in percent) and type. In column 1, winter barley sites are marked (*), all others are winter wheat.

site	growing period	length [days]	gap-filled NEE [%]	av. temp. [°C]	precip. [mm]	soil texture (Cl:Sa:Si [%]) and type
Auradé	27.10.05-29.06.06	245	43.9	9.7	374	32.3:20.6:47.1 luvisol
Gebesee(a)*	17.09.04-16.07.05	302	29.2	7.9	366	35.8:3.9:60.3 chernozem
Gebesee(b)	09.11.06-07.08.07	271	45.9	10.6	447	
Grignon	28.10.05-14.07.06	259	40.3	8.2	327	18.9:7.0:74.1 luvisol
Klingenberg	25.09.05-06.09.06	347	42.2	6.0	607	44.1:21.7:34.24 pseudogley
Lamasquère	18.10.06-15.07.07	270	52.4	11.3	531	54.3:12.0:33.7 luvisol on alluvium
Oensingen(a)*	29.09.04-07.07.05	281	46.6	7.5	548	43.0:9.5:47.54 eutric-stagnic cambisol
Oensingen(b)	19.10.06-16.07.07	270	52.5	10.2	1051	

We selected six sites from the CarboEurope database (Figure 2.1), and data collected over the years 2005-7. The sites are located in France (Auradé + Lamasquère (Béziat *et al.*, 2009), Grignon), Germany (Gebesee (Anthoni *et al.*, 2004), Klingenberg) and Switzerland (Oensingen, (Dietiker *et al.*, 2010)). They vary in latitude (from

43.6°N to 51.1°N) and longitude (from 1.1°E to 13.5°E), and represent considerable variety in terms of western-central European climate. Average temperatures measured during the various growing periods (sowing–harvest) ranged from 6.0 to 11.3 °C, and precipitation from 327 mm to 1051 mm. These climates result in a substantial variation in growing periods over the six sites. Particularly high average temperatures and precipitation totals have been recorded for the growing seasons of those crops planted in late 2006 and harvested in the summer of 2007. The amount of precipitation measured during growing season Oensingen(b) is outstanding with a reported value of ∼1050 mm in 270 days. Growing periods not only varied with respect to timing (with sowing dates ranging from mid September to early November, i.e. a difference of 53 days maximum) but also overall length (from 245 to 347 days, Table 2.1). Field measurements of soil texture values indicate varying local pedo-climatic conditions, although loamy soils predominate.

Overall, the selection of study sites and years offers a broad spectrum of western-central European climatic conditions, which were used to test model performance. Using these data, we compared simulated and observed NEE for winter wheat (ww) and winter barley (wb) over 6 (ww) and 2 (wb) growing periods. Wheat and barley are the two main cereals (including grain maize but not green or silage maize) in Europe (EU-27), with a harvested production in 2007 of 46% (wheat) and 22% (barley) of the total for cereals (∼260 million tonnes) (Eurostat, 2008).

2.2.2 Model description

Photosynthesis, energy and water balance

The Soil Plant Atmosphere (SPA) model (Williams *et al.*, 1996, 2001b) is a process-based model that simulates ecosystem photosynthesis and water balance at fine temporal and spatial scales (30 minute time-step, up to ten canopy and twenty soil layers). The scales of parameterisation (leaf-level) and prediction (canopy-level) have been designed to allow the model to diagnose eddy flux data and to provide a tool for scaling up leaf

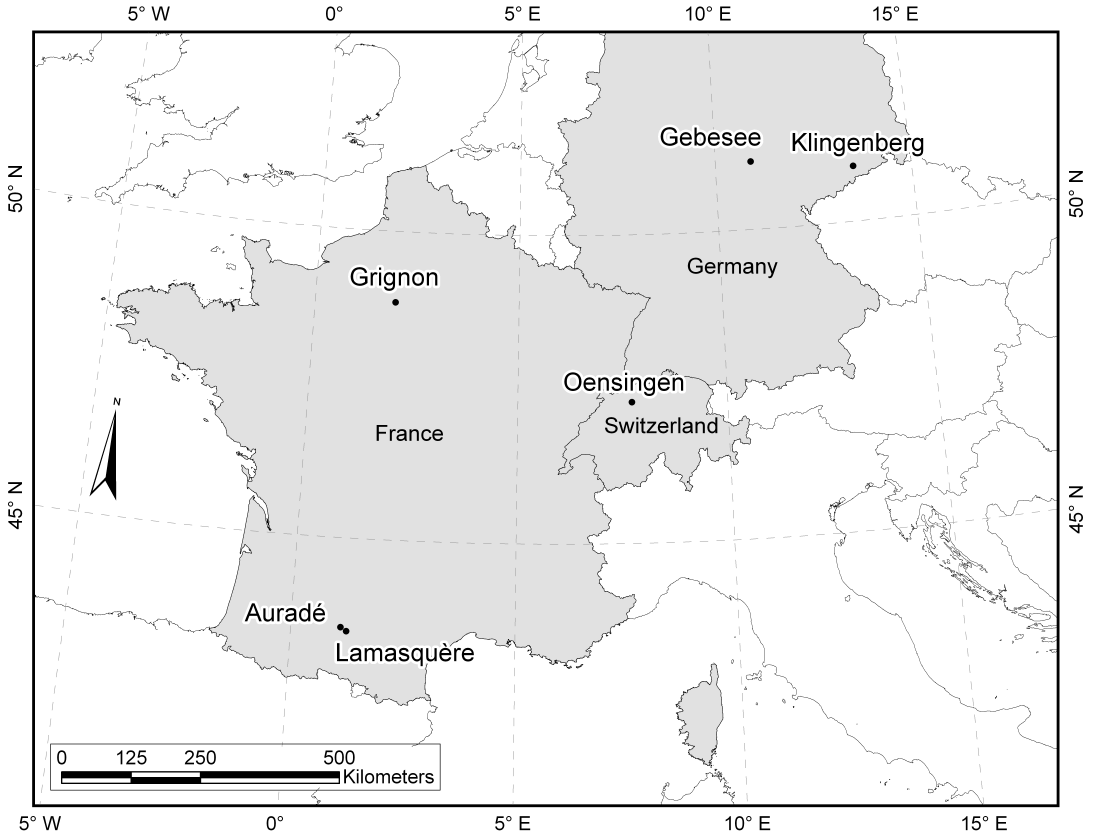

Figure 2.1: Locations of study sites.

level processes to canopy and landscape scales (Williams *et al.*, 2001b). The SPA model employs some well-tested theoretical representations of ecophysiological processes, such as the Farquhar model of leaf-level photosynthesis (Farquhar and von Caemmerer, 1982), and the Penman-Monteith equation to determine leaf-level transpiration (Jones, 1992). These two processes are linked by a model of stomatal conductance that optimizes daily C gain per unit leaf nitrogen, within the limitations of canopy water storage and soil to canopy water transport. Stomata adjust in order to maximize C assimilation within the limitations of the hydraulic system, so stomatal resistance is adjusted to balance atmospheric demand for water with rates of water uptake and supply from soils. As a consequence, evapotranspiration is maintained at a rate that keeps leaf water potential [Ψ_l] from falling below a critical threshold value, below which potentially dangerous cavitation of the hydraulic system may occur (Williams *et al.*, 1996).

Plant hydraulics within SPA are represented as the change of leaf water potential over

time. This change is a function of soil water potential, capacitance of the hydraulic system, evapotranspiration, and above and below ground hydraulic resistance. Based on these assumptions and the biochemical parameters for maximum carboxylation capacity (V_{cmax}) and maximum electron transport rate (J_{max}), for each canopy layer and time-step an iterative procedure is used to determine the maximum sustainable stomatal conductance (g_{s}) and the assimilation rate associated with this conductance. SPA also contains a detailed representation of soil hydrology and thermal dynamics, allowing the surface energy balance to be solved as a function of down-welling radiation reaching the soil surface by estimating the soil surface temperature. Net radiation is then partitioned into sensible, latent and ground heat fluxes (Williams *et al.*, 2001a). For each soil layer, changes to water content are regulated by precipitation and evaporation (surface layer only), abstraction by roots (rooted layers only), and gravitational drainage, whilst soil porosity and water retention curves of each layer are estimated according to empirical relationships with soil texture. Plant root distribution is determined by total fine root biomass, maximum root biomass per unit volume, and depth of rooting. LAI is calculated by dividing live leaf C mass by the C per leaf area parameter C_{la}. The SPA model has been applied in natural ecosystems ranging from the 70°N to 2°S (Williams *et al.*, 1998, 2000). More recently, a C mass balance model has been developed (Williams *et al.*, 2005) to link to SPA.

Below, we describe modifications that have been made in order to simulate the dynamics of agroecosystems. These modifications are (1) the addition of a new developmental module dependant on ambient temperature, daylength, and vernalization and (2) the modification of the C allocation pattern in terms of adding/removing C pools and introducing a dependence of C allocation on crop developmental stage.

Carbon partitioning scheme

The C partitioning scheme embedded within SPA version 2 – Crop (hereafter referred to as SPAc; SPA as modified for the simulation of crop C dynamics) is based on observations of field crops with a series of harvests and crop growth analyses

(Penning de Vries *et al.*, 1989). Time series of C allocation fractions to the various crop plant organs (root, leaves, stem, storage organs) are derived from the patterns of increase in biomass. These fractions account for the efficiency of glucose conversion into structural dry matter. We chose this crop C partitioning scheme as corresponding tables have been published in Penning de Vries *et al.* (1989) for 14 different annual crop types such as wheat, barley, maize, potato, rice, sugar-beet, and soybean among others. As a consequence, information on C partitioning for wheat and barley were readily available for this study and new crop functional types can easily be added to SPAc. The original range of developmental stages, as can be found in Penning de Vries *et al.* (1989), has been extended to account for pre-emergence development as proposed by Wang and Engel (1998).

Crop developmental model

In the scheme outlined above, C allocation keys are given as a function of developmental stage (DS), which quantifies a crop plant's physiological age, and is related to its morphological appearance (for an example see Figure 2.2). It is important to correctly simulate crop plant development, as the C allocation pattern is directly related to it (Penning de Vries *et al.*, 1989). The model representation of crop developmental stage is introduced into SPAc by a new state variable, ranging from -1 at sowing to 2 at maturity (see Table 2.2 for intermediate phases and stages). DS is calculated as the sum of daily values of developmental rate (DR).

$$DS = \sum DR \qquad [d^{-1}] \tag{2.1}$$

A modified Wang & Engel model (Streck *et al.*, 2003) was implemented in SPAc to calculate crop developmental rate on the basis of justifiable non-linear functions for three environmental factors: temperature *f(T)*, photoperiod *f(P)*, and vernalization *f(V)*. Only severe water stress is known to have a direct influence on crop development (Penning de Vries *et al.*, 1989), and so soil moisture effects are not considered here.

In detail, DR is calculated as the product of a maximum developmental rate DR_{max} (the maximum possible DR under optimal ambient conditions for development) and the three developmental response functions.

$$DR = DR_{max} \times f(T) \times f(P) \times f(V) \qquad [d^{-1}] \tag{2.2}$$

The temperature response function is:

$$f(T) = \frac{[2(T - T_{min})^{\alpha} \times (T_{opt} - Tmin)^{\alpha} - (T - T_{min})^{2\alpha}]}{(T_{opt} - T_{min})^{2\alpha}} \tag{2.3}$$

for $T_{min} \leq T \leq T_{max}$. $f(T) = 0$ for $T < T_{min}$ or $T > T_{max}$. The exponent α is given by:

$$\alpha = \frac{ln2}{ln[(T_{max} - T_{min})/(T_{opt} - T_{min})]} \tag{2.4}$$

T_{min}, T_{opt}, and T_{max} are the cardinal temperatures for development (minimum, optimum, and maximum), and T is the mean daily temperature calculated from the 48 half-hourly temperature values.

The photoperiod response function is:

$$f(P) = 1 - exp[-\omega(P - P_c)] \tag{2.5}$$

where P is the actual photoperiod, P_c the critical photoperiod below which no development occurs, and ω is a cultivar specific photoperiod sensitivity coefficient.

The effective vernalization days, VD, are calculated from sowing as:

$$VD = \sum fvn(T) \tag{2.6}$$

where fvn(T) is the daily vernalization rate (per day), calculated using Equation 2.3 and Equation 2.4 with the cardinal temperatures for vernalization ($T_{min,v}, T_{opt,v}$, and

$T_{max,v}$). The vernalization response function is:

$$f(V) = \frac{(VD)^5}{(VD_h)^5 + (VD)^5} \tag{2.7}$$

where *f(V)* is the vernalization function that varies from 0 (unvernalized) to 1 (fully vernalized plants). Parameter VD_h is the effective vernalization days when plants are 50% vernalized, and the exponent 5 provides the sigmoidal shape of the response to VD. We understand vernalization as "the acquisition or acceleration of the ability to flower by a chilling treatment" (Chouard, 1960). According to Slafer and Rawson (1994), it is generally accepted that exposure to vernalising temperatures after seed imbibition (i.e. absorption of water by seed) can affect wheat developmental rate during the vegetative stages. For a more detailed description of these functions see Streck *et al.* (2003).

Table 2.2: Relation of SPAc developmental stages (DS) to crop growing phases and stages. DS [d^{-1}] ranges between -1 at sowing and +2 at maturity. After: Wang and Engel (1998).

phase	start of stage	DS
pre-emergence	sowing	-1.
	germination	-0.5
pre-anthesis	emergence	0.
(vegetative)	floral initiation	0.2
	terminal spikelet	0.45
	flag leaf	0.65
	heading	0.9
post-anthesis	anthesis	1.
(reproductive)	milk development	1.15
	dough development	1.5
ripening	ripening	1.95
	maturity	2.

In SPAc, *f(P)* and *f(V)* affect development only in the vegetative phase (*f(T)* in the vegetative and reproductive phases), and different $DR_{\max}$ are assumed for the vegetative and reproductive phases (Streck *et al.*, 2003). In our experiments, developmental rate is initially limited by low *f(V)* values. However, as *f(V)* saturates quickly through the winter period (*f(V)* = 1), *f(P)* and *f(T)* become the only limiting factors on crop development during the vegetative phase (Figure 2.2 a)). *f(T)* remains limiting until crop maturity, but exhibits a continuously weakening influence (*f(T)* close to 1) as mean daily temperatures increase throughout spring towards summer. As a result, DS remains low until the beginning of February, after which it rises gradually. By

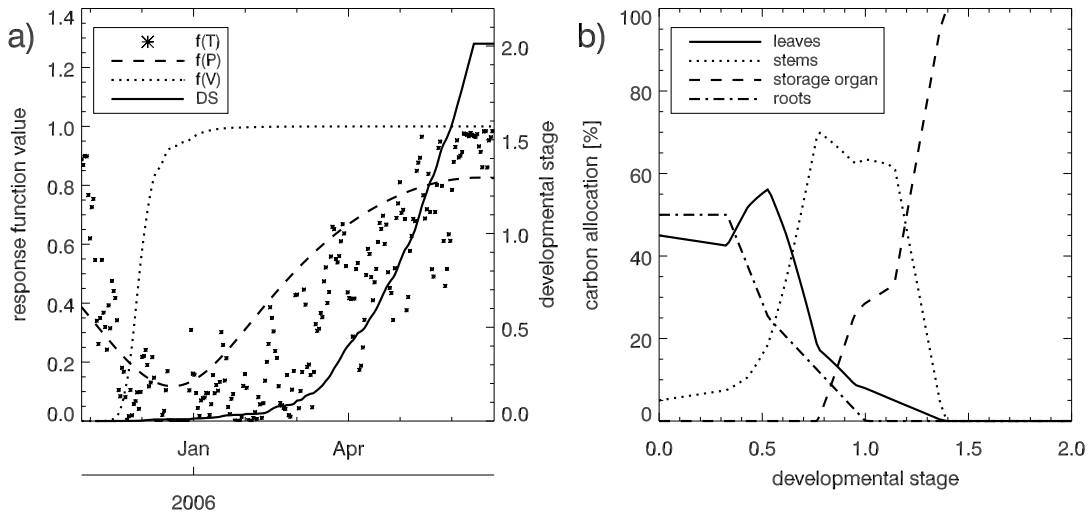

Figure 2.2: a) Time vs. developmental response function values ($f(T)$ = temperature function, $f(P)$ = photoperiod function, $f(V)$ = vernalization function) plus developmental stage (DS) and b) DS vs. carbon allocation pattern for growing season Auradé (winter wheat) as implemented in SPAc. In order to maximise plotting space, DS values <0 (sowing to emergence) are not shown in a) + b).

mid-March, developmental rate increases significantly so that DS rises in an quasi-exponential fashion until crop maturity. Due to space restrictions, Figure 2.2 a) shows the progression of DS for Auradé only. However, all the other sites show a relatively similar phenological pattern, and all crop plants reached maturity (DS = 2) before harvest.

In the study of Streck *et al.* (2003), the modified Wang & Engel model produced a root mean squared error (*RMSE*) of simulated winter wheat development which was up to 45% lower compared to the original model. The only difference between the modified Wang & Engel model (Streck *et al.*, 2003) and the way it is being used in SPAc is that we do not split the vegetative phase into two sub-phases. In the modified Wang & Engel model, *f(V)*, *f(P)*, and *f(T)* are used in sub phase I (0 <DS< 0.4), and *f(V)* is deactivated in sub phase II (0.4 <DS< 1). In SPAc, *f(V)*, *f(P)*, and *f(T)* affect developmental rate throughout the vegetative phase (DS < 1), but only *f(T)* is used in the reproductive phase (DS> 1). Another advantage of the modified Wang & Engel model is that both the temperature and vernalization response functions can easily be modified by changing their cardinal temperatures in order to improve representativeness

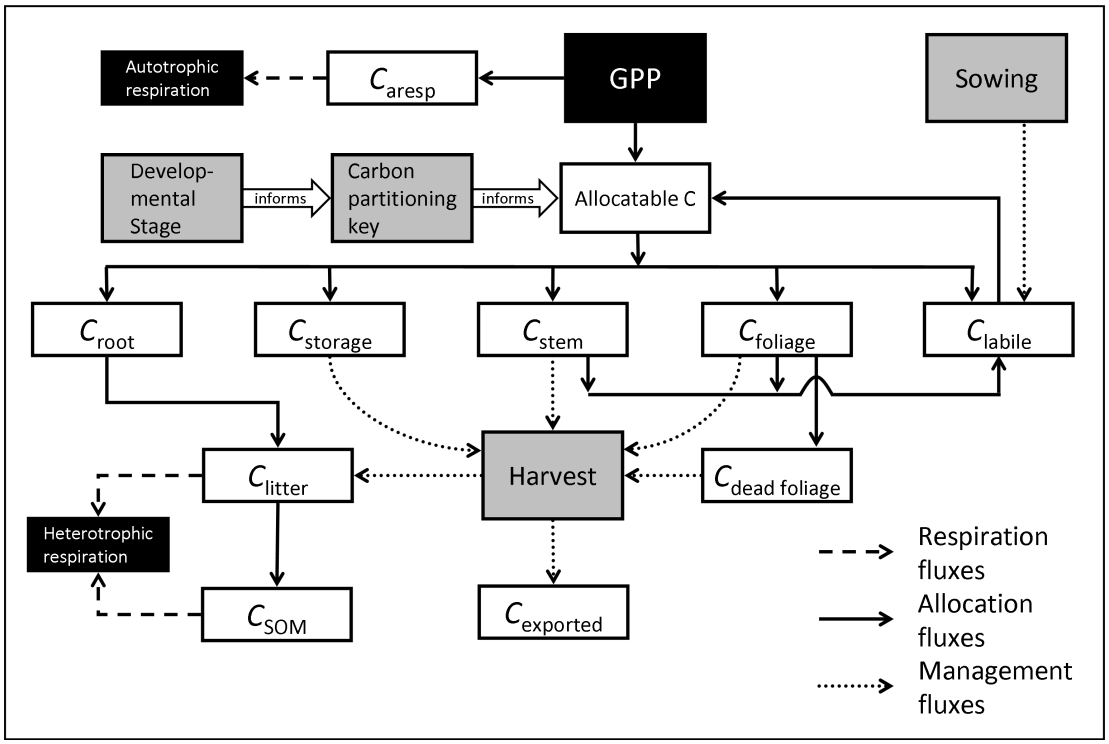

Figure 2.3: Schematic of SPAc respiratory processes and photosynthesis (black boxes), carbon pools (white boxes), fluxes (arrows), and external drivers (grey boxes).

for different developmental stages, agricultural regions and crop types or cultivars if required (though the vernalization function was found to be cultivar independent (Streck *et al.*, 2003)). Similarly, the photoperiod response function can be adapted by changing either the photoperiod sensitivity coefficient or the critical photoperiod.

Carbon fluxes: growth, respiration, senescence, and remobilisation

Based on this development-linked C allocation pattern, SPAc simulates the allocation of carbohydrates to one root and four above ground (i.e. shoot) C pools (labile, foliage, stem and storage organ C pools, Figure 2.3). Around sowing (DS<0), C gained through photosynthesis (after having subtracted autotrophic respiration as a fixed fraction (f_a) of gross primary productivity (GPP, Waring *et al.* (1998); Gifford (2003)) is mainly allocated to leaves and roots at approximately equal amounts (Figure 2.2 b)). In the case of winter cereals, the root share decreases continuously from DS≈0.3 onwards, leaf

allocation considerably drops from DS≈0.5, whilst stem allocation reaches maximum values (0.7<DS<1.2). For DS>1.2, allocation to the storage organs (here cereal grains) increases sharply with declining partitioning to the stem C pool. All available C will be allocated entirely to the storage organ pool for DS>1.4.

A litter C pool receives litter fluxes originating from the shoot and root C pools (Figure 2.3). The root litter flux is a function of developmental stage and commences at flowering (DS=1). Shoot litter fluxes only occur at harvest and are dependent on the amount of above ground biomass left on field after harvest. Decomposition fluxes are then calculated as a function of litter C content, specific turnover rate parameters and temperature (based on a Q_{10} temperature relationship). In the same fashion, mineralization fluxes of the litter and soil organic matter C pools (i.e., heterotrophic respiration) are calculated (Williams *et al.*, 2005). C originating from the fraction of GPP to be respired enters a respiratory C pool. The autotrophic respiration flux itself originates from the gradual turnover of this pool, and thus occurs throughout day and night, but is not directly determined by temperature.

The model runs were initiated at the reported sowing date, when, based on thermal time, SPAc calculates the duration of the period from sowing to emergence (a phase of non-activity). In the current version, SPAc does not explicitly account for germination and growth of roots and shoots from germination until emergence. At emergence, the gradual turnover of the labile C pool content (representing the amount of C contained in the seeds) is the only initial source available for growth. As leaves grow, photosynthesis initiates and new C is available for allocation. In SPAc, seedlings do not fully exhaust their seeds, as photosynthesis takes over the C supply once C available from photosynthesis is greater than C available from seed reallocation (Penning de Vries *et al.*, 1989). The remaining labile (or seed) C will be turned over and added to the litter C pool. Photosynthesis continues throughout the late autumn and winter months at a reduced rate, only limited by local meteorology (i.e. no additional constraint on growth was introduced to represent the effect of "dormancy"), and will increase considerably with rising ambient temperature and global irradiation levels in spring.

Later, in the reproductive phase, carbohydrates from the foliar and stem C pools are remobilized and transferred to the labile C pool. Remobilization of stem C is triggered once the running mean of the storage organ growth rate drops below a previously attained value. Leaf senescence rate on the other hand occurs either due to self shading as a function of leaf area (if LAI is higher than the critical LAI threshold value) or ageing as a function primarily of developmental stage, whichever is higher (van Laar *et al.*, 1997). 50% of the senescing leaf C flux is treated as remobilized carbohydrate (Penning de Vries *et al.*, 1989; van Laar *et al.*, 1997), whilst the other half enters a dead foliage C pool (Figure 2.3). We assume that wheat/barley plants do not shed their leaves before harvest. Root death commences at flowering with a minimal value and linearly approaches and maintains its maximum rate at developmental stage 1.3 and beyond. In this simulation, dying roots are assumed not to contribute remobilised C to the labile C pool. Each of the remobilization processes involves a fixed respiratory cost due to the conversion between starch and glucose (Goudriaan and van Laar, 1994). In the reproductive phase, young storage organs may not have the capacity to accept all the carbohydrates provided (allocated NPP plus remobilized reserves from stems and leaves), as there may be a high total number of receiving growing points, which still might have too small an overall sink size, though. Consequently, the growth rate of the storage organ is limited by a maximum potential growth rate per day, which is set to about a third of the overall storage organ pool (Goudriaan and van Laar, 1994). If this maximum growth rate is exceeded, any surplus C will be allocated to the labile C pool.

At harvest (date as reported in Table 2.1), the fraction of the above ground C mass exported from the field is given by the storage organ content plus a reported fraction of harvested stem and leaf C, and the residual crop C mass enters the litter C pool. The longer term fate of crop residues depends on the local residues management such as ploughing frequency or straw incorporation. Accordingly, crop residue decomposition and mineralization rates are affected by management type and timing, which have to be accounted for when simulating post-harvest ecosystem respiration fluxes. The model results presented here are only truly representative of the growing period between sowing

and harvest, as ploughing, post-harvest sowing, and re-growth of volunteers are not explicitly considered.

Model set-up

The input drivers for the SPAc model are time-series of gap-filled half-hourly observations of temperature, ambient CO_2, wind speed, global radiation, vapour pressure deficit, precipitation and air pressure. Moreover, soil texture is prescribed as reported from the individual flux sites, and initial soil organic matter as well as labile C contents (i.e. seed C content) are estimated based on field observations reported in the literature (Anthoni *et al.*, 2004; Aubinet *et al.*, 2009; Halley and Soffe, 1988). Accordingly, initial values of soil organic matter in the top 40 cm soil layer and labile C content have been set to 7200 gC m^{-2} and 9 gC m^{-2}, respectively. SPAc has been set up to include 4 canopy and 20 soil layers. The runs were initiated at sowing (date as reported in Table 2.1) and terminated by the end of the following year, even if cover crops were grown (e.g. Oensingen(a)). The effects of fertilization have not been taken into account, but reported harvest dates and crop residue management are considered in the model runs.

2.2.3 Sensitivity analysis and parameterisation

An analysis of model output sensitivity to a set of parameters has been performed in order to rate parameters by their importance in determining model behaviour. As a result, we are able to evaluate model reliability in more detail and recommend further needs of research on specific model processes and related parameters.

A single parameter sensitivity index (S) has been applied in this study. This index quantifies model sensitivity by relating the relative change of the state variable of interest with the relative change of the model parameter of interest. S is given by

$$S = \frac{R_a - R_n}{R_n} / \frac{P_a - P_n}{P_n} \tag{2.8}$$

where R_a and R_n are responses for altered and nominal model state variable(s) or statistics, and P_a and P_n are the altered and nominal parameters respectively. We analysed model sensitivity for cumulative NEE (sowing to harvest) for the winter wheat growing period of Auradé. The relative changes to the diagnostics have been quantified for a set of 32 model parameters used within various SPAc modules, such as those simulating photosynthesis, crop development, plant hydraulics, and ecosystem respiration. For each sensitivity test, the particular parameter of interest was altered by adding (subtracting) 25% to (from) its nominal value, so that the denominator of equation (2.8) is always equal to either +0.25 (parameter increased by 25%) or -0.25 (parameter decreased by 25%). Consequently, if S = 1, a 25% increase (decrease) of a parameter leads to a 25% increase (decrease) of cumulative NEE. The following parameters are altered in a different fashion: only the absolute value of minimum leaf water potential Ψ_l is modified (as its nominal value is already negative), leaf nitrogen distribution through the canopy layers is compared to a uniform distribution, only the decimal places of stomatal efficiency are altered, and each of the cardinal temperatures was varied by ±2 °C.

An overview of model parameters, nominal values, and references is given in Table A.1. The parameterisation is based on an extensive literature review, ensuring that all of our parameter values range within realistic, previously reported limits. We decided to use this single parameterisation (except for V_cmax, J_max, and C_la, which are crop type specific here) for each of the sites included in this study in order to examine whether it is possible to find a generic parameterisation that allows for a realistic field-scale simulation of winter wheat/barley C budgets over western-central Europe, and to highlight which parameters might need recalibration with varying latitudes and longitudes.

2.3 Results

2.3.1 Results for modelled carbon exchange data

Daily NEE flux data and residuals

A comparison of observed with modelled NEE flux data showed that SPAc modelled both the overall magnitude, and especially the seasonality, of C exchange for all of the 8 growing periods with high accuracy (mean $R^2 = 0.83$ (linear Pearson correlation coefficient), mean $RMSE = 1.47$ gC $m^{-2}d^{-1}$, Figure 2.4). In general, a rather gradual decrease of observed NEE from sowing onwards (i.e. a gradual strengthening of the ecosystem's C uptake potential) until early spring compared well to modelled values. By the beginning of March, the assimilation of C increased considerably until reaching its peak value in a period between May and June. The observations were largely reproduced by the simulated NEE values, with SPAc results matching observations best for Auradé (ww), Gebesee(a) (wb), and Grignon (ww). Note that in Figure 2.4 a), two modelled lines are shown. The line with higher post-harvest NEE displays results for all modelled above ground C (except for grains) remaining on field after harvest, whereas the line with lower post-harvest NEE represents model results for 90% of both leaf and stem C having been exported. As a consequence, post-harvest decomposition and mineralisation (and thus NEE) fluxes are considerably different between the two. The highest observed daily rate of C assimilation was rather similar for all sites and ranged in between -8 and -12 gC $m^{-2}d^{-1}$, except for Oensingen(b) (ww), which had some days with productivity in excess of these values. Here, the observed peak value of C assimilation was $\sim$-15 gC $m^{-2}d^{-1}$, and the corresponding modelled value was considerably smaller in magnitude ($\sim$-8 gC $m^{-2}d^{-1}$). After this phase of peak C assimilation, the observations showed that NEE became less negative (i.e. the ecosystems assimilatory capacity decreased) in a very rapid fashion towards crop maturity and harvest. The data indicated that all of the studied ecosystems were net sources of C by harvest, and this shift in C flows was well simulated.

There was a mismatch in terms of the timing of the onset of spring C assimilation for Klingenberg (ww). Modelled NEE decreased considerably around early March, whereas observations implied an onset of the peak growing season approximately a month and a half later.

At harvest, the reported fraction of crop residue and harvested biomass determined the allocation of above ground C mass to either the litter C pool or the exported C pool. Consequently, modelled heterotrophic respiration increased at harvest proportionally to the amount of crop residue instantly available for decomposition and mineralization. Observed harvest-time NEE fluxes compared well to the simulated values, with exceptions: growing seasons Gebesee(a) (wb), Grignon (ww), and Klingenberg (ww) showed an increase in NEE around harvest date, whereas a much smaller (if any) influence of harvest on NEE could be seen for Gebesee(b) (ww), and Lamasquère (ww). Also a comparison of post-harvest values showed that for Lamasquère (ww) there was a relatively small difference in modelled and observed NEE fluxes, whilst this difference was considerably higher for Gebesee(b) (ww) and especially Oensingen(a) (wb), where a cover crop was sown after the wb harvest. There was a clear sensitivity in the model to assumptions about residues. Post-harvest decomposition and mineralisation (and thus NEE) fluxes were considerably different depending on whether all above ground C (except for grains) was left on the field after harvest, or whether 90% of both leaf and stem C were exported (Figure 2.4 a)).

For simplicity, we are not showing a comparison of modelling results of GPP and ecosystem respiration with values derived from NEE observations. However, these data are analysed in a companion paper in this special issue for growing periods Auradé, Gebesee(b), Grignon, Klingenberg, and Oensingen(b). Mean values of the Kendall tau rank correlation coefficient (r, modelled vs. observed values) for these sites are 0.65 (GPP) and 0.63 (ecosystem respiration). For a detailed analysis of these data please see Wattenbach *et al.* (2010).

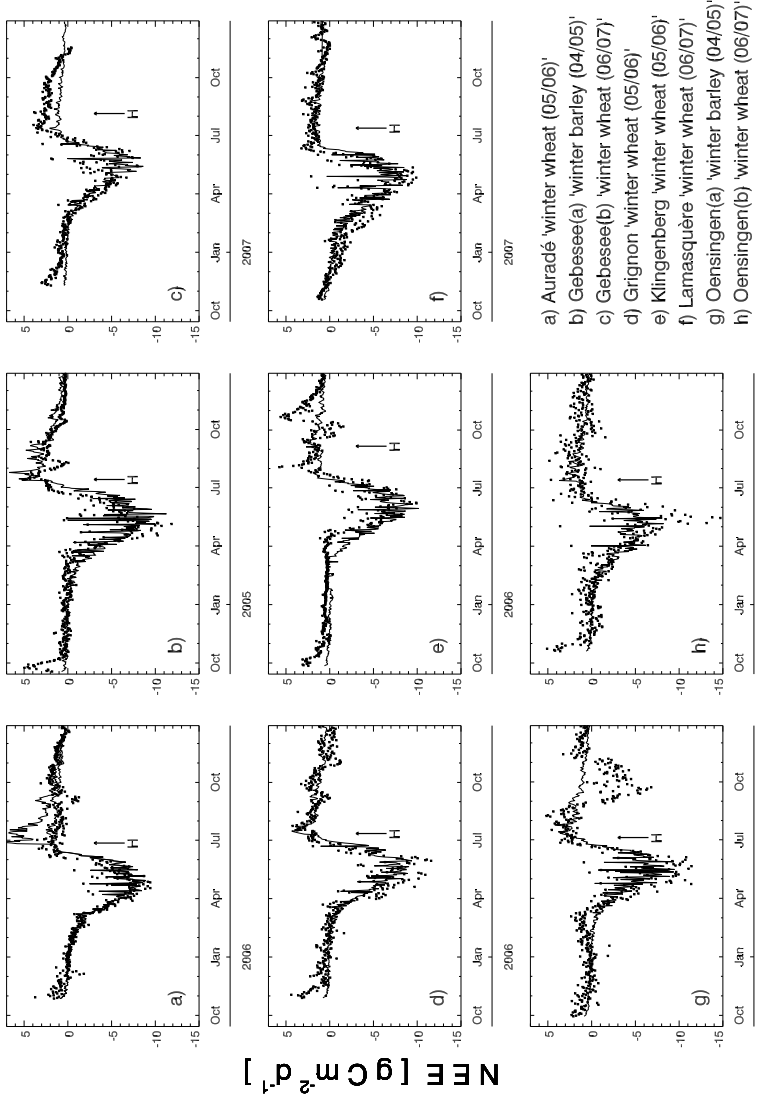

Figure 2.4: Observed (boxes) and modelled (solid line) daily values of NEE in gC $m^{-2}d^{-1}$ for each of the study sites and years. The timing of harvest (H) is indicated by arrows. Plotted values begin at sowing date as reported. In panel a), two lines are shown for model results with 90% (lower NEE at harvest) and 0% (higher NEE at harvest) of the above ground C mass (except for grains, which are always entirely exported) removed from the site at harvest.

Residuals of NEE (i.e. observed minus modelled NEE) indicated some clear periods of autocorrelation, associated with either crop development or post-harvest periods (Figure 2.5). The large post-harvest residuals for Oensingen(a) were associated with growth of newly seeded crops or cover crops following harvest. For example, in Dietiker *et al.* (2010), the second Oensingen crop 2005 (a Phacelia-based cover crop mixture) was modelled as a grassland with 50% above ground and 50% below ground biomass. These crops were not modelled by SPAc, and so corresponding residuals can be ignored in further discussion. The residuals in the pre-harvest phase do not show a clear pattern among sites. For instance, the model tended to estimate weaker sinks at Oensingen than the data in the month before harvest. In Auradé and Gebesee, the opposite was true, with the model suggesting a stronger sink than was measured pre-harvest. As expected, residuals were closest to 0 in the winter months when C fluxes generally are minimal, and (with exceptions) highest in the pre-harvest growing period.

Statistical description of daily and hourly NEE flux data

A linear fit between observed and modelled daily NEE (gC $m^{-2}d^{-1}$, sowing to harvest only) indicated that the R^2 was lowest for Oensingen(b) (0.74), and highest for Auradé and Oensingen(a) (0.88 each, Table 2.3). The slope of the linear fit was lower than 1 for all sites, indicating model bias. As negative intercept values suggested, sink strength was generally overestimated. Cumulative NEE (between sowing and harvest) were almost always lower than what had been observed, with a mean difference of ∼-134 g C m^{-2}. The R^2 of observed vs. modelled cumulative NEE for all site years was 0.27. *RMSE* was lowest for Auradé and highest for Oensingen(b), and ranged between 1.15–1.85 gC $m^{-2}d^{-1}$.

Five days (15.–20.05.06) within growing period Auradé (ww) were chosen to display half hourly values of modelled and simulated NEE (Figure 2.6). The observed diurnal cycle of NEE, with the ecosystem's net C uptake during daytime and net C release C during night-time, was reproduced by SPAc with high accuracy, both in terms of magnitude and timing.

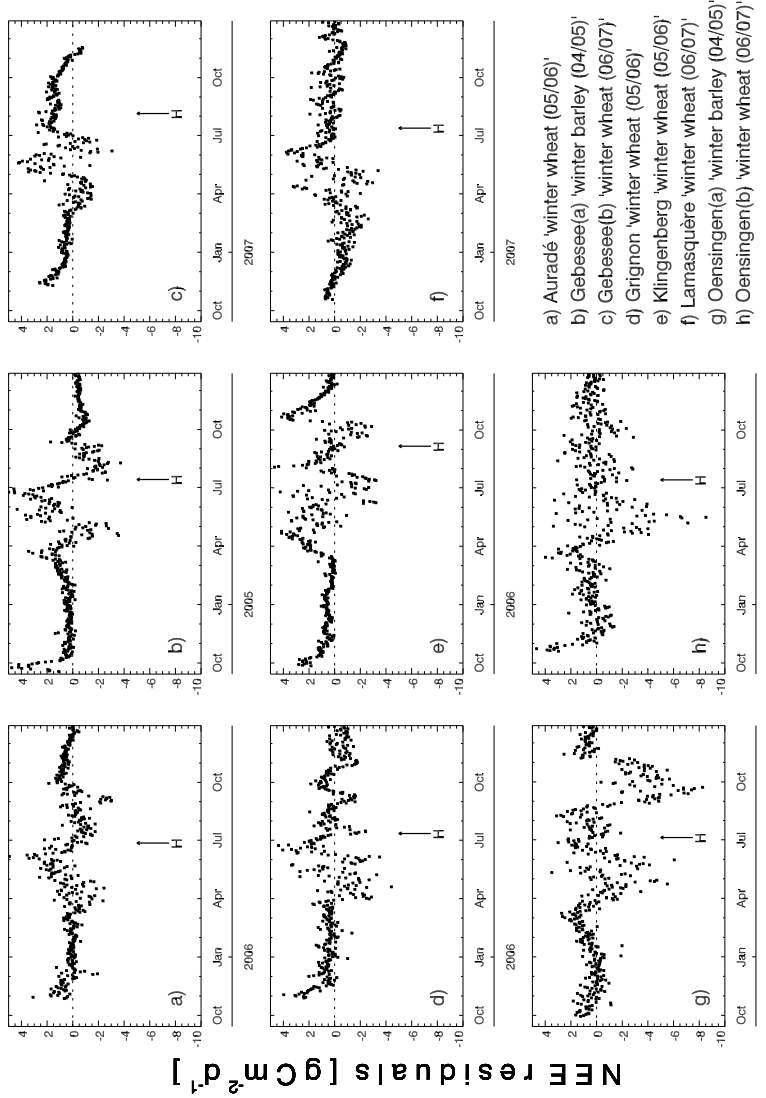

Figure 2.5: Observed minus modelled values of NEE (= NEE residuals) in gC $m^{-2}d^{-1}$ for each of the study sites and years. The timing of harvest (H) is indicated by arrows.

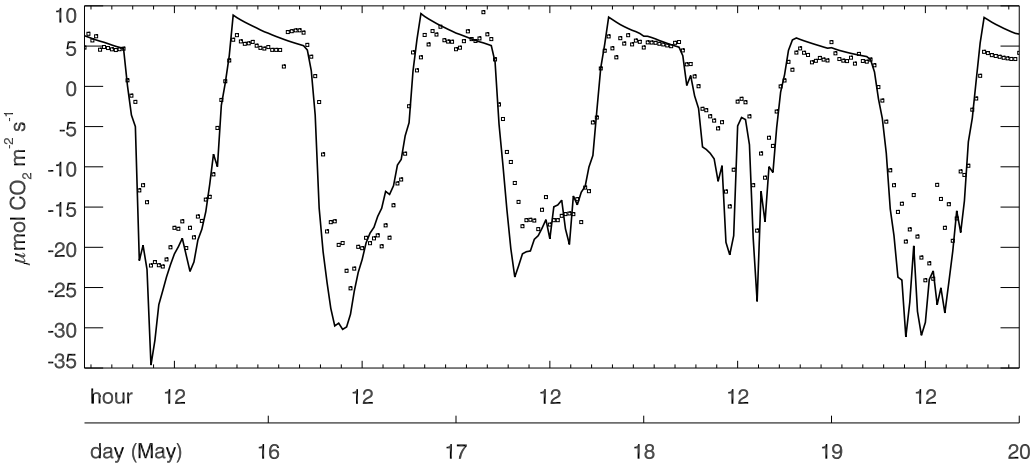

Figure 2.6: Observed (boxes) and modelled (solid line) half hourly values of NEE in μmol CO_2 $m^{-2}s^{-1}$ for the 15th–20th of May 2006, Auradé (ww).

Moreover, elevated vapour pressure deficit (∼1.8 kPa in early afternoon hours on the 17th) and considerably reduced short-wave radiation levels (∼100 Wm^{-2} around noon on the 18th) coincided with midday depressions in C assimilation rates, which were recognisable in plotted values of both observed and modelled NEE. The maximum temperature on the 17th was ∼10 °C higher than on the following day. Peak C assimilation rate seemed to be slightly overestimated by SPAc for each of the 5 days.

2.3.2 Results for modelled biometric data

We compared simulations of leaf area index (LAI) and leaf C mass with independent measurements for all growing periods, except for Oensingen(a) and (b), for which no time series of observations of both LAI and leaf dry mass were available. Moreover, observed total leaf C mass values (i.e. not reported separately as both live and dead leaf C mass, except for Gebesee(a)+(b)) will contain a certain share of live and dead leaf C, depending on the crop developmental stage. Presumably, all reported values of total leaf C for the vegetative crop phase are live leaf C mass. During the reproductive phase with commencing and accelerating senescence, the fraction of dead leaf C contained in reported total leaf C values will increase continuously towards maturity, when finally all observations are for dead leaf C only. We have time series of observed total leaf C mass

for Auradé, Grignon, Klingenberg, and Lamasquère, and both live and dead leaf C mass for Gebesee(a)+(b). We subsequently converted leaf dry mass to leaf C mass assuming the same fixed leaf C content of 0.459 (Penning de Vries *et al.*, 1989) for total, live, and dead leaf dry mass. Various on-site measurements during the study periods indicated that leaf C content is relatively similar for both live and dead leaves. Similarly, we used C content fractions for stem, root, and grains (following Penning de Vries *et al.* (1989)) to convert from reported values given as dry biomass per area to gC m^{-2}.

SPAc modelled LAI and leaf C mass with average accuracy overall (mean R^2 values: 0.58 (LAI), 0.41 (live leaf C mass), 0.36 (total leaf C mass), Figure 2.7), but seasonal dynamics are relatively well captured nonetheless. There was a greater agreement between predicted and observed peak leaf C mass than LAI values. There was a good match between observed and modelled LAI for the Grignon site, whereas modelled LAI was considerably higher than measured for all of the 4 remaining field sites. For Auradé, observed LAI values were ∼50% lower than simulated. The timing of peak LAI and also senescence was represented well by the model for all but one of the sites: the modelled onset of the peak growth phase of LAI and leaf C was 20–30 days earlier than observed for Klingenberg.

Modelled live leaf C mass values were close to measurements of total leaf C during the vegetative phase (i.e. before the peak of LAI and leaf C), often within the uncertainty range of ±1 standard deviation (rows 2 + 4 in Figure 2.7). They decreased considerably towards maturity as senescence accelerated, and just before harvest were 0 for all sites. In contrast to that, observed total leaf C mass values decreased at a slower rate and thus maintained higher values during the reproductive phase throughout. At harvest time, total leaf C mass typically was ∼50% of its peak value (panels b), h), and l)). Only for Klingenberg (panel j)) the total leaf C mass dropped to a very low value (∼20 gC m^{-2}) at crop maturity. The observed pattern of total leaf C mass decrease during the reproductive phase is better matched when considering modelled standing dead leaf C mass (dashed line). Dead leaf C mass increased from the late vegetative phase until maturity, and, even though it then was considerably larger than observed values of total leaf C, was able to more closely follow the observed pattern.

Table 2.3: Statistical description of modelling results (RMSE and linear fit between observed and simulated daily NEE from sowing to harvest, columns 2–5) and comparison of simulated vs. observed values of cumulative NEE (from sowing to harvest, gC m^{-2}), yield (gC m^{-2}), and LAI (m^2 m^{-2}, columns 6–11).

	NEE comparison				$NEE_{harvest}$		yield		LAI_{max}	
site	RMSE	R^2	slope	intercept	obs	mod	obs	mod [% of obs]	obs	mod [% of obs]
Auradé	1.15	0.88	0.89	-0.82	-447	-551	283	239 [84]	3.13	7.05 [225]
Gebesee(a)	1.64	0.82	0.87	-1.05	-314	-603	292	240 [82]	3.36	6.43 [191]
Gebesee(b)	1.37	0.81	0.81	-0.81	-169	-359	387	205 [53]	3.24	5.66 [175]
Grignon	1.44	0.87	0.76	-0.80	-411.6	-526	350	230 [66]	6.20	6.56 [106]
Klingenberg	1.55	0.80	0.87	-0.90	-275.8	-482	318	257 [81]	3.22	6.49 [202]
Lamasquère	1.28	0.84	0.80	-0.35	-529	-524	394	253 [64]	4.48	6.89 [154]
Oensingen(a)	1.44	0.88	0.67	-0.55	-357	-397	287	184 [64]	4.30	5.05 [117]
Oensingen(b)	1.85	0.74	0.58	-0.68	-339	-387	255	213 [83]	5.40	6.08 [113]

For Gebesee(a)+(b), observations of both live and dead leaf C mass are shown (panels d) and f)), indicating that dead leaf C mass accumulation starts earlier and reaches higher at-harvest values than modelled. Observed values of peak LAI ranged from ∼3.1 to ∼6.2 m^2 m^{-2} compared to a modelled range from ∼6.5 to ∼7 m^2 m^{-2}. On average, modelled peak LAI was 60% higher than measured. Observed peak leaf C mass data ranged from ∼70 to ∼125 gC m^{-2} compared to simulated values ranging from ∼125 to ∼140 gC m^{-2}. On average, modelled peak live (total) leaf C mass was 24% (44%) higher than measured.

Yield was always underestimated by SPAc for all field sites and years (harvested grain C mass in gC as reported from the site, columns 8 + 9 in Table 2.3: 71% of observed, on average), whereas maximum LAI was continuously higher than the measurements in field (columns 10 + 11: 160% of observed, on average). The R^2 of observed vs. modelled yield for all site years was 0.05, with no significant correlation.

2.3.3 Sensitivity analysis

The model showed highest sensitivity to the parameters that determined the fraction of GPP allocated to autotrophic respiration (f_a) and the minimum photoperiod for development (PH_{cr}, Table 2.4). The nominal value of cumulative NEE at harvest was -550.62 gC m^{-2}. Considerable model sensitivity was evident for parameters describing the leaf mass per area (C_{la}), the maximum development rate in both the vegetative and reproductive phases ($r_{\mathrm{max,v/r}}$), the parameters relating temperature to development ($T_{\mathrm{min/opt/max}}$), and the photoperiod sensitivity coefficient (PH_{sc}). Most of these parameters were applied within the crop developmental module. Model sensitivity was particularly low to vernalization-related parameters and to those parameters used for estimating the rate of decomposition and mineralization processes.

Model sensitivity to the distribution of leaf nitrogen (N_{frac}) through the four canopy layers (not listed in Table 2.4) was tested by comparing the leaf N distribution based

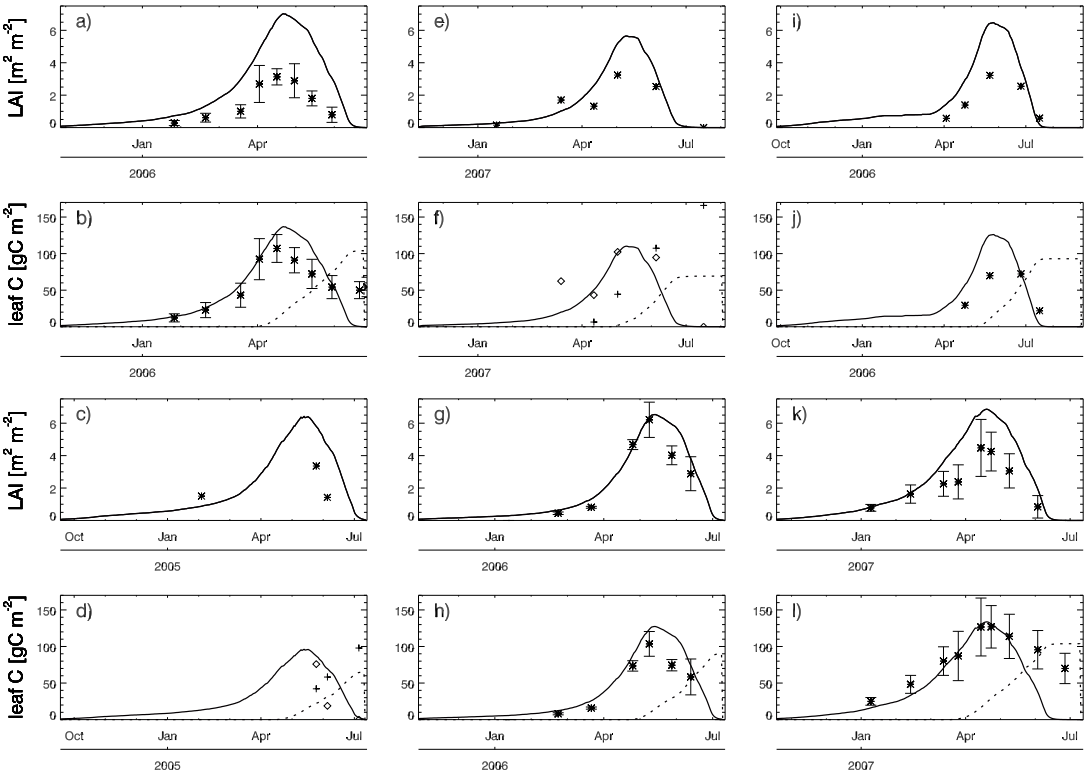

Figure 2.7: Rows 1 + 3: Modelled (solid line) and observed (∗) values of LAI. Rows 2 + 4: Modelled live (solid line) and standing dead (dashed line) leaf carbon mass values, together with observed time series of total (∗), live (⋄), and dead (+) leaf carbon mass. Error bars are ± 1 standard deviation, where available. a) + b) Auradé, c) + d) Gebesee(a), e) + f) Gebesee(b), g) + h) Grignon , i) + j) Klingenberg, k) + l) Lamasquère.

on Hirose and Werger (1987) with a uniform distribution, resulting in a new cumulative NEE of -523.17 gC m^{-2} (a relative change of 5%).

Table 2.4: Results of sensitivity analysis for each of the parameters in Table A.1 except for N_{frac} (in text). Nominal NEE value (NEE_{nom}) is -550.62. Columns 2+3 contain values of absolute change in NEE (i.e. $\Delta NEE = NEE - NEE_{nom}$), both for a 25% increase and decrease of the parameter concerned. Columns 4+5 contain values for sensitivity coefficient S. For the cardinal temperatures of development, each parameter was altered by ± 2 °C, and no S value could be calculated.

parameter	Δ NEE (%)		S	
	+25%	-25%	+25%	-25%
g_{plant}	-4.04 (-0.7)	6.63 (1.2)	0.03	0.05
Ψ_{l}	-44.71 (-8.1)	70.20 (12.7)	0.32	0.51
I	4.79 (0.9)	-4.34 (-0.8)	-0.03	-0.03
C	-5.57 (-1.0)	5.66 (1.0)	0.04	0.04
R_{r}	42.07 (7.6)	-44.46 (-8.1)	-0.31	-0.32
V_{cmax}	-10.95 (-2.0)	28.11 (5.1)	0.08	0.20
J_{max}	-94.04 (-17.1)	111.65 (20.3)	0.68	0.81
C_{la}	111.65 (20.3)	-158.92 (-28.9)	-0.81	-1.15
r_{dc}	-0.08 (0.0)	0.08 (0.0)	0.00	0.00

f_a	264.97 (48.1)	-261.33 (-47.5)	-1.92	-1.90
t_{root}	2.72 (0.5)	-2.76 (-0.5)	-0.02	-0.02
m_{lit}	2.02 (0.4)	-2.34 (-0.4)	-0.01	-0.02
m_{SOM}	25.02 (4.5)	-25.45 (-4.6)	-0.18	-0.18
t_{lab}	-20.30 (-3.7)	31.20 (5.7)	0.15	0.23
r_{tr}	17.76 (3.2)	-18.06 (-3.3)	-0.13	-0.13
t_{ar}	0.00 (0.0)	-0.01 (0.0)	0.00	0.00
GDD_{em}	0.00 (0.0)	0.00 (0.0)	0.00	0.00
trl_{stem}	2.03 (0.4)	-2.15 (-0.4)	-0.01	-0.02
$r_{\mathrm{max,v}}$	76.51 (13.9)	-103.85 (-18.9)	-0.56	-0.75
$r_{\mathrm{max,r}}$	33.59 (6.1)	-49.00 (-8.9)	-0.24	-0.36
T_{min}	-35.62 (-6.5)	28.39 (5.2)		
T_{opt}	-150.81 (-27.4)	152.11 (27.6)		
T_{max}	63.01 (11.4)	-75.91 (-13.8)		
$T_{\mathrm{min,vn}}$	-0.62 (-0.1)	0.22 (0.0)		
$T_{\mathrm{opt,vn}}$	0.24 (0.0)	-0.61 (-0.1)		
$T_{\mathrm{max,vn}}$	0.66 (0.1)	-0.74 (-0.1)		
VD_{h}	-1.84 (-0.3)	3.16 (0.6)	0.01	0.02
LAI_{cr}	-15.59 (-2.8)	26.99 (4.9)	0.11	0.20
dsh_{max}	6.59 (1.2)	-7.74 (-1.4)	-0.05	-0.06
PH_{cr}	-159.27 (-28.9)	101.14 (18.4)	1.16	0.73
PH_{sc}	40.60 (7.4)	-60.30 (-11.0)	-0.29	-0.44

2.4 Discussion

2.4.1 Modelled carbon exchange data

For all of the study years presented, SPAc was able to simulate the seasonality of C fluxes with high accuracy (mean $R^2 = 0.83$, daily NEE data between sowing and harvest of all growing periods). This seasonality greatly depends on the developmental model and C allocation and remobilization patterns associated with it (Table 2.4). Seeds germinated soon after sowing in autumn, so SPAc simulated (rather low) photosynthesis and gradual growth of LAI during autumn and winter. In the winter and early spring months, photosynthesis was limited by low temperatures and global irradiation levels, which SPAc was able to represent. However, throughout late spring and summer, the crop plants matured relatively quickly. As a consequence, only a short peak C assimilation phase was observed, followed by rapid senescence, which the modelling captured effectively (Figure 2.4).

We define winter cereal "dormancy" as a period of relatively low rates of photosynthetic activity during autumn and winter, rather than a period of non-photosynthetic-activity. Observed values of hourly NEE data show a daily pattern of C assimilation and release during the entire growth period, including autumn and winter months (data not shown). Accordingly, we did not add a temperature-dependant "dormancy" parameter in order to additionally limit photosynthesis in SPAc during winter.

As the ecosystem's assimilatory capacity is closely related to its developmental stage through shifting C allocation patterns, remobilization, and senescence, the modelling approach adopted within SPAc is able to represent typical winter wheat/barley C flux dynamics. Growing period Klingenberg was exceptional, as the observed onset of the peak growing phase occurred about 1.5 months later than modelled. Moreover, due to a rainy period from end of July to end of August 2006, this season's harvest date was 1–2 months later than those of the other sites. Currently, SPAc is not accounting for a delaying factor (probably in order to limit photosynthesis rather than development) that could improve model results for this single growing season.

SPAc was closest to observations during the winter and early spring months (the "dormancy" phase), whereas daily NEE was lower than observed (i.e. C assimilation overestimated) for most of the sites during the peak growth phase itself. Correspondingly, for all but one of the growing seasons, (Lamasquère (ww) was this exception) the modelled cumulative NEE at harvest was lower than observed, and all intercept values of lines fitted to observed vs. modelled scatter plots were negative (Table 2.3). The R^2 value of 0.27 of observed vs. modelled cumulative NEE (sowing to harvest) for all site years further indicates that SPAc needs to be improved in order to allow for an enhanced representation of cumulative NEE for different years and site locations. We expect major improvements by increasing the initial litter C content (thus increasing post-sowing heterotrophic respiration), as observed NEE was generally higher than modelled in the days following sowing. The seasonality of C exchange was mainly a function of the crop's maturity (developmental stage), but the magnitude of daily NEE was largely determined by the photosynthesis-related modules within SPAc. Correspondingly, adjusting related parameters, for instance those describing carboxylation rate (V_{cmax} and

J_{max}), will likely improve model performance. This overestimation of net C assimilation is further confirmed through the modelled hourly NEE data for Auradé (Figure 2.6), which in daytime was almost always more negative than observed. However, SPAc simulated the effects of high vapour pressure deficit (17.05.06) and low global irradiation levels (18.05.06) effectively.

SPAc predictions of NEE are only truly representative of the period between sowing and harvest, as no post-harvest regrowth of volunteers or land management actions have been considered. This largely explains differences between modelled and observed post-harvest NEE values (Figure 2.5). For example, manure application in October 2006 ($\sim$176 gC m^{-2}) could explain high observed values of NEE for Klingenberg, and the sowing of a cover crop (*Phacelia sp.*, *Avena sp.*, and *Trifolium alexandrinum*; 20.07.05) caused a later second C assimilation phase observed at Oensingen(a).

The reported fraction of crop biomass remaining on field after harvest was considered in all SPAc model runs to simulate realistic amounts of crop residue decomposition and mineralisation (i.e. heterotrophic respiration). During the growing period at Auradé, only the grains have been exported, and the remaining above ground biomass was left on the field after harvest. Due to this large litter flux, SPAc initially modelled a considerable contribution of decomposing crop residue to post-harvest respiration, further increasing NEE for this period (thin solid line in panel a) of Figure 2.4). However, NEE observations did not show any large amount of crop residue decomposition and mineralisation after harvest. The crop residue was incorporated into the soil at ploughing on the 30.09.06. As summer precipitation had been relatively low, the residues might have dried out on the surface, and consequently, decomposition might have not started before ploughing. Additionally, small voluntary regrowth occurred after harvest, which would have further influenced post-harvest NEE (E. Céschia, personal communication). Thus, model results were much closer to observations with a parameterisation where only 10% of the above ground biomass (except for grains) remained on the site after harvest. More data are needed in order to improve the limited understanding of how land management influences crop residue decomposition and mineralisation rates. In the crop growth model APSIM, decomposition rate is set

to decrease as the crop residue dries up, based on potential evaporation (Keating *et al.*, 2003). Data on direct observations of soil respiration fluxes would further help to constrain the estimation of heterotrophic respiration during and outside of crop growth periods, as proposed by Wang *et al.* (2005).

2.4.2 Modelled biometric data

Except for Grignon, SPAc generally overestimated LAI when compared to observations (R^2 of observed vs. modelled LAI_{max} was <0.01), but simulated values of leaf C compare considerably better to measurements (R^2 of observed vs. modelled maximum leaf C was 0.33, Figure 2.7). As not only LAI, but also (though to a smaller extent) live leaf C mass are often overestimated by SPAc, the fraction and/or duration of C allocation to leaves might be too high. Alternatively, increasing parameter C_{la} (C per leaf area) would make it more "C expensive" to grow leaves, thus reducing LAI. Due to high model sensitivity, a change in C_{la} would certainly make an impact on overall C assimilation capacity. However, very similar total leaf C mass values have been observed at Auradé and Grignon, but there are large differences in LAI. This difference could be explained by either alternative methods of measuring LAI (due to the contributions of green stems and ears, the LAI measured above the canopy can be quite different to the LAI measured through destructive green leaf sampling (Hoyaux *et al.*, 2008)) or different C per leaf area (C_{la}) values. Another potential error source in this model is the assumption of a constant C_{la} over the growing period (Kucharik and Twine, 2007).

In other studies, observed values of LAI_{max} for winter wheat were ∼3 (Lokupitiya *et al.*, 2009), 4–6 (Wang *et al.*, 2007), and ∼5 $\mathrm{m}^2\ \mathrm{m}^{-2}$ (Arora, 2003; Wang *et al.*, 2005). In Huang *et al.* (2009a), measured LAI_{max} correlated positively with synthetic fertilizer N application rates (0–200 $\mathrm{kgN\ ha}^{-1}$), and ranged from 1–6.5 $\mathrm{m}^2\ \mathrm{m}^{-2}$. Their data suggest that we might be predicting LAI for winter cereals under optimal growth conditions. Thus, a more detailed consideration of cultivar specific parameters affecting LAI, but also land management issues such as fertilization, pest/weed control, and irrigation would result in a more realistic prediction of LAI for various sites and years.

Another improvement to SPAc would be to account for the contribution of green stems and ears to overall photosynthesis. In SUCROS, a mechanistic crop growth model on which the modelling approach adopted in SPAc is greatly based upon, ear photosynthesis is accounted for by assuming half of the ear area index (EAI, in $m^2\ m^{-2}$) to contribute to overall light absorption. Moreover, the significance of not only green ear, but also stem photosynthesis, has been demonstrated in Hoyaux *et al.* (2008). Their study, a model-data comparison of C flux data for winter wheat in Lonzée, Belgium, showed that highest model uncertainty resulted from varying C assimilation rates of stems and ears. When only considering green leaf photosynthesis, cumulative GPP was underestimated by 23%. If stem and ear photosynthesis were considered in SPAc, leaf C mass, and as a consequence LAI, could be reduced without considerably reducing the crop plant's assimilatory capacity.

For Klingenberg, we modelled an earlier onset of peak LAI and leaf C mass growth than observed. As this lag can also be seen in the daily flux data, SPAc seems to have overestimated photosynthesis in the early spring months, leading to an increase in LAI and leaf C mass not supported by measurements made on site. SPAc has also slightly overestimated GPP during the winter months, resulting in a (rather gradual) build-up of foliar biomass during this period. By the onset of the peak growth phase in spring, this winter growth could have resulted in too high initial values of LAI and leaf C mass, allowing for higher than observed photosynthetic rates. In this context, measurements of LAI or leaf dry matter (DM) made during the "dormancy" phase would help to further explain and constrain model behaviour.

Compared to SPAc runs with one single foliar C pool, the addition of a standing dead foliage C pool led to an improved prediction of at-harvest total foliar C mass, which was measured to be considerably >0 for most of the sites (Figure 2.7). At maturity, the observable leaf C of winter cereals was predominately standing dead leaf C mass, which remained after leaf mass loss through senescence and remobilization. Without a modelled standing dead foliage C pool, leaf C mass at maturity would be largely underestimated by SPAc. Final dead leaf C mass is higher than observed values of

total leaf C at harvest for all sites, but were considerably lower than measured dead leaf C at Gebesee(a)+(b).

Leaf senescence is triggered in SPAc at an LAI of $\geq$4, thus the dead foliage C pool began to receive C whilst the alive foliar C mass was still growing. This is realistic, as self-shading can induce senescence of lower leaves while the foliar biomass in upper levels might still be increasing. An alternative way of modelling leaf senescence would be to connect LAI to leaf N content: leaves will begin to senesce when the leaf N concentration drops below a value required for photosynthesis (Kucharik and Twine, 2007).

Based on the observed data available, it is difficult to conclude whether we are actually under- or overestimating dead leaf C mass at maturity. Whichever is true, the model could be improved by changing the conditions of triggering leaf senescence or by altering the fraction of senescing leaf biomass allocated to the dead foliage C pool (currently 0.5, the other half being treated as remobilized C, which will finally be allocated to the storage organ).

In another study, leaf senescence was found to be poorly represented, resulting in a considerable mismatch between observed and simulated LAI (Kucharik and Twine, 2007). Improving the representation of crop senescence in agroecosystem modelling is of further importance: standing dead C mass during the reproductive phase, but more importantly the post-harvest crop residue layer, together have the potential to improve the surface energy balance when considered in simulations, as they affect surface albedo and other physical properties (Kucharik and Twine, 2007). Moreover, an advanced representation of crop senescence and its effect on vegetation greenness will increase the usability of remote sensing data (e.g. MODIS 250 m NDVI) for data assimilation and validation. We see in the modelling approach followed here a step forward in representing leaf senescence and estimating standing dead leaf C mass for these purposes.

We might expect that with a stronger simulated C sink than measured, the simulated

grain yield would be an overestimate. However, model simulations actually underestimated grain yield in all cases by a mean value of ∼100.4 gC m^{-2} (72% of observed), and the R^2 value for all site years was 0.05. The biometry and flux residuals seem to suggest that less C is allocated to foliage. If this were so, then leaf C stocks would be reduced, and C sink strength would be decreased as a result of resultant reductions in GPP. However, of the smaller amount of C assimilated, a larger fraction and larger absolute amount must be allocated to grain filling. Data on root allocation and turnover would be valuable to better constrain below ground allocation and resolve these discrepancies. Moreover, the already discussed consideration of green ear and stem photosynthesis would allow for lower leaf C allocation without considerably reducing total C assimilation.

There are different approaches in the crop growth modelling community in predicting yield. For example, growth of the storage organs is source-limited in the EPIC model, whereas it is both source and sink-limited in CERES (Mearns *et al.*, 1999). However, the questions remain whether grain number is the controller of yield formation (sink limited) or rather a reflection of yield formation (source limited, Jamieson *et al.* (1998): the Sirius crop growth model successfully predicted yield without an explicit dependence on grain population. In SPAc, yield growth is both source and sink-limited.

Improving the simulation of cumulative NEE, LAI, and yield will be the focus of future research with SPAc, as these entities are currently represented with relatively low accuracy by the model.

2.4.3 Which are the parameters with highest model sensitivity?

We found high model sensitivity to a range of different parameters, which can be distinguished into two main groups: photosynthesis-related and development-related parameters. In the first group, parameter f_a (the fraction of GPP respired) is a major control on model sensitivity, as it largely determines the amount of C available for growth. Indeed, it is known that f_a not only varies over a relatively broad range

for crops (0.3–0.6 for maize, rice, and wheat), but also that it changes with crop development, rather than being constant throughout the plant's life span (Amthor, 2000). Crop f_a is lower than for natural vegetation, as the crop breeders' selection of genotypes with large harvest indexes may indirectly have led to the selection of reduced autotrophic respiration (Amthor, 2000). We conclude that both model sensitivity and parameter uncertainty are high for f_a. Our simulations of autotrophic respiration fluxes might be improved if we more explicitly simulated growth and maintenance respiration as separate processes, an approach with a long tradition in models of higher-plant respiration (Amthor, 2000). However, this change would come at the cost of increasing model complexity set against a lack of detailed data constraints. Moreover, formulations of growth and maintenance respiration are purely notional functional constructs, and they are not biochemically distinct from each other. Their coefficients are not fundamental but are defined only operationally by a particular measurement protocol and assumptions associated with it (Gifford, 2003). Thus, the philosophy of modelling autotrophic respiration in SPAc was chosen to be more simplistic.

The amount of leaf C per area (C_{la}) is another important parameter with a high influence on crop canopy development, and correspondingly high model sensitivity. Maximum electron transport rate (J_{max}) is directly used within SPAc's photosynthesis module and thus a crucial factor in estimating the amount of C available for growth. Additional studies would help in determining to which extent these parameters are cultivar dependent and thus might explain site-to-site and year-to-year differences in the magnitude of overall C assimilation through one crop type. Comparably low model sensitivity was evident for parameters used for modelling plant hydraulics, reflecting a lack of water stress impacts on C dynamics and plant development. SPAc was also relatively insensitive to changing decomposition and mineralisation rates, although the importance of residue management was clearly demonstrated. As the model's insensitivity to parameter GDD_{em} suggests, it seems to be unlikely that SPAc is considerably sensitive to potential shortcomings in the model structure itself. These shortcomings are still present as a lack of detail in simulating seed germination and growth of roots and shoots until emergence.

We also found high model sensitivity to a range of development-related parameters. In particular those coefficients estimating the influence of daylength (photoperiod) on developmental rate play an important role in establishing developmental stage and thus shifting C allocation patterns, senescence and C remobilization. Even though some modern crop varieties are known to have little or no sensitivity to daylength (to facilitate management over various cropping systems and larger regions), this sensitivity is still a desirable trait to keep harvest dates constant in areas of largely varying sowing dates (Penning de Vries *et al.*, 1989). Photoperiod sensitivity is still the norm and a very powerful adaptive mechanism (Craufurd and Wheeler, 2009). Together with maximum developmental rates in both the vegetative and reproductive phases, photoperiod-related parameters exhibit notable model sensitivity in SPAc and thus need to be well constrained. We found considerable model sensitivity for non-vernalisation related cardinal temperatures of development, highlighting that a well defined set of parameters is of paramount importance. An improvement could be to use different cardinal temperatures for various sub-phases, e.g. as shown in Porter and Semenov (2005) and Streck *et al.* (2003). Temperature is crucial in determining the duration of important phases such as leaf growth (C assimilation/vegetative phase) and grain filling (senescence/reproductive phase). There already exists a set of studies that provide estimates of these cardinal temperatures (Li *et al.*, 2008; Porter and Semenov, 2005; Streck *et al.*, 2003; Wang and Engel, 1998; Xue *et al.*, 2004), however these still vary considerably in relation to the number of sub-phases and cardinal temperature values themselves. Especially in the context of regional studies, which require generic estimates of these parameters for one single crop type, it is important to have a better estimate of the full range of parameter space. In SPAc, a 2 °C cardinal temperature change results in a considerable change in NEE (Table 2.4). More research is needed in order to determine whether the application of various different sets of cardinal temperatures (one for each individual sub-phase as in Porter and Semenov (2005) and Streck *et al.* (2003)) is superior over one/two single parameter sets which are constant from emergence to maturity. An increased number of cardinal temperature sets would result in increased model accuracy but also complexity. The temporal and spatial scale at which a certain model is applied will largely determine what is more important: accuracy or simplicity.

2.4.4 Is the modelling of developmental stages reliable?

The simulation of crop developmental stages is a novel part of SPAc and a key element in controlling fundamental model processes such as C partitioning, senescence, and remobilization. In another study, grain yield prediction was found to be much more dependent on the simulation of crop development and LAI than of the various components of yield, such as number of ears or grains (Jamieson *et al.*, 1998). Unfortunately, no on-field observations of developmental or phenological stages have been made during the study periods presented here. We are currently developing and testing a methodology that would enable us to observe the timing of key crop developmental stages and land management operations from space, based on MODIS 250 m NDVI data time series. These timings will probably be sowing date (summer crops), break of winter "dormancy" (i.e. the onset of the peak growth phase of winter cereals), and maximum LAI/flowering date. This new source of data would enable us to compare our estimates of crop development solely based on local meteorology with an independent means of data, and also provide input data for future regional modelling. The potential usefulness of MODIS data and their applicability for crop phenology detection have been highlighted in several studies (Huang *et al.*, 2009a; Kucharik and Twine, 2007; Sakamoto *et al.*, 2005).

Overall, our results suggest that SPAc captures the typical seasonality of winter wheat/barley NEE reasonably well (Figure 2.4), leading to the conclusion that the developmental model predicts the key timings of vegetation growth in a realistic manner. Growth during the winter period is restricted mainly through low temperatures and global irradiation, and thus photosynthesis. In all our model runs we see a small initial growth of leaves and roots soon after the sowing date, having accounted for a delay due to germination. At many sites, an initial high efflux of C has been observed around sowing, which then drops sharply. This C emission can possibly be explained by crop residue decomposition and/or ploughing shortly before sowing, which we are not considering in our model runs. The rapid decline of NEE can be seen as a result of initial growth of the winter crop sown.

In general, C assimilation during the vegetative phase appears to be controlled by photosynthesis as a function of local meteorology, whereas crop development causes the rapid increase of NEE in the reproductive phase. Crop development controls this shift from increasing to decreasing C assimilation through (1) a shift in C partitioning (from leaves and roots to stems and grains), and (2) the onset and acceleration of senescence as the crop matures. As all model runs reproduce the timing of these various stages with high accuracy (Figure 2.4), we are confident that SPAc realistically models crop developmental stages.

Even though we are not accounting for any land management operations other than sowing and harvest, such as ploughing, fertilization, and application of herbicides, modelled NEE are still considerably close to observations. It is possible that some pests are responsible for the reduced productivity observed.

2.4.5 Is a generic winter wheat/barley parameterisation acceptable?

SPAc effectively modelled the seasonality of NEE for winter wheat/barley over a range of western-central European climatic conditions and crop cultivars. Moreover, model inconsistencies were largely consistent across the different sites (a general overestimation of the C sink, Table 2.3), suggesting that small changes to the model parameterisation would improve results for all sites. It is debatable whether a few parameters should be isolated from this set in order to be allowed to vary with latitude/longitude or local climatic conditions. More research is needed for establishing the variability of cardinal temperatures, and especially photoperiod coefficients, for various spatial scales and climates.

A more cultivar-specific parameterisation would certainly improve model results. However, it is desirable to keep model complexity low for larger scale studies, so a trade-off between model accuracy and model precision is unavoidable. This study demonstrated that a generic cereal parameterisation allowed for rather accurate than precise predictions of cropland C fluxes over 6 different locations in Western-Central Europe. We

are convinced that an improved *generic* parameterisation, together with changes in model structure regarding green stem/ear photosynthesis, would result in considerably more precise simulations of both cereal C fluxes and stocks for Western-Central Europe. Overall, there was no evidence suggesting different parameters were required for wheat and barley.

2.4.6 Need for further measurements

The crop modelling approach followed here is largely based on, and compared with, a time series of biometric measurements. In this context, more data are required for model calibration and validation, especially regarding below ground partitioning coefficients and rates and determinants of senescence. Ideally, these empirical studies would be accompanied by observing the timing of key crop developmental stages. Also, as crop residue decomposition/mineralisation rates were found to be sensitive to land management, more C flux observations for varying amounts of crop residue biomass and land management operations would help to improve the representation of model processes in the post-harvest phase. Further parameters with high model sensitivity, but also high uncertainty (and thus requiring further research), are the fraction of GPP respired (f_a), the amount of leaf C per area (C_{la}), Farquhar parameters, developmental coefficients, and C allocation patterns.

2.5 Conclusions

We have demonstrated the coupling of a crop developmental model with a model of ecosystem C balance. The coupled model is capable of effectively describing the timing and magnitude of C exchanges for cereal crops in western-central Europe, compared against flux and biometric data. We found relatively high model accuracy for predicting daily C NEE fluxes over six different cropland sites and eight study periods (mean $R^2 = 0.83$, mean $RMSE = 1.47$ gC $\mathrm{m}^{-2}\mathrm{d}^{-1}$). However, SPAc simulated cumulative NEE (sowing–harvest) with lower accuracy (mean $R^2 = 0.27$). We conclude that

the high quality of modelled daily NEE data is a result of realistically modelling cereal crop development, senescence, and remobilization. The simulation of crop development is a key new part of the model, making a crucial contribution in more realistically simulating C assimilation during the reproductive phase through shifts in C partitioning coefficients and the onset and acceleration of senescence. The general overestimation of photosynthesis is possibly a result of model weaknesses in terms of model parameterisation and structure, leading to a larger C sink size than observed (mean cumulative NEE difference (observed - modelled) ∼-133.9 gC m^{-2}). However, further data on fine root or below ground C allocation patterns is required in order to explain the overestimated sink strength whilst underestimating yield. As model error was found to be largely consistent over the various study sites, we conclude that an improved single parameterisation will be able to produce realistic predictions of winter cereal C balance for western-central Europe.

Moreover, observed daily NEE data suggested active photosynthesis during the entire crop growth period, including the so-called winter "dormancy" months. SPAc was able to match these observations solely based on local meteorology and without further restrictions on photosynthesis, such as a threshold temperature value defining the duration of this "dormancy" period. This suggests that the concept of "dormancy", as it is known from natural ecosystems, is not directly applicable to winter cereal crops.

The model was also able to generally simulate realistic patterns of post-harvest decomposition and mineralisation fluxes as a function of crop residue C mass. However, these fluxes were clearly overestimated when no crop residue was exported from the field. We expect improved simulation of decomposition and mineralisation rates when accounting for the effects of crop residue moisture on these rates.

LAI was overestimated by 60% on average, indicating that we predict LAI for optimal non-stressed conditions, but yield was underestimated (∼71% of observed). We require a parameter calibration or model structure that will (1) decrease LAI, (2) slightly reduce live leaf C mass, and (3) increase yield whilst (4) decreasing the overall C assimilation strength. These changes could result from alterations to the parameter for C per leaf

area and the dynamics of root allocation. Additionally, a significant improvement could be made to the model structure by accounting for the contributions of green ears and stems on overall photosynthesis, allowing for lowering LAI and live leaf C without lowering C assimilation more than necessary.

Another crop C budget model novelty was the inclusion of a dead leaf C pool, which allowed for a more realistic prediction of at-harvest above-ground C stocks. Moreover, we expect an improved simulation of the surface energy balance (mainly through albedo effects), and of optical properties of the crop canopy, which is important for future studies based on remote sensing data (e.g. MODIS 250 m NDVI time series).

Further studies should focus on improving the development parameterisations for photoperiod and temperature, and ascertaining the allocation of photosynthate to autotrophic respiration. Additionally, more estimates of C per leaf area values but also C allocation patterns to both above and below ground organs of cereal crops are required.

Chapter 3

The carbon balance of European croplands: A cross-site comparison of simulation models

This chapter was written and published in collaboration with Wattenbach *et al.* (2010). M. Wattenbach provided paper outline, text, Figures, and Tables. I contributed with SPAc model outputs (as in chapter 2) and text editing. I wrote section 3.2.2, and made further changes in Figure selection and Tables compared to the published version. Due to space restrictions, Appendix Figures in the published paper are not included here.

Abstract

Croplands cover approximately 45% of Europe and play an important role in the overall carbon (C) budget of the continent. However, the estimation of their C balance remains uncertain due to the diversity of crops and cropping systems together with the strong influence of human management. Here, we present a multi-site model comparison for four cropland ecosystem models, namely the DNDC, ORCHIDEE-STICS, CERES-EGC

and SPA models. We compare the accuracy of the models in predicting net ecosystem exchange (NEE), gross primary production (GPP), ecosystem respiration (R_e) as well as actual evapo-transpiration (ETa) for winter wheat (*Triticum aestivum L.*), winter barley (*Hordeum vulgare L.*) and maize (*Zea mays L.*) derived from eddy covariance measurements on five sites along a gradient of climatic conditions from eastern to south-westerly Europe. The models are all able to simulate daily GPP. The simulation results for daily ETa and R_e are, however, less accurate. The resulting simulation of daily NEE is adequate except in some cases where models fail due to a lack in phase and amplitude alignment. ORCHIDEE-STICS and SPA show the best performance. Nevertheless, they are not able to simulate full crop rotations or the multiple management practices used. CERES-EGC, and especially DNDC, although exhibiting a lower level of model accuracy, are able to simulate such conditions, resulting in more accurate simulation of annual cumulative NEE. [1]

3.1 Introduction

Croplands are an important component of the European carbon (C) balance (Janssens *et al.*, 2003, 2005; Schulze *et al.*, 2009; Kutsch *et al.*, 2010). They cover a large area between 1.10 (EPA-Corine2000) and 1.24 Mkm^{-2} (Gervois *et al.*, 2008), within the EU27 plus Switzerland, and there have been a number of integrated studies that attempted to quantify, at the continental scale, their C balance. Each previous study has used different approaches, from extrapolation of regional statistics, through remote sensing to modelling (Vleeshouwers and Verhagen, 2002; Janssens *et al.*, 2003; Smith, 2004; Smith *et al.*, 2005a; Bondeau *et al.*, 2007; Gervois *et al.*, 2008; Ciais *et al.*, 2010). However, CO_2 emissions are largely determined by the temporal and spatial sequence of human activity and there remains a considerable degree of uncertainty (Smith *et al.*, 2005a; Osborne *et al.*, 2010). Regional- or continental-scale statistics are not consistently available for the entire area of Europe (Ramankutty *et al.*, 2008) and

[1] Published as: Wattenbach, M., Sus, O., Vuichard, N., Lehuger, S., Williams, M. et al. (2010). The carbon balance of European croplands: A cross-site comparison of simulation models. *Agriculture, Ecosystems & Environment*, **139**, 419 – 453.

available experimental data are scarce, and come from heterogeneous sources. Remote sensing products lack the accuracy and precision to reflect the degree of temporal and/or spatial heterogeneity of croplands (Reeves *et al.*, 2005; Osborne *et al.*, 2010). In the case of modelling, the records now available through the CarboEurope network are the first comprehensive high resolution flux data suitable for use in parameterising process based agroecosystem models across Europe (Smith *et al.*, 2010).

Croplands may play an important role in climate change mitigation (Denman *et al.*, 2007; Smith *et al.*, 2008). It is therefore imperative to establish a better understanding of processes in order to reproduce the current pattern of cropland C dynamics. In the framework of the CarboEurope integrated project, detailed information about soil, vegetation and C and water fluxes from eddy covariance systems, in connection with comprehensive crop management data covering entire crop rotations, are available. The network of sites covers all main regions of EU25 and Switzerland, reflecting regionally specific crops and management (Céschia *et al.*, 2010; Eugster *et al.*, 2010; Kutsch *et al.*, 2010). Here, we present a multi-site model comparison for four ecosystem models, namely the DeNitrification DeComposition model (DNDC, Li *et al.* (1992, 1994, 2005)), the coupled vegetation-crop model "Organising carbon and Hydrology In Dynamic EcosystEms – Simulateur mulTIdisciplinaire pour les Cultures Standard" (ORCHIDEE-STICS, de Noblet-Ducoudré *et al.* (2004); Gervois *et al.* (2008)), the "Crop Environment REsource Synthesis Environnement et Grandes Cultures" (CERES-EGC, Gabrielle *et al.* (2006); Lehuger *et al.* (2009, 2010)) model and the Soil Plant Atmosphere model (SPAc, Williams *et al.* (1996); Sus *et al.* (2010)). These models represent a cross-cut of widely applied model species that are currently used to analyse the C dynamics of croplands. These include site-scale semi-empirical models, biogeochemical regional-scale process models, soil-vegetation-atmosphere transfer models (SVATs), and coupled global vegetation models (Li *et al.*, 1997; Smith *et al.*, 1997; Williams and Rastetter, 1999; Law *et al.*, 2000; Brown *et al.*, 2002; Zhang *et al.*, 2006; Lehuger *et al.*, 2007, 2009; Gervois *et al.*, 2008; Vuichard *et al.*, 2008). We compare the models in terms of their performance in simulating the cycling of C and water between vegetation and the atmosphere on a daily time scale. This study does not include other

greenhouse gases, due to the lack of high resolution measurements at the sites, and the limitation of ORCHIDEE-STICS and SPAc to simulation only the C cycle.

The key elements of the C cycle are the fixation of atmospheric C dioxide (CO_2) by photosynthesis and its release by autotrophic and heterotrophic respiration. The net flux as the sum of these three components is the net ecosystem exchange (NEE) which can be measured by eddy covariance systems (Baldocchi *et al.*, 1996; Black *et al.*, 1996; Moncrieff *et al.*, 1997; Baldocchi, 2003; Reichstein *et al.*, 2005; Aubinet *et al.*, 2009; Smith *et al.*, 2010). NEE is the net uptake or release of C by terrestrial ecosystems influenced by climatic and by non-climatic factors like the plant water supply, leaf area index and soil C dynamics, which are again influenced by crop type and associated management.

The terrestrial water cycle includes the precipitation that reaches the vegetation surface from the atmosphere, which is subsequently partitioned into rain intercepted by the canopy, surface and sub-surface run-off, and water infiltrating the soil profile. The water which enters the soil profile either evaporates, is taken up by plant roots and subsequently transpired, or percolates out of the rooting zone. The sum of the first two, evaporation and transpiration, is the process of evapotranspiration (Bosch and Hewlett, 1982; Zhang *et al.*, 2001; Farley *et al.*, 2005; Falloon and Betts, 2010). The two processes of water release and C uptake are closely interlinked by plant stomatal conductance of water and CO_2 (Beer *et al.*, 2007).

Besides being a key factor in the exchange of C and water between the plant and atmosphere, the soil water status also influences the microbial decay of C which is strongly constrained by soil moisture conditions, as either too much or too little water reduce microbial activity (Pastor and Post, 1986; Davidson *et al.*, 2006).

A number of previous studies have evaluated SVAT models for simulating C fluxes from croplands (Wang *et al.*, 2005, 2007; Adiku *et al.*, 2006; Huang *et al.*, 2009a). Elsewhere in this issue, three papers present detailed evaluations of the SPAc (Sus *et al.*, 2010), CERES-EGC (Lehuger *et al.*, 2010) and the DNDC (Dietiker *et al.*, 2010)

models. However, the combined evaluation of water and C fluxes is relatively rare in the literature (Adiku *et al.*, 2006). Three previous studies have had comparable aims (Kramer *et al.*, 2002; Morales *et al.*, 2005; Grant *et al.*, 2007). The study by Grant *et al.* (2007) evaluates only one model against cropland eddy covariance data for latent heat and net biome productivity (NBP) measured over an irrigated and rain fed Maize-Soybean rotation in the US. Kramer *et al.* (2002) and Morales *et al.* (2005), on the other hand, compare a number of biogeochemical and coupled global vegetation models including ORCHIDEE against global FLUXNET data, but in that case, for global forest biomes and not cropland ecosystems.

Here we focus on the accurate representation of the main components of the cropland C cycle: net ecosystem exchange, ecosystem respiration (R_e) and gross primary production (GPP) in connection with actual evapotranspiration (ETa). This model evaluation is conducted on a daily time scale, and over a gradient of environmental conditions in Europe ranging from the eastern part of Germany (mean annual temperature (T) = 7.3 °C; precipitation (P) = 850 mm) over a central mountainous alpine region in Switzerland (T = 9.0 °C; P = 1100 mm), to the central and southern part of France (T = 12.9 °C; P = 700 mm). This multi-criterion, multi-model, multi-site evaluation provides insights into the applicability of the models to simulate the C balance of cropland ecosystems within Europe.

3.2 Materials and methods

3.2.1 The cropland sites

The four models were run at four sites (Oensingen, Grignon, Auradé, Klingenberg) for one year of winter wheat (*Triticum aestivum*) at each site, one year for winter barley (*Hordeum vulgare*) at Gebesee, and one year for maize (*Zea mays*) at Grignon. However, the extent of our comparison is limited by model differences in the number of crop types simulated and the type of output data produced. For example, SPAc has no maize, and

ORCHIDEE-STICS no winter barley implementation yet, and CERES-EGC produces no estimate of R_e. The combinations of sites, models, crops and years are given in Table 3.1. Model results were compared accordingly. A more detailed description of the sites is given in other papers in this special issue (Kutsch *et al.*, 2010; Céschia *et al.*, 2010).

3.2.2 Models

The DNDC model

The DNDC model (in this study version 9.2), is a general model of C and N biogeochemistry in agricultural ecosystems (Li *et al.*, 1992, 1994, 2005). It is a process-oriented simulation model, which contains four interacting sub-models for soil climate, de-nitrification, decomposition and plant growth. The model has been tested against numerous field data sets of nitrous oxide (N_2O) emissions (Frolking *et al.*, 1998; Tonitto *et al.*, 2007a; Abdalla *et al.*, 2009; David *et al.*, 2009) and soil C dynamics (Li *et al.*, 1997; Smith *et al.*, 1997; Brown *et al.*, 2002; Zhang *et al.*, 2006).

Plant Growth. DNDC simulates plant growth using an empirical approach calculating photosynthesis, respiration, water and N demand, C allocation, crop yield, and litter production on a daily time step for about sixty different crops. Photosynthesis is calculated using the radiation use efficiency approach (Aber and Federer, 1992), with interception of light depending on leaf areas index based on Beer's law (Falge *et al.*, 2005). Phenology is simulated using accumulative thermal degree days approach. A user defined amount of litter either from roots or aboveground residue after harvest is assumed to enter the C cycle of the model (Qiu *et al.*, 2009).

Soil organic C dynamics. Soil organic C (SOC) dynamics are simulated by assuming four main pools: plant residue, microbial biomes, active humus, and passive humus. Each of the main pools is subdivided into one or more sub-pools with different

properties. The daily decomposition rate is calculated depending on the relative size of each sub-pool and is regulated by each pool size, its decomposition rate, the soil clay content, N availability, soil temperature and moisture, and its depth in the soil profile. In the process of the decomposition simulation, C is transferred to the soil pool with the next lower decomposition rate, partially assimilated into microbial biomes, and partially converted into CO_2 (Qiu *et al.*, 2009).

Latent heat flux. Potential evapotranspiration (ET) in DNDC is calculated using a daily average value from the Thornthwaite formula (Thornthwaite and Hare, 1965). Subsequently, potential ET is separated into potential evaporation and transpiration. To calculate the potential transpiration, the water demand of plants is calculated based on the daily biomass increment using the water/biomass ratio of the crops. The actual plant transpiration is then calculated by taking the actual soil water content of the soil profile into account (Li *et al.*, 2006).

The ORCHIDEE-STICS model

ORCHIDEE-STICS is a coupled model (de Noblet-Ducoudré *et al.*, 2004; Gervois *et al.*, 2008) consisting of a dynamic global vegetation model ORCHIDEE (Krinner *et al.*, 2005), and a process-oriented crop model STICS (Brisson *et al.*, 1998, 2002, 2003).

The ORCHIDEE model calculates, for diverse vegetation types (plant functional types), surface CO_2, water vapour and heat fluxes driven by varying weather, and the soil water and C pool dynamics. It contains a biophysical module, dealing with photosynthesis and energy balance calculations each 30 min, and a C dynamics module, dealing with phenology, growth, allocation, mortality and SOM decomposition, on a daily time step. For better representing cultivated plants, their phenology and management-related growth is calculated by the STICS model which is coupled to ORCHIDEE, providing daily foliar index, root density profiles, nitrogen stress, vegetation height, and irrigation requirements. These variables are then sequentially assimilated into ORCHIDEE each day to further calculate accurately gross primary production.

Table 3.1: The combination of sites, models and crops and the lengths of the simulation period for the comparison in days of the year (DOY).

Site	Crop	Time period			Model			
		Start	End	DOY	CERES	SPAc	ORCHIDEE	DNDC
Oensingen	Winter wheat	19/10/2006	16/07/2007	270		x	x	x
Grignon	Maize	09/05/2005	28/09/2005	142	x		x	x
	Winter wheat	28/10/2005	14/07/2006	259	x	x	x	x
Auradé	Winter wheat	27/10/2005	29/06/2006	245	x	x	x	x
Klingenberg	Winter wheat	25/09/2005	06/09/2006	346	x	x	x	x
Gebesee	Winter barley	17/09/2004	16/07/2005	302	x	x	x	x

Currently, the ORCHIDEE-STICS model has been used for simulating wheat, soybean and maize although STICS has sufficiently generic parameterisations to allow simulation of other crop species. The processes of the STICS sub model are:

Plant growth. Crop growth is driven by the plant C accumulation and solar radiation intercepted by the foliage. According to the plant type, crop development is driven either by a thermal index (degree-days), a photothermal index, or a photothermal index taking into account vernalisation. The vernalisation factor is the ratio between the sum of vernalising days since planting and plant vernalisation requirements. Water stress and nitrogen stress, if any, reduce leaf growth and biomass accumulation, based on stress indices that are calculated in water and nitrogen balance modules (Brisson *et al.*, 1998, 2002, 2003).

Soil organic C dynamics. Soil organic matter (SOM) decomposition is modelled based on the work of Parton and Rasmussen (1994). SOM decomposition results in C fluxes within three C pools (active, slow, and passive). These fluxes are a function of time constants under reference temperature and moisture values and vary with temperature and moisture inhibition functions that are used to parameterise the decrease of soil metabolic activity under cold, dry, or anaerobic conditions. The fractions of these fluxes that are attributed to the other C pools and as CO_2 flux to the atmosphere, are also prescribed.

Latent heat flux. The latent heat flux calculation accounts for soil evaporation, foliage water (i.e. intercepted precipitation and dew), evaporation, canopy transpiration and snow sublimation. Each of these fluxes is driven by the gradient of specific humidity between the evaporating surface and the overlaying air and limited by a set of resistances (Krinner *et al.*, 2005).

The SPAc model

The Soil Plant Atmosphere model (Williams *et al.*, 1996) is a process-based model that simulates ecosystem photosynthesis and water balance at fine temporal and spatial scales (up to 30 min time step, ten canopy and twenty soil layers). The scale of parameterisation (leaf-level) and prediction (canopy-level) have been designed to allow the model to diagnose eddy-flux data and to provide a tool for scaling up leaf level processes to canopy and landscape scales (Williams *et al.*, 2000).

Plant growth. The SPAc model employs the Farquhar approach of leaf-level photosynthesis (Farquhar and von Caemmerer, 1982) to calculate the amount of carbohydrates synthesised at each time step. The carbohydrates are then allocated to one root and four above-ground C pools (labile, foliage, stem and storage organ C pools, Penning de Vries *et al.* (1989)), and the model further accounts for autotrophic and heterotrophic respiratory processes. The C allocation pattern itself is dependent on the developmental stage (DS) of the crop plant. DS is calculated as the sum of daily developmental rates, which are a function of temperature, photoperiod, and vernalisation (Sus *et al.*, 2010). Senescence is calculated as a function of either mutual shading effects of canopies with an LAI >4, or developmental rate in the reproductive phase, whichever is dominant. Senescent C is either remobilised and subsequently reallocated to the growing storage organ, or added to a standing dead leaf biomass C pool.

Soil organic C dynamics. At harvest, the fraction of the aboveground biomass exported from the field is estimated by the storage organ C content plus non-crop residue leaf and stem C mass. The residual crop biomass gradually enters the litter C pool. The fraction of crop residue entering either the litter or soil C pool further depends on land management and can be adjusted accordingly. Following this approach, SPAc models the C mass balance for winter/spring barley and wheat (Sus *et al.*, 2010).

Latent heat flux. SPAc uses the Penman-Monteith equation to determine leaf-level transpiration (Penman, 1948; Monteith, 1965; Monteith and Moss, 1977). It is linked to the photosynthesis module by a novel model of stomatal conductance that optimizes daily C gain per unit leaf nitrogen, within the limitations of canopy water storage and soil to canopy water transport.

The CERES-EGC model

The original CERES model is a soil-crop model (Jones and Kiniry, 1986). It was extended to CERES-EGC (Gabrielle *et al.*, 2006; Lehuger *et al.*, 2009) by moving the focus towards the simulation of nitrogen-cycle-related processes such as nitrate leaching, emissions of N_2O and nitrogen oxides. CERES-EGC runs on a daily time step, and requires daily rain, mean air temperature and Penman potential evapotranspiration (Penman, 1948) as forcing variables to calculate actual evapotranspiration.

CERES-EGC simulates water, C and nitrogen in the soil-crop system in a number of sub modules. A physical sub-model simulates heat, water and nitrate movement in the soil. It is also responsible for the calculation of soil evaporation, plant water uptake and transpiration. A biological sub-model simulates the growth and phenology of the crops.

Plant growth. The model calculates net photosynthesis as a linear function of intercepted radiation according to the Monteith approach (Monteith and Moss, 1977), with light interception depending on leaf area index based on Beer's law. The key species specific parameter in this calculation is the radiation use efficiency (RUE) defined as the dry biomass produced per unit of radiation intercepted. Photosynthates are partitioned on a daily basis to currently growing organs (roots, leaves, stems, fruits) according to crop development stage. The latter is driven by the accumulation of growing degree days, as well as cold temperature and daylength for crops sensitive to vernalisation and photoperiod. Lastly, crop N uptake is computed through a supply/demand scheme,

with soil supply depending on soil nitrate and ammonium concentrations and root length density.

Soil organs C dynamics. A micro-biological sub-model simulates the turnover of organic matter in the plough layer. Decomposition, mineralisation and N-immobilisation are modelled with three pools of organic matter (OM): the labile OM, the microbial biomass and the humads. Kinetic rate constants define the C and N flows between the different pools. Direct field emissions of CO_2, N_2O, NO and NH_3 into the atmosphere are simulated with different trace gas modules (Lehuger *et al.*, 2010).

Latent heat flux. The Penman potential evapotranspiration (Penman, 1948) is used as forcing variables to calculate actual evapotranspiration based on the water status of the soil and crop, respectively.

Simulation set-up

Input data. Models are driven by meteorological variables derived from half hourly measurements at each site. Simulation time steps differ among models (and consequently time resolution of input meteorological variables): from daily (for DNDC) and CERES-EGC) to half-hourly (for SPAc and ORCHIDEE-STICS). The number of meteorological variables used also differs among the models: from only two for DNDC (temperature and precipitation) to up to six for ORCHIDEE-STICS (temperature, precipitation, incident long and short-wave radiation, relative humidity and wind speed).

In case of gaps in the on-site daily time series, data from the nearest climate station from the ECAD dataset were used to gap-fill daily values for models with daily time steps (Klein Tank *et al.*, 2002). In case of gaps in the half hourly data required by ORCHIDEE-STICS and SPAc, data were gap filled with long term site-specific half-hourly average values.

The soil texture is determined from measurements made at each site (Kutsch *et al.*,

2010; Sus *et al.*, 2010) and prescribed accordingly for all four models. Management events, such as fertilization, irrigation, planting, harvest or ploughing are also defined by on-site observed values (Kutsch *et al.*, 2010). In the SPAc model, the effects of fertilization are not taken into account, but reported harvest dates and crop residue management are considered in the model runs.

The three simulated crops, winter wheat, winter barley, and maize, were parameterised for each model using "standard" published values (Kätterer *et al.*, 1997; López and Arrue, 1997; van den Boogaard *et al.*, 1997; Juskiw *et al.*, 2001; Lohila *et al.*, 2003; McMaster and Wilhelm, 2003; Mueller *et al.*, 2005) or data provided by site observations. For the DNDC model, values given in Table 3.2 are for the time of harvest as prescribed in the DNDC user manual. For the estimation of plant C/N ratios in DNDC, site data for biomass and C and nitrogen content were used. ORCHIDEE-STICS, SPAc and CERES-EGC use generic parameterisations for all sites. Where C and N content data were not available, fertilizer application data, provided by the site managers, were used to derive site specific C/N ratios under the assumption of optimum nitrogen supply during growth.

Initialisation procedure. For the initialisation of the soil C and nitrogen pools, the DNDC model was run for ten years using daily ECAD weather data from the nearest weather station (Klein Tank *et al.*, 2002). The litter input for the initialisation period was manually adjusted so that modelled matched measured total soil organic C at the beginning of the simulation period. The fertilizer input for this initialisation period was assumed to be in the same order of magnitude as the mineral fertilizer input during the simulation period.

For simulations performed by ORCHIDEE-STICS, the soil C pools were initialised to their steady state equilibrium values after a thousand-years spin-up during which climate and management practice of the simulated year were repeatedly cycled.

For SPAc simulations, initial soil organic matter as well as labile C contents are estimated based on field observations reported in the literature (Halley and Soffe, 1988;

Anthoni *et al.*, 2004; Aubinet *et al.*, 2009). The initial labile C content is equal to the seed C content at sowing in the SPAc model.

The CERES-EGC model was run for two rotations at all sites before the measurement period to stabilize the C and N soil pools and dampen the initial conditions. The same meteorological data were repeatedly used in case the historical data were not available.

DNDC was set up to run for the full crop rotation using litter inputs based on the calculated crop growth. The optimum yield parameter was adjusted to match the site specific yields. The DNDC model does not incorporate the concept of crop germination and emergence; it assumes an initial biomass at the day of sowing with the immediate start of photosynthesis. In order to simulate a realistic crop growth we assume 20 days for the crop to emerge from the day of seeding to the start of photosynthesis (Stone *et al.*, 1999; McMaster and Wilhelm, 2003).

For the ORCHIDEE-STICS runs, one simulation was performed for each crop season. The SPAc runs have been initiated at sowing (date as reported from the site) and terminated by the end of the following year.

It is important to note that the SPAc outputs are only truly representative of the actual growth period from sowing to harvest, as no post-harvest voluntary re-growth, ploughing or sowing have been considered. However, reported fractions of crop residual biomass were considered for the simulation of post-harvest heterotrophic respiration fluxes (Sus *et al.*, 2010).

The simulations of CERES-EGC were set up for full crop rotations. The sowing date of each crop was initiated in the management file and harvest time was simulated when crops attained physiological maturity. Grain and straw were exported from the field while crop residues and roots were incorporated into the SOM pools at the date of post-harvest tillage. Catch crops (at Grignon) and volunteers from the previous crop (at Auradé) were simulated between the crop seasons of a winter crop (barley and wheat) and a spring crop (maize and sunflower).

Table 3.2: The site specific crop parameters used to run the DNDC model for the site comparison.

Parameter name	Unit	Winter wheat					Maize	Barley
		Values site Oensingen	Values site Auradé	Values site Gebesee	Values site Grignon	Values site Klingenberg	Values site Grignon	Values site Gebesee
Total biomass	kg DM ha^{-1}	7900	7600	7600	7600	7600	6500	8200
Portion of grain		0.40	0.40	0.40	0.40	0.40	0.44	0.30
Portion of shoot		0.55	0.55	0.55	0.55	0.55	0.49	0.65
Portion of root		0.05	0.05	0.05	0.05	0.05	0.07	0.05
Total plant C/N ratio		68.00	36.09	36.09	36.09	36.09	52.00	84.00
Grain C/N ratio		35.00	28.00	28.00	28.00	28.00	37.00	40.00
Root C/N ratio		100.00	54.00	54.00	54.00	54.00	75.00	160.00
Shoot C/N ratio		100.00	44.00	44.00	44.00	44.00	75.00	160.00
Water requirement	kg water kg DM^{-1}	200.0	150.0	150.0	150.0	150.0	50.0	100.0
Max LAI	m^2 m^{-2}	7.0	7.0	7.0	7.0	7.0	4.5	5.0
Max height	m	0.7	0.7	0.7	0.7	0.7	2.4	1.0
Thermal degree days	°C	2400	2400	2400	2400	2600	2400	2500

Model comparison

We used the site eddy covariance derived data for GPP, NEE, R_e (Reichstein *et al.*, 2005) and latent heat flux aggregated on a daily time step for the model comparison. The data were provided in gap filled format, which was checked for errors and outliers and aggregated for different time intervals from half hourly to weekly in the CarboEurope IP ecosystem database (LEVEL 4, Reichstein *et al.* (2005); Papale *et al.* (2006a,b); Moffat *et al.* (2007)).

The statistical methods of the model comparison were based on Smith *et al.* (1997); Morales *et al.* (2005). The data analysis itself was performed in the statistical package *R* (*R*, 2009). To determine if the daily measured NEE, GPP and R_e data were normally distributed, we used the Shapiro-Wilk implementation in *R* (Royston, 1992) independently for each site and each year of the comparison. The highly significant result of the test ($p < 0.01$) indicates a very high probability that the data are not from a normally distributed population. Subsequently we used the non-parametric Kendall tau rank correlation coefficient or r, to assess if simulations and measurements were associated:

$$r = \frac{n_c - n_d}{(1/2)n(n-1)} \tag{3.1}$$

where r is the correlation coefficient, n is the number of observations, n_c is the number of concordant pairs, and n_d is the number of discordant pairs. We estimated the significance based on Best and Gipps (1974).

To analyse the association between measured and simulated data we calculated a locally weighted polynomial regression (Cleveland, 1979, 1981), the "lowess" smoother, within 1:1 scatter plots of measured against simulated values. The lowess fit function is a continuous fit to subsets of the data without requiring a predefined fitting model. Thus, the fitted line describes the best model fit for a subsection of data by a moving window indicator. A change in the slope of the fitted line indicates a change in the correlation

between measured and modelled values due to shifting from low to high values. In all pair plots, the right hand side panel shows the r values in black for significant correlation coefficient results ($p < 0.05$), and in light grey for non-significant associations ($p > 0.05$). The size of the text indicates the strength of the association. We use a 95% confidence interval as suggested by Smith *et al.* (1997); Morales *et al.* (2005).

The model efficiency factor E (Nash and Sutcliffe, 1970) is another measure of model performance. It compares the squared sum of the absolute error with the squared sum of the difference between the observations and their mean value. It compares the ability of the model to reproduce observed data variability with a much simpler model that is based on the arithmetic mean of the measurements:

$$E = 1 - \frac{\sum_{i=1}^{n} (O_i - P_i)^2}{\sum_{i=1}^{n} (O_i - \bar{O}_i)^2} \tag{3.2}$$

where O_i are the observed values, P_i are the simulated values, n are the total number of observations and i the current observation. E ranges from 1 to -∞. Any model giving a negative value shows a poor performance, a value of 0 indicates that the model does not perform better than using the mean of the observations, and values close to 1 indicate a "near-perfect" fit.

To compare the annual C balance of the sites, the total annual flux is calculated for observed and simulated NEE:

$$m_{o,i} = \sum_{i=1}^{n} O_i + m_{o,i-1} \tag{3.3}$$

$$m_{p,i} = \sum_{i=1}^{n} P_i + m_{p,i-1} \tag{3.4}$$

where $m_{o,i}$ is the cumulative sum of the daily (i) observed fluxes and $m_{p,i}$ the cumulative sum of the simulated flux. The difference of the two, observed minus modelled, is the

absolute error Δx presented in Table A.2. We tested the median of the two cumulative flux distributions for significant differences on the 95% confidence level by using the R implementation of the Wilcoxon rank sum test (Hollander and Wolfe, 1973; Corder and Foreman, 2009).

3.3 Results

The statistical results of r and E for all sites are summarised in Table A.2 and in the figures that show the site to site performance in terms of r. There are common patterns for all sites and for all models which are:

- Poor performance of all models in reproducing low C fluxes ranging between -2 gC m^{-2} day^{-1} and 2 gC m^{-2} day^{-1} (Figure 3.1 and Annex Figs. A1-A5 in Wattenbach *et al.* (2010)).

- All models have problems with capturing crop phenology, which is indirectly indicated by either an overestimation of the amplitude of growth in the later stage of crop development (mainly the case for ORCHIDEE-STICS, SPAc and CERES-EGC model) or a phase shift of growth as seen for DNDC (especially for winter wheat and barley, by simulating the onset of growth to early in the season, Figure 3.2 and Annex Figures A6-A10 in Wattenbach *et al.* (2010)).

- A good to very-good fit for GPP and R_e at fluxes below, and respectively, above the -2 gC m^{-2} day^{-1} and 2 gC m^{-2} day^{-1} flux rates, but a relatively poorer fit for NEE.

- DNDC and CERES-EGC: a relatively poor performance in reproducing the latent heat flux in contrast to a better performance for NEE, GPP and R_e, suggesting weaknesses in coupling water and C fluxes in these models.

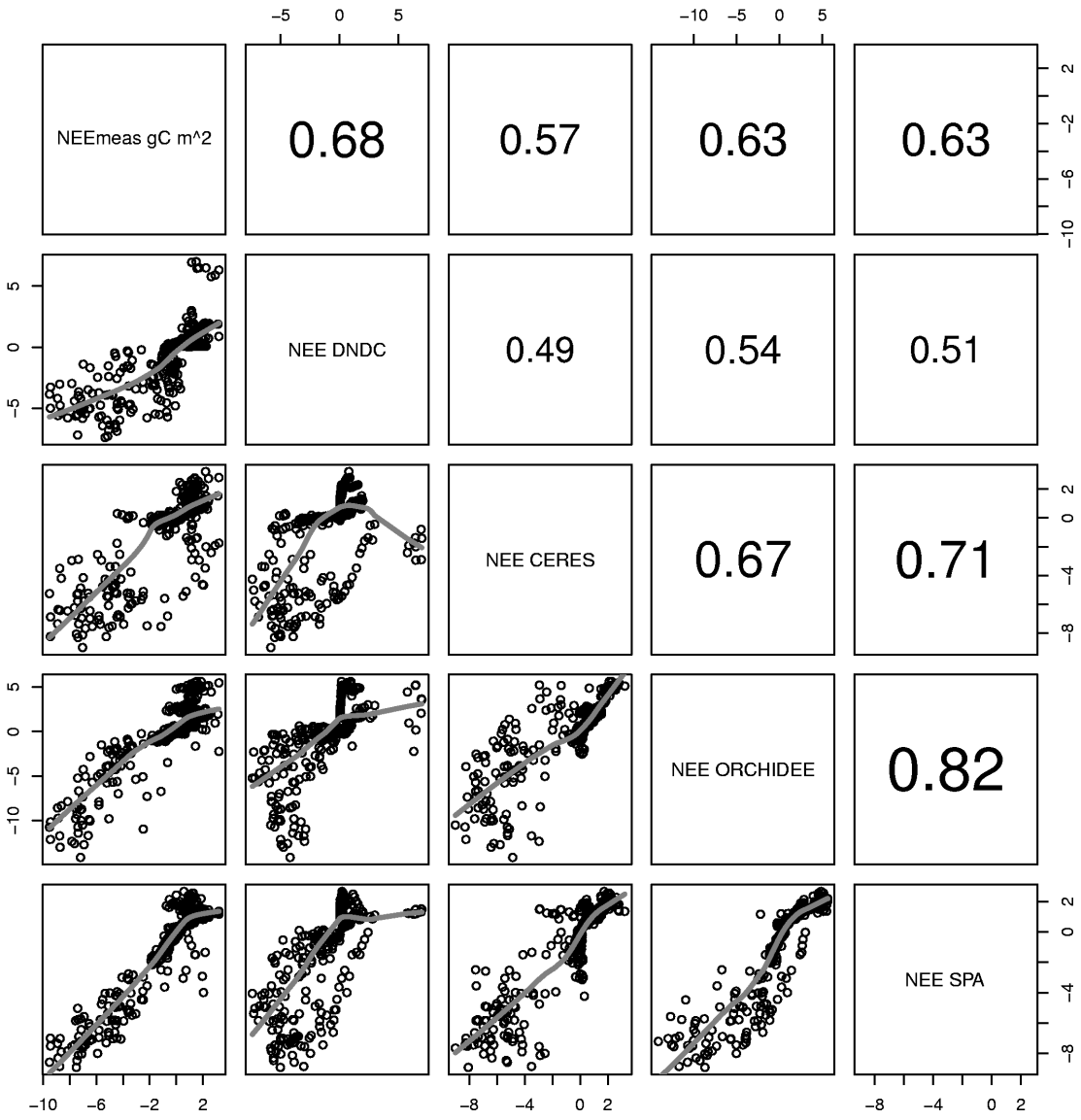

Figure 3.1: Scatter plots of simulated versus measured NEE for site Auradé 2006 (winter wheat). The grey line indicates the lowess regression. Values in the upper-right panels are Kendall correlation coefficients. The size of the number indicates the strength of the association. In this case all models capture observed NEE with good levels of association.

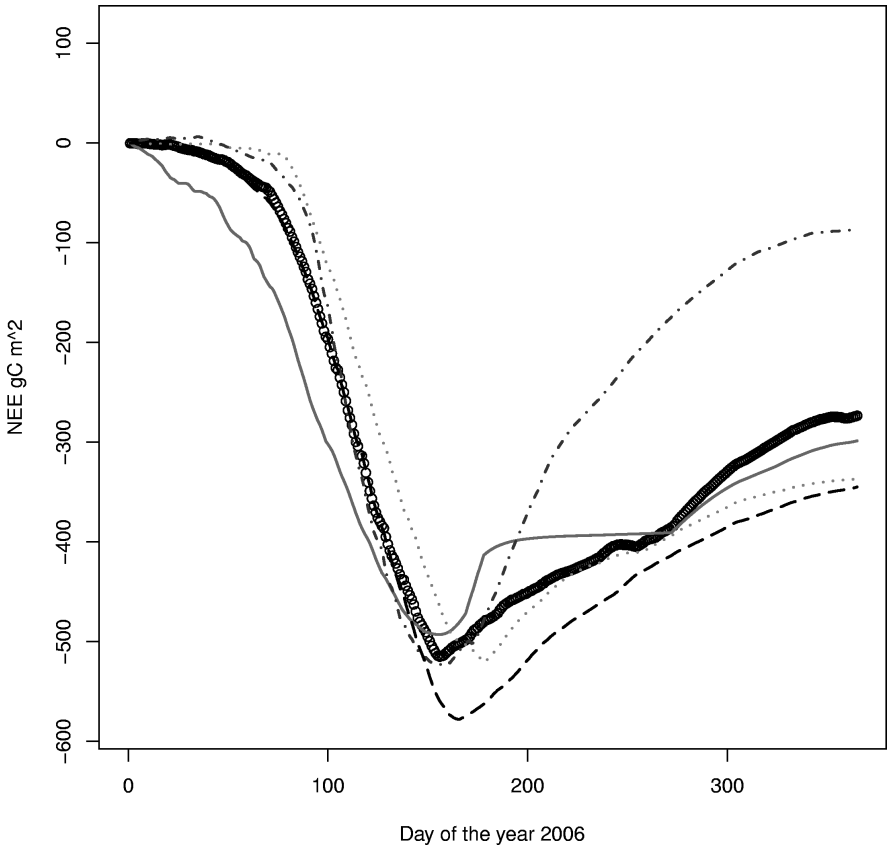

Figure 3.2: Cumulative NEE for year 2005 at site Auradé, winter wheat. DNDC: grey solid line, ORCHIDEE-STICS: darkgrey dash-dot line, CERES-EGC: grey dots, SPAc: black dashed line, measurements indicated by open circles. Besides capturing the daily dynamics of fluxes (Figure 3.1), ORCHIDEE-STICS fails to capture the fluxes after the growing season.

3.3.1 NEE

There is a wide range in the performance of the various models in reproducing measured NEE patterns at different sites and in different years, and also between models at one site in the same year. Correlations range from $r = 0.28$, $p < 0.05$ for DNDC simulating maize in year 2005 at Grignon to $r = 0.81$, $p < 0.05$ for the SPAc model simulating winter barley at Gebesee in 2007 (see Table A.2). In general, all models perform better for simulating winter crops (site mean: $E = 0.56$, $r = 0.61$) than the summer maize crop at Grignon (site mean: $E = 0.46$, $r = 0.42$).

In general, there is a better inter-model agreement between SPAc and ORCHIDEE-STICS, except for the Klingenberg site, where we observe a slightly better agreement

between SPAc and DNDC than between ORCHIDEE-STICS and DNDC. When comparing average correlation of all models per site, models perform on average best at Gebesee with winter barley in 2007 ($r = 0.68$), followed by Auradé ($r = 0.65$), Klingenberg ($r = 0.61$), Grignon 2006 ($r = 0.58$), Oensingen ($r = 0.52$) and the maize crop in Grignon in 2005 ($r = 0.42$). Even though these results are relatively good, all models poorly reproduce low fluxes in the range of -2 gC m^{-2} day^{-1} to 2 gC m^{-2} day^{-1} at all sites.

If we compare cumulative NEE fluxes (Figure 3.2 and Annex Figures A6-A10 in Wattenbach *et al.* (2010)), we observe a mismatch for all models in the early stage of the growing season, when low fluxes predominate. The DNDC model shows a stronger divergence from measurements compared to the other models in the first 100 days of year (DOY). The ORCHIDEE-STICS, SPAc and CERES-EGC models start with very similar trajectories but begin to diverge between DOY 100 and 200 at most of the sites, except for maize at Grignon in 2005. A common pattern for the three models is to overestimate the NEE peak and the failure to reproduce senescence and post harvest fluxes. This leads to a mismatch in simulated vs. observed annual cumulative NEE (Table A.2). In general, the SPAc model shows the best performance when expressed as r and E for NEE over all sites, even though deficiencies remain in reproducing cumulative NEE because of lacking peak and post-harvest fluxes.

3.3.2 $\mathbf{R}_e$

When ranking the models according to their association with the data, ORCHIDEE-STICS shows the best performance on average over all sites (model mean: $r = 0.72$, $p < 0.05$). This model is also consistent in its performance over all sites with comparable r values (Table A.2). Between models, the r values vary strongly from $r = 0.38$ for DNDC in Auradé to $r = 0.79$ ($p < 0.05$) for ORCHIDEE-STICS at Klingenberg in 2006. Similar as for the simulation of NEE, we can identify the highest significant agreement between SPAc and ORCHIDEE-STICS (note that CERES-EGC does not simulate R_e), and a lower association between these two models and DNDC. However,

the pattern with contrasting behaviour of all models for fluxes below 2 gC m^{-2} day^{-1} is again clear (Figure 3.3 and Annex Figures A11, A12 in Wattenbach *et al.* (2010)), and a considerable scatter is seen for high flux rates. This is also reflected in low mean model efficiency values: E = -1.02, E = 0.44 and E = 0.33 for DNDC, ORCHIDEE-STICS and SPAc, respectively.

3.3.3 GPP

Model performance for simulating GPP is comparable to NEE (mean r = 0.85), with correlation coefficients that vary from r = 0.43 (ORCHIDEE-STICS at Oensingen) to r = 0.75 (SPAc at Gebesee, $p < 0.05$, Figure 3.4, Annex Figures A13, A14 in Wattenbach *et al.* (2010), and Table A.2).

Overall, the models agree better with each other (mean correlation between models for all sites: r = 0.68) than with measurements (mean correlation between models and observations: r = 0.58). In this respect, ORCHIDEE-STICS and SPAc are the two models that show highest agreement with measurements (mean r = 0.76), followed by DNDC (mean r = 0.67). DNDC and ORCHIDEE-STICS disagree the most (mean r = 0.6). Concerning the good agreement between ORCHIDEE-STICS and SPAc, the scatter between the two models is lower than in their respective reproduction of the measured values, which suggests a common reason for the misfit with the data.

Model-data comparisons exhibit a strong mismatch for low fluxes, indicated by an almost "flat" shape of the regression line at low measured values (see Figure 3.4 and Annex A13, A14 in Wattenbach *et al.* (2010)).

Overall, model-data agreement as evaluated by E is relatively high, being generally greater than 0.55. It is minimal for DNDC at Grignon in 2006 (E = 0.31) and goes up to 0.80 for three model-site combinations (ORCHIDEE-SITCS and SPAc at Grignon 2006 and SPAc at Gebesee).

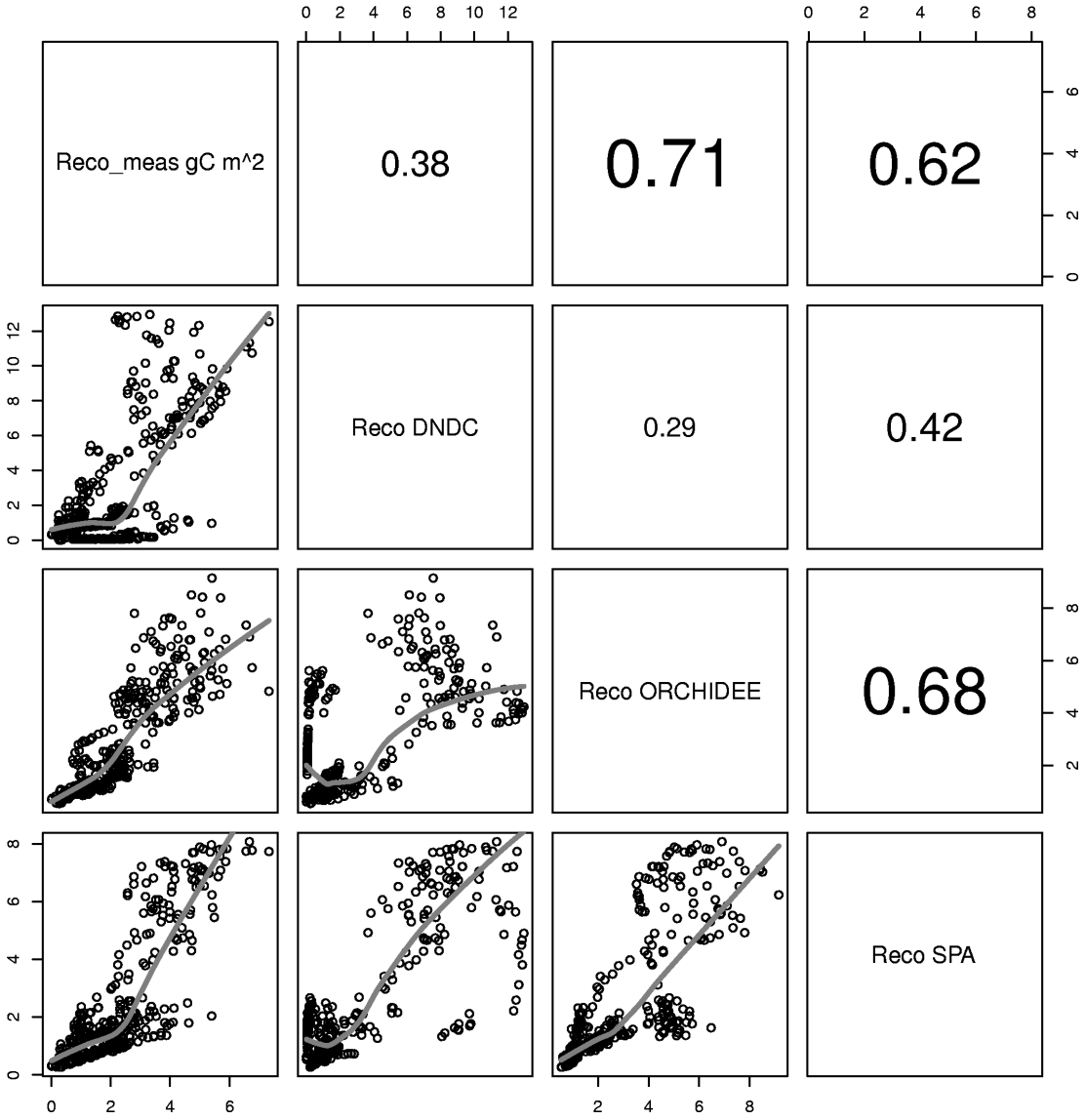

Figure 3.3: Scatter plots of simulated versus measured R_e for site Auradé, winter wheat, in 2005. The grey line indicates the lowess regression. Values in the upper-right panels are Kendall correlation coefficients. The size of the number indicates the strength of the association. The pattern of lack of fit for small fluxes appears now more pronounced for ORCHIDEE-STICS and SPAc as in Figure A11 in Wattenbach *et al.* (2010).

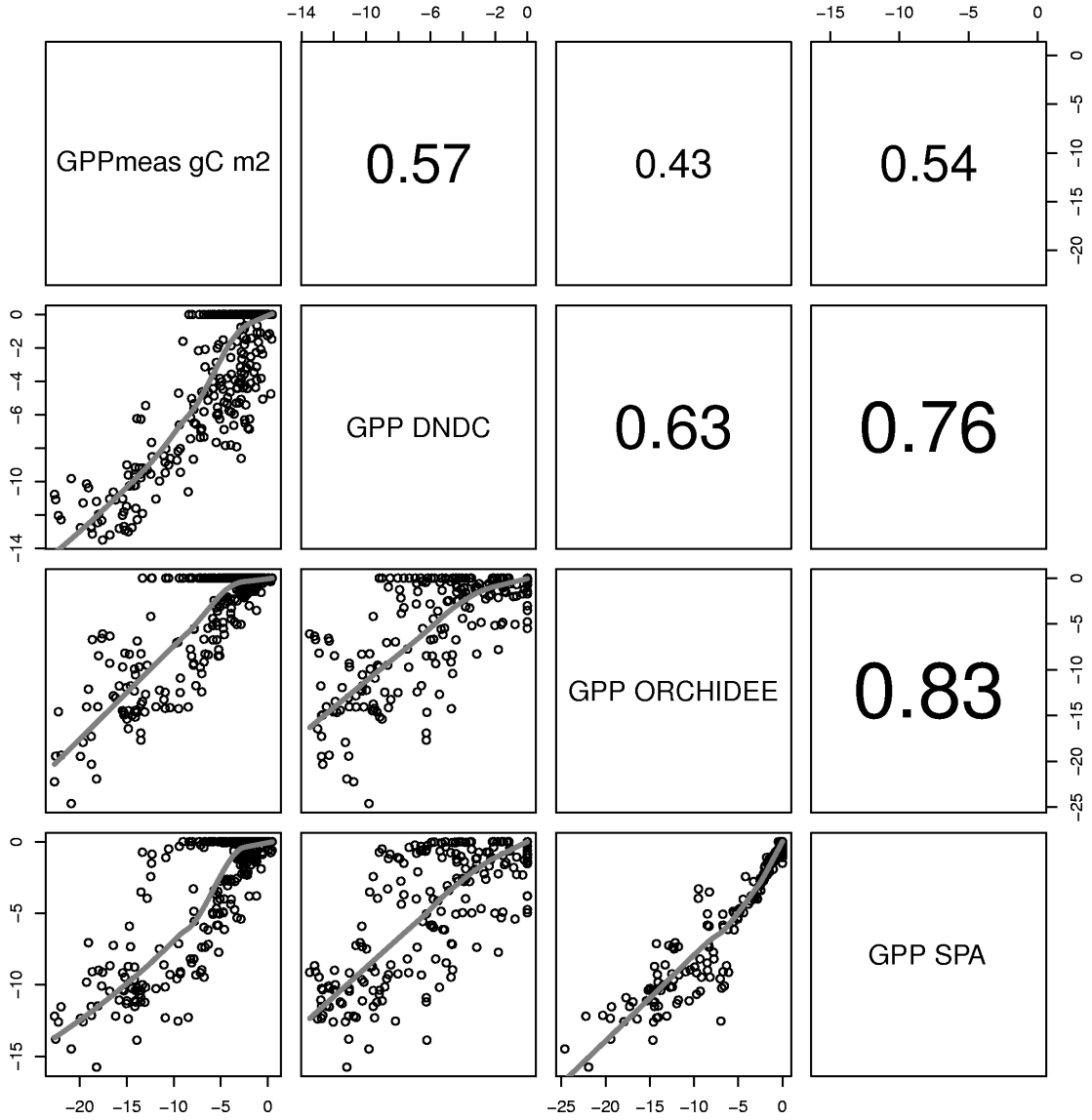

Figure 3.4: Scatter plots of simulated versus measured GPP for site Oensingen, winter wheat, in 2007. The grey line indicates the lowess regression. Values in the upper-right panels are Kendall correlation coefficients. The size of the number indicates the strength of the association. There is a good reproduction of GPP by the models and a less pronounced small flux disagreement. Interesting here is the high agreement between ORCHIDEEE-STICS and SPAc indicating, again, the high similarity of model response to external drivers.

3.3.4 ETa

The comparison of observed and modelled evapotranspiration fluxes generally shows that ORCHIDEE-STICS and SPAc model data correlate most with measurements (mean r for all sites: 0.60 for ORCHIDEE-STICS, 0.69 for SPAc). Again, these models also exhibit a considerable degree of cross-correlation, indicating a general agreement in the response to driving variables. In relation to that, the accuracy of modelled ETa as simulated by CERES-EGC (mean $r = 0.38$) and DNDC (mean $r = 0.45$) is considerably lower. For CERES-EGC and DNDC, the relationship between modelled and observed ETa, expressed by the slope of the lowess fit curve, is changing around a value of 1 mm d^{-1}. Beyond this value, the fit curve gradually takes over a quasi-logarithmic behaviour for most scatter plots. For certain sites (e.g. both Grignon years), DNDC and CERES-EGC fail to reproduce high flux rates, indicated by a high degree of scattering around the fit curve. The correlation of modelled values is high between DNDC and CERES-EGC, and even higher than with observations at the Gebesee site.

We found low values of model efficiency for DNDC and CERES-EGC, which were negative for Grignon 2006, Gebesee and Klingenberg. For SPAc and ORCHIDEE-STICS, E ranges from 0.2 (SPAc at Oensingen) to 0.78 (ORCHIDEE-STICS at Grignon 2006). Thus, the overall efficiency of these two models is higher and broadly satisfying.

In general, lower evapotranspiration fluxes were captured with higher accuracy by all models, which is indicated by an increasing data spread beyond 1 mm d^{-1} in most of the scatter plots (Figure 3.5 and Annex Figures A15-A19 in Wattenbach *et al.* (2010)).

3.4 Discussion

The aim of the paper was to test four models for accuracy in simulating the main components of the C cycle (net ecosystem exchange, ecosystem respiration, and gross primary production) in connection with actual evapotranspiration on a daily time scale over a gradient of environmental conditions in Europe. The results show a heterogeneous

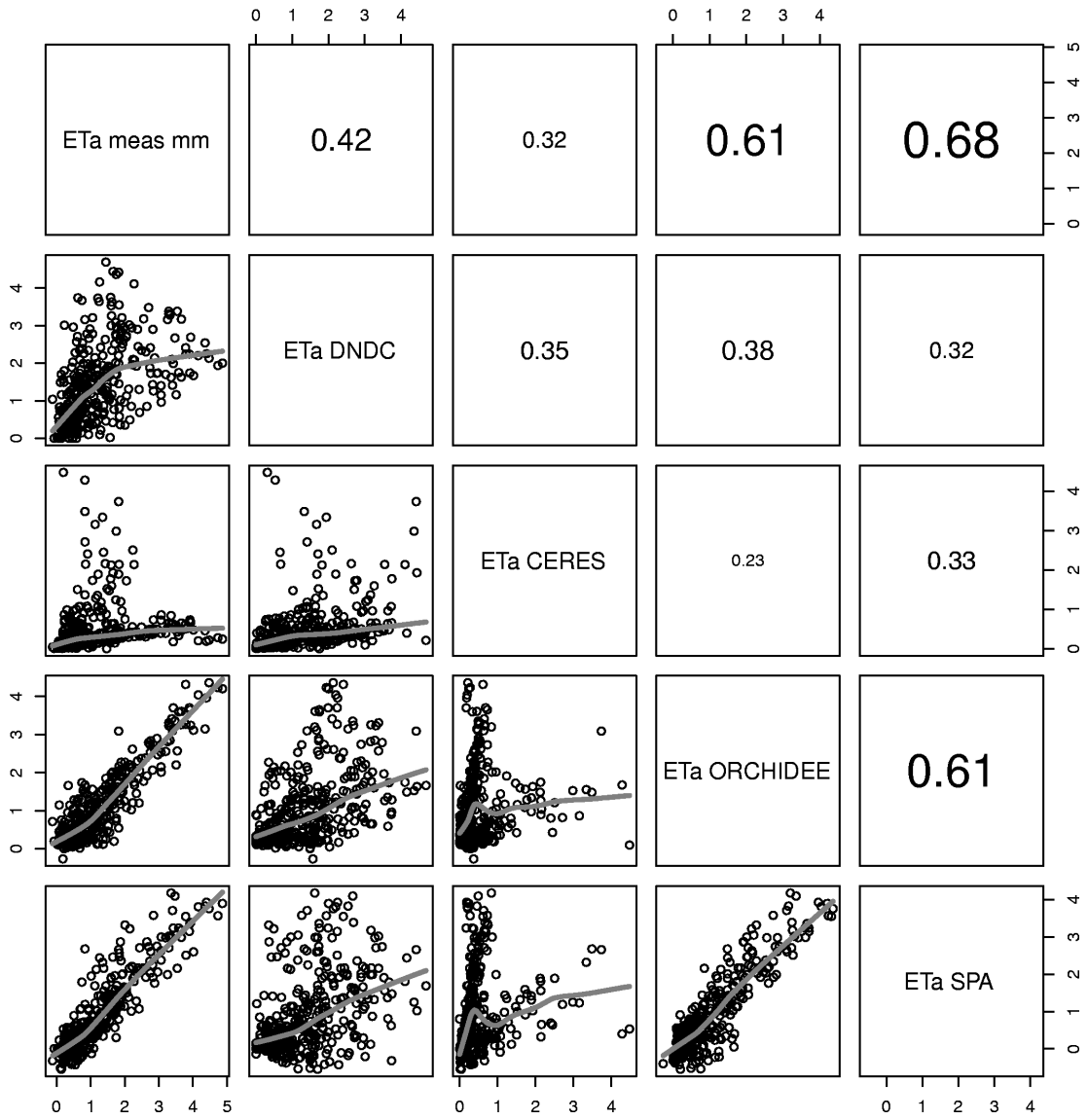

Figure 3.5: Scatter plots of simulated versus measured ETa for the Grignon site, winter wheat, in 2006. The grey line indicates the lowess regression. Values in the upper-right panels are Kendall correlation coefficients. The size of the number indicates the strength of the association. CERES-EGC and DNDC are deficient in reproducing observed high flux rates.

picture, with differences between models and between sites. The two models with the highest accuracy for simulating daily NEE and latent heat over all sites are SPAc and ORCHIDEE-STICS. Both models run on a half hourly time step with a high process resolution, so they are able to capture the diurnal variability of processes, leading to a high level of agreement when measurements are aggregated to daily fluxes. They are strong, in particular, in simulating water fluxes. For these, They clearly out-perform the two other models, which is most probably a result of the more process oriented representation of latent heat flux in the models (subsection 3.2.2).

However, the models are not able to simulate crop rotations due to the limited number of crops parameterised, and due to their current limitation of modelling growing period processes only. Consequently, they cannot produce accurate annual cumulative NEE fluxes at Grignon, Klingenberg, and Gebesee, and at Oensingen in case of ORCHIDEE-STICS. However, even though models are limited to winter wheat and winter barley for SPAc, and winter wheat and maize for ORCHIDEE-STICS, they are able to capture 43% and 37%, respectively, of the crop area of the EU27 (Kutsch *et al.*, 2010). Through their joint ability to simulate these three crops, the two models cover more than 50% of the EU27. However, for the purposes of examining a wide range of mitigation options envisaged for agriculture in the context of climate change (Denman *et al.*, 2007; Smith *et al.*, 2008), the models need to be extended to simulate a number of post-harvest activities, like catch and cover crops, and crop management options like low tillage and non-tillage systems.

On the other hand, the CERES-EGC and DNDC models are less accurate in their representation of daily NEE. In the model comparison presented here, DNDC fails to reproduce NEE at Grignon, and exhibits a poor performance at Oensingen. One possible factor leading to the failure of DNDC at the Grignon site in 2006 was the particularly mild winter, with temperatures rising above +10 °C in the first 100 days of the year. The DNDC model seems to be more sensitive to these temperatures than the other models. DNDC responds with immediate growth, leading to a strong overestimation of early GPP and to early senescence. In contrast to the other models, DNDC simulates phenology based on the GDD approach, which causes the strong

phase mismatch with measurements and with the other models. Another important factor determining the accuracy of the DNDC model is the lack of consideration of germination/emergence as well as vernalisation in the model, which leads to unrealistic growth in the early stage of the growing season. These factors lead to a relatively poor performance of the model when simulating NEE in particular.

The lack-of-fit for the simulation of water fluxes for DNDC can be explained by the models use of the Thornthwaite formula (Thornthwaite and Hare, 1965) to calculate evapotranspiration. The Thornthwaite formula is known to underestimate potential latent heat flux, especially under arid and semiarid conditions (Amatya *et al.*, 1995; McKenney and Rosenberg, 1993). This explains poor model performance for all sites except Oensingen, where highest precipitation values combined with a relatively low mean annual temperature have been recorded. Moreover, deficiencies within the hydrological component in DNDC have been reported, especially regarding the calculation of water filled soil pore space (Tonitto *et al.*, 2007a,b).

There are a number of factors that limited the performance of DNDC in comparison to the other models. The first and most important point (compared to the best performing models, SPAc and ORCHIDEE-STICS) is the simulation of full crop rotations at all sites. Whereas SPAc and ORCHIDEE-STICS were initialised to determine the initial conditions only for the current simulation year, DNDC had to use conditions inherited from the previously cultivated crop. The model also considers all management options applied at the sites including manure applications, tillage, and the growth of cover crops. DNDC's comparably high level of complexity regarding the above factors has a profound impact on model uncertainty, further increasing the chance of poorer model fit to measurements.

In the case of CERES-EGC, we see a comparable performance to ORCHIDEE-STICS and SPAc when we compare simulated to measured NEE. However, the model was calibrated for the sites in Grignon and Auradé (Lehuger *et al.*, 2010), limiting the degrees of freedom when simulating fluxes at these sites. If we compare the performance

for the un-calibrated site in Gebesee though, model performance is still good in simulating NEE.

In general, these results are in agreement with other studies examining C fluxes. A direct comparison of models simulating C and water fluxes at FLUXNET forest sites, including the two model classes presented in this study (biogeochemical and dynamic global vegetation models), showed very similar results (Morales *et al.*, 2005). In that study, great variability of model accuracy across all sites was found. A main problem was the representation of water fluxes in the southern European region, where models performed poorly. We observe that especially DNDC performs comparably poorly at all sites, except for Oensingen. CERES-EGC exhibits problems at Grignon in 2005 and 2006 and at Gebesee, and in terms of model efficiency at Auradé in 2006.

3.4.1 Why do models fail to simulate low fluxes?

The lack of accuracy when simulating C fluxes close to zero is the most obvious feature observed in this model comparison across sites and across models. There are two possible explanations. The first is that the concepts implemented in the models under comparison are not adequate to simulate the underlying processes. The second is that the measured fluxes are unrealistic due to the inherent properties of uncertainty of eddy covariance measurements, such as u* correction, gap filling, outlier filtering, advection, and flux partitioning (Hollinger and Richardson, 2005; Reichstein *et al.*, 2005; Richardson and Hollinger, 2005; Lasslop *et al.*, 2008; Osborne *et al.*, 2010; Smith *et al.*, 2010). The results show that the models fail to reproduce low fluxes in all flux components, namely NEE, GPP and R_e. It is also very important to note that the models are inconsistent in how they simulate these fluxes, but still show partial consistency when directly compared to each other (this is especially true for ORCHIDEE-STICS and SPAc). Measurements and models approach these quantities from completely different directions. The entity measured in eddy covariance systems is NEE. The values for GPP and R_e are derived from NEE using flux partitioning (Reichstein *et al.*, 2005), which uses measured weather data as drivers. The models, on the other hand, use the

same weather data as drivers to simulate GPP and R_e, providing NEE. So, given the same driving variables, we arrive at different results for these low fluxes.

If we look at the results of GPP and R_e simulations, we find a generally higher agreement for fluxes below -2 gC m^{-2} day^{-1} and above 2 gC m^{-2} day^{-1}, respectively, which indicates that the underlying assumptions for these fluxes are consistent. The time when these low fluxes appear are the early growing stages of the crop or the intercropping period, which might hold one key to answer the question about the inconsistency. In this part of the growing season, NEE fluxes are dominated by heterotrophic respiration of soil organic matter and litter C. This respiration flux is clearly higher than photosynthesis of the small and slowly growing crop biomass. As a consequence, initial values of soil organic matter, but more importantly litter C, largely determine the overall match of modelled vs observed NEE in the early growth phase. For example, we found clearly improved SPAc results for early season low NEE fluxes when increasing initial litter C content (from 0 gC m^{-2}, the initial litter C content for all runs shown here, to 200 gC m^{-2}, results not shown). ORCHIDEE-STICS and SPAc, the models with the highest agreement between each other for these low fluxes, are the two models that only simulate growing season processes with a limited implementation of management actions, which can explain the mismatch. On the other hand, DNDC shows a good performance in simulating GPP (and in some cases R_e), but was not able to adequately reproduce the temporal development of the crop, which in turn caused a lack of alignment between the peaks in GPP and R_e. Because NEE is calculated as the difference of the two, errors amplify. This is especially the case at the end of the growing season: then, the model simulates senescence, reducing GPP, which in parallel increases ecosystem respiration due to a higher soil C input. However, the inherent properties of eddy covariance measurements also have effects on the model comparison. There are a number of papers discussing the influence of different assumptions on aggregated NEE fluxes at agricultural sites (Anthoni *et al.*, 2004; Aubinet *et al.*, 2009; Moureaux *et al.*, 2008), which show a considerable systematic uncertainly in the flux estimates varying from 10 gC m^{-2} y^{-1} to 40 gC m^{-2} y^{-1}. Estimates of NEE at Gebesee in 2003 ranged from -185

gC m^{-2} y^{-1} to -245 gC m^{-2} y^{-1}, based on different assumptions in data processing (Anthoni *et al.*, 2004).

Especially for low fluxes (with low photosynthetic activity in the early, late or inter growing season), nocturnal flux measurements (when turbulent mixing is insufficient) are becoming over proportionally important, because they are also used to derive daytime R_e. These data need also to be gap filled in order to be used to calculate daily values. The error introduced by gap filling can be estimated as follows: at daytime, maximum observed errors were $\pm$0.20 gC m^{-2}, and at night time the maximum was $\pm$0.14 gC m^{-2} per percentage of day filled (Falge *et al.*, 2001). The percentage of gap-filled half hourly data range from as low as 29.2% for 302 days at Gebesee 2005 up to 58.9% for 347 days at Klingenberg 2005, which could explain the inconsistent reproduction of NEE data by models.

3.5 Conclusions

Overall, the models tested in this study show an acceptable to very good performance when simulating NEE with significant associations and efficiencies above zero (beside DNDC at Grignon 2006). All models have problems in reproducing fluxes between -2 gC m^{-2} day^{-1} and 2 gC m^{-2} day^{-1}, which most probably results from the combined effects of various common deficiencies: a lack of accuracy in simulating the correct temporal sequence of development stages, problems in capturing the ecosystem respiration flux, and not considering all management actions.

For European-scale application, models likes SPAc and ORCHIDEE-STICS are highly accurate in simulating net carbon fluxes (NEE) and water fluxes. However, they are only able to simulate the seasonal carbon balance of a limited number of crops with a limited consideration of management. Thus, they are not yet capable of evaluating the wide range of mitigation options envisaged for agriculture in the context of climate change (Denman *et al.*, 2007; Smith *et al.*, 2008). They are also not able to accurately

simulate annual carbon budgets, because they do not consider post-harvest effects (such as intercropping or regrowth).

On the other hand, models like CERES-EGC and DNDC are less accurate in simulating NEE and are especially poor in reproducing latent heat fluxes. They are however capable of simulating mitigation options, because they can simulate full crop rotations and associated management effects. CERES-EGC and DNDC also consider other greenhouse gases like N_2O, and in case of DNDC also CH_4, which further affect the GHG balance. In this study, DNDC is the model with the widest range of implemented crop types and management options under irrigated and non-irrigated conditions (Leip *et al.*, 2008), but shows lowest accuracy in daily carbon flux simulation. However, CERES-EGC and DNDC fail to accurately reproduce associated water fluxes. This might limit their ability to simulate possible drought effects, which will have an increasing importance in predictive simulations due to climate change (Seneviratne *et al.*, 2002; Salinger, 2005; Falloon and Betts, 2010).

Finally, this model comparison shows that multiply constrained model evaluation is clearly improved with high temporal resolution data sources, such as those from eddy-flux data, in combination with detailed management information, such as that provided at the CarboEurope IP sites.

Chapter 4

Diagnosis of a crop carbon mass balance model through the assimilation of observed winter wheat flux and biometric data

Abstract

Studying the carbon (C) cycling of croplands is important for improving the understanding of the terrestrial C cycle and associated ecosystem services such as agricultural yield. Crop models have been used to provide answers to these pertinent questions, but several key processes are simplistically captured or poorly understood, and parameter uncertainty is large. Crop models are generally empirical, provide no uncertainty estimate of key state variables, and have low predictive capacity.

In this study, we have assimilated measurements of eddy covariance (EC) derived fluxes of net ecosystem exchange (NEE) of C and independent measurements of biometry (i.e. C stocks and leaf area index (LAI)) into a crop C mass balance model (SPAc)

using the Ensemble Kalman Filter (EnKF). We use observations of C fluxes and stocks made at the Klingenberg (Germany) CarboEurope flux site for one growing cycle of winter wheat (2005/2006), and thus are applying a multiple-constraints approach for interpreting both observed and modelled annual C sums. The overall research rationale was to diagnose key processes of a crop model through explicit consideration of independent, multiple constraints. In fact, we expect our crop model to be deficient and oversimplified, and here we aim for detecting and resolving these deficiencies through data assimilation (DA).

We found that DA clearly provided important, quantitatively identified insights into model shortcomings. Constraints on aboveground biometry (in particular LAI and foliar C) and key crop processes were resolved in NEE flux data, which served as a strong diagnostic tool for model analysis brought about by DA. Assimilated flux data identified model shortcomings in structure and parameterisation. We noted temporal parameter variability as a response to C flux DA, which is indicative of ecosystem processes that are resolved in NEE data but are not captured by model structure. Moreover, observational constraints are stronger for physiological than developmental parameters.

Our results suggest that wheat crop models benefit from accounting for temporal and/or canopy layer variability in leaf thickness and fraction of autotrophic respiration. NEE data constraints on crop developmental stage (DS) on the other hand are less obvious, as DS is a non-tangible, rather abstract model state variable. A general weakness of this generalized crop C mass balance model is the lack of a mechanistic representation of C partitioning. We further found that SPAc is deficient in reproducing flux data when biomass and LAI meet external constraints, which is supposedly related to shortcomings in simulating plant hydraulics and photosynthesis of non-leaf green surfaces (i.e. stems and ears). Frequent sampling of key biometric variables is warranted to improve the understanding of rapidly changing agroecosystem processes such as development, C allocation, and senescence.

4.1 Introduction

Studying the carbon C cycling of croplands is important for improving the understanding of the terrestrial C cycle and associated ecosystem services such as agricultural yield. In the year 2000, ≈12% of the ice-free land surface was cropland (Ramankutty *et al.*, 2008; Leff *et al.*, 2004), which further represents 10-15% of the total global biological productivity (Haberl *et al.*, 2007). Modelling can be used to determine C budgets for the diagnosis of the current situation of agricultural source-sink relationships. Such diagnosis also allows for the derivation of best-practise recommendation for a less C intensive cropland management. Improved agricultural land management has great potential for increasing soil C sequestration (Smith, 2008). However it is expected that by 2050 at least 50% more agricultural production will be needed to feed the world population (Tilman *et al.*, 2001). Answering the question of how humankind will be able to simultaneously increase global crop yield in a sustainable fashion whilst exploiting the C sequestration potential of croplands is of paramount importance.

Over several decades, agricultural models have been used for crop biomass growth and/or yield simulations (see Sus *et al.* (2010)). More recently, land-surface models have been equipped with crop C cycling sub-modules (e.g Bondeau *et al.* (2007); Kucharik and Twine (2007); de Noblet-Ducoudré *et al.* (2004)) and crop C budget models have been developed (Huang *et al.*, 2009b; Arora, 2003; Adiku *et al.*, 2006; Wang *et al.*, 2005). However, the use of crop modelling as a diagnostic and predictive tool of agricultural yield and C cycling is still limited for a number of reasons. The lack of reliable information on land management, soil properties, and climate data complicates large-scale crop modelling (Wang *et al.*, 2007; Smith *et al.*, 2010), whereas the largest source of uncertainty stems from parameter uncertainty in local applications (de Wit and van Diepen, 2007). Several processes in a crop C budget model are representations of non-linear responses to changes in environmental conditions. For instance, C fluxes are highly sensitive to phenological processes (Baldocchi, 1994). These processes are poorly understood and non-linear (Xue *et al.*, 2004; Yin *et al.*, 1995),

interactive (Yan and Wallace, 1998; Slafer and Rawson, 1994), and inadequately simulated due to parameter uncertainty. There exists a range of competing phenological model concepts, parameterisations of which show considerable cultivar dependence (Xue *et al.*, 2004; Yan and Hunt, 1999; Slafer and Rawson, 1994). Moreover, environmental variables such as temperature and daylength merely serve as surrogates for complex biochemical pathways to simulate crop phenology (Setiyono *et al.*, 2007).

Crop models are generally empirical, and provide no uncertainty estimate of key state variables (SV, de Wit and van Diepen (2007)). Their simplified description of a natural system and inaccurate parameterisation result in a low predictive performance (Dorigo *et al.*, 2007). There is a lack of enough datasets to completely constrain crop C budgets, and model equifinality remains unresolved. Thus, we need multiple independent observations on modelled states in order to create a situation where the model dynamics have to satisfy the demands provided by a range of independent observations (Smith *et al.*, 2010; Baldocchi, 2003).

In this study, we are applying a multiple-constraints approach for interpreting both observed and modelled growing season crop C sums. In doing so, we are able to diagnose presumed key model shortcomings as outlined above. We have assimilated flux measurements of EC derived net ecosystem C exchange (i.e. NEE) and independent measurements of dry matter (i.e. C stocks) into a crop C mass balance model (SPAc, Sus *et al.* (2010)) using the EnKF. We use observations of C fluxes and stocks made at the Klingenberg (Germany) CarboEurope flux site (Prescher *et al.*, 2010) for one growing cycle of winter wheat (2005/2006). We explicitly account for various sources of uncertainty in both model and observations through an ensemble of model and measurement realizations. The model ensemble also provides an uncertainty estimate for simulated SV and parameters. Modelled SV and parameters are updated by assimilated observations through a weighting function, which is directly related to both model and observation uncertainties. State estimation is a useful tool for keeping the model linked to observations, ensuring that an improved estimate of model state at the current time step (e.g. fluxes of C assimilated and respired, leaf and storage organ (i.e. yield) C stocks) will lead to an improved state estimation at future time steps when

no observations are available. Simultaneously, key parameters of SPAc are updated to gain insight into model deficiencies, parameter uncertainty, and improved parameter estimates. In fact, we expect SPAc to be deficient and oversimplified, and here we aim for detecting and resolving these deficiencies.

Our overall objective is to use multiple and independent data constraints to assess a crop C model. The motivations of this study are threefold. (1) To assess the informational content of flux versus biometric data for crop models, addressing the question of whether multiple model constraints (i.e. the simultaneous assimilation of C fluxes and stocks) lead to a significant improvement of modelled C pools and fluxes. We hypothesise that the assimilation of both flux and biometric data is complementary in a sense that these independent, orthogonal data types are related to, and thus provide information about, a range of different model processes which are all important controls of photosynthesis, respiration, and crop development. (2) To estimate key model parameters and their uncertainty for prognostic applications and for the guidance of more detailed field studies. Do the temporally highly resolved flux data provide a strong constraint on crop developmental parameters? How realistic are the a priori values of key physiological parameters? We hypothesise that a forward model run with posterior parameter values will be in better agreement with observations than runs using prior parameters. (3) To determine whether the temporal richness of C flux data is fully exploited when assimilated into the model. Are residuals between observations and model estimates equally reduced, independent of daytime and season? When is flux DA most effective?

Overall, addressing these objectives will provide insights into C cycling of cereal crops and DA methodology, critical uncertainties, and requirements for future research. The primary novelty of this study is that it is the first combined assimilation of C fluxes and biometric data into a crop C mass balance model.

4.2 Data and methods

4.2.1 Crop model and data assimilation scheme

The soil-plant-atmosphere crop model (SPAc)

The Soil Plant Atmosphere (SPA) model (Williams *et al.*, 1996) is a process-based model that simulates ecosystem photosynthesis and water balance at fine temporal and spatial scales (30min time-step, up to ten canopy and twenty soil layers). SPA employs some well-tested theoretical representations of ecophysiological processes, such as for the calculation of photosynthesis (the Farquhar model, Farquhar and von Caemmerer (1982)) and leaf-level transpiration (Penman-Monteith equation, Jones (1992)). These two processes are linked by a model of stomatal conductance, which optimizes the daily gain of C per unit of leaf nitrogen within the limits of canopy water storage and soil to canopy water transport (Williams *et al.*, 1996). The amount of irradiation intercepted by the canopy depends on LAI, which is calculated by dividing the live leaf C mass by the C per leaf area parameter (C_{la}). A C mass balance model has been added to SPA more recently, including autotrophic respiration, C allocation to plant tissues, their turnover, and mineralization of dead organic matter (Williams *et al.*, 2005).

Moreover, a C partitioning scheme and a crop developmental model have been added (SPA version 2 - Crop (Sus *et al.*, 2010), hereafter referred to as SPAc). The C partitioning scheme is based on empirical values of field crop growth analyses (Penning de Vries *et al.*, 1989). This scheme considers C allocation to one root and four above ground C pools (labile, foliage, stem and storage organ C pools), and is a function of crop developmental stage (DS). DS is calculated as the sum of daily crop developmental rate (DR), which is estimated on the basis of non-linear functions for three environmental factors: temperature *f(T)*, photoperiod *f(P)*, and vernalization *f(V)* (Streck *et al.*, 2003; Sus *et al.*, 2010; Wang and Engel, 1998). In contrast to *f(T)*, both *f(P)* and *f(V)* affect DR only in the vegetative phase (wheat is assumed to be insensitive to photoperiod after anthesis, Slafer and Rawson (1994)). *f(V)* reduces DR

only during the first winter months, as it saturates relatively quickly. For a more detailed description of the developmental model applied in SPAc, see Sus *et al.* (2010).

Data assimilation scheme - the Ensemble Kalman Filter (EnKF)

DA can be considered as a set of techniques that aims for finding an optimal combination of observations and models, referred to as the "analysis" (Evensen, 2003). Measured and modelled states of a system are weighted in DA according to errors in both observations and numerical forecasts, providing new SV or parameter estimates. Parameters are considered as physical and time-invariant descriptions of particular characteristics or processes of the system in concern. Fluxes and storages of water, energy, or C, propagated in time by the model processes, are typical examples of model SVs. The overall success of DA lies in an unbiased model state prediction, which in turn is largely dependent on accurate parameter estimation (Moradkhani *et al.*, 2005). The popularity of EnKF-based DA for state estimation in the geosciences has increased in the past decade (Hu *et al.*, 2010; Moradkhani *et al.*, 2005). The EnKF has been applied in studies of various disciplines (Evensen, 2003). More recently, the EnKF was used in the context of C cycling of terrestrial ecosystems (Williams *et al.*, 2005; Quaife *et al.*, 2008; Chen *et al.*, 2008), global vegetation phenology (Stöckli *et al.*, 2008), and crop modelling (de Wit and van Diepen, 2007).

The generic Kalman Filter (KF) is a sequential filter method: a model is being integrated forward in time and uses observations whenever available to reinitialize (= the "analysis") the model with updated states and parameters at the very same time step. The KF interpolates and extrapolates data into data void regions in time and space, keeping the model in agreement with the observed data in a forecast-observe-update feedback loop (Williams *et al.*, 2005). The analysis is a weighted linear combination of the model forecast ψ^f and model forecast error covariances $P^f H^T$, corresponding to each of the measurements contained in array d. H is the observation operator, which relates an observed value to a SV of interest within the model through a set of relationships (Mathieu and O'Neill, 2008). If the measured variable is also a SV

in the model, the observation operator is directly linear (e.g. observed and modelled NEE or leaf C). H relates the true model state ψ^t to the observations d under the consideration of measurement error ϵ by:

$$d = H\psi^t + \epsilon \tag{4.1}$$

The weights applied within the KF are a function of model forecast (P^f) and measurement (R) covariances, and the difference between forecast and measurement, also called the innovation (Evensen, 2003).

The EnKF applies an ensemble of forecasts to extend linear sequential DA to non-linear applications (Turner *et al.*, 2008). The estimation of priori model covariance is not needed for the analysis step, but instead the EnKF uses straightforward ensemble statistics as an approximation of model uncertainty. The error covariance matrices for the forecast and analysed estimate (P^f and P^a) are given by

$$P^f \cong P_e^f = \overline{(\psi^f - \overline{\psi^f})(\psi^f - \overline{\psi^f})^T} \tag{4.2}$$

$$P^a \cong P_e^a = \overline{(\psi^a - \overline{\psi^a})(\psi^a - \overline{\psi^a})^T} \tag{4.3}$$

Subscript e denotes that the error covariance is derived from the ensemble statistics using the average over the ensemble as the best estimate of model state. Superscripts f and a represent the forecast and analysed model state, respectively. Error statistics are represented by an appropriate ensemble of model states created by Monte Carlo sampling, which is then used to represent specific probability density functions (PDF), and approximate estimates for moments of these PDFs can be derived. Model uncertainty itself is represented using stochastic forcing (Mathieu and O'Neill, 2008). In this study, we used the normalized *RMSE* ratio (*NRR*) as a method of quantifying the appropriate amount of stochastic model uncertainty. The *NRR* is a comparison between the spread of an ensemble and the ensemble mean forecast error. A deficiency

in model spread is hereby seen as a measure of uncertainty associated with the ensemble mean (Moradkhani *et al.*, 2005).

Observations are represented as a randomized ensemble of samples, whose mean and standard deviation correspond to the first-guess observation and measurement error, respectively (Evensen, 2003). The ensemble of observations is given by

$$d_j = d + \epsilon_j, \tag{4.4}$$

where j is counting from 1 to the number of ensembles. Finally, the analysis is formulated as

$$\psi_j^a = \psi_j^f + K(d_e - H\psi_j^f), \tag{4.5}$$

where K is the Kalman gain matrix, represented by $P_e^f H^T (H P_e^f H^T + R_e)^{-1}$. K is "proportional" to the uncertainty in the model forecast, and "inversely proportional" to the measurement noise (Gelb *et al.*, 2001).

The accuracy of SV estimation is lowered if a potential temporal evolution of parameter values is not incorporated (Chen *et al.*, 2008). While in theory parameters should remain constant, evidence of temporal change in parameters from the EnKF is indicative of poor process representation, and thus a useful diagnostic. Through a joint SV and parameter estimation, we explicitly acknowledge that model behaviour might change over time, necessitating subsequent adjustments in parameters. SV and parameter values are concatenated in one single joint state vector, an approach which is also referred to as "state augmentation" (Moradkhani *et al.*, 2005).

We selected a set of nine parameters (Table 4.1) for which we found particular model sensitivity in a previous study (Sus *et al.*, 2010). While two of these (C_{la}, f_{a}) are important controls of the C assimilation strength of an ecosystem, the remaining seven parameters are crucial components in the phenology routines.

- C_{la} prescribes the C cost of developing leaf area (i.e. leaf thickness, lower C_{la} fosters leaf area growth), and f_{a} prescribes the fraction of autotrophic respiration (the lower f_{a}, the more C available for biomass growth).
- The cardinal temperatures for development (T_{min}, T_{opt}, T_{max}) are important controls on the influence of ambient temperature on DR. *f(T)* (which is largest at ambient temperature close to T_{opt}) is proportional to the difference between T_{min} and T_{max} (the overall temperature range allowing for development).
- DR is inversely proportional to PH_{cr} (the daylength threshold, below which no development occurs). The amplitude of *f(P)* is proportional to PH_{sc}, i.e. the impact of daylength seasonality on development is dampened (intensified) with a low (high) PH_{sc}.
- $r_{\mathrm{max,v}}$ and $r_{\mathrm{max,r}}$ are the maximum potential DR under optimal environmental conditions in the vegetative and reproductive growth phases, respectively.

As the "true" values of these sensitive parameters are considerably uncertain and cultivar dependant (Streck *et al.*, 2003; Setiyono *et al.*, 2007; Porter and Semenov, 2005; Suleau *et al.*, 2011; Birch *et al.*, 1999), additional constraints provided by DA are clearly beneficial.

4.2.2 The Klingenberg CarboEurope site

The Klingenberg CarboEurope cropland site is located around 20-30 km south west of Dresden (Germany). The local climate is characterised by mean annual precipitation values of 819 mm at the nearby forest site (∼4 km north of the cropland site). Precipitation records show a convective summer maximum and a secondary frontal winter maximum. The annual mean temperature (1959-2000) is 7.7 °C and the mean monthly minimum and maximum temperatures are -1.0 °C and 16.6 °C respectively (Goldberg *et al.*, 2002).

The Klingenberg cropland site has been under continuous crop cultivation since 1975.

Previous to the winter wheat (*Triticum aestivum*) cultivation in 2005/2006, rapeseed (*Brassica napus*) was grown in 2004/2005. In 2007, maize (*Zea mays*) was grown as a summer crop following a more than half-year fallow period since the harvest of winter wheat in autumn 2006. In general, during the typical fallow periods between two crop cultivations, vegetation growth is dominated by volunteer seedlings or weed species (Prescher *et al.*, 2010).

The organic soil horizon (Ap) overlying the drained Gleysol is a medium clayey loam with a mean thickness of ∼0.2 m, followed by a slightly sandy clay and clayey sandy loam in the B horizon. The total soil C stock up to a depth of 60 cm was found to be ∼9700 gC m^{-2}. In addition to mineral fertilization (08/04/06, 22/04/06, 04/05/06, 04/06/06) and herbicides application (9 times ∼0.5 l ha^{-1} on average during the cultivation period), organic manure was applied to the field in August 2004 (32,000 kg ha^{-1}) and October 2006 (22,000 kg ha^{-1}). The soil was tilled before sowing up to a depth of 12 cm. Winter wheat was sown on the 25/09/05 and harvested on the 06/09/06 (Prescher *et al.*, 2010).

Fluxes of C, momentum, latent and sensible heat were measured using the EC method. NEE (Figure 4.1) was determined as the sum of Fc (the C flux, calculated and corrected in agreement with the EUROFLUX methodology (Aubinet *et al.*, 1999; Grünwald and Bernhofer, 2007)) and Sc (the C storage change, estimated based on the temporal changes of C concentration for the respective EC level). A u*-correction was applied to replace unreliable data due to low-turbulence conditions (Prescher *et al.*, 2010). Meteorological data include precipitation, air temperature, air humidity, soil temperature, and shortwave incoming radiation. Temperatures close to or below freezing were observed from mid-November until early April. Considerably low precipitation values were measured in July (Figure 4.2, Prescher *et al.* (2010)). On a monthly basis, replicated measurements of above- and belowground biomass were taken from three vegetation clear-cuts of a set area. The corresponding dry matter and LAI were measured in the laboratory (Prescher *et al.* (2010); Marga Wartinger, *personal communication*).

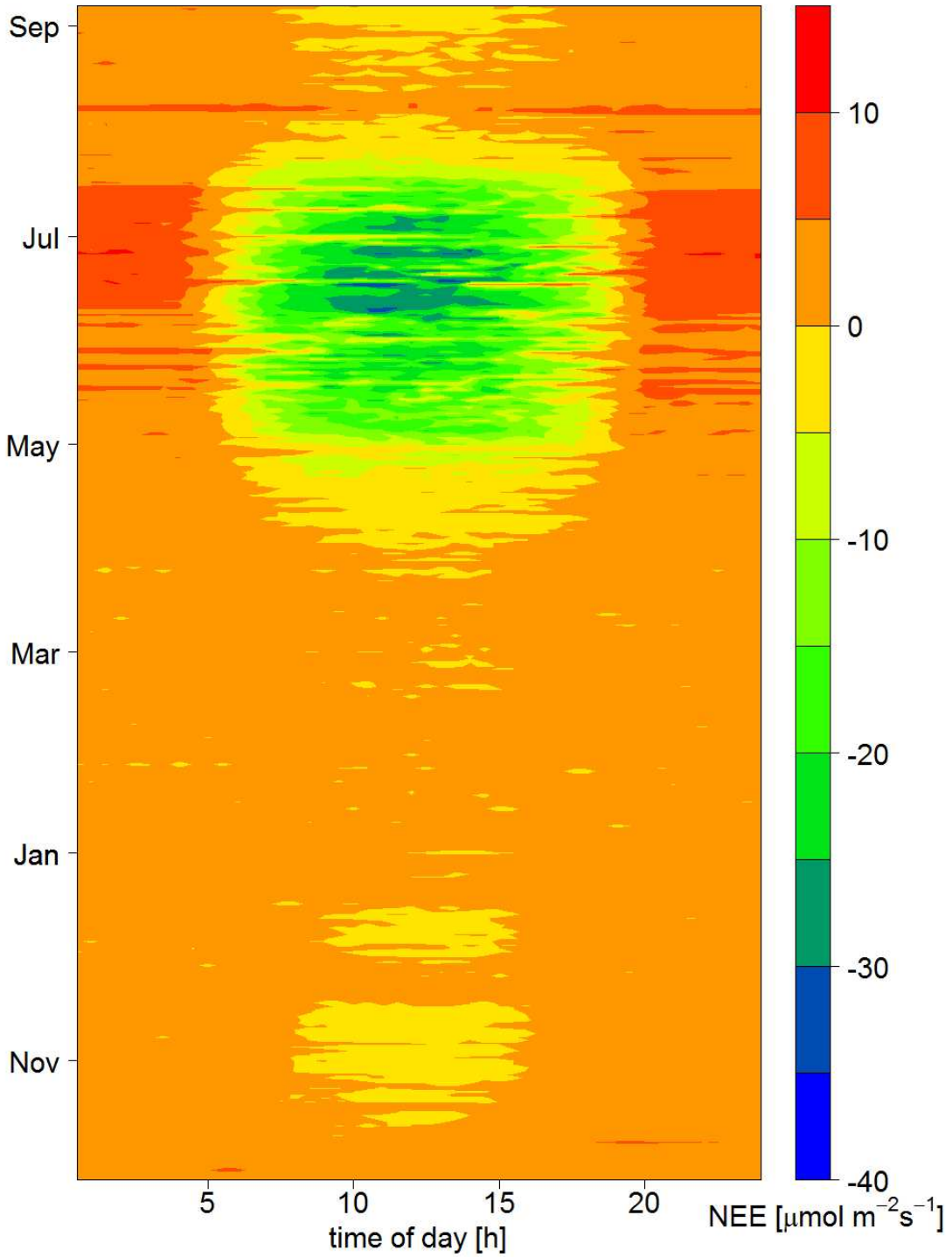

Figure 4.1: Contour plot of half hourly fluxes of NEE in μmol m^{-2} s^{-1}. Note that plotted data include both gap-filled an non-gap-filled values.

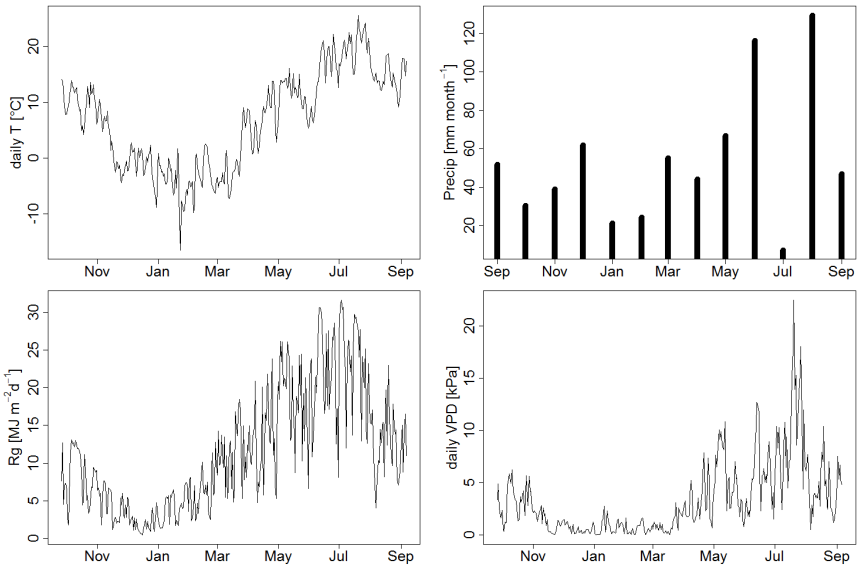

Figure 4.2: Measured values of temperature (T), precipitation (Precip), global irradiation (Rg), and vapour pressure deficit (VPD) for the Klingenberg 2005/2006 winter wheat growing season (period from sowing to harvest shown).

4.2.3 Assessment of NEE data uncertainty

We used the Hollinger *et al.* (2005) "paired observations" approach to quantify uncertainty of non-gap-filled half-hourly NEE data observed during the Klingenberg winter wheat 2005/2006 study period. In general agreement with the findings of Hollinger *et al.* (2005), the flux errors follow a double-exponential (Laplace) distribution (left panel in Figure 4.3) and are heteroscedastic (right panel in Figure 4.3). We found a standard deviation of 1.6 μmol CO_2 m^{-2} s^{-1}, which we used as a constant measure of observation error in the NEE DA procedure.

4.2.4 Assessing model uncertainty and ensemble size

For each time step (here half-hourly) the model uncertainty on biometry, C fluxes, and parameters is sampled from a normal distribution with zero mean. The standard deviation of this distribution is calculated as the product of the uncertainty given in Table 4.1 and Table A.3 and the absolute modelled value. Uncertainty estimates on measured biometry are given in percent of the absolute observed value, whereas the

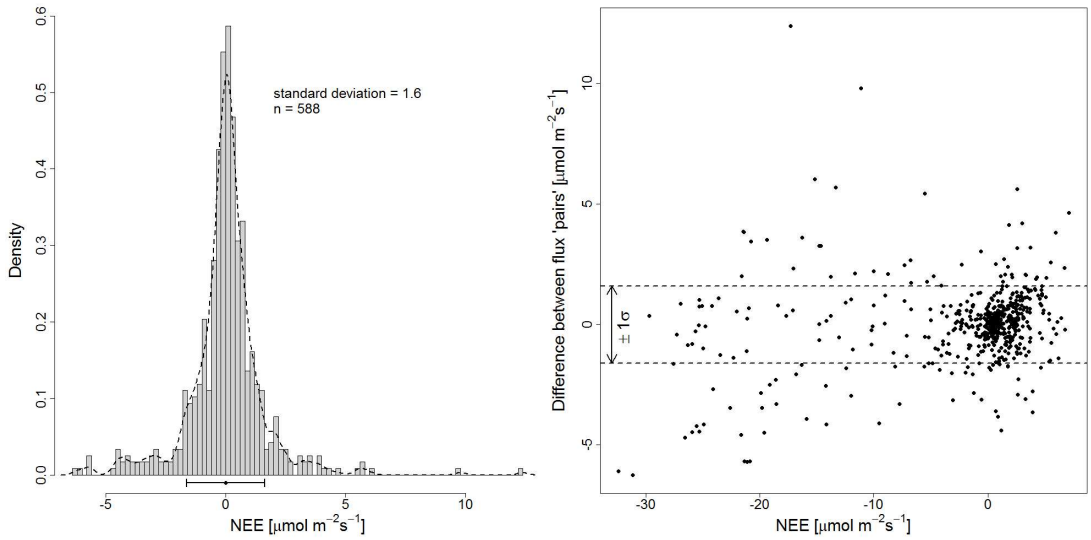

Figure 4.3: Flux uncertainty for net ecosystem exchange (NEE). Left: Histogram of flux "deviations" following the Hollinger *et al.* (2005) successive days approach. Also shown is the ∼66% confidence interval ($\pm 1\ \sigma$) below the histogram as a horizontal error bar. Right: Observed NEE plotted against corresponding differences between paired NEE observations.

flux uncertainty is represented by a constant absolute value (0.035 gC m^{-2} time step^{-1}, which corresponds to a daily cumulative flux uncertainty of 1.68 gC m^{-2} d^{-1}) as in Williams *et al.* (2005).

We found that a large amount of model uncertainty (20% on all modelled fluxes) is needed in order to satisfy the prerequisite of a unit *NRR*. With this model flux error, the observed NEE data points are almost entirely within the $\pm 1\ \sigma$ confidence interval of the model, whereas it is more desirable that this confidence range encompasses about 66% of the data. We decided to halve the uncertainty on modelled fluxes (i.e. to 10%, Table A.3). Now, model spread as described by the *NRR* is too low ($NRR = 1.22$), but we observe a better relationship between model confidence interval and observed NEE (Figure 4). Moreover, uncertainty on C stocks has to be much lower than on fluxes, as model uncertainty builds up relatively quickly due to the cumulative nature of the stocks. We chose to equally emphasize the impact of DA on C stocks, LAI, and parameters by setting model uncertainty for all to 0.1% per time step (Table 4.1, Table A.3). We used the same initial parameter values as shown in Sus *et al.* (2010).

We analysed the relationship between varying ensemble sizes (N) and the *RMSE* of

Table 4.1: Initial parameter values and model uncertainty. Also shown are the low/high bounds within which each parameter is allowed to vary. For each parameter, initial uncertainty was set to 5% of the allowed range.

Parameter	Description [unit]	Initial value	Low/high bounds	Model uncertainty ts^{-1} (d^{-1}) [%]
C_{la}	Leaf C per leaf area [gC m^{-2}]	19.5	15/25	0.1 (4.8)
f_{a}	Fraction of G respired [-]	0.44	0.3/0.5	0.1 (4.8)
T_{min}	Minimum temperature for development [°C]	0	-2/2	0.1 (4.8)
T_{opt}	Optimum temperature for development [°C]	24	22/26	0.1 (4.8)
T_{max}	Maximum temperature for development [°C]	35	33/37	0.1 (4.8)
PH_{cr}	Minimum (or critical) photoperiod for development [h]	8.25	7/9	0.1 (4.8)
PH_{sc}	Photoperiod sensitivity coefficient [-]	0.25	0.1/0.5	0.1 (4.8)
$r_{\mathrm{max,v}}$	Maximum development rate in vegetative phase [d^{-1}]	0.04	0.01/0.1	0.1 (4.8)
$r_{\mathrm{max,r}}$	Maximum development rate in reproductive phase [d^{-1}]	0.035	0.01/0.1	0.1 (4.8)

NEE for the ensemble mean (based on an estimated "truth" model run with N = 500). The *RMSE* of the ensemble mean drops considerably to lower levels for N = 50 (further increases in N lead to further, but gradual reductions). These results correspond to the observations made by de Wit and van Diepen (2007) and Reichle *et al.* (2002). In these studies, N values of 50 and 30, respectively, are considered to be sufficient for the estimation of the ensemble mean. Even though an ensemble size of 50 members seems sufficient, we chose an N of 100 in our DA modelling experiments as a safety margin.

4.2.5 DA experiments

DA experiments were conducted with the assimilation of only one single data type first (Table 4.2). Then, various combinations of observations were assimilated. Finally, forward run (*fwd*) and all data (NEE_{Biometry}) assimilation experiments were repeated, however initialised with posterior parameter estimates as derived from NEE_{Biometry}.

In doing so, we assessed posterior parameter quality by testing whether a forward run with posterior parameter estimates provides an improved estimation of C cycling (fwd_{post}). We further tested posterior parameter quality by analysing their temporal variability when all data are assimilated (DA_{post}). Parameter values stabilizing around their posterior estimates are assumed to be well defined by experiment NEE_{Biometry}.

4.3 Results

4.3.1 Daily and hourly C fluxes

SPAc was run on a half hourly time step for one entire winter wheat growing season (sowing to harvest 2005/2006) at the Klingenberg CarboEurope flux tower site. For the *fwd* run, the squared Pearson correlation coefficient R^2 (NEE observed vs. modelled) was 0.79, the Nash-Sutcliffe model efficiency E (see Wattenbach *et al.* (2010) for a definition) was 0.73, and the cumulative NEE value was -233 $\pm$ 91 gC m^{-2} (Figure 4.4 a)). Accordingly, C assimilation is overestimated by $\sim$35 gC m^{-2} in the *fwd* run compared with the cumulative NEE derived from the observations (-198 gC m^{-2}, Table 4.2), but within uncertainty limits. It is important to keep in mind that the observed cumulative NEE is a sum of observed (44%) and gap-filled (56%) values, thus has uncertainties also.

The *fwd* run data further show that SPAc is largely able to capture the seasonality and magnitude of net ecosystem exchange of C (Figure 4.4 a)), explaining 79% of the variability in observed NEE. Both observations and model data reflect prevailing meteorological conditions: an initial phase of low C assimilation (due to low irradiation) and respiration (low temperatures) rates in September-November 2005 is followed by a long period of nearly absent C exchange from December 2005-April 2006 (Figure 4.1, Figure 4.4). Observed crop germination and sprouting in autumn 2005 soon after sowing are well reproduced. Autumn daytime C uptake is still outweighed by mineralisation of litter and soil organic matter (SOM, Figure 4.1, Figure 4.4). Apparent is an earlier than

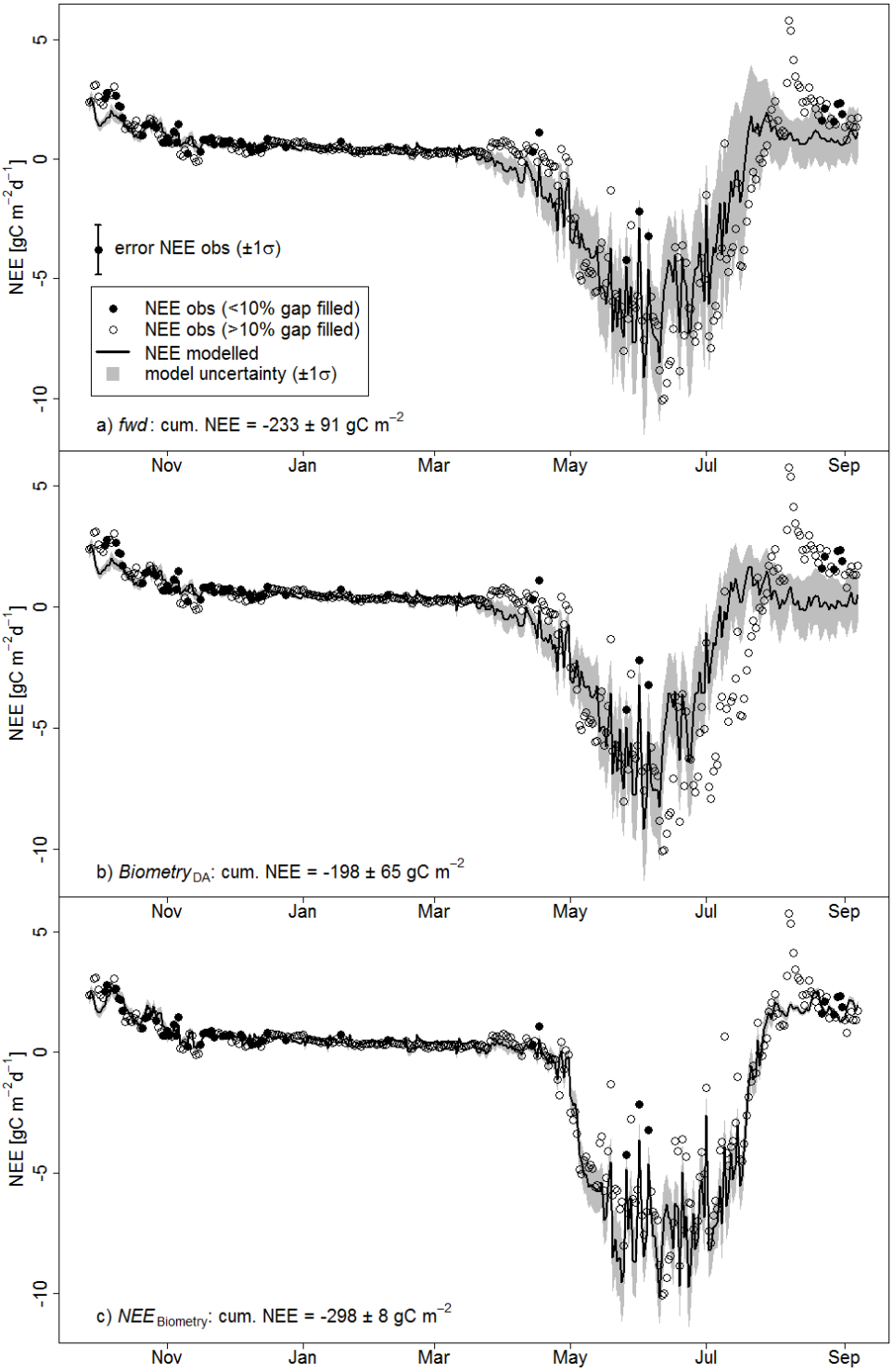

Figure 4.4: Modelled (line) and observed (open and closed circles) fluxes of net ecosystem exchange of C in gC m^{-2} d^{-1} for Klingenberg 2005-2006 and three different simulation scenarios (see legend and Table 4.2). Closed (open) circles represent daily NEE values containing less than 10% (more than 10%) gap-filled half-hourly estimates.

observed timing of the source-sink crossover point (low temperatures and snow cover in March/April were reported for Klingenberg in 2006) and premature senescence. SPAc generally underestimates the C sink strength in the daytime hours of early May, and more considerably from mid-June to mid-July (Figure 4.5). Phases of an overprediction of C assimilation occur in the early morning hours throughout the growing season, and during daytime in April and early to mid-June. Night-time respiration appears underestimated from mid-June to mid-July and from the beginning of August until harvest (Figure 4.5). Once the crop matured (∼early August), the sign of observed NEE changes and the ecosystem is a net source of C until harvest, which was delayed due to high rainfall in August. SPAc clearly underestimates NEE during this relatively short-lived respiration peak.

For experiment $Biometry_{\mathrm{DA}}$, the uncertainty in simulated cumulative NEE at harvest is reduced (from ±91 gC m^{-2} in the *fwd* run to ±65 gC m^{-2}), but R^2 (0.69) and E (0.51) decrease. The estimated C sink strength now closely matches the observed value. However, sink strength is underestimated by mid-June until sink-source crossover in August (Figure 4.4 b)). Model discrepancies in the *fwd* run such as the premature initiation of the peak growth phase and the underestimation of heterotrophic respiration in early August could not be resolved. Model uncertainty on cumulative NEE is clearly lowest for experiment NEE_{Biometry} (±8 gC m^{-2}, Figure 4.4 c)). Modelled and observed NEE correspond very well in their overall magnitude and seasonality ($R^2 = 0.95$, $E = 0.94$). Remaining model discrepancies are persistent in terms of a brief phase of daytime underestimation of C assimilation in mid-June and an overestimation of C assimilation around sunrise and during daytime in late May (data not shown).

For all experiments, night-time respiration is highest after sunset and lowest just before sunrise. This pattern is largely explainable by the way SPAc calculates autotrophic respiration (R_a). R_a is the result of the constant turnover of an autotrophic respiration pool (C_{aresp}). C_{aresp} receives all autotrophically respired C during daytime (∼55% of overall photosynthesis). C_{aresp}, and thus night-time R_a, are largest after sunset.

The impact of assimilated NEE is largest during daytime, when differences between

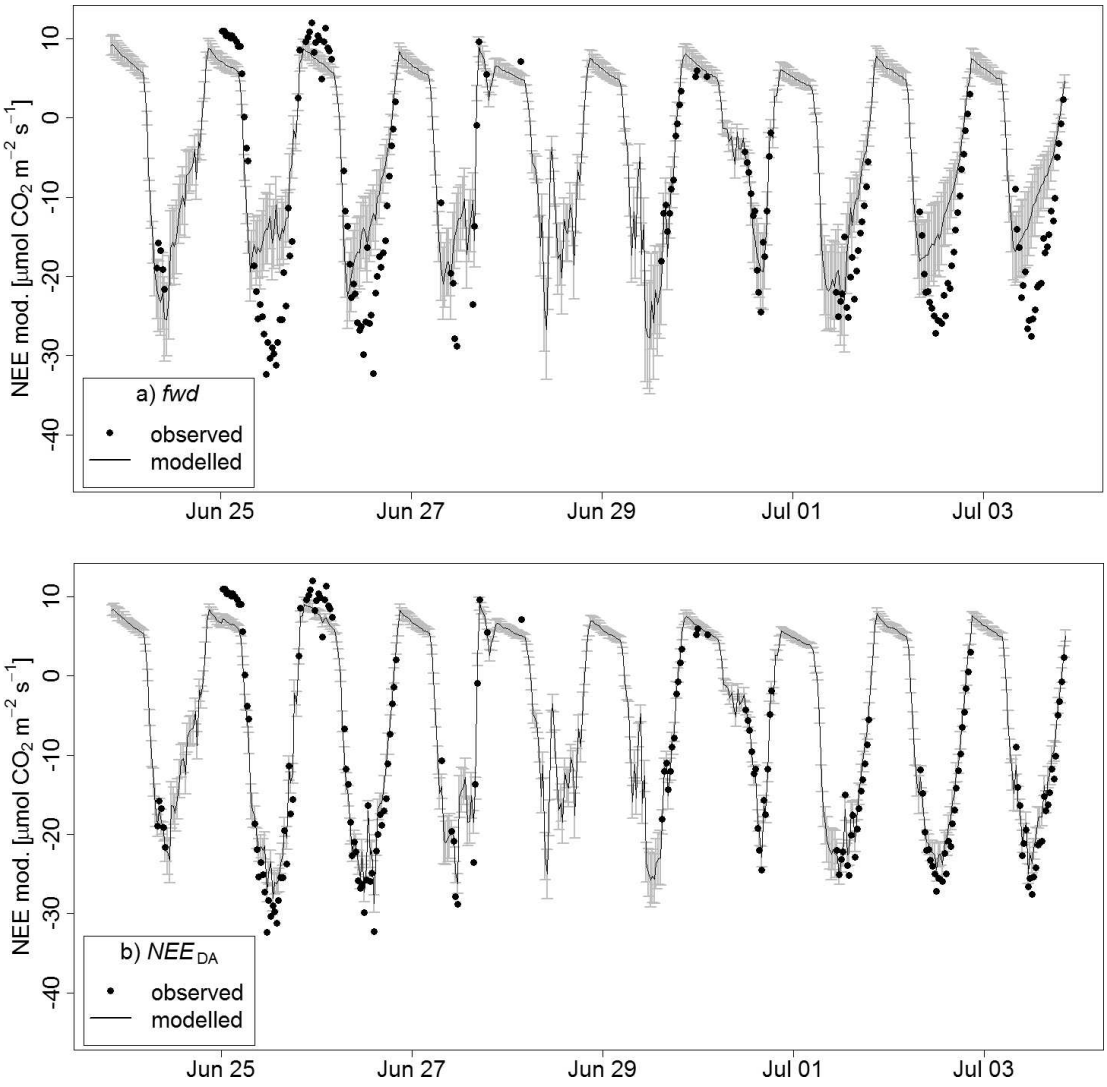

Figure 4.5: Half-hourly observed NEE and modelled NEE for experiments a) *fwd* and b) NEE_{DA}. The grey error bars indicate the ± 1 σ standard deviation.

observations and *fwd* model data are largest (e.g. June 25th and July 2nd in Figure 4.5) and more non-gap filled data are available. The DA update impact is especially large during the crop senescence phase beginning in June and lasting until early August (Figure 4.4 c)). During this phase, SPAc-simulated daily NEE is underestimated due to premature initiation of senescence. The EnKF analysis corrects for this deficiency at observational time steps. During longer data gaps (i.e. those lasting > 1 day), *fwd* and NEE_{DA} estimates are largely similar. The suppression of modelled photosynthesis due to relatively low irradiation values on June 30th compares well to observations (Figure 4.5 a)). These results show that model deficiencies during the late crop growing

phase from June to August are largely attributable to weaknesses in simulating the timing and magnitude of senescence.

The assimilation of C flux data improves daytime more than night-time estimates of C exchange (Figure 4.6). For daytime observations, the overall data fit is largely improved (*fwd* R^2 = 0.69, NEE_{DA} R^2 = 0.86) and residuals are reduced (*fwd RMSE* = 4.15 μmol CO_2 m^{-2} s^{-1}, NEE_{DA} *RMSE* = 2.82). We also find an improvement of the fit between night-time simulations and observations for NEE_{DA}, though this improvement is somewhat smaller (*fwd* R^2 = 0.63, NEE_{DA} R^2 = 0.73). Residuals are only slightly lowered (*fwd RMSE* = 1.23, NEE_{DA} *RMSE* = 1.09), and the slope of the linear fit remained largely unchanged. The study period sum of night-time flux residuals is 29.9 gC m^{-2} (*fwd*), and 28.4 gC m^{-2} (NEE_{DA}).

4.3.2 Cumulative NEE

Experiment *fwd* (-233 gC m^{-2}) overestimates observed at-harvest cumulative NEE (-198 gC m^{-2}), but model and measurements are in close agreement for experiment $Biometry_{\mathrm{DA}}$ (-198 gC m^{-2}, Table 4.2). Experiments Cr_{DA} and LAI_{DA} show highest at-harvest cumulative NEE (-120 gC m^{-2} and -129 gC m^{-2}, respectively). In contrast to that, experiment Cf_{DA} leads to a relatively small reduction in the sink strength (-183 gC m^{-2}), which is generally overestimated whenever NEE data are assimilated (from -263 gC m^{-2} to -309 gC m^{-2}). The temporal evolution of cumulative NEE for all model runs shows that the "measured" end value is additionally influenced by the late-season respiration event in early August (Figure 4.7). This causes a relatively rapid sign change in the observed NEE curve slope around late July. Even though the estimated timing of this sink-source crossover point is improved when NEE data are assimilated, the magnitude of this upward trend is not reproduced. The cumulative amount of C respired during this period is ∼90 gCm^{-2} (observed), and ∼33 gC m^{-2} (NEE_{DA}). This difference corresponds to ∼77% of the gap between observed at-harvest cumulative NEE and experiment NEE_{DA}. SPAc generally fails to reproduce this peak in C loss (Figure 4.4), independent of the amount and type of data assimilated. Prior

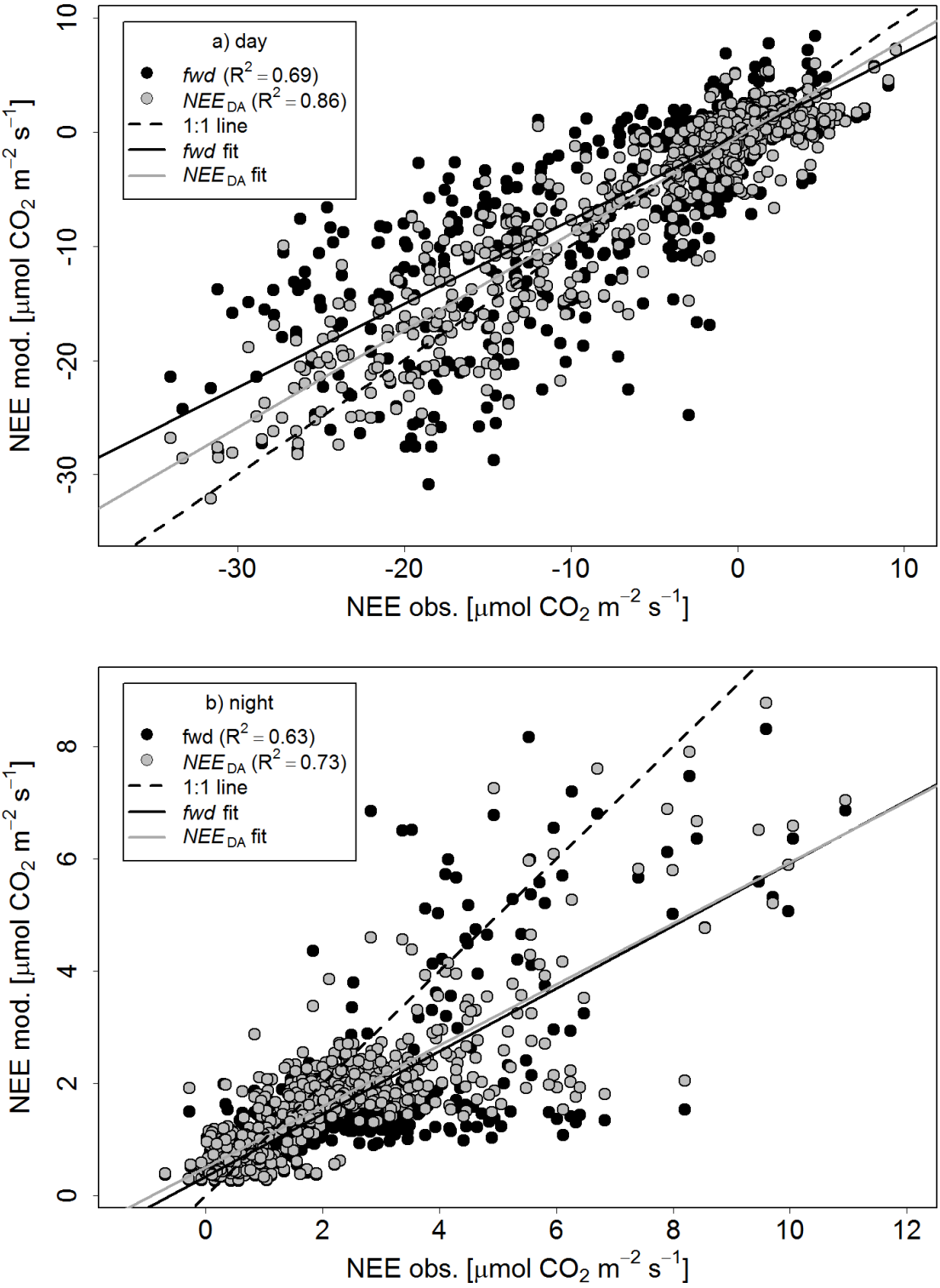

Figure 4.6: Daytime (top) and night-time (bottom) scatter plots of observed (x-axis) versus modelled (y-axis) NEE. Model data are shown for DA experiments *fwd* and NEE_{DA} together with corresponding linear fit lines.

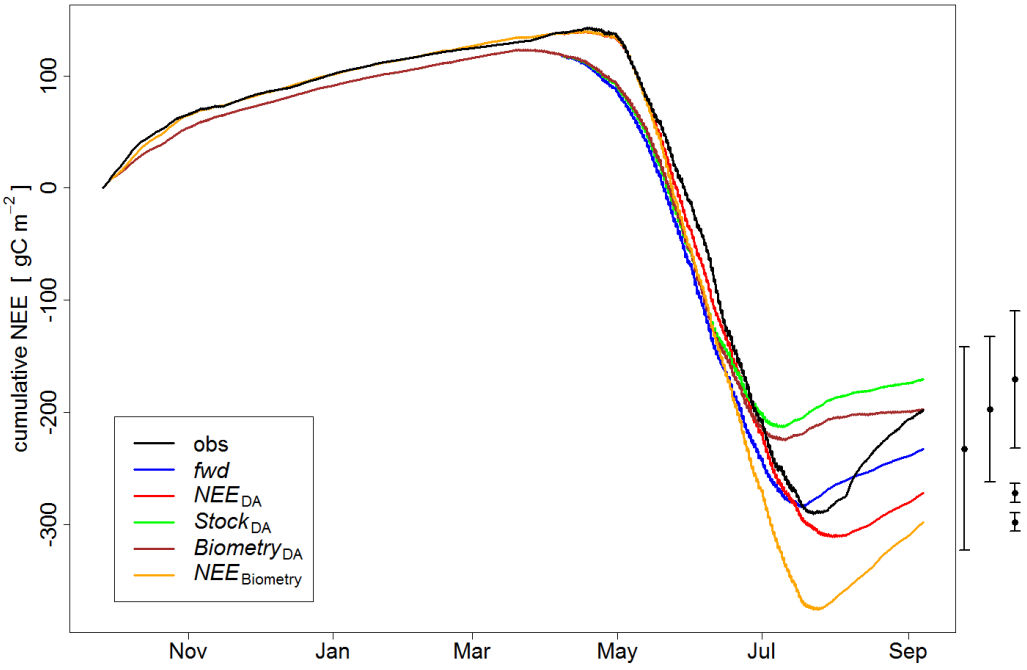

Figure 4.7: Cumulative NEE (from sowing to harvest) in gC m^{-2} for four DA experiments (see legend and Table 4.2), the forward run (*fwd*), and as derived from observations (obs). The ± 1 σ confidence interval on final simulated estimates of cumulative NEE are shown as error bars to the right of the plot.

to this respiration phase, experiment NEE_{DA} reproduces observations best. NEE_{DA} appears successful in improving early season crop C exchanges, but fails to do so after crop maturity. The assimilation of biometric data with or without LAI lowers pre-maturity sink strength. The agroecosystem turns into a weak source of C from early July until harvest. All non-NEE DA experiments underestimate R_e in the first weeks following sowing (related to deficiencies in estimated initial conditions in litter and SOM C and corresponding rates of decomposition and mineralisation), and are premature in predicting the start of the growing season.

The uncertainty on cumulative NEE is successively reduced the more data are assimilated (Figure 4.7). After the assimilation of stock (or +LAI) data, the resulting uncertainty is about half the uncertainty of the *fwd* experiment. Especially when NEE data are assimilated in any combination, uncertainty is largely reduced from ± 91 (*fwd*) to about ± 8 to ± 13 gC m^{-2} (Table 4.2).

4.3.3 Biometric data

The assimilation of NEE data was useful in constraining the C content of several crop organs, especially in conjunction with biometry DA (experiment NEE_{Biometry}, Figure 4.8). Compared to the *fwd* run, all aboveground biometric pools are improved by NEE_{DA} (data not shown). However, C_r is considerably higher than observed. As expected, assimilating all available biometric data ($Biometry_{\mathrm{DA}}$) leads to a considerably improved simulation of most C stocks. C_r is clearly reduced compared to the forward run, and C_{stor} is now within 4 gC m^{-2} of the observed value (300 gC m^{-2} at harvest). C_f is now smaller than observed during the senescence period, but LAI remains relatively close to measurements. For experiment NEE_{DA}, C_f is clearly reduced ($\sim$30 gC m^{-2} smaller peak value than in *fwd*), and C_r is considerably higher than observations and *fwd* data from late-June until harvest. Moreover, peak LAI is clearly reduced but overall remains close to observations. Final C_{stor} is overestimated by $\sim$50 gC m^{-2}.

For experiment NEE_{Biometry}, LAI and all stocks except for C_r are close to their observations. Under this DA scenario, SPAc provides the best estimate of final yield (298 ± 41 gC m^{-2}). Whenever NEE data are assimilated, modelled C stock and LAI estimates show high temporal variability. This pattern is likely to be related to state estimate adjustments in response to assimilated NEE data, indicating mass balance breaches. C_f and LAI appear more susceptible to these state adjustments due to higher cross-correlations with C flux estimates within the SV. We generally observe that the large amount of assimilated NEE data leads to a considerable reduction in model biometry uncertainty. Despite this reduction in uncertainty, observed biometric data are still able to constrain model state at observational time steps by constraining corresponding modelled pools (Figure 4.8, bottom row). The impact of assimilated NEE data clearly dominates, but adjustments through assimilated biometric data still have obvious effects on corresponding pools.

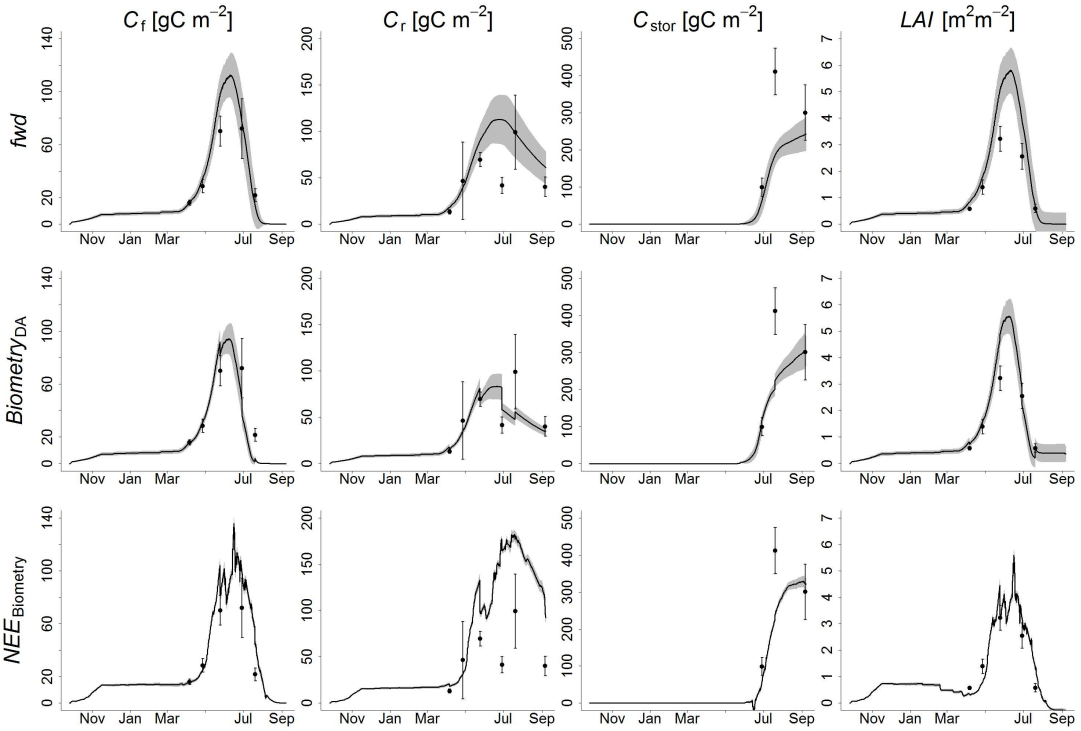

Figure 4.8: C stock time series of foliage, fine roots, and storage organ (columns 1 to 3), and time series of LAI (column 4). The $\pm 1\ \sigma$ confidence interval on the model mean (black solid line) is shown by the shaded grey area. Observations of C stocks and LAI are shown as points together with a $\pm 1\ \sigma$ measurement uncertainty as error bars. Time series are plotted for experiments *fwd* (row 1), $Biometry_{\mathrm{DA}}$ (row 2), and NEE_{Biometry} (row 3).

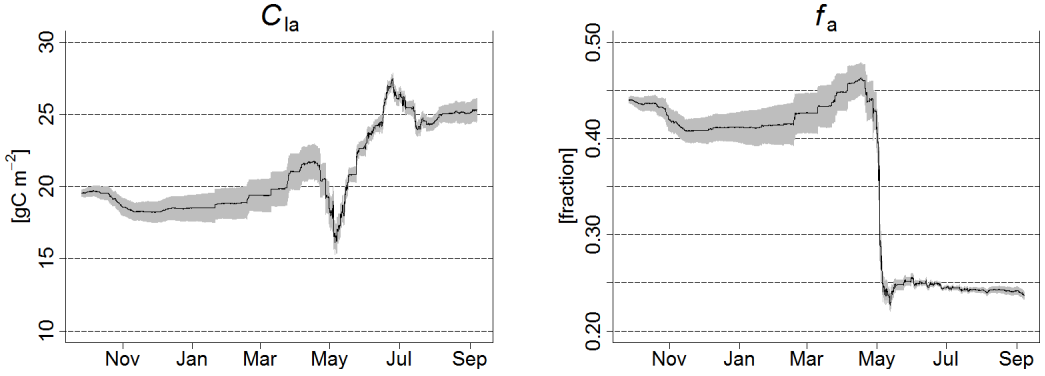

Figure 4.9: Temporal evolution of two out of nine parameters contained in the model state vector for experiment NEE_{Biometry}.

Table 4.2: Statistical summary of model experiments with different data types assimilated.

DA experiment name	Data assimilated	*RMSE*	R^2	*E*	slope	intercept	NEE_{cum} (obs: -198)	Yield (obs: 300)
1. *fwd* (prior *fwd* run)	./.	0.064	0.79	0.73	1.01	0.001	-233 ± 91	243 ± 45
2. NEE_{DA}	NEE	0.032	0.95	0.94	1.06	0.006	-272 ± 8	352 ± 11
3. Cf_{DA}	C_f	0.068	0.76	0.64	1.07	-0.002	-183 ± 77	219 ± 40
4. Cr_{DA}	C_r	0.081	0.67	0.4	1.09	-0.008	-120 ± 60	195 ± 33
5. Cs_{DA}	C_s	0.074	0.72	0.63	0.96	-0.004	-189 ± 73	255 ± 43
6. $Cstor_{\mathrm{DA}}$	C_{stor}	0.066	0.78	0.7	1.02	0.002	-235 ± 92	304 ± 45
7. LAI_{DA}	LAI	0.074	0.74	0.48	1.18	-0.006	-129 ± 58	196 ± 27
8. $Stock_{\mathrm{DA}}$	3 to 6	0.079	0.69	0.47	1.07	-0.003	-171 ± 61	283 ± 38
9. $Biometry_{\mathrm{DA}}$	3 to 7	0.078	0.69	0.51	1.05	-0.001	-198 ± 65	304 ± 41
10. NEE_{LAI}	2+7	0.031	0.95	0.94	1.06	0.005	-263 ± 12	345 ± 14
11. NEE_{Stock}	2+8	0.032	0.95	0.94	1.07	0.006	-309 ± 13	404 ± 17
12. NEE_{Biometry}	2+9	0.032	0.95	0.94	1.04	0.002	-298 ± 8	322 ± 15
13. fwd_{post} (posterior *fwd* run)	./.	0.096	0.74	0.7	0.69	0.016	-703 ± 109	530 ± 78
14. DA_{post} (posterior NEE_{Biometry} run)	2+9	0.032	0.94	0.94	1.05	0.004	-299 ± 10	370 ± 17

4.3.4 Parameter evolution - prior initials

For experiment NEE_{Biometry}, general observations are that 1) parameters are showing trends in their temporal evolution towards a new value, 2) there is evidence for a seasonal variation of C_{la}, and 3) parameter uncertainty is reduced during the peak growth phase after thawing of all soil layers by early April and during periods of model sensitivity for specific parameters (Figure 4.9). C_{la} first decreases to about 16 gC m^{-2} around early May, then rises to ∼27.5 gC m^{-2} before senescence, and falls again to ∼25 gC m^{-2} around harvest. This simulation corresponds to the growth of thinner leaves of the young crop plant, whilst leaf growth becomes more C expensive as the crop matures. With the end of leaf C allocation around early July, parameter uncertainty begins to gradually increase. Parameter f_{a} decreases throughout the growing season, leading to an increased availability of assimilated carbohydrates for growth. A ∼0.2 drop occurs over a relatively short time period in early May, and f_{a} remains at ∼0.25 until harvest (Figure 4.9). Compared to the initial f_{a} value (0.44), the crop now only respires ∼25% of C gained and is thus more productive.

Parameter r_{max} is relatively close to its initial value before flowering ($r_{\text{max,v}}$, prior: 0.04, posterior: 0.037), but is clearly reduced by DA during the reproductive phase ($r_{\text{max,r}}$, prior: 0.035, posterior: ∼0.02, temporal variability of developmental parameters not shown). This translates into a shortening of the reproductive period, which is dominated by storage organ growth. The increase in PH_{sc} from 0.25 to 0.3 increases the seasonal amplitude of *f(P)*, which now delays development more strongly at short daylengths. As PH_{cr} is reduced (prior: 8.25, posterior: 7.6), the overall range of daylengths allowing for development increases, which has the general effect of accelerating crop development. Finally, temporal trends in the cardinal temperatures of development are obvious. T_{min} appears well constrained and approaches a new value of ∼-1.7 °C before senescence. The temporal evolution of parameter T_{opt} suggests that prior and posterior values are in close agreement, even though temporal variability exists. T_{max} rises considerably and is close to 39 °C. For all model experiments with NEE DA, there were similar trends in parameter behaviour (data not shown), however with varying magnitude. Most obvious

Table 4.3: Prior and posterior (as estimated by DA experiment NEE_{Biometry}) values of model parameters.

Parameter	C_{la}	f_{a}	T_{min}	T_{opt}	T_{max}	PH_{cr}	PH_{sc}	$r_{\mathrm{max,v}}$	$r_{\mathrm{max,r}}$
Prior	19.5	0.44	0	24	35	8.25	0.25	0.04	0.035
Posterior	16	0.25	-1.7	24	38.7	7.6	0.3	0.04	0.02

is a temporal variability in C_{la} and the prior overestimation of f_{a}. Due to their temporal scarcity, biometric data provide no clear parameter constraints. Model sensitivity for all parameters analysed is greatest during the peak growth season from May to July, whilst parameter uncertainty increases during the autumn and winter months after sowing and after crop senescence in the weeks before harvest.

4.3.5 Parameter evolution - posterior initials

SPAc was driven with posterior parameter values as derived from experiment NEE_{Biometry} (Table 4.3) in order to examine whether parameter values stabilise around derived posterior estimates (experiment DA_{post}, data not shown). Compared to experiment NEE_{Biometry}, C_{la} shows the same pattern of initial low values in the early season (growth of thinner leaves) and rises throughout the growing period until before senescence, when it stabilises around 21 gC m^{-2}. However, this rise is lower than in experiment NEE_{Biometry}, where pre-senescence C_{la} is $\sim$27.5 gC m^{-2} (Figure 4.9). Parameters f_{a}, T_{min}, and $r_{\mathrm{max,r}}$ clearly stabilise around their corresponding posterior values. The photoperiod parameters (PH_{cr}, PH_{sc}) exhibit seasonal variability, but their final values at flowering (DS = 1) are close to the initial estimate. T_{max} is the parameter with largest variability. It shows a clear trend towards higher values and is finally edge-hitting ($\sim$42 °C) by late June.

The *fwd* run driven with the posterior parameter values (fwd_{post}, Table 4.3) clearly shows though that modelled NEE is now considerably underestimated during the vegetative phase of crop growth (Table 4.2). The magnitude of peak daily C uptake is clearly higher ($\sim$-13 gC m^{-2} compared to $\sim$-10 gC m^{-2} observed), and the timing of the source-sink crossover is about a month premature. At-harvest cumulative NEE is

$\sim$-703 gC m^{-2}, which corresponds to an overestimation of the sink strength by $\sim$500 gC m^{-2}. Because the same model state and parameter perturbation values were used as for experiment *fwd*, model uncertainty for cumulative NEE are comparable for experiments fwd_{post} and *fwd*. However, correlation statistics are only slightly lowered ($R^2 = 0.74$, $E = 0.70$), and the *RMSE* rises from 0.064 gC m^{-2} to 0.096 gC m^{-2}. Overall, the ecosystem is much more productive than observed, and the timing and magnitude of C exchange are of lower quality compared to experiment *fwd*. These results indicate structural model deficiencies. There is evidence that temporally varying parameters improve on model performance, thus underlying processes explaining this variability are not captured within SPAc. Consequently, posterior parameter values (especially for f_{a}) are not applicable to the entire crop developmental process.

4.4 Discussion

4.4.1 Does the assimilation of NEE observations improve modelled biometry?

We find that the assimilation of NEE data improves the state estimate of most biometric variables. This improvement is most obvious for C_{f} and LAI, two SV which are directly associated with the photosynthetic capacity of the ecosystem. It is due to this direct link that NEE data have high information content on aboveground green biomass, as daytime C fluxes are dominated by GPP. As forward modelled C_{f} and LAI follow rather gradually changing patterns of growth and decline, rapid temporal changes in these two pools are associated with mass balance breaches in the EnKF, i.e. these two pools absorb daytime NEE information and noise on photosynthesis.

For experiment NEE_{DA}, C_{f} and LAI are considerably lower than in the *fwd* run. The flux data constrain timing and magnitude of growth and decay of C_{f}, with this constraint being largest during peak-season (mid-May to early July). For this period, NEE data show relatively high day-to-day variability but appear to fluctuate

around a mean level. The flux data suggest that the peak-season average magnitude of photosynthetic capacity has a broad plateau, rather than a narrow peak as seen in *fwd* data. C_f is adjusted accordingly and fluctuates around a mean level of ∼80 gC m^{-2} during this period, but model and observational data are still within close agreement. In fact, the biometric data allow the interpretation that both patterns of growth and decay of photosynthetic biomass (broad plateau vs. narrow peak) appear plausible, as measurements during this period are sparse. Overall, the C flux data suggest that SPAc might trigger senescence too early. NEE_DA indicates that C_f and LAI should remain rather constant during a pre-senescence plateau period (as in Gervois *et al.* (2004)).

The effect of NEE_DA on C_s and C_stor is less considerable. Both C pools begin to grow at a later crop developmental stage, and exhibit no control on plant physiology (which could be introduced through mechanistic modelling of C partitioning dynamics (Minchin, 2007) and through stem photosynthesis (Aubinet *et al.*, 2009)). Nonetheless, C_s and C_stor are closer to observations after DA, suggesting that NEE data indirectly constrain these two variables through state vector interconnections.

C_r overestimation through NEE_DA largely coincides with periods of underestimated model C assimilation. This is somewhat surprising, as we assume synchronized growth of C_f and C_r (Baret *et al.*, 1992), conserving the shoot:root ratio. Instead, as C_f is lowered and C_r rises with NEE_DA, the belowground partitioning coefficient might be underestimated. C_r is a strong control on root water uptake and overall plant water status. Thus, it is possible that the EnKF analysis successively increases C_r (and thus lowers the shoot:root ratio, *fwd* = 7.3, NEE_DA = 6.6 at maturity) as a response to the lowered C assimilation capacity due to reduced C_f. A lower shoot:root ratio reduces the detrimental effect of water limitations on stomatal opening and photosynthesis, and thus partly balances the decrease in photosynthetic C uptake potential. In fact, stomatal conductance is larger during July (the driest month, Figure 4.2) for experiment NEE_DA than *fwd* (data not shown). As C partitioning is a dynamic process adjusting to environmental conditions (Minchin, 2007), it is reasonable that actual root partitioning could have been favoured in response to suboptimal water supply (Lambers *et al.*, 1995) or nutrient deficiency (Amos and Walters, 2006).

Further, observed C_r does not represent the total amount of C partitioned to roots, as C loss through root exudates and sloughed-off material is not accounted for (40% to 45% of total allocated root C, Buyanovsky and Wagner (1987)). As experiment $Biometry_{DA}$ suggests (Figure 4.8), SPAc potentially underestimates fine root water uptake and transport, or, in other words, overestimates plant drought stress given realistic state estimates of C_r (considerably lowered in $Biometry_{DA}$ compared to *fwd* run) and LAI.

4.4.2 Why is ecosystem C sink strength underestimated with assimilated biometry?

With assimilated biometry, the fit between modelled and observed NEE is of lower quality. Even though the at-harvest cumulative NEE is closest to the observational value, C assimilation during the peak growth phase, and especially during the reproductive period, is largely reduced. Except for C_{stor}, the assimilation of biometric data clearly reduces the C sink strength (with this reduction being largest for experiments Cr_{DA} and LAI_{DA}, Table 4.2).

The impact of the assimilation of C_r data is generally twofold. Firstly, because C_r appears overestimated in experiment *fwd* (but note that root exudation and sloughing-off (Grayston *et al.*, 1997) are not captured by observations), the assimilation procedure directly reduces C_r and thus exacerbates the impact of drought stress on stomatal opening and photosynthetic potential as discussed above. Secondly, we find that C_r and C_f are positively correlated within the state vector, so responses to Cr_{DA} are synchronized. As forward modelled C_r generally appears to be an overestimate, the DA procedure not only reduces C_r, but also C_f and LAI (most obvious by end-June) and thus photosynthetic potential. Measurements of C_r are particularly labour intensive and prone to high uncertainties, which are reflected as large standard deviations in the observational data (Figure 4.8). Thus, DA experiments with C_r data are to be assessed with caution, bearing in mind that the observational evidence might be less certain than for other crop organs.

Similarly, assimilated LAI data clearly reduce C sink strength. When assuming that LAI measurements are not negatively biased, the evidence is strong that SPAc is not able to reproduce observed carbon exchange fluxes under realistic foliar biomass values. This indicates that SPAc might be deficient in not accounting for photosynthesis of green crop organs other than leaves. According to Penning de Vries *et al.* (1989), non-leaf photosynthesis is often of second order importance and can be disregarded, but might be relevant for young crop plants. Hoyaux *et al.* (2008) found that observed GPP of a winter wheat crop was best reproduced when accounting for stem photosynthesis, with a stem photosynthetic capacity of 63% of that of leaves. The authors conclude that accounting for non-leaf green area is critical for scaling wheat C assimilation from the leaf to canopy scale. Broge and Mortensen (2002) find that up to 25% of the total green area of a winter wheat crop can be represented by stems prior to heading, and this fraction further increases during senescence. LAI data at Klingenberg were collected through destructive leaf sampling and areameter measurements (Marga Wartinger, *personal communication*). Projected stem area data were not assimilated, and these show that stem area index (SAI) is as low as ∼14% of LAI in the vegetative growth phase, but SAI is considerably higher than LAI during crop senescence (e.g. $>$ 200% of LAI at the 19th of July, data not shown). Because measured LAI underestimates canopy green area, the assimilation leads to an underestimation of photosynthetically active plant surface and thus total C assimilation capacity, with this underestimation being largest in the senescence phase (Figure 4.4 b)).

4.4.3 Parameter estimation and temporal evolution under the "all data" experiment

We generally find that not all parameters are equally well constrained by the assimilation of observational data. For experiment DA_{post}, we find that some parameters exhibit clear temporal variability, while others tend to stabilise around their initial values. Constraints appear to be stronger for C_{la} and f_{a} than for developmental parameters.

For both NEE_{Biometry} and DA_{post}, we find strong evidence of a temporal variability in C_{la}, a parameter with high model sensitivity (Sus *et al.*, 2010; Ceglar *et al.*, 2011). That C_{la} increases with advancing crop development is a plausible process, which has been reported in the literature (Birch *et al.*, 1999; Penning de Vries *et al.*, 1989). Penning de Vries *et al.* (1989) find that with a temporally varying C_{la} value the development of leaf area is more realistically approximated, as low C_{la} at the beginning of leaf growth speeds up the development of leaf area. They assume that C_{la} rises by up to 50% during the growing season relative to its base value. Our findings confirm that wheat (and probably cereals in general) crop models benefit from accounting for temporal variability in C_{la}.

There is strong evidence that the initial guess of f_{a} (0.44) was too high for the entire growth period. The winter wheat crop appears to utilize a considerably higher fraction of photosynthesised C for growth. Estimates of f_{a} for winter wheat range between 0.3 to 0.6 (Amthor, 2000; Gifford, 1995; Aubinet *et al.*, 2009). Suleau *et al.* (2011) found an overall f_{a} of 0.45 for winter wheat, however there was no evidence for a constant ratio between R_a and GPP, as respiration responses to GPP were assumed to be dependent of developmental stage. Aubinet (2008) found a mean $f_{\text{a}} = 0.3$ for three crop types (including two winter wheat seasons), which remained fairly constant over the growing season but increased during senescence. This late season f_{a} increase appears to be a wheat (probably cereal) specific phenomenon, and is assumed to be related to processes such as dough development (Aubinet, 2008), C translocation, and grain growth (Amthor, 2000). Several studies suggest that the ratio between plant respiration and photosynthesis (R/P) is conservative over a wide array of plant ages, sizes, growth rates, CO_2 concentrations, and temperatures (Gifford, 2003) and varies between 0.3 to 0.6 (Amthor, 2000; Gifford, 2003) or within an even narrower range of 0.4 to 0.5 (Thornley, 2011). Only drastic destructive events (such as canopy removal through grazing or tree felling) can push this ratio outside the aforementioned range (Gifford, 2003). For most higher plants, the absolute R/P minimum is a result of various respiration-intensive processes, such as growth costs (R/P = 0.15–0.20), soil ion uptake, phloem transport, N assimilation (R/P increased to about 0.20–0.30),

and structure maintenance (raising long-term R/P to 0.30–0.40). A maximum R/P of >0.75–0.85 appears implausible considering the evolutionary history of higher plants (Amthor, 2000). Our final derived estimate of $f_{\mathrm{a}} = 0.25$ is below the range of usual reported values and the conservative minimum. Accordingly, this posterior value cannot be regarded as a robustly calibrated estimate of ratio R/P, but is rather an expression of model deficiency in reproducing productivity under given constraints on photosynthetic biomass and C flux exchange. Experiment fwd_{post} also suggests that $f_{\mathrm{a}} = 0.25$ is an underestimate. The winter wheat crop now clearly appears to be too productive (Table 4.2), indicating that posterior parameter values (especially for f_{a}) are not applicable to the entire life-cycle of the crop. For some parameters, temporal variability improves model performance, so SPAc needs to account for additional processes that are reflected in this parameter behaviour. The studies above (Suleau *et al.*, 2011; Aubinet, 2008; Amthor, 2000) suggest that f_{a} varies with DS, and in particular the question of how late-season processes associated with yield formation affect R_a needs improved assessment. The distribution of leaf area over various canopy layers could be simulated as a function of DS, and each canopy layer could be associated with a specific C_{la}. However, low temperatures until mid-spring might have caused frost damage in the winter crop, which could then explain the observed delay and dampening of the ecosystem's C assimilation phase. In another SPAc crop modelling study (Sus *et al.*, 2010), the Klingenberg flux data were found to temporally lag behind modelled estimates of C exchange, whereas the timing of peak C assimilation of eight other study periods (from four other CarboEurope sites) was estimated with much better accuracy.

The posterior estimates of developmental parameters generally cause an accelerated vegetative crop development in experiment fwd_{post} (anthesis (DS = 1) advanced by 23 days), implying that the phase of leaf and root C allocation in experiment *fwd* might be too long. The timing of senescence, which is largely controlled by DS in SPAc (but see Yin *et al.* (2000) for a leaf N driven crop senescence model), appears well estimated by fwd_{post} (data not shown). However, for some developmental parameters there is considerable seasonal variability in experiment DA_{post} (data not shown).

Nonetheless, posterior estimates of developmental parameters remain within plausible limits. For instance, values of $r_{\mathrm{max,v}}$ (ranging between 0.029 to 0.035 d^{-1} for various cultivars), PH_{SC} (0.16 to 0.34 h^{-1}) and PH_{CR} (7.0 to 9.5 h) were found to be cultivar dependent (Xue *et al.*, 2004). Modelled seasonal parameter variability stays close to these literature values even though allowable a priori parameter space is considerably wider. Moreover, *f(T)* and *f(P)* are known to interact, e.g. the more delaying *f(P)*, the narrower the temperature range allowing for development (Yan and Wallace, 1998). This could explain why assimilation experiments NEE_{Biometry} and DA_{post} are not reproducing equal parameter behaviour. The altered posterior photoperiodic parameters (Table 4.3) might have pushed the cardinal temperatures in a new regime, or vice versa.

A literature review by Porter and Gawith (1999) provided that wheat temperature sensitivity changes during the course of crop development, and cultivar differences can be as large as 35%. Wheat development was found to be less sensitive to temperature during its vegetative phase, and cardinal temperatures are highest during grain-filling. We find evidence that cardinal temperatures rise with crop development (data not shown), but end season estimates of T_{opt} (24 °C) and T_{max} (38.7 °C) are higher than mean values reported by Porter and Gawith (1999) (20.7 °C and 35.4 °C, respectively). T_{min} (-1.7 °C) is generally lower than literature values, and also shows no seasonal variability (T_{min} rises from 1.5 to 9.5 °C in Porter and Gawith (1999)). Wang and Engel (1998) assume that T_{min} is rather constant throughout development (0 °C), and they expect T_{opt} and T_{max} to be 5 °C higher during the reproductive phase. A Bayesian calibration of cardinal temperatures for maize yielded maturity values for T_{opt} (24.8 °C) and T_{max} (39.0 °C, Ceglar *et al.* (2011)) comparable to our estimates. Generally speaking, our NEE_{Biometry} estimates of cardinal temperatures appear plausible, but we suspect that the overall temperature range is overestimated. Published values have to be assessed with caution though, as they are attained under specific environmental conditions (field or laboratory, daylength and temperature regimes, Slafer and Rawson (1994)), or derived from or formulated for differing phenological model concepts.

Our general observation that developmental parameters are not as well constrained as structural vegetation parameters (i.e. C_{la} and f_{a}) corresponds to the findings of Stöckli *et al.* (2008). Using the EnKF, they assimilated MODIS (Moderate Resolution Imaging Spectroradiometer) data into a global phenology model, and concluded that vegetation parameters are more explicitly related to the assimilated data than phenological states, which are an implicit part of the phenology model. Similarly, we find that EC NEE data more explicitly constrain structural vegetation parameters (C_{la} and f_{a}), and that developmental parameters are rather implicitly reflected in measurements (modelled DS remains to be physiologically integrated, Weixing *et al.* (2002)). Moreover, an improved estimation of DS would improve the timing of shifts in C allocation and senescence, but the allocation parameters themselves still remain unaltered. A general weakness of generalized crop C mass balance models is the lack of a mechanistic representation of C partitioning (see Marcelis and Heuvelink (2007) for alternatives). C allocation is the result of plant growth and development, and not their driver (Minchin, 2007).

4.4.4 Why are assimilated nocturnal and post-senescence C fluxes not improving model estimates?

The EnKF analysis weights observations and model data according to their relative uncertainties. The larger the uncertainty in an observation compared to its corresponding model estimate, the lower the magnitude of the analysis update. We find that model uncertainty on nocturnal NEE fluxes (then $\mathrm{R}_a + \mathrm{R}_h$) is considerably lower than during daytime (Figure 4.6). On the other hand, our estimate of measurement uncertainty is a constant value day and night (1.6 μmol m^{-2} s^{-1}). As a result of that, the EnKF analysis weights nocturnal model estimates more than during daytime.

Night-time R_e of a wheat crop was found to be independent of canopy temperature before heading, but sensitive to temperature thereafter (Baldocchi, 1994). Accordingly, model underestimation of R_e might be related to a lack of mechanical understanding

of how crop senescence affects R_a. Kucharik and Twine (2007) identified a night-time underestimation of observed R_e by 50% during the growing season of a maize-soybean rotation. The authors assume that model deficiencies are not primarily a result of neglecting residue dynamics, but rather result from fundamental shortcomings in model formulation and parameterisation, and in particular of soil respiration. However, the mineralization flux of fresh crop residues is significant, supplying 70% to 75% of total respiration in the first weeks once available (Buyanovsky and Wagner, 1987). We conclude that experiment NEE_{DA} is a powerful tool for constraining daytime C fluxes, but poorly constrains underestimated night-time R_e. In agreement with Kucharik and Twine (2007), we assume that structural and parametral model deficiencies are responsible for this underestimation, and key parameters need to be incorporated into the state vector for an improved diagnosis and state estimation. NEE flux data provide no sufficient constraints for state estimation of C_{SOM} and C_{lit}.

The EnKF fails to improve the reproduction of observed post-senescence C fluxes (model R_h only, as the wheat crop has already matured). Any assimilated NEE observations during this post-senescence phase until harvest have no considerable impact on model data, as 1) model uncertainty on respiration-only C fluxes is relatively low, 2) no parameters constraining heterotrophic respiration are contained in the state vector, and 3) EnKF changes in SOM and litter C pools are not sufficient to compensate the underestimation of heterotrophic respiration fluxes. Heterotrophic respiration is strongly dependant on the amount of available organic matter and soil temperature sensitivity (Q_{10}). Determining appropriate mineralisation and decomposition rates is confounded by land management through soil mixing, physical disruption of aggregates, aeration (Arevalo *et al.*, 2010), and the previous year's soil C input (Anthoni *et al.*, 2004).

Deficiencies in simulating the agroecosystem respiration flux appear to be a common feature of current crop C budget models, and might be related to shortcomings in modelling developmental phases and not considering all relevant land management actions (Wattenbach *et al.*, 2010). To improve our understanding of agroecosystem C cycling, we need to know more about SOM dynamics (Anthoni *et al.*, 2004). At

Klingenberg, the effects of mechanical treatment of the top soil layers through harvest and fertiliser machinery have not been analysed, however increased respiration rates after management are expected (Prescher *et al.*, 2010). In its current formulation, SPAc does not account for land management effects on heterotrophic respiration rates, but our results suggest that this is warranted.

4.4.5 Methodological difficulties and needs for further research

The poor temporal resolution of biometric data clearly reduces their potential for constraining important model parameters. An annual crop plant is relatively short lived and characterised by rapid changes in parameter values. The winter wheat crop analysed here is largely dependent on its internal developmental "clock", which informs about shifts in allocation and leaf growth strategies in order to maximise leaf area and yield within one single growing season. Biometric data need to be frequently measured in order to capture this rapidly varying behaviour, which clearly differs from more long-lived, perennial plant functional types which have to balance short-term gains in photosynthates and biomass growth with long-term survivability. A potential way forward is to interpolate between observational values and create a gap-filled biometric measurement record. The selection of an appropriate interpolation method would be based on the assumption that the growth and decline of crop biomass are gradual processes with smooth temporal shifts, such as provided by spline or shape-preserving "upper-envelope" interpolation methods. Generalised interpolation functions could also be derived from crop model biometry data outputs.

In this study, the 7,292 NEE observations clearly outnumber the total of 22 biometric measurements and thus dominate any multiple-constraints DA experiment. With a temporally highly resolved biometric data record, C allocation fractions could be directly constrained in a DA experiment. NEE data probably contain valuable information on the approximate duration of leaf and root growth, the root:shoot ratio, and senescence rate. However, NEE data provide low constraints on C partitioning to stems and storage organs, as these have no physiological meaning within SPAc.

Because of their first order importance, parameters controlling plant hydraulics need improved calibration before NEE_{DA} can unfold its supposable potential on constraining partitioning coefficients. An alternative way of constraining simulated biometry with temporally highly resolved observations is the assimilation of remotely sensed data with appropriate spatio-temporal sensor resolution. MODIS 250 m VI data have been used within crop classification and assimilation studies (Wardlow and Egbert, 2008; Doraiswamy *et al.*, 2004), where they were found suitable as crop type specific green canopy area constraints. Their assimilation allows for upscaling crop C cycle studies in space and time, which largely improves our assessment of cropland C flux seasonality. MODIS data bear the potential to compensate for the lack of knowledge about regional land management patterns, to inform about unforeseen disturbance events (e.g. droughts, frost damage, pest infestation), and to improve simulated crop growth and development when their model representation is deficient.

In general, a complicating factor for parameter estimation is ensemble spread collapse (Stöckli *et al.*, 2008). The only source of parameter variance is the a priori defined additive noise perturbation, here $\sim$5% d^{-1} (Table 4.1). We find evidence that parameter ensemble spread may be too low considering the large amount of NEE data samples assimilated (Figure 4.9), so that observations have progressively smaller impact. Parameter ensemble spread is known to be reduced by spurious correlations between a predicted measurement and a variable. This will lead to a small nonphysical update of the variable in concern. This problem is ubiquitous in EnKF applications and can lead to filter divergence (Evensen, 2009). In a synthetic simulation experiment, Evensen (2009) found that ensemble variance of 100 ensemble members only stabilised after 50 analysis timesteps, however at $\sim$60% of the initial estimate. This means that spurious correlations, however small they may be, can have a considerable cumulative effect on any parameter estimation exercise with the EnKF, so that covariance inflation methods need to be considered for enhanced trustability of derived results. Kernel perturbation methods exist that guarantee that parameter ensemble variance is kept above a pre-defined threshold by variance scaling, but without altering the shape of the ensemble distribution (Stöckli *et al.*, 2008; Moradkhani *et al.*, 2005). There is

so far no consensus on the methodology best applied in this context: it can be a simple inflation factor (which scales the deviation of each individual parameter sample from the ensemble mean, typically inflated by ∼1%, Evensen (2009)), a conditional covariance inflation (ensemble spread is inflated back to a minimum value, e.g. defined as 25% of initial variance, Aksoy *et al.* (2005)), kernel smoothing of parameter samples (Chen *et al.*, 2008), or a covariance inflation which is proportional to the variance reduction due to spurious correlations, which can be quantified with an independent (i.e. not model driven) ensemble (Evensen, 2009). As we did not correct for parameter ensemble spread collapse in this study, we acknowledge that parameter evolution is affected by the aforementioned processes. When ensemble variance is reduced, the EnKF analysis puts more weight on model values, with the consequence that parameters are less sensitive to the model update when assimilating observations. In other words, we underestimate potential parameter variability. Clearly, posterior parameter values should be considered with caution, and should not be regarded as a result of robust model calibration. Instead, they reveal structural model shortcomings and calibration uncertainties, highlighting further needs of model improvement.

The robust estimation of uncertainties, both in measurements and model, is key to the success of any DA study (Keenan *et al.*, 2011). According to Raupach *et al.* (2005), results reached without an explicit consideration of uncertainty might as well not have been reached at all. However, most DA studies are not explicitly (if at all) describing how uncertainty measures have been quantified (Keenan *et al.*, 2011). This is probably because DA in ecosystem ecology is still in the infant stage, even though gradually becoming a more active research subject (Luo *et al.*, 2009). Only recently, a code of best-practice has been published, which outlines the various steps necessary for more robust, comparable, and detailed descriptions of DA studies (Keenan *et al.*, 2011). In our study, measurement uncertainties were clearly defined for biometric field data by site PIs (in standard deviations derived from repeated destructive measurements of crop organs), but we had to approximate the error in EC flux data by means of the Hollinger *et al.* (2005) "paired observations" approach. Despite of the heteroscedastic nature of flux data uncertainty, we chose the absolute value of measurement error to

be independent of the instantaneous flux magnitude. In doing so, the uncertainty on low fluxes (e.g. at night-time) is possibly overestimated, and underestimated for high fluxes (e.g. daytime during peak growth). This could also partly explain the weakness of assimilated nocturnal fluxes to update model state and parameters. However, the considerably more problematic challenge in DA is the quantification of model uncertainty. As models are, by definition, simplifications of reality, uncertainty is an inherent component and ubiquitous. It can best be approximated by model-model intercomparison, or through alternately activating equally plausible structures applied within one and the same model. However, these approaches are relatively time-consuming and have rarely been applied in DA studies of ecosystem ecology (Keenan *et al.*, 2011). An alternative approach of quantifying the absolute range of model uncertainty necessary for parameter estimation is to conduct a synthetic data or twin experiment (Eknes and Evensen, 2002; Keenan *et al.*, 2011). In this case, data to be assimilated are produced by a forward run of the very same model. Initial parameter values are altered compared to the forward run, so that the twin experiment can establish whether the DA framework is able to reproduce the known truth. Unless this study is successful, there is no point in applying the methodology with real data (Eknes and Evensen, 2002). As this success is further dependent on model uncertainty, the twin experiment can reveal whether a given model uncertainty allows for correct parameter estimation: if it is too low, model parameters are not sufficiently informed by observations, if it is too high, parameters will not stabilise within the allowable range. However, that way the true model uncertainty is not necessarily estimated, but rather a level of model uncertainty that allows for realistic parameter estimation. We have not conducted such experiments in our study (which aims for model diagnosis rather than parameterisation), and estimated model uncertainty through trial and error. This is clearly not satisfactory, and we acknowledge that the code of best-practice as proposed by Keenan *et al.* (2011) should be adopted within future studies of ecosystem parameter estimation. The results further show that the problem of equifinality among parameters, but also among parameters and state variables, could not be resolved satisfyingly. This appears to be a common problem of current DA studies in ecosystem modelling (Hill *et al.*, 2011b; Tang and Zhuang, 2008). Moreover, steady-state assumption on

initial stocks were found to bias parameter estimates (Carvalhais *et al.*, 2008): the uncertainty in initial C pools has considerable implications for parameter estimation with the EnKF (or DA in general, Hill *et al.* (2011b)). Accordingly, the EnKF analysis implies a high degree of parameter certainty (due to low parameter spread) in our study that does not appear to be justified. We therefore acknowledge that the EnKF framework as applied here provides uncertainty estimates on parameters and stocks that require careful judgement.

Further, observed chamber data on soil respiration fluxes would be beneficial in constraining modelled R_h, which we found to be underestimated. Assimilated respiration flux data could be a valuable source of information on litter and belowground C stocks, and on corresponding mineralization and decomposition rates. NEE_{DA} is complicated by a potential "noise" sink behaviour of belowground C pools (Williams *et al.*, 2005). The results of Suleau *et al.* (2011) indicate that the magnitude and fraction of belowground R_a of a winter wheat crop varies with DS, and thus is probably proportional to fine root C allocation.

A general problem we identified is that high frequency stock changes (caused by mass balance breaches through the EnKF analysis) absorb part of the signal contained in the assimilated data and thus might obscure structural or parametric model deficiencies. We described this phenomenon for C_{f} and LAI, whose strong response to DA possibly reduces the potential constraint of observed NEE data on model parameters. We suggest that for a pure crop parameter estimation study, ideally only temporally highly resolved data should be assimilated (e.g. NEE or soil respiration data), and biometric stocks should not form part of the model state vector.

4.5 Conclusions

We assimilated observations of biometry and C exchange for one winter wheat growing season into an agroecosystem BGCM (the SPAc model). The overall research rationale was to diagnose key processes of a crop model through explicit consideration of

independent, multiple constraints. External control of state estimation through assimilated measurements reveals model behaviour under realistic conditions, whilst confidence limits on simulated and observed data are explicitly respected for. DA clearly provided important, quantitatively determined insights into model shortcomings, and explanations and potential solutions were highlighted. We found that expected constraints on key crop processes are resolved in NEE flux data, which serve as a strong diagnostic tool for model analysis brought about by DA. The time richness of EC flux data is an important commodity for detailed model testing through revealing time variability in parameters. Observation of biometry also provided useful insights into model shortcomings, but their comparably low temporal resolution does not allow for detailed analysis of underlying processes. The winter wheat crop is a short-lived, annual plant that undergoes rapid changes in growth strategies compared to non-managed vegetation cover. Thus, frequent sampling of key biometric variables is warranted to improve the understanding of ecosystem dynamics such as development, C allocation, and senescence. These findings are summarized in more detail in the following.

The assimilation of NEE data improves the state estimate of aboveground biometric variables, largely constraining the timing and magnitude of growth and decay of foliar C and LAI. The flux data indicate a premature simulated senescence, further suggesting a phase of constant LAI during peak growth rather than a narrow peak. The temporal lag between the end of LAI growth and the beginning of its senescence is larger after DA. NEE constraints on belowground allocation allow for the diagnosis of fine root water uptake and transport, but belowground C pools exhibited noise sink behaviour.

We find that SPAc is deficient in reproducing flux data when biomass and LAI meet external constraints. Assimilation of biometric variables clearly reduces the ecosystem's C sink strength. The model overestimates plant drought stress given realistic state estimates of C_{r}. Further, as the quality of fit to observed NEE data declines through LAI assimilation, SPAc appears deficient in not accounting for photosynthesis of green crop organs other than leaves. NEE observations clearly outnumber biometric measurements and thus dominate the multiple-constraints DA experiments presented here. An alternative way of constraining simulated biometry with temporally highly

resolved observations is the assimilation of remotely sensed data with appropriate spatio-temporal sensor resolution (e.g. MODIS).

Temporal variability is indicative of ecosystem processes that are resolved in NEE data (parameter constraints through biometry are negligible due to their poor temporal resolution) but are not captured by model structure. Rather than providing defendable, calibrated, posterior parameter values (which is nonetheless possible if a model is well calibrated and analysed parameters are carefully selected), DA reasonably confirmed model deficiencies that were indicated through model-observation comparisons in previous studies (Sus *et al.*, 2010; Wattenbach *et al.*, 2010). We found that observational constraints on parameters with high model sensitivity are stronger for physiological than developmental parameters. Wheat (and probably cereals in general) crop models benefit from accounting for temporal and/or canopy layer variability in leaf thickness and fraction of autotrophic respiration. Further, the crop appears to utilize a considerably higher fraction of photosynthesised C for growth (f_{a} prior = 0.44; posterior = 0.25). The late season f_{a} increase after NEE_{DA} is assumed to be related to processes such as dough development, C translocation, and grain growth.

Through NEE_{DA} we further aimed for independent constraints on developmental parameters, which are commonly derived empirically from laboratory or field observations of crop phenology. Posterior estimates of cardinal temperatures appear plausible, realistically reproducing timing of senescence. However, their overall range is presumably overestimated. Crop developmental stage is a non-tangible, abstract model state variable. It is not well integrated into physiological processes, and thus corresponding parameters are rather implicitly resolved in NEE data. A general weakness of this generalized crop C mass balance model is the lack of a mechanistic representation of C partitioning, which is approximated through developmental controls on temporal allocation shifts.

NEE DA could not resolve deficiencies in simulating the agroecosystem respiration flux . This shortcoming appears to be a common feature of current crop C budget models, and might be related to weaknesses in modelling senescence controls on $\mathrm{R_a}$. $\mathrm{R_e}$

is largely constrained through initial conditions in C_{SOM} and C_{lit} and corresponding rate constants of decomposition and mineralization. These are in turn considerably influenced by land management, and this influence necessitates more detailed study.

Chapter 5

A data assimilation framework for constraining upscaled cropland carbon flux seasonality and biometry with MODIS

Abstract

Agroecosystem models are heavily dependent on information on land management patterns for regional applications. Land management practices play a major role in determining global yield variability, and add an anthropogenic signal to the observed seasonality of atmospheric CO_2 concentrations. However, there is still little knowledge on spatial and temporal variability of important farmland activities such as crop sowing dates, cultivar selection, and fertilisation application, and thus these remain rather crudely approximated within carbon (C) cycle studies.

In this study, we present a framework allowing for spatio-temporally resolved simulation of cropland C fluxes under observational constraints on land management and canopy

greenness. We apply data assimilation (DA) methodology in order to explicitly account for information on sowing dates and model leaf area index (LAI), two key variables that are resolved within field patch specific Moderate Resolution Imaging Spectroradiometer (MODIS) 250 m vegetation index (VI, MOD13Q1, version 5) time series data. MODIS data were assimilated both variationally (for sowing date estimation) and sequentially (for improved model state estimation, using the Ensemble Kalman Filter (EnKF)) into a crop C mass balance model (SPAc). In doing so, we are able to accurately quantify the multiannual (2000-2006) regional C flux and biometry seasonality of maize-soybean crop rotations surrounding the Bondville Ameriflux eddy covariance (EC) site, averaged over 104 pixel locations within the wider area.

At the point scale (i.e. the Bondville site), we find that MODIS-derived sowing dates allow for highly accurate simulations of growing season C cycling at locations for which ground-truth sowing dates are not available. Moreover, sequential MODIS DA improves model performance by reducing a negative bias in forward model LAI, which is most effective in years of delayed sowing progress. Important land management practices (fertilisation, irrigation, cultivar selection, double cropping) and disturbance events (frosts and droughts) are probably indirectly resolved in assimilated temporal VI profiles. This framework enables modellers to accurately simulate current (i.e. last 10 years) C cycling of major agricultural regions.

Averaged over the 104 field patches analysed, relative spatial variability for biometry and net ecosystem exchange (NEE) ranges from ≈7% to ≈10%, but variability in net biome productivity (NBP) is considerably larger (≈24% to ≈32%). Regional patterns of land management are important drivers of agricultural C cycling and major sources of uncertainty if not appropriately accounted for. Moreover, observing C cycling at one single field with its individual sowing pattern is not sufficient to constrain large-scale agroecosystem behaviour. Study area average growing season length (GSL) is 20 days longer than observed at Bondville, primarily because of an earlier estimated start of season (SoS). Differences between Bondville and upscaled NEE are especially large in years with non-optimal weather conditions for sowing. Finally, reproducing multiannual C budgeting is not achieved even when temporally highly

resolved local meteorological driver data, sowing dates, soil conditions, and satellite-derived observations of vegetation greenness are considered. Additional information on cropland management and belowground C cycling still needs to be considered, as MODIS data cannot provide such constraints.

5.1 Introduction

Agricultural ecosystems (excluding managed grasslands, herein referred to as agroecosystems as in Kucharik and Twine (2007)) are of major importance to humankind. There are clear links between climate change, population growth (Zhang *et al.*, 2011), and fluctuations in agricultural production (Lee *et al.*, 2008). The carrying capacity of agroecosystems shrinks significantly in a deteriorating climate (Zhang *et al.*, 2011): cooling shortens the potential GSL, whilst warming reduces the duration from sowing to harvest (and thus the duration of grain filling) through accelerating development (Andrade, 1995; Brown and de Beurs, 2008; Lobell and Field, 2007). Global food demand is expected to double by 2050 (Tilman *et al.*, 2001). Further agricultural intensification might have considerable detrimental effects on several crucial ecosystem services, including food production itself (Foley *et al.*, 2005).

Land management practices play a major role in determining global yield variability, of which only ≈30% was found to be attributable to climate variables (Lobell and Field, 2007). Whilst first coarse global datasets on agricultural management have been developed (Sacks *et al.*, 2010; Siebert *et al.*, 2006), there is still little knowledge on detailed spatial and temporal variability of important farmland activities such as crop sowing dates, cultivar selection, and fertilisation application. These practices have been used as important tools for crop yield improvements during the "Green Revolution" (Foley *et al.*, 2005), and they will be applied in future efforts so that supply of agricultural yield will meet its demand.

Novel measurements using EC to measure net C fluxes are now being combined with simultaneous observations of crop biometry. These constraints on cropland C budgeting

and climate controls are currently being used to improve biogeochemical models (BGCM) on various scales (e.g. Bondeau *et al.* (2007); de Noblet-Ducoudré *et al.* (2004); Kucharik and Twine (2007); Sus *et al.* (2010)), which traditionally lacked a crop specific plant functional type. Unrepresented agroecosystem C cycling was estimated to be a major source of uncertainty within four BGCMs simulating global C and water cycles (McGuire *et al.*, 2001). Generally, BGCMs would benefit from a better representation of interannual phenological variability (Schwalm *et al.*, 2010), which is poorly understood (Craufurd and Wheeler, 2009; Stöckli *et al.*, 2008).

Agroecosystem models are heavily dependent on information on land management patterns for regional applications. Remote sensing (RS) data have been used in crop growth modelling studies to estimate related parameters (e.g. sowing or emergence date, Brown and de Beurs (2008); Dente *et al.* (2008); Doraiswamy *et al.* (2004); Launay and Guerif (2005); Karkee *et al.* (2009)) and initial conditions (e.g. soil water content, Inoue and Olioso (2006)), mostly applying variational DA techniques. These studies are based on findings that RS VI data are related to crop canopy chlorophyll density or green leaf biomass, and that several growth phases (e.g. emergence, canopy establishment, senescence, maturity) are detectable from VI time series data (Tucker *et al.*, 1979). MODIS 250 m resolution VI data have been used for crop type classification (e.g. Wardlow and Egbert (2008)) and yield estimations (e.g. Doraiswamy *et al.* (2004)) in the U.S., being suitable for providing regional crop type specific VI time series for field patch sizes of >25 ha Doraiswamy *et al.* (2004). However, no study so far attempted to assimilate RS time series of various field patches into a crop model simulating agroecosystem C exchange. Upscaled model estimates of cropland NEE fluxes are forced with uncertain information on land management, climate, and environmental conditions. In particular the variability of sowing dates in space and time remains rather crudely approximated within C cycle studies.

In this study, we present a framework for spatio-temporally resolved simulation of cropland C fluxes under observational constraints on land management and canopy greenness. We apply DA methodology in order to explicitly account for information on sowing dates and model LAI, two key variables that are resolved within field

patch specific MODIS 250 m VI (MOD13Q1, version 5) time series data. DA is a technique for merging the information contained in both models and observations, and useful for creating a best possible estimate of cropland C cycling (Demarty *et al.*, 2007). Sequential DA techniques such as the Ensemble Kalman Filter (EnKF, Evensen (2003)) have been developed and applied successfully within BGCMs (Chen *et al.*, 2008; Quaife *et al.*, 2008; Williams *et al.*, 2005; Gove and Hollinger, 2006). Here, we sequentially assimilated MODIS data at observational time steps, using the EnKF, into a crop C mass balance model (SPAc, Sus *et al.* (2010)) for improved C flux and biometry estimation, and compared model outputs against independent validation data sets. We acquired 104 MODIS VI data time series, with pixel coordinates centred on field patches of sufficient size surrounding the Ameriflux Bondville (Illinois, U.S.) EC flux tower site.

In doing so, we provide a new estimate of the uncertainty in cropland C cycling due to unknown regional land management patterns. In the following, we address the following research questions: (1) do MODIS 250 m VI time series contain appropriate information for improving crop C fluxes at the point scale? As a proof of concept, we compare model outputs before and after DA against observations of NEE (as measured by EC at Bondville) for seven full maize-soybean crop rotation (MSCR) cycles (2000-2006), including fallow periods. (2) How large is the spatio-temporal variability in upscaled cropland C fluxes and biometry when averaged over the 104 pixel locations? Are the Bondville EC flux data representative of regional cropland C exchange, considering spatial heterogeneity in land use? (3) Do the MODIS data carry further information on yield formation, i.e. are both C fluxes and stocks simultaneously improved? (4) Are the region's MSCR a net sink of C when fallow season C uptake is not accounted for/modelled? We hypothesise that the pure crop growing season (sowing to harvest) C balance is positive (i.e. a C source), and might be negative only when fallow season weed grass growth and management are considered.

Table 5.1: Overview of tasks accomplished, and data and methods involved, at each major step of the study.

Step	Task	Data and methods
1	Crop model calibration and application at the point scale	Bondville EC C flux data, SPAc
2	Building maize/soybean crop masks for study area	USDA crop data layers (CDL)
3	Extracting single-field crop VI time series	Crop masks, MODIS M(O/Y)D13Q1 subset grids
4	Determination of individual sowing dates for each pixel	MODIS-derived LAI time series, model LAI (SPAc), NASS crop progress reports (for validation)
5	Model upscaling through MODIS VI DA	EnKF, SPAc, NASS yield data (for validation)

5.2 Data and Methods

In this study, we followed several consecutive steps in order to move from a calibrated agroecosystem BGCM at the point scale (step 1, Table 5.1) to an upscaled regional estimate of C (step 5). We accounted for highly-resolved information on crop type classification (varying both in space and time) in order to build maize and soybean crop masks (step 2). We then used these to extract MODIS VI time series for single field patches of sufficient size, avoiding mix-pixel effects (step 3). Before final model upscaling, we determined individual sowing dates for each pixel of the study area through variational DA (step 4). Each of these steps are described in detail in the following sections.

5.2.1 Step 1: Crop model calibration and application at the point scale

Study area and C flux data

The MSCR of the wider study area can be considered as a model ecosystem for biogeochemical studies due to the flat terrain, homogeneous land-use pattern, and independent data sets available. MSCR are the dominant land-use type within

the U.S. Corn Belt, representing 83% of the land surface devoted to agriculture (Hollinger *et al.*, 2004). MSCR have been analysed in various studies for their C sequestration potential under reduced or no-till management (Grant *et al.*, 2007; Hollinger *et al.*, 2004; Verma *et al.*, 2005; Baker and Griffis, 2005). We selected a study area of approximately 800 km^2 (32 km E-W, 25 km N-S, Figure 5.1), the centre pixel of which is close to the Ameriflux Bondville EC flux tower site (Ameriflux site ID: US-Bo1, latitude: 40.01, longitude: -88.29, located in the county of Champaign, Illinois (USA), Figure 5.1, Figure 5.3). The climate of the region around Bondville is, according to the Köppen climate classification scheme, humid continental (class Dfa). Cold winters are in stark contrast to the warm to hot, rather humid summers (annual temperature amplitude $\geq$25 °C for all study years). Annual average precipitation over the period 2000 to 2006 is 754 mm, and range between a low value of 577 mm in 2001 and a high value of 928 mm in 2004.

At Bondville, half-hourly C exchange fluxes between the atmosphere and the biosphere have been measured continuously from 1996-present. Forcing meteorological variables (radiation, temperature, wind, humidity, and precipitation, all half hourly) have been recorded for diagnostics (see Meyers and Hollinger (2004) for a detailed description). For several years, measurements have been taken of several aboveground plant biometric variables.

The Bondville agricultural site has been used in no-till management of a soybean (*Glycine max*) - maize (*Zea mays*) crop rotation, with maize grown in odd years and the crop residues left on the field after harvest. The area surrounding the flux tower is characterised by predominantly well drained silt loam soils with little surface slope (Wilson and Meyers, 2007). The flux data analysed in this study are half-hourly observations of NEE, that were gap-filled based on a light use efficiency model (for daytime values) and a respiration function (for night-time values, Bernacchi *et al.* (2005); Hollinger *et al.* (2004)) to derive daily sums. The higher sink strength of the maize crop growing periods largely reflects the difference between C_3 (soybean) and C_4 (maize) net photosynthesis rates (Hollinger *et al.*, 2004; Baldocchi, 1994).

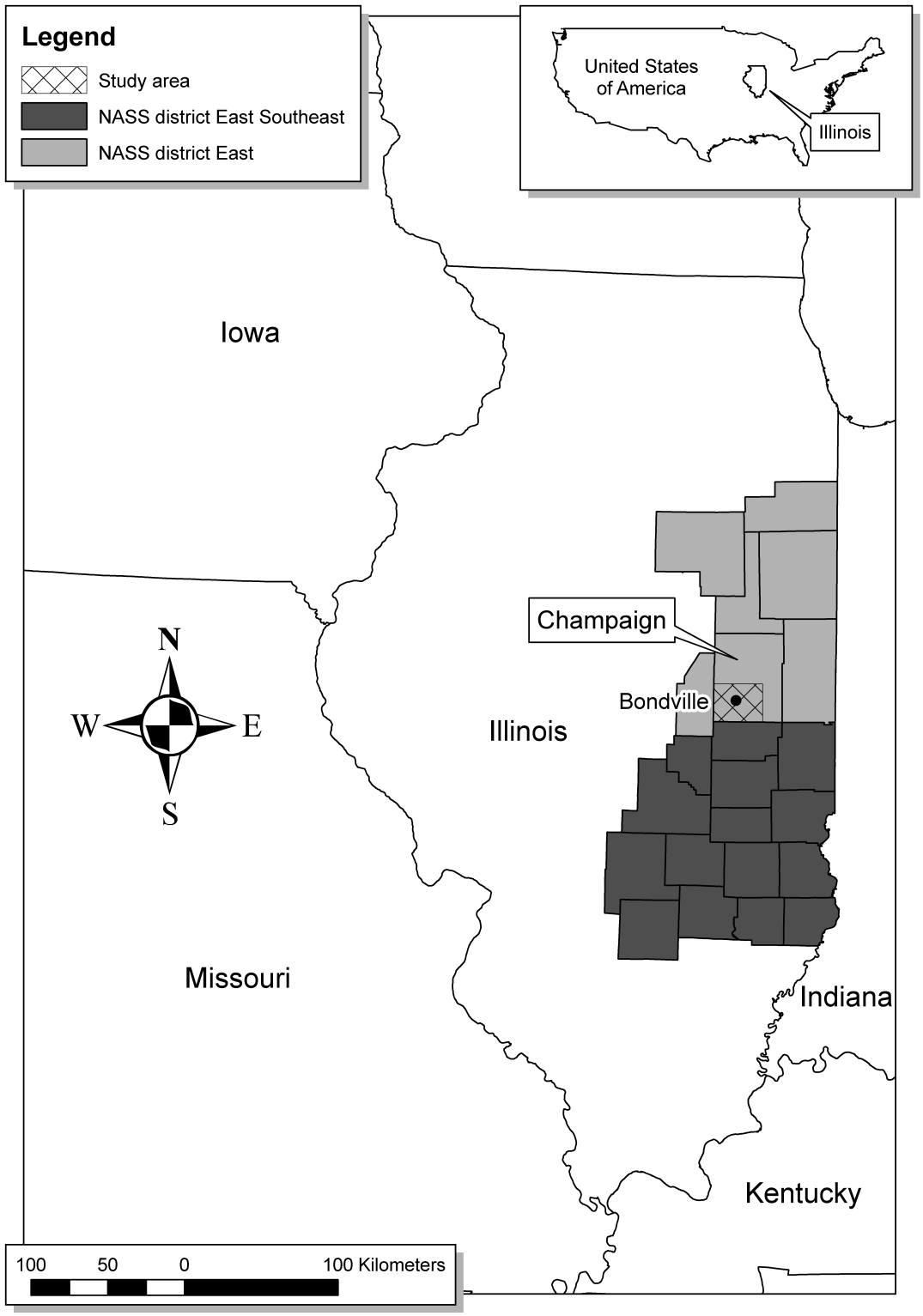

Figure 5.1: Location of the Bondville EC-flux tower site, study area (checked box), and NASS crop progress report districts (grey and dark grey counties).

Crop model: structure, parameterization, and initial conditions

The Soil Plant Atmosphere (SPA) model (Williams *et al.*, 1996, 2001b) is a process-based model that simulates ecosystem photosynthesis and water balance at fine temporal and spatial scales (30min time-step, up to ten canopy and twenty soil layers). SPA employs some well-tested theoretical representations of ecophysiological processes, such as for the calculation of photosynthesis (the Farquhar model, Farquhar and von Caemmerer (1982)) and leaf-level transpiration (Penman-Monteith equation, Jones (1992)). These two processes are linked by a model of stomatal conductance, which optimizes the daily gain of C per unit of leaf nitrogen within the limits of canopy water storage and soil to canopy water transport (Williams *et al.*, 1996). For each canopy layer and time-step an iterative procedure is used to determine the maximum sustainable C assimilation rate. The amount of irradiation intercepted by the canopy depends on LAI, which is calculated by dividing live leaf C mass by the C per leaf area parameter (C_{la}). A C mass balance model has been added to SPA more recently (Williams *et al.*, 2005), and a C_4 photosynthesis model based on Collatz *et al.* (1992) was integrated.

Moreover, a crop C partitioning scheme and a developmental model have been added (SPA version 2 - Crop (Sus *et al.*, 2010), hereafter referred to as SPAc). The C partitioning scheme is based on empirical values of field crop growth analyses (Penning de Vries *et al.*, 1989). This partitioning pattern, considering C allocation to one root and four above ground C pools (labile, foliage, stem and storage organ C pools), is a function of crop developmental stage (DS). DS of maize and soybean is calculated as the sum of daily crop developmental rates (DR), which are estimated on the basis of non-linear functions for two environmental factors: temperature *f(T)* and photoperiod *f(P)* (Streck *et al.*, 2008; Sus *et al.*, 2010; Wang and Engel, 1998; Setiyono *et al.*, 2007). For maize, *f(T)* is the only control on developmental rate throughout the crop's life cycle within SPAc (Streck *et al.*, 2008). For soybean, crop development is affected by *f(T)* from sowing to maturity, and by *f(P)* until DS = 1 (as in Setiyono *et al.* (2007), but simplified). The soybean photoperiod function is applied as shown in Setiyono *et al.*

(2007). Leaf senescence for both crops is calculated as the bigger value of leaf senescence rate due to mutual shading (SR_{sh}, if LAI >5), and leaf senescence rate as a function of physiological maturity or age (SR_{age}, if DS >1, van Laar *et al.* (1997)). In order to find a better match with observed patterns of leaf biomass senescence and associated C fluxes observed at Bondville, we set SR_{age} to increase exponentially with DS.

SPAc runs were conducted for three different plant functional types: maize, soybean, and C_3 weed grasses growing in fallow periods between harvest and sowing. We used the same parameter values as in Sus *et al.* (2010); parameter values that were altered are given in Table A.4. The initial conditions for the SPAc modelling runs were a soil organic matter (SOM) C content of 3,600 gC m^{-2} (for which modelled SOM C is in rough equilibrium, i.e. litter decomposition flux into the soil and soil mineralisation flux are approximately equal), a litter C content of 400 gC m^{-2} (adjusted to reflect annual variability in litter C as observed by Verma *et al.* (2005)), and a labile C content of 10 gC m^{-2} at sowing for soybean and maize (i.e. the seed C content, approximated from Aubinet *et al.* (2009)) and of 1 gC m^{-2} after harvest for the fallow period C_3 weed crop (approximated value).

5.2.2 Step 2: Building crop type masks

For the identification of MODIS VI time series coordinates that are centred over single field MSCR's, USDA-NASS (U.S Department of Agriculture–National Agricultural Statistics Service) Cropland Data Layers (CDL) were used as a classification basis. The CDL raster data are geo-referenced, crop-specific land cover data layers (see Boryan *et al.* (2011) for a detailed description). The 28 land cover categories contained in the CDL data are accuracy tested based on independent validation samples, showing that the cover categories for maize and soybean are well characterized within NASS' CDL (total crop mapping accuracies range from 85% to 95% for major crop categories, Boryan *et al.* (2011)). We acquired seven CDL raster images (2000-2006) in World Geodetic System (WGS) 1984 Universal Transverse Mercator (UTM) projection (zone 16N). We further resampled the 2006 CDL (which is based on 56 m AWiFS data, others

on 30 m Landsat TM data) to a finer 30 m pixel resolution using a nearest neighbour approach.

We used the seven NASS CDL raster images (one for each year in 2000-2006) to extract time series of those MODIS pixels for which we find minimum requirements of crop type coverage to be satisfied. These requirements were that within a search window of 500 m x 500 m centred over the composite pixel centre coordinates, the mean coverage of a prescribed crop type (i.e. either maize or soybean as classified by a CDL) is >95% for each year of the study period, and maize and soybean crops alternate in their annual rotational succession. We built two crop masks (with either maize or soybean as the prescribed "starting" crop type in year 2000, and crop types alternating each year) that quantify the minimal percentage coverage of a particular crop type rotation over the entire study period and for each pixel within the MODIS subset, satisfying the requirements outlined above. The size of each MODIS subset scene covering the study area and of the two crop masks is 132 x 102 pixels, or 13,362 pixels in total. Out of these, we found 104 pixels that met the defined requirements, 59 with maize sown in year 2000, and 45 with soybean (Figure 5.2).

We downloaded MODIS Terra (MOD13Q1) and Aqua (MYD13Q1) collection 5 (C5) 250 m data subsets from the Oak Ridge National Laboratory Distributed Active Archive Center (ORNL, 2010). The size of the 500 m x 500 m search window was defined in order to encompass four at-nadir MODIS 250 m pixels. This was necessary in order to reduce the likelihood of "contamination" of extracted MODIS single crop time series by VI signals of neighbouring fields with a different cultivated crop type and/or sowing date. As one MODIS repeat cycle is completed in no less than 16 days (Wolfe *et al.*, 1999), the true coordinates of each pixel within a MOD13Q1/MYD13Q1 time series are likely to differ, as they might originate from different MODIS orbits. In theory, each 250 m pixel can be located everywhere within the 500 m x 500 m search window centred over the composite coordinates (Figure 5.3).

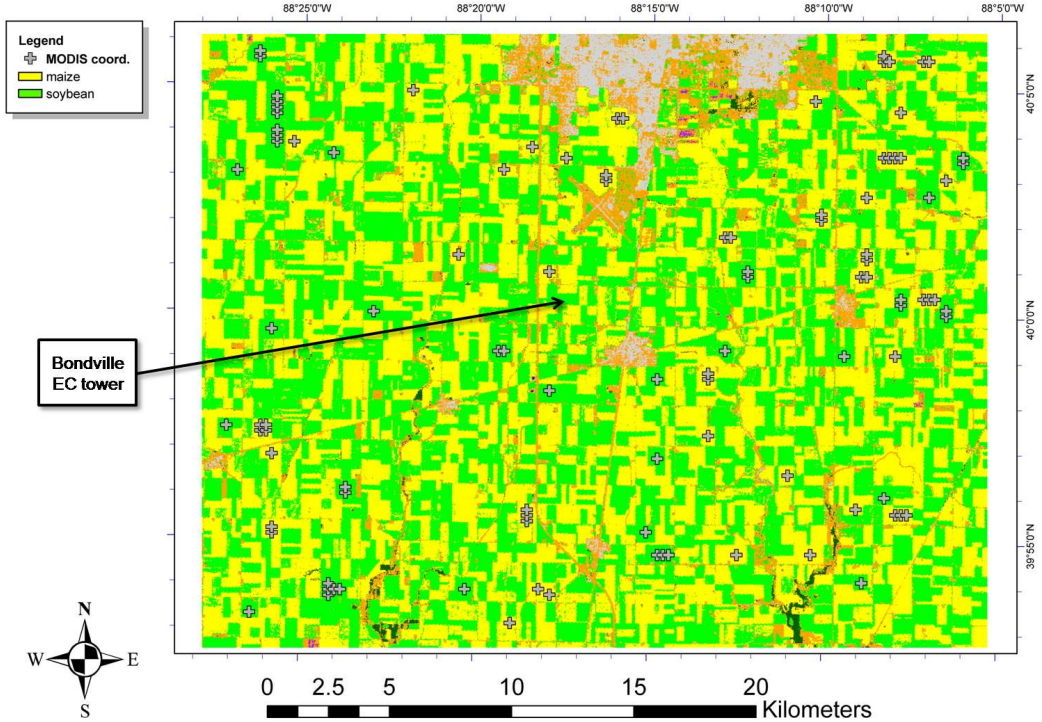

Figure 5.2: The USDA CDL of the study area. Selected MODIS composite coordinates are indicated. The study area is dominated by maize (yellow) and soybean (green) cultivations.

Large off-nadir views can lead to additional distortions. For example, the size of the MODIS observation footprint can increase fourfold at viewing angles beyond 60° (Wolfe *et al.*, 1998). Sakamoto *et al.* (2005) removed MODIS pixels with a viewing angle of >32.25° in their study to avoid neighbouring effects. We decided to remove all MODIS observations with a viewing angle >40°, which eliminates all pixel distortions of factor >1.6 (Wolfe *et al.*, 1998). For example, ∼16% of all pixel values contained in the Bondville MODIS time series were removed due to viewing angle filtering. At this site, our criteria for minimum field patch size as defined earlier are not strictly met. However, we chose the same viewing angle threshold value in order to retain a sufficient amount of MODIS observations for testing our DA concept. A MODIS 250 m observation at Bondville with a viewing angle close to 40° (distorted pixel size ∼400 m) is certain to suffer from a neighbouring effect (Figure 5.3). However, only 20% of the retained Bondville pixels have viewing angles >30° (distorted pixel size >325 m), and 60% have viewing angles <20° (distorted pixel size <290 m). Thus, we expect only minor (negligible) neighbouring effects in the retrieved Bondville MODIS data time series (in the MODIS data time series of selected composite locations in the entire study area).

5.2.3 Step 3: Extracting single-field crop VI time series

MODIS data subsets contain a series of geo-referenced, gridded values of two VIs (the normalized difference vegetation index (NDVI) and the enhanced vegetation index (EVI)), red (ρ_{red}, 620-670 nm wavelength band, 250 m pixel resolution), blue (ρ_{blue}, 459-479 nm, 500 m), and near infra-red (ρ_{NIR}, 841-879 nm, 250 m) reflectance, pixel reliability and quality flags, and viewing geometry angles. An algorithm converts MODIS surface reflectances to VI values after correcting for molecular scattering, ozone absorption, aerosols, and off-nadir effects using a BRDF (bidirectional reflectance distribution function) model (Huete *et al.*, 1999). Only high quality data are retained for compositing within a 16 day time window, and quality flags (based on degree of cloud contamination and viewing geometry) are allocated to each observation. As a result of this filtering procedure, spatially adjacent selected pixel values may originate

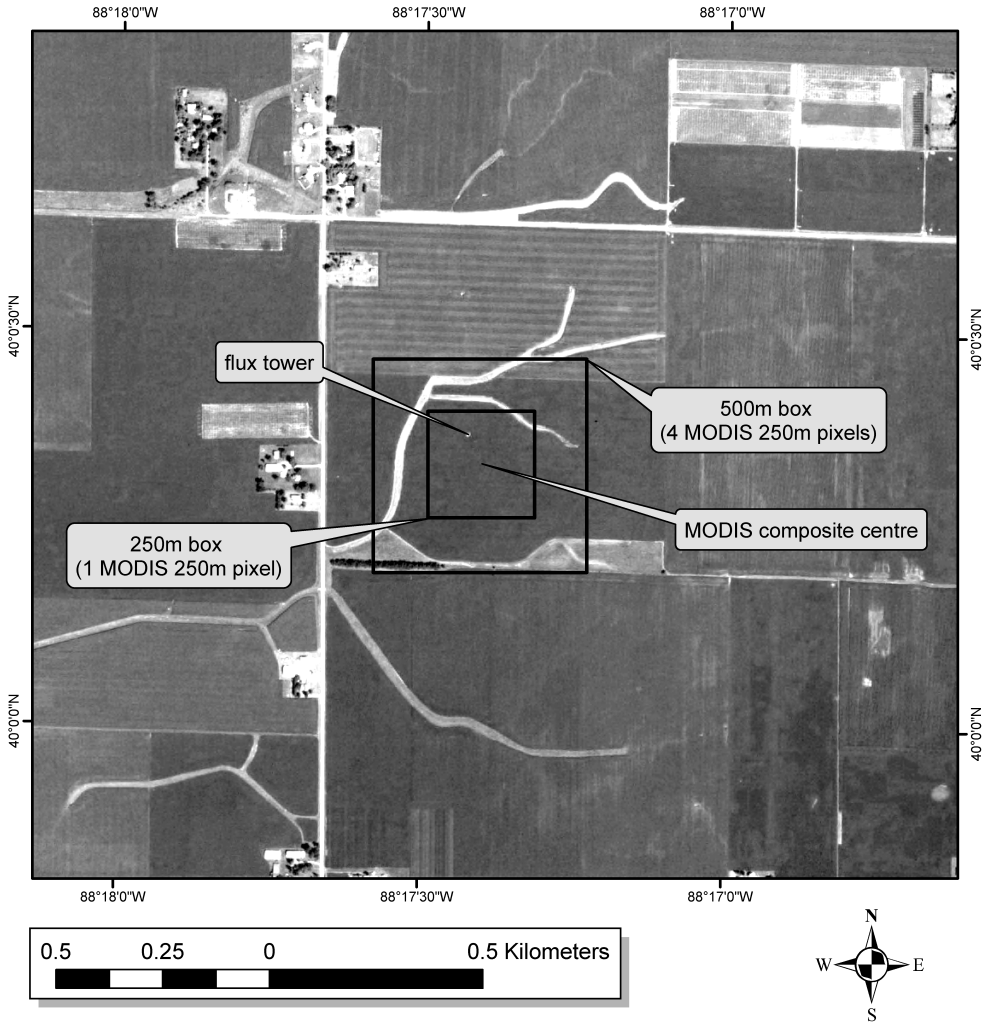

Figure 5.3: The Bondville flux tower site. The selected MODIS composite centre location is indicated, together with approximated at-nadir extents of one 250 m MODIS pixel, and one 500 m MODIS pixel.

from different days (Solano *et al.*, 2010), and every MODIS VI time series has irregular temporal spacing.

The C5 Terra and Aqua data streams are processed 8 days out of phase, providing a quasi-8-day temporal frequency. Another new feature of C5 is the inclusion of the "Composite day of year" information (CMPDOY, Solano *et al.* (2010)). The CMPDOY provides information on the real date of the selected MODIS observation (two consecutive observations of a single sensor can be between 1 to 32 days apart), and thus considerably improves temporal accuracy of retrieved time profiles of reflectances or VIs.

Guindin-Garcia (2011) found that the consideration of CMPDOY within agricultural studies based on MODIS data is of crucial importance, which is especially true for observations of maize crops in the vegetative stage. Previous studies commonly assumed that the MODIS composite DOY refers to the first, central, or last day within the 16-day time window (e.g. Wardlow *et al.* (2006); Chen *et al.* (2006)).

We remapped all selected MODIS subset scenes to the WGS 1984 UTM (zone 16N) projection. Using the crop type masks created, we extracted MODIS time series information for all non-masked pixels within each gridded subset scene. We applied a filter to screen for pixel values affected by thick clouds by excluding all composite data with a blue reflectance value of >10% (Sakamoto *et al.*, 2005), and removed all composite data with a reliability of >1 (i.e. pixels most probably cloudy, ORNL (2010)).

We applied an empirical relationship to scale from modelled LAI to modelled VI. This modelled VI estimate is then directly related to satellite derived VI. The empirical relationship applied here, based on the Renormalized Difference Vegetation Index (RDVI), was developed by Haboudane *et al.* (2004) for maize and soybeans grown in Ottawa (Canada). The RDVI has been developed in order to attain a more linearised relationship with vegetation biophysical variables compared to the NDVI (Roujean and Breon, 1995), which asymptotically saturates in high biomass regions with a maximum value of 0.9 (Huete *et al.*, 2002). The RDVI is defined as

$$RDVI = \frac{\rho_{NIR} - \rho_{red}}{\sqrt{\rho_{NIR} + \rho_{red}}} \tag{5.1}$$

In Haboudane *et al.* (2004), the RDVI was retrieved from Compact Airborne Spectrographic Imager (CASI) data, using hyperspectral narrow bands centred at 670 nm (ρ_{red}) and 800 nm (ρ_{NIR}) with a bandwidth of 7.5 nm. The empirical relationship between LAI and RDVI was determined using simulated data from leaf and canopy reflectance models, based on the CASI central wavelengths and bandwidths for ρ_{red} and ρ_{NIR}. The resulting predictive equation was found to be

$$LAI = 0.0918 * \exp^{6.0002 * RDVI} \quad (5.2)$$

A comparison of CASI retrieved LAI values based on Equation 5.2 against ground truth measurements showed that LAI was predicted with high accuracy overall: R^2 = 0.95 and $RMSE$ = 0.75 for soybeans, and R^2 = 0.90 and $RMSE$ = 0.66 for maize (Haboudane *et al.*, 2004). The authors further found an overestimation of LAI values >5 m^2 m^{-2}.

The coupling of a canopy transfer model to the crop C mass balance model for the provision of a modelled VI output is beyond the scope of this study, but has been tested by Quaife *et al.* (2008), who assimilated MODIS spectral reflectance rather than LAI-product data into an ecosystem model. Here, we are focussing on the analysis of ground measured versus satellite derived LAI time series for maize and soybean at Bondville as an assessment of the overall merits of Equation 5.2 for LAI prediction and its applicability to MODIS data. Moreover, in our DA approach we expect the EnKF to account for the overestimation of RDVI-derived LAI at high biomass values, as it explicitly traces correlations between members of its state vector. As the correlation between RDVI and LAI diminishes for LAI values >5 m^2 m^{-2} (the RDVI asymptotically approaches a saturation value around 0.7), so will the impact of an assimilated MODIS RDVI value on the model, if modelled LAI >5 m^2 m^{-2}.

The MODIS Land Discipline Team (MODLAND, http://modis-land.gsfc.nasa.gov/, see also Justice *et al.* (2002)) quantified the average MODIS VI uncertainty over a range of biomes and seasonality to ±0.025 (NDVI) and ±0.015 (EVI). Our independently quantified estimate (based on the Hollinger and Richardson (2005) approach on uncertainty estimation in EC data) produced a comparable value of ±0.017. We referred to this uncertainty estimate in all DA runs.

5.2.4 Step 4: Determination of individual sowing dates for each pixel

We expect that the DA procedure will correct for deficiencies in modelled patterns of crop leaf area growth and senescence. However, it was necessary to find an individual sowing date for each pixel and each year of the study area (no regional field patch specific observations of sowing dates were available as model input). This is important because crop developmental progress, the calculation of which is initiated at sowing, determines the duration of growth phases of the various crop organs (e.g. leaves, storage organs). The crop model will only be able to respond to assimilated MODIS observations as long as modelled LAI is greater than zero. Also, the assimilation of MODIS data can correct for deficiencies in modelled LAI, but has no impact on the simulated developmental stage of a crop. If individual sowing dates were not determined, there would be a mismatch in updated modelled LAI and modelled crop developmental stage after DA.

In order to determine pixel-specific sowing dates, we ran the crop model in the forward mode (no data assimilated, forced with Bondville observed meteorology) to provide modelled curves of crop LAI evolution. For each year of the study period we ran SPAc 80 times, but each time with a different sowing date (spanning a range of DOY from 90 to 170). We chose this range in order to encompass reported usual sowing dates of maize and soybean for Illinois (USDA, 1997), which are DOY 112-148 for maize, and DOY 126-167 for soybean. Out of the resulting 80 modelled LAI curves, we solved for the sowing date with the minimum sum of squared residuals between its corresponding modelled LAI and the MODIS-derived LAI data.

In order to compare our estimation of modelled sowing dates with general patterns of land management within the wider area, we referred to NASS crop progress reports. These reports are published per crop census district as the smallest spatial unit. As the study site lies within the NASS East crop census district, but is bordering to the NASS East-South East district, we used crop progress reports from both regions (Figure 5.1). The study area is considerably smaller than these census districts, and thus lacks spatial representivity with respect to the observed sowing dates reported on a larger scale. In our analysis, we focus on a qualitative interpretation of modelled

versus reported sowing dates, further investigating whether effects such as delayed sowing due to high late-spring rainfall levels are reflected in model data. Further, this comparison will indicate potential model deficiencies in the simulation of both early crop establishment/development and leaf senescence.

5.2.5 Step 5: Model upscaling through MODIS VI DA

DA can be considered as a set of techniques that aims for finding an optimal combination of observations and models, referred to as the "analysis" (Mathieu and O'Neill, 2008). In this study, the EnKF approach is used (Evensen, 2003; Williams *et al.*, 2005). The model state vector contained all above- and belowground biometric variables (the C masses of leaves (C_{f}), stems (C_{s}), storage organs (C_{stor}), roots (C_{r}), LAI) and the RDVI. We selected a model uncertainty of 1% for all biometric variables, and an uncertainty of 10% for the RDVI. We chose a higher uncertainty level for modelled RDVI in order to account for additional uncertainties in scaling from LAI to RDVI using Equation 5.2. Also, as modelled RDVI is not a cumulative sum of daily C fluxes (but instead scaled from LAI), there is no uncertainty propagation between time steps, and so we set modelled RDVI uncertainty constant at 10%. Measurement uncertainty of MODIS-derived RDVI is an absolute value of ± 0.017 RDVI on all observations (see subsection 5.2.3). Accordingly, model uncertainty is greater than measurement uncertainty for RDVI greater than 0.17. We chose an ensemble size of 50 members, for which we found stabilising RMSE between SPAc modelled and observed NEE in a previous study (chapter 4). Similarly, de Wit and van Diepen (2007) found that the soil moisture ensemble mean of a crop model can be well estimated with an ensemble size of 50, and improvements are small when this metric is increased to 100.

NASS provides county estimates of yearly yields for maize and soybean, which we used to validate our upscaled estimates of modelled storage organ C mass. NASS values are reported in bushels acre^{-1}. One bushel of shelled maize corresponds to 56 pounds (25.4 kg), and one bushel of soybeans weighs 60 pounds (27.2 kg, USDA (1992)). We converted these values into gC m^{-2} under the assumption of a grain moisture content of

15.5% for maize and 13% for soybeans and a C fraction in the grain of 0.447 for maize and 0.54 for soybeans (Hollinger *et al.*, 2004). While the NASS yield data report net grain weight harvested for maize and soybeans, modelled outputs in this study are given in C allocated to the entire storage organ (i.e. the total maize ear weight (including husks and the cob with grains), or total soybean pod weight (including beans and pod walls)). Field measurements of both total storage organ weight and grain weight for maize were available at the Bondville Ameriflux site for 3 years, according to which maize grain weight is typically ∼84% of total storage organ weight at maturity. We account for the bias between the NASS yield data and the SPA model results for maize by multiplying the NASS data with a factor of 1/0.84 (i.e. converting from NASS yield to total storage organ weight). Following Gent (1983), the average ratio of soybeans to total pod weight is 0.78, and we corrected NASS soybean yield data accordingly.

5.3 Results

5.3.1 Simulated sowing dates

Modelled sowing dates broadly reflect reported trends of planting progress (Figure 5.4) as a response to spring precipitation events. In 2000, >90% of both maize and soybean crops are modelled to be sown by early May, a year of record sowing progress due to reported suitable weather conditions. We expect soybean to be sown about at least 1 to 2 weeks after maize (USDA, 1997), a pattern which is generally reproduced (except for 2003). Reported delay of crop sowing progress in 2002 due to high spring rainfalls is reflected by model data for soybean, whereas simulated maize sowing progress appears rather constant for all years. Modelled sowing dates for maize, which are closest to NASS reported values in 2003 and 2005, often appear premature (up to 1 month in 2000 and 2002), and are less sensitive to interannual variability in sowing conditions than soybean. Modelled soybean sowing dates meet reported patterns particularly well in 2001, 2002, 2004, and 2005. For years with larger discrepancies, soybean sowing

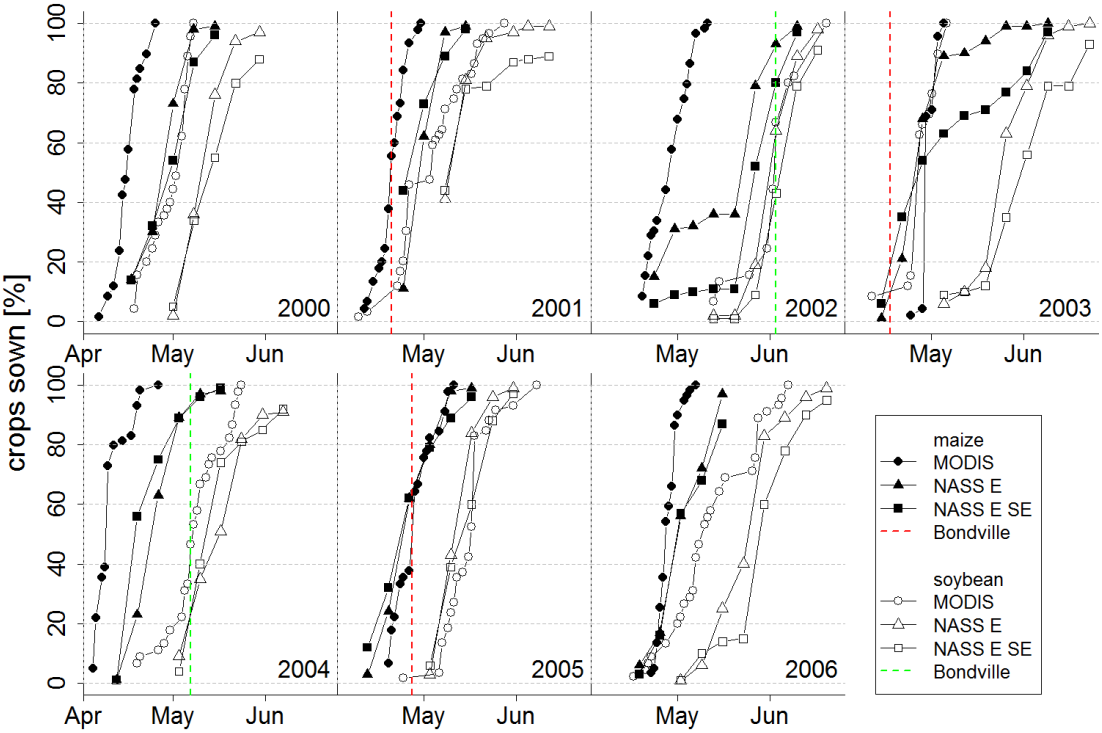

Figure 5.4: Crop sowing progress for the study area and the two surrounding NASS census districts (East and East-South East) for the seven study years (2000-2006). MODIS-derived model estimates (circles) and NASS reported values (triangles and squares) are shown as percentage of crops sown within the respective regions. Reported sowing dates for the Bondville EC flux site are indicated by dashed vertical lines (red: maize, green: soybean).

dates are biased towards lower DOYs (2000 and especially 2003, when modelled maize and soybean sowing dates coincide).

On the other hand, a comparison of farmer reported and simulated sowing dates for the Bondville site shows that modelled maize sowing DOYs tend to be overestimated (by 11 to 12 days, except for 2001), whilst soybean sowing DOYs are only slightly underestimated (1 to 4 days, Table 5.2). The Bondville data also show that reported sowing of the 2002 soybean crop is clearly delayed (by ∼4 weeks compared to the other soybean growing period in 2004) due to abnormal precipitation in April-June, which is well reproduced by the MODIS-based model value. Except for 2003, Bondville observations are within the 40–80% range of modelled sowing progress (Figure 5.4). These results stand in contrast to NASS data suggesting that model maize sowing

Table 5.2: Farmer reported sowing dates and model estimates, and the difference between the two (in DOY). Values are shown for five years (2001-2005, sowing dates for remaining years not available) of the Bondville EC flux tower site, with maize (soybean) grown in odd (even) years.

year	Crop type	Farmer reported sowing date	Modelled sowing date
2001	Maize	109	108
2002	Soybean	153	152
2003	Maize	106	118
2004	Soybean	127	123
2005	Maize	116	127

dates are premature. However, as only five observations are available at Bondville, the limited database does not allow for firm conclusions.

5.3.2 Proof of concept - assimilation of MODIS RDVI time series at Bondville

Bondville observations of EC-derived NEE fluxes and biometry are an important data source for ground-truth testing of the MODIS RDVI-LAI relationship, and enable investigation of whether assimilated MODIS data time series contain information that improves simulated maize/soybean C cycling and aboveground biomass. Our assessment in this section is twofold: firstly, to analyse whether MODIS DA improves C flux and biomass estimation when SPAc is driven with reported sowing dates. Secondly, we conduct the same analysis for SPAc outputs under satellite-derived (i.e. modelled) sowing dates. This second assessment is the actual proof of our DA hypothesis: that we are able to retrieve a reliable estimate of crop C cycling and biometry with a model that is driven with modelled sowing dates and updated by assimilated MODIS RDVI values. We conducted the following model experiments: 1) model forward (no DA) run forced with farmer reported sowing dates (FWrep), 2) as FWrep but with MODIS DA (DArep), 3) model forward run forced with modelled sowing dates (FWmod), and 4) as FWmod but with MODIS DA (DAmod).

We find a good agreement between ground-observed and MODIS-derived LAI at Bondville for years 2001–2006 ($R^2 = 0.74$, $RMSE = 1.08$ m^2 m^{-2}), but MODIS data are negatively biased (mean error (i.e. MODIS LAI minus Bondville ground-truth) = -0.49

m^2 m^{-2}, Figure 5.5). This agreement is particularly strong with regards to the observed seasonality of LAI evolution of maize and soybean, which is in turn largely controlled by site-specific sowing dates. The periods of rapid LAI increase in May and senescence in September as shown by the ground-truth data are well captured by MODIS. However, maximum ground-observed LAI values often appear underestimated (e.g. by ∼0.5–1 m^2 m^{-2} for maize 2003 and soybean 2005) by MODIS, but is overestimated for soybean ground-observed LAI > 6 m^2 m^{-2} (2004). The data show large interannual differences in peak LAI values, and both data sources reproduce a pattern of highest LAI in 2004 and lowest values in 2005. MODIS-derived LAI are <0.3 m^2 m^{-2} during fallow periods, with the exception of a slight increase during the weeks before sowing in 2002 and 2004. In 2001, the lack of MODIS Aqua data (the sensor started operation in May 2002) is responsible for larger gaps in the observational record.

The assimilation of MODIS RDVI data generally improves the simulation of LAI by reducing a negative bias (mean error (i.e. mod. minus obs.) = -0.45 m^2 m^{-2} (FWrep), -0.41 (DArep), -0.57 (FWmod), -0.40 (DAmod)) and constraining seasonality (Figure 5.5). FWmod data show that, compared to the ground-truth data, modelled LAI is underestimated in all years (R^2 = 0.68 (0.70 with reported sowing dates), *RMSE* = 1.27 (1.20) m^2 m^{-2}). The seasonality of observed LAI is generally better captured than its overall magnitude. Late sowing of the summer crop extends the duration of C_3 grass growth (Table 5.2), and leads to particularly large pre-sowing LAI values of >4 m^2 m^{-2} in 2002 (see also Hollinger *et al.* (2004)). With the assimilation of MODIS RDVI (DAmod), modelled LAI is generally closer to ground-truth data (R^2 = 0.78 (0.78 with reported sowing dates), *RMSE* = 1.02 (1.03) m^2 m^{-2}). The assimilation impact is particularly evident for years 2002 to 2004 (improved peak LAI value), and 2002 and 2003 (improved seasonality through MODIS constraints shortly after sowing and/or before harvest). The long data gap in early 2001 leads to a late "correction" of model maize LAI by mid-June. Growth of C_3 grass is reduced due to the assimilation of relatively low RDVI during fallow periods. DAmod fallow weed LAI is largest before sowing in 2002 (up to ∼0.9 m^2 m^{-2}). DA successfully informed about rapid growth following late sowing of the soybean crop in 2002 (which was underestimated by

FWmod), and thus appears suitable for correcting model deficiencies during anomalous years.

Growing season observed NEE data are generally well reproduced in terms of magnitude and seasonality by all model experiments, with model fits for DAmod ($R^2 = 0.63$) > FWmod (0.59) > DArep (0.58) > FWrep (0.55, Figure 5.6). There are only small adjustments in *RMSE* estimates (all within 3.67 gC m^{-2} d^{-1} to 3.73 gC m^{-2} d^{-1}), but positive model bias is reduced through DA (mean error (i.e. mod. minus obs.) = 0.99 gC m^{-2} d^{-1} (FWrep), 0.65 (DArep), 1.15 (FWmod), 0.76 (DAmod)). For experiments with reported sowing dates, model improvements through MODIS DA are largest for soybean and are generally negligible for maize years. Compared to FWmod, experiment DAmod shows improved R^2 for all growing seasons but maize 2003.

FWrep data reveal a model deficiency in the timing and/or rate of senescence during maize years (Figure 5.6 a)). Magnitudes of peak C uptake are generally well reproduced and reflect expected patterns of a C_3/C_4 photosynthesis type crop rotation. With warming temperatures in the spring months, but also in late autumn, daily negatives of NEE are associated with the growth of weed grass (Hollinger *et al.*, 2004), which was particularly intense in spring 2003 (Figure 5.6). This pattern is not well reproduced by FWrep data. Simulated fallow period C uptake is only evident in the weeks before sowing in 2002 and 2004, but is otherwise largely balanced by heterotrophic respiration. MODIS DA (DArep) produces a slightly better fit (mean $R^2 = 0.55$ FWrep, 0.58 DArep) between observed and simulated NEE for all growing seasons (sowing to harvest) but 2005 (Figure 5.6 b)). Fit improvement is largest for soybean years. Compared to FWrep, FWmod experimental data show that SPAc explains ~4% more of the observed variability solely through adjustments in sowing dates (Figure 5.6 c)). However, there are still discrepancies in terms of a delayed start of the crop C assimilation phase (2002), timing of senescence, and of an underestimation of the growing season sink strength (all years, but particularly 2003 and 2005). When RDVI data are assimilated (DAmod), this positive bias in NEE is reduced (from 1.15 gC m^{-2} d^{-1} to 0.76 gC m^{-2} d^{-1} (mean error), Figure 5.6 d)).

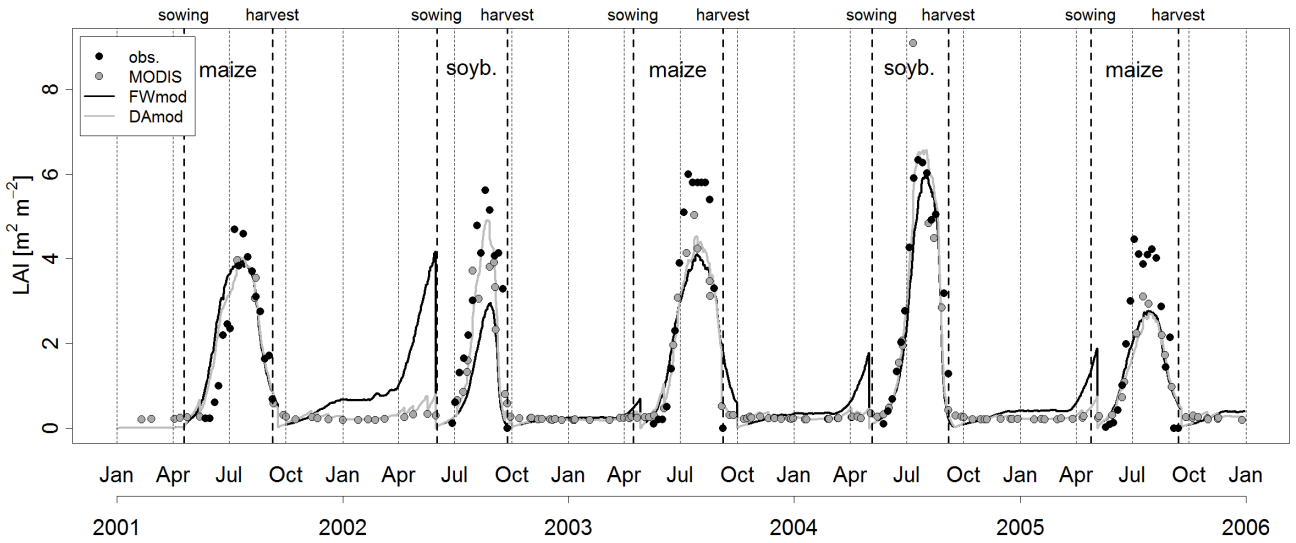

Figure 5.5: Observed (black circles), MODIS-derived (grey circles), and modelled LAI (experiments FWmod and DAmod, black and grey lines) for the Bondville EC flux tower site, 2001-2006. The vertical dashed lines denote farmer reported sowing and harvest dates for the flux site.

Closer agreement between observed and modelled growing season NEE after MODIS DA is brought about in two ways: 1) The assimilation of low RDVI reduces weed grass growth and related litter fluxes during fallow periods. Consequently, litter C content at crop sowing is lower in DA than forward runs, and subsequent growing season litter C mineralization is reduced. 2) MODIS DA increases the agroecosystem's photosynthetic potential during the growing season. As the LAI data suggest (Figure 5.5), MODIS DA increased growing season sink strength by increasing the crop's green canopy surface. When comparing observation-derived and modelled gross primary productivity (GPP, data not shown), we clearly see that growing season photosynthesis (and the quality of fit between observed and modelled GPP) increased through MODIS DA, with largest gains for experiment DAmod. MODIS DA appears generally useful to correct for model deficiencies during growing seasons, but carries relatively little informational content about fallow season C_3 grass growth and C assimilation, which are poorly reproduced in all experiments.

Forward simulated C_{stor} (FWrep and FWmod, Figure 5.7) is, except for soybean 2004, generally lower than observed. Nonetheless, interannual variability is largely reproduced, with modelled and observed maize C_{stor} in 2003 > 2001 > 2005. Observed data are subject to uncertainty for years 2004 and 2005, when differences between in-field dry matter (DM) measurements and farmer reported C_{stor} (published in bushels acre^{-1}) are particularly large. Visual analysis of DM time series data indicates that the final C_{stor} value in 2005 is probably an overestimate, as observations of previous days remained on a constant lower level closer to the farmer's observation ($\sim$490 gC m^{-2}, data not shown). Forward model soybean C_{stor} is underestimated in 2002, but very close to the DM measurement in 2004. In contrast to maize, soybean model values show rather little sensitivity to sowing dates (i.e. FWrep and FWmod data similar).

MODIS DA improves the simulation of C_{stor} in 2001 and 2002 by reducing a negative bias, but increases the gap between model and observations in other years. C_{stor} is generally increased by two means: 1) an increase of the total amount of C partitioned to the storage organ due to successive LAI (and thus C uptake) increases, and 2) immediate adjustment of the C_{stor} state estimate at the DA time step through the correlation of

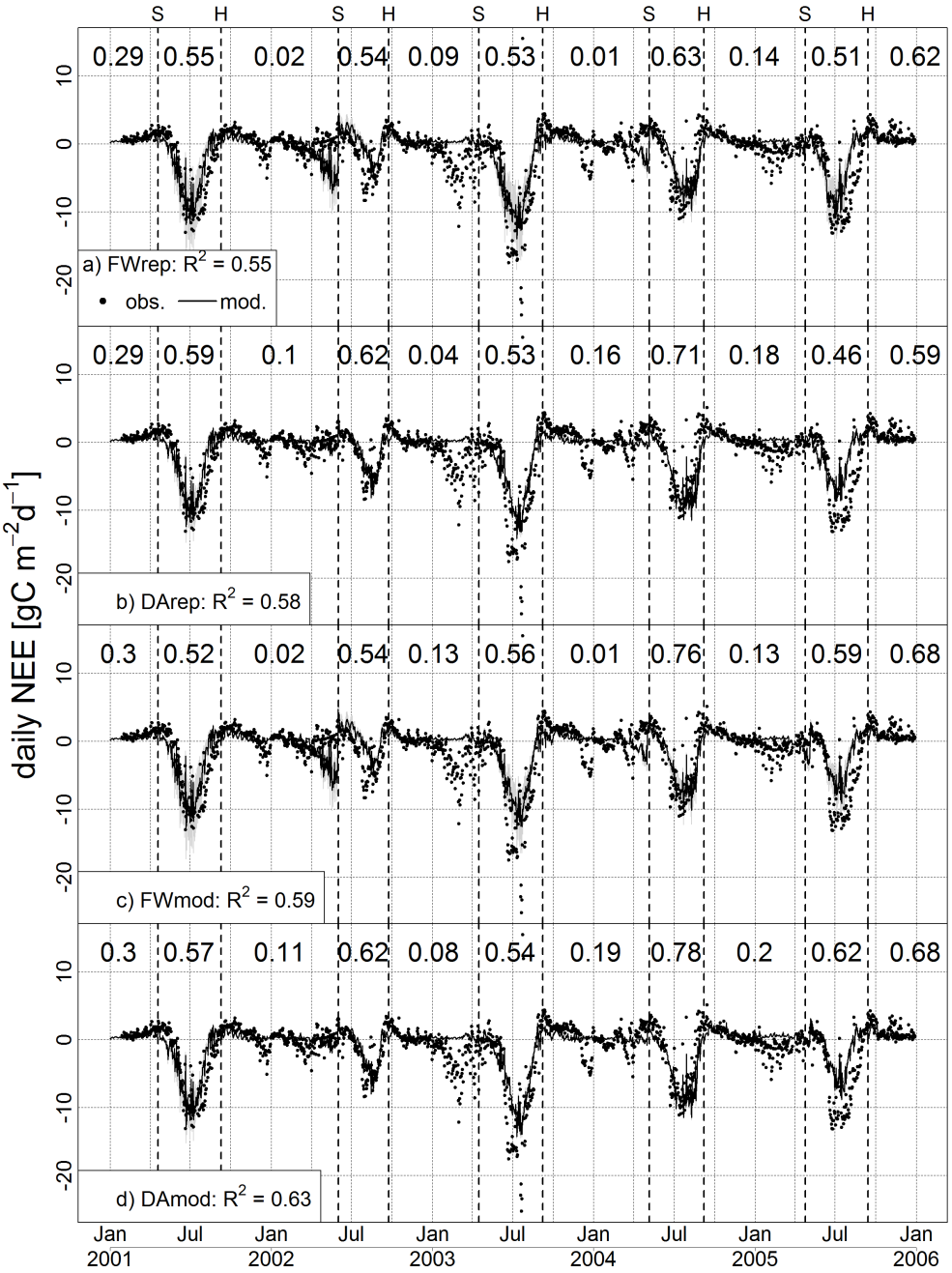

Figure 5.6: Observed (dots) and modelled (black line) daily NEE [gC m^{-2} d^{-1}] from 2001-2006 for the Bondville EC flux tower site (maize in odd years, soybean in even years). Model ensemble spread (or uncertainty, $\pm 1\ \sigma$) is shown as the shaded grey area, vertical dashed lines denote farmer reported sowing (S) and harvest (H) dates. Model values are shown for the four DA experiments (a-d). Squared correlation coefficients (R^2) between observations and modelled NEE are shown for each sub phases at the top of each panel (growing seasons: black values, fallow periods: grey), and as the 2001-2005 growing season average in the legend.

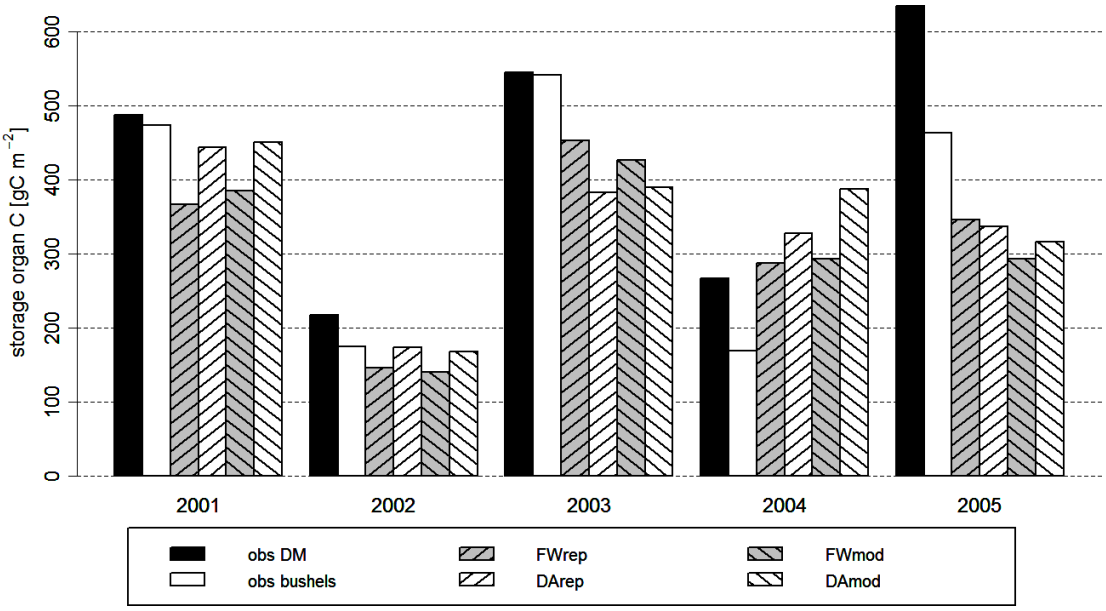

Figure 5.7: C_{stor} [gC m^{-2}] as observed at Bondville (derived from dry matter measurements ("obs DM") and derived from farmer reported yield in bushels ("obs bushels")), and for the four model experiments (see legend) from 2001-2005. Odd years: maize, even years: soybean.

RDVI and C_{stor} within the model state vector (both positive and negative). Model time series data (not shown) indicate that 1) was the main reason for C_{stor} increases in all years but 2003, and 2) for reductions in C_{stor} after DA in 2003 (mass balance breaches of ∼-60 gC m^{-2}). After DA, soybean C_{stor} is overestimated in 2004.

Cumulative NEE is generally overestimated (i.e. sink strength underestimation) by all model experiments (by ∼900 gC m^{-2} after 5 years), with this underestimation being ∼100 gC m^{-2} larger for experiments with modelled sowing dates (data not shown). In general, there is little difference in final estimates between FW and DA experiments. Observations and experimental data are rather close until before spring 2003. Partly because SPAc poorly reproduces fallow weed grass growth (and/or underestimates crop GPP), the gap between observations and model values increases (especially in 2003 and 2005). A careful analysis of these data should bear in mind that "observed" cumulative NEE is estimated on the basis of both measured and gap-filled half-hourly NEE. Of the data shown here, ∼51% of half-hourly NEE is gap-filled.

Presumably all C contained in the storage organs that were removed from the field at

harvest is consumed and thus respired afterwards. Consequently, C_{stor} has to be added to cumulative NEE in order to derive an estimate of observed Net Biome Productivity (NBP, here ∼-210 gCm^{-2} for the study period, Table 5.3). Measurements suggest that this no-till agroecosystem is still a C sink after accounting for harvested C mass (but not for the C-fuel emissions from production equipment). Cumulative NBP is overestimated by all model experiments, and this overestimation increases when MODIS data are assimilated (NBP mod. minus obs. ≈ 200 gC m^{-2} (FWrep), 260 gC m^{-2} (DArep), 260 gC m^{-2} (FWmod), 450 gC m^{-2} (DAmod), data not shown). Compared to cumulative NEE, the gap between FArep and FAmod reduced, but differences between forward and DA values increased (especially true for DAmod). Forward model data suggest that this agroecosystem is about C neutral after accounting for exported C. Compared to the two FW experiments, the increase in NBP through DA (final NBP for DAmod ∼240 gC m^{-2}) is mainly related to 1) the suppression of fallow season weed grass C assimilation and 2) C_{stor} mass balance breaches due to correlations with RDVI within the model state vector. However, gains and losses in C_{stor} through mass balance breaches are about balanced (data not shown). Accordingly, our experimental data show that it is the failure of MODIS DA to inform about fallow season C uptake that explains the gap between FW and DA model data (in fact, MODIS DA increased crop LAI and GPP).

5.3.3 Upscaling — Simulated LAI, C_{stor}, and cumulative NEE of the study area after MODIS DA

Statistical assessment of study area model averages and observations

Considering the field-patch specific sowing dates, and after the assimilation of corresponding MODIS RDVI time series, average (of 104 pixels) annual cumulative NBP of the study area is positive for both crops (152 ± 94 gC m^{-2} y^{-1} for maize and 77 ± 65 gC m^{-2} y^{-1} for soybean, Table 5.3), and crop rotations are net C sources in all years including fallow periods. Through DA, we are able to quantify a considerable variability of cumulative NEE and NBP within the study area. For NEE, this variability has a mean standard deviation of 56 gC m^{-2} y^{-1} for maize and 39 gC m^{-2} y^{-1} for soybean,

and is almost double for NBP (see above) because of the additional consideration of modelled C_{stor} variability.

While, in terms of NBP, all study years are net sources of C, variability is considerably large so that estimates are often not significantly different from zero. This is especially true for most soybean years (except for 2000 and 2002) and maize in 2002, 2003, and 2006. The region's C source strength varies between a low for both crops in 2003 and 2006 (NBP only slightly positive for both crops) and a clear high in 2000. Observed NBP is positive for four years, and strongly negative only in 2003. This strong sink strength in 2003 is largely responsible for overall negative observed NBP after five years, as the ecosystem loses on average ∼60 gC m^{-2} y^{-1} during other years (but note considerable uncertainty due to reported C_{stor} and the flux data themselves, not explicitly shown in Table 5.3). Model NBP is positively correlated with NEE ($R = 0.78$ and 0.96 for maize and soybean, respectively), and weakly to negatively correlated with yield (R = 0.19 and -0.50) and LAI (R = -0.13 and -0.03). Model NEE is generally strongly negative (significantly different from zero when accounting for study area variability) except for 2000, when NEE of both crops is close to zero. In terms of NEE, sink size is larger for maize than soybean (by ∼54 gC m^{-2} y^{-1}), but maize is a stronger source of C (by ∼75 gC m^{-2} y^{-1}) in terms of NBP. Observed NEE is clearly lower than modelled for maize, but (except for 2002) larger during soybean years (note that bold model values in Table 5.3 are same crop types as cultivated at Bondville during given year).

Compared to Bondville observations, model C_{stor} is lower for maize, and about equal to larger for soybean. C_{stor} mass is largest (smallest) in 2004 (2002) for maize and in 2006 (2002) for soybean, and is on average ∼130 gC m^{-2} higher for maize than soybean. Yield variability is ∼10% of the study area mean for both crops. Maximum LAI of soybean is on average ∼2.6 m^2 m^{-2} greater than that of maize, and study area variabilities of both crops are comparable (∼0.5 m^2 m^{-2}). Again, 2002 is the year with lowest values on record. Differences between model values and observations are generally within 0.5 m^2 m^{-2}, except for 2004 (1.5 m^2 m^{-2} mod. > obs.).

Table 5.3: Observed (at Bondville, where available) and study area model averages and standard deviations for maximum LAI, storage organ C at maturity, and cumulative NEE and NBP (all year). Observed storage organ C is shown for field dry matter samples, and farmer reported values (in parentheses). Bold model values are same crop types as at Bondville. Model values are averages of all soybean or maize field patches in a given year.

year	LAI max [m^2 m^{-2}]			Storage organ [gC m^{-2}]			Cum. NEE [gC m^{-2} y^{-1}]			Cum. NBP [gC m^{-2} y^{-1}]		
	obs	soybean	maize	obs	soybean	maize	obs	soybean	maize	obs	soybean	maize
2000	-	7.9 ± 0.4	4.8 ± 0.5	-	278 ± 28	464 ± 39	108	17 ± 28	-49 ± 39	-	295 ± 40	415 ± 55
2001	4.7	7.3 ± 0.3	5.2 ± 0.4	487 (474)	278 ± 24	441 ± 38	-405	-223 ± 42	-268 ± 72	82 (69)	55 ± 48	173 ± 81
2002	5.6	6.1 ± 0.6	3.8 ± 0.7	217 (174)	204 ± 24	239 ± 45	-143	-76 ± 27	-140 ± 73	74 (31)	128 ± 36	99 ± 86
2003	6	7.4 ± 0.4	5.5 ± 0.3	545 (542)	297 ± 22	472 ± 36	-927	-285 ± 40	-434 ± 48	-382 (-385)	12 ± 46	38 ± 60
2004	6.3	7.9 ± 0.5	4.9 ± 0.3	267 (169)	329 ± 34	509 ± 33	-252	-302 ± 48	-374 ± 49	15 (-83)	27 ± 59	135 ± 59
2005	4.5	7.7 ± 0.5	4.1 ± 0.4	635 (463)	312 ± 29	383 ± 38	-570	-298 ± 34	-236 ± 66	65 (-107)	14 ± 45	147 ± 76
2006	-	7.6 ± 1	5.3 ± 0.7	-	334 ± 25	435 ± 38	-22	-329 ± 52	-378 ± 44	-	5 ± 58	57 ± 58
mean	-	7.4 ± 0.5	4.8 ± 0.5	-	290 ± 27	420 ± 38	-316	-214 ± 39	-268 ± 56	-29 (-95)	77 ± 65	152 ± 94
$\sum$	-	-	-	-	-	-	-2211	-1496 ± 105	-1879 ± 152	-	536 ± 175	1064 ± 252

Time series analysis of modelled and observed NEE, NBP, and C_{stor}

Study area average model values are nearly identical to the Bondville cumulative NEE flux data value (∼-2970 gC m^{-2}) when only considering the growing season C balance (sowing-harvest, Figure 5.8 c)). Both crop rotation types (maize-soybean (i.e. maize sown in even years), and soybean-maize rotations (i.e. soybean sown in even years)) and observations are within <100 gC m^{-2} after the seven study years. Bondville observed data for growing season cumulative NEE are supposedly positively biased because of the ongoing decomposition of fallow weed grass residue during the growing season itself (which is much lower in model runs, as MODIS DA largely restricts fallow season growth). Assuming an average weed grass litter C input of ∼200 gC m^{-2} y^{-1} at sowing (probably an overestimate), the cumulative mineralization flux of this litter component is ≤15 gC m^{-2} between sowing and harvest, or ≤105 gC m^{-2} after the seven study growing periods (see Buyanovsky *et al.* (1987) for crop litter mineralization rates).

For all season NEE data (Figure 5.8 b)), the gap between modelled and observed NEE is considerably larger. Modelled NEE is ∼500–650 gC m^{-2} higher than Bondville observations by end-2006 (note that data in Figure 5.8 are for crop rotations, but for single crop types in Table 5.3). For both modelled crop rotations, the observed fallow season C uptake is virtually absent and instead continuous heterotrophic respiration C losses prevail. By end-2006, the study area-wide modelled NEE variability has a standard deviation of ∼ ±130 gC m^{-2}.

For 2001-2005, observed cumulative NBP data indicate a net C sink of ∼-210 gC m^{-2}, whereas modelled crop rotations indicate a net C source of ∼315 gC m^{-2}–513 gC m^{-2} (Figure 5.8 a)). Model data are close to Bondville observations until after autumn 2001 (dashed line in Figure 5.8 a)), but a gap continuously builds up during fallow periods (especially spring 2003).

Compared to large-scale observational data, study area averages of modelled C_{stor} are of rather similar quality with or without DA, but residuals could be reduced (Figure 5.9). Clearly, NASS observed interannual variability of maize C_{stor} (which

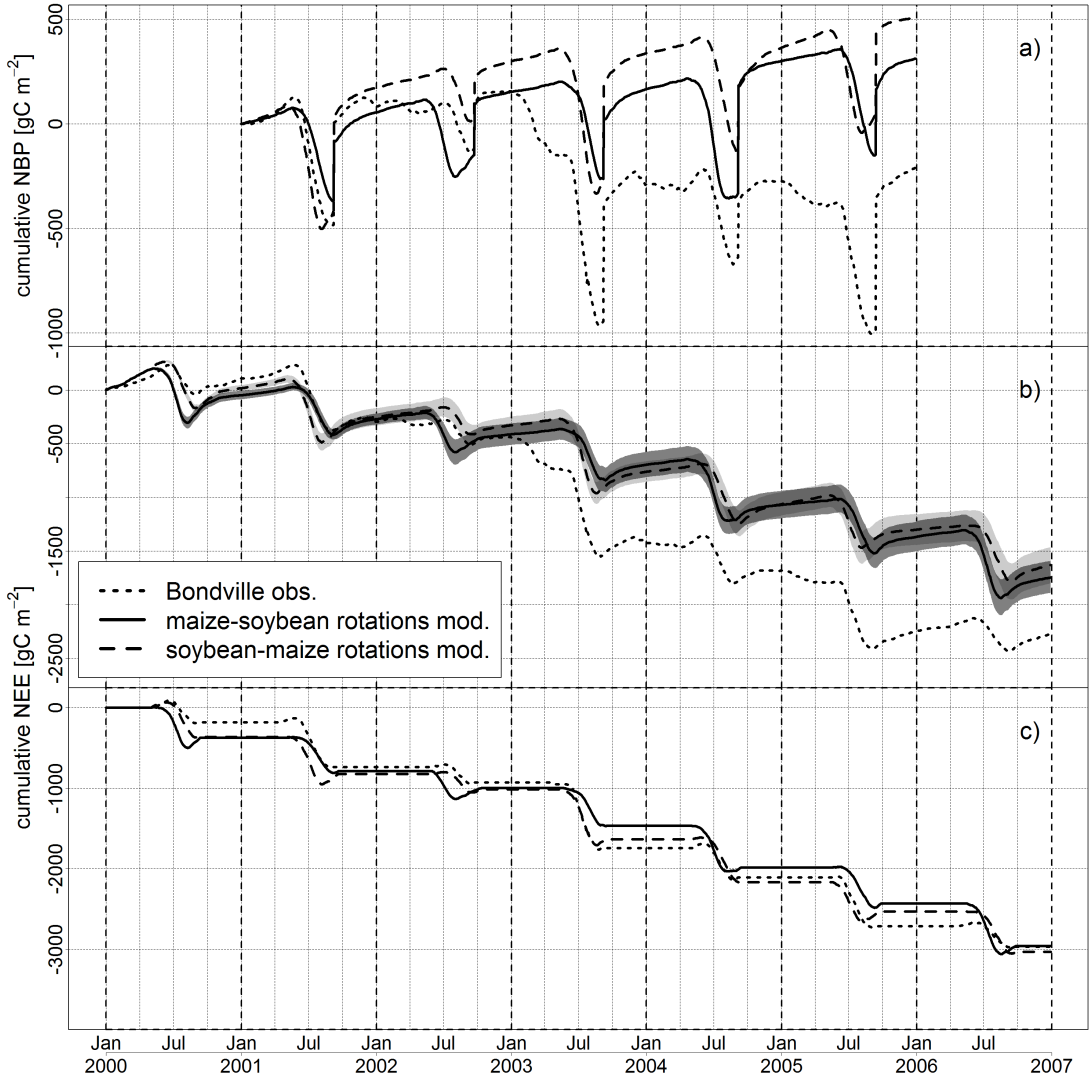

Figure 5.8: Study area model averages (experiment DAmod) and Bondville EC measurements of a) cumulative NBP (from 2001-2005), b) cumulative NEE, and c) cumulative NEE for growing periods (sowing to harvest) only. Model data are shown for pixels with maize sown in even (odd) years, i.e. maize-soybean (soybean-maize) rotations. All values are in gC m^{-2}. The shaded areas in panel b) denote ± 1 σ study area model variability.

is considerably larger than for soybean) is reproduced by study area averages of both model experiments. DA basically resulted in an overall shift of model data to lower values, which is most obvious in 2002. The statistical fit between NASS observations and model is of lower quality after DA (R = 0.70 for forward and 0.60 for DA simulations), but residuals are reduced nonetheless (from $RMSE$ = 92.2 to 78.9 gC m^{-2}). For soybeans, the forward data fit with observations is rather poor (R = -0.18), and is improved by DA (R = 0.06). $RMSE$ is clearly reduced from 177.3 to 92.2 gC m^{-2}, but a positive bias in modelled soybean C_{stor} remains. As observations show, relatively high soybean C_{stor} was reported in 2002 despite of the considerably delayed sowing progress. For this year, model estimates are the lowest on record, but are brought closer to observations through DA.

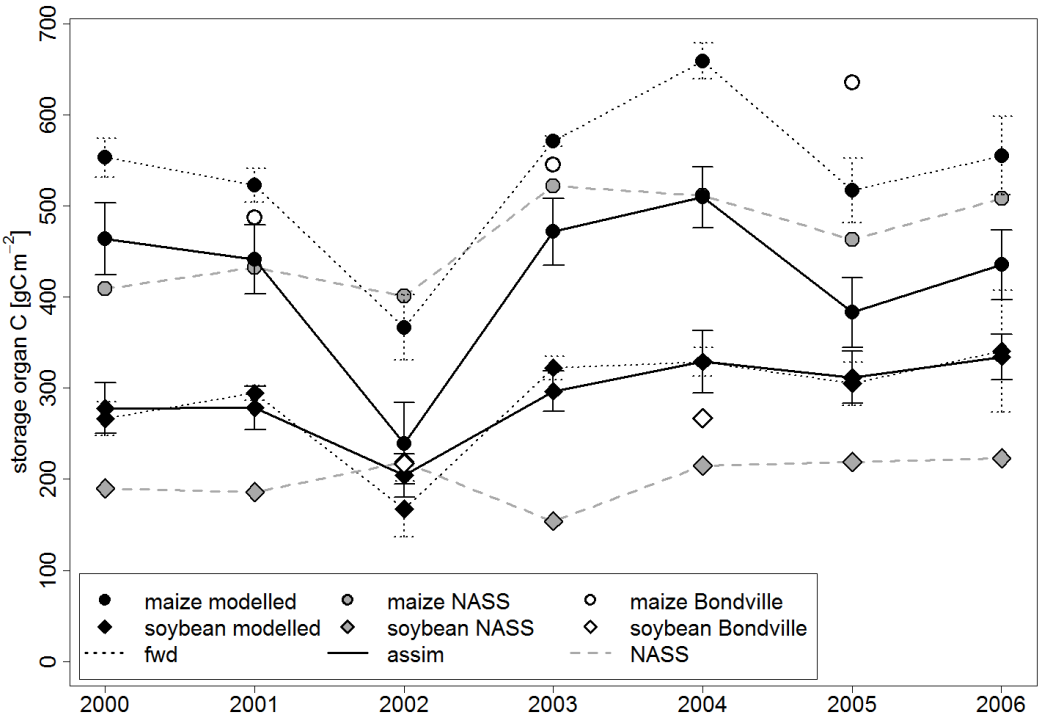

Figure 5.9: Modelled (black symbols) and observed (NASS: grey symbols, Bondville: open symbols) C_{stor} at maturity. Model data are shown for experiments FWmod (black dotted lines) and DAmod (black solid lines), together with their corresponding study area variability over the 104 MODIS pixel locations ($\pm 1\ \sigma$ uncertainty bars). NASS observations (Champaign county) are connected with grey dashed lines.

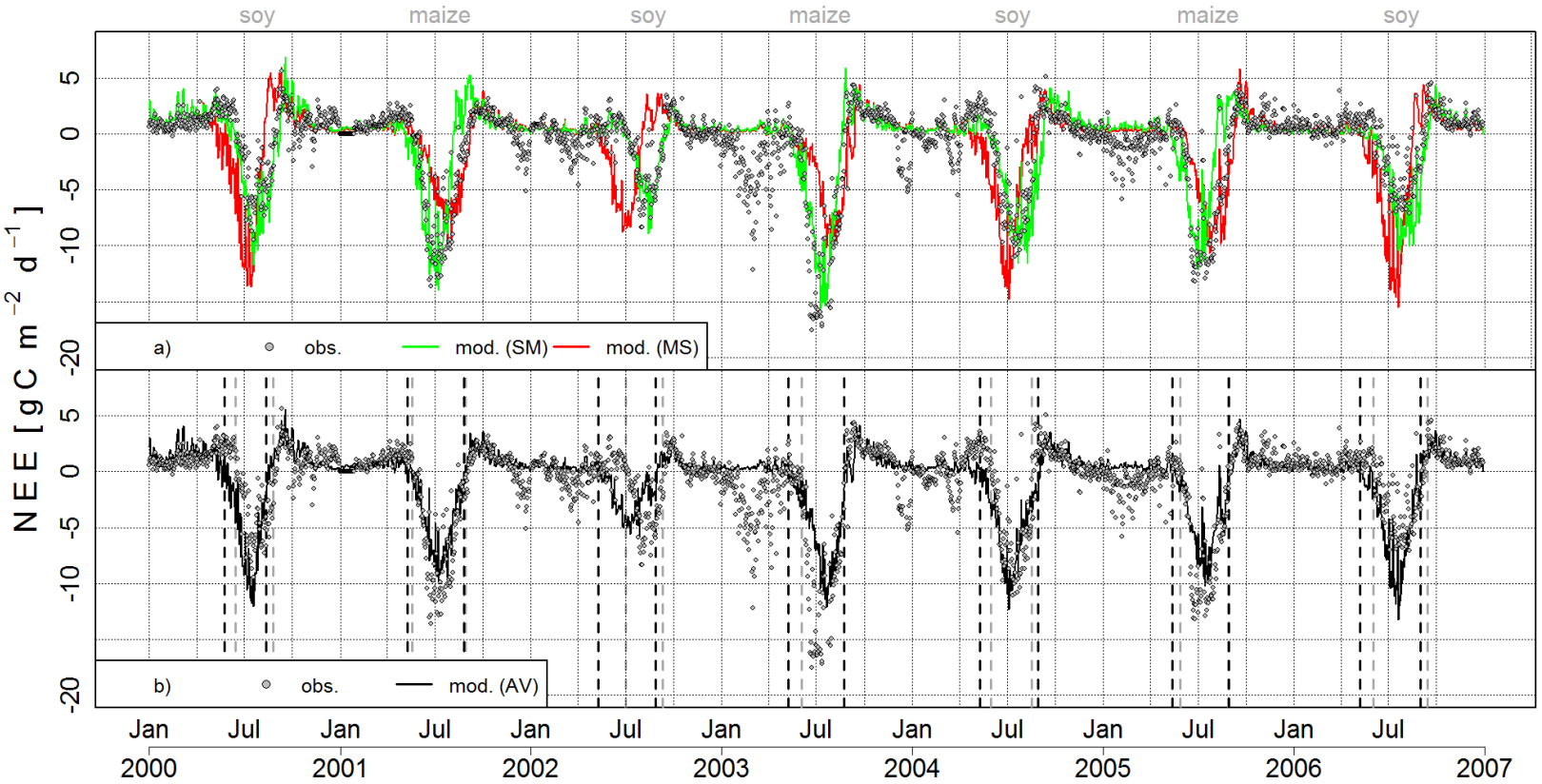

Figure 5.10: Study area averages of modelled NEE fluxes (lines) and as observed at Bondville EC site (grey circles). Model data shown are a) crop rotations with soybean sown in even years (green line, soybean-maize (SM), as Bondville site rotation), soybean sown in odd years (red line, MS), and b) means over all 104 MODIS pixel locations (black line, average (AV), i.e. not crop type specific). Vertical dashed lines in b) denote SoS and EoS dates as estimated from model data (black) and observations (grey).

Model data suggest clear differences in the seasonality of MSCR C fluxes within the study area compared to observations. These differences are mainly attributable to earlier estimated start of season (SoS, i.e. timing of sink-crossover after sowing using a 10 day moving average of the time series analysed) values. Study area averages of modelled soybean-maize rotations generally reflect interannual patterns in SoS and end of season (EoS, i.e. timing of source-crossover after SoS) as observed at Bondville (Table 5.4), but discrepancies exist. Model-derived SoS are generally lower than Bondville values (by ∼2 weeks on average, soybean-maize (SM) rotations in Table 5.4), and DOYs are closer to Bondville values for soybean than maize years. This prematurity in SoS is even larger for maize-soybean (MS) rotations (∼25 days) and the study area flux average (AV, ∼23 days). In 2002, model SoS values are >1.5 months premature (MS and AV). These discrepancies are lower for EoS estimates, which are again generally earlier than "observed" by ∼5 days (SM), ∼11 days (MS), and ∼4 days (AV). Consequently, modelled average growing season length (GSL = EoS - SoS) is about 9 to 20 days longer than derived from Bondville measurements.

Further, we see that the magnitude of modelled growing season C fluxes reflects observed patterns well (green line in Figure 5.10 a)). Fallow season weed growth (C uptake) and decay (C emission) are not reproduced, but post-harvest NEE fluxes (dominated by crop residue decomposition) are close to measurements. The Bondville flux data appear representative of SM rotations within the study area. However, modelled MS rotations (red line in Figure 5.10 a)) clearly differ in growing season C uptake magnitude and seasonality during all study years.

The pattern of study area mean model fluxes reveals the year-to-year variability in regional ecosystem sink strength (black line in Figure 5.10 b), which is the average of all maize and soybean pixels for each year), rather than sink strength variability due to C_3/C_4 crop type rotation. The magnitude of C sink strength in 2002, when sowing dates have been reported to be particularly late, is considerably lower compared to other years. As expected, model data show larger (lower) C uptake during Bondville soybean (maize) growing periods than observed. Clear seasonality shifts towards earlier DOYs are most obvious during Bondville soybean years (especially 2002).

Table 5.4: Observed (obs., at Bondville) and modelled (mod.) start of season (SoS), end of season (EoS) DOYs, and growing season length (GSL) in days. Model data are shown for pixels with soybean grown in even years (soybean-maize (SM), as Bondville site rotation), with soybean grown in odd years (maize-soybean (MS)), and averaged over all pixels (AV).

year	SoS				EoS				GSL			
	obs.	mod. (SM)	mod. (MS)	mod. (AV)	obs.	mod. (SM)	mod. (MS)	mod. (AV)	obs.	mod. (SM)	mod. (MS)	mod. (AV)
2000	166	160	126	145	238	244	216	225	72	84	90	80
2001	139	123	139	131	242	216	246	239	103	93	107	108
2002	184	182	130	131	254	256	212	241	70	74	82	110
2003	155	127	132	130	236	229	252	236	81	102	120	106
2004	152	145	110	131	231	249	219	243	79	104	109	112
2005	150	130	156	135	242	215	252	244	92	85	96	109
2006	155	132	128	130	259	256	227	245	104	124	99	115
mean	157	143	132	134	243	238	232	239	86	100	95	106
mod.-obs. (from mean)	-	-14	-25	-23	-	-5	-11	-4	-	14	9	20

5.4 Discussion

5.4.1 Does MODIS DA improve model reproduction of Bondville ground-truth data?

We generally find that all model experiments are able to reproduce the seasonality in observed C fluxes at the Bondville EC site, but deficiencies in magnitude and fallow season C cycling are evident. Our main focus lies on analysing whether we can use MODIS RDVI time series for sowing date estimation and assimilation to compensate for model deficiencies and the scarcity of land management data. Hereby, we made the observation that with MODIS-derived sowing dates, SPAc is not only able to reproduce observed C flux seasonality, but the fit to observed data is even better when compared to model runs driven with reported sowing dates. MODIS DA further improves model performance in anomalous growing seasons. Accordingly, we developed a crop modelling framework that is readily applicable to major agricultural regions of the U.S. without necessitating a priori information of sowing dates, and probably of further land management practices (fertilisation, irrigation, cultivar selection, double cropping, Bondeau *et al.* (2007)) and disturbance events (frosts and droughts, Viña *et al.* (2004)).

Model improvement through simulated sowing dates

Our forward model proved to be deficient in reproducing peak photosynthetic capacity and timing and rate of senescence. SPAc appears to underestimate crop LAI, which is particularly true for maize. The current model calibration provides a reasonable overall fit to observations, but interannually, model performance strength is variable (e.g. lowest in 2002 and 2005). The model appears deficient due to its simplified structure of simulating crop development and senescence, and due to its rather generic calibration that should render SPAc suitable for spatio-temporal runs on larger scales.

Modelled sowing dates as input to our forward experiment (FWmod) improve the statistical fit of growing season NEE to observations (an R^2 gain of 0.04 compared

to FWrep), however cumulative NEE is now slightly higher than for FWrep (data not shown). Thus, modelled sowing dates improve NEE seasonality at the expense of a reduced C uptake potential. An independent constraint on crop LAI (MODIS RDVI) was used for finding the model sowing date which best reproduces observed seasonality in green aboveground biomass. This procedure clearly constrains the seasonality of cropland NEE. We aimed for improving simulated GSL by using all available MODIS data for each particular growing season in our fitting procedure. Most probably, we could have produced a better sowing date estimate by using only (and temporally more highly resolved) MODIS data during the vegetative phase (i.e. when LAI is increasing, as in Doraiswamy *et al.* (2004)). However, this approach would probably be detrimental for the merits of our DA procedure during senescence, the simulated timing and rate of which still need improvement (Kucharik and Twine, 2007; Suyker *et al.*, 2005; Sus *et al.*, 2010). It is further possible that fallow weeds might have introduced an early bias in retrieved sowing dates (Wardlow *et al.*, 2006), but MODSI RDVI showed little sensitivity to pre-crop vegetation (Figure 5.5).

Differences between MODIS-derived sowing dates and observed values (Figure 5.4) are indicative of deficiencies in model LAI and photosynthetic potential under ambient climatic conditions (when assuming that study area sowing patterns are representative of large-scale observations). Because modelled maize sowing dates are mostly premature (and earlier sowing dates generally produce larger model LAI), simulated maize green biomass is probably underestimated. The reported delay in sowing progress in 2002 is well captured for soybeans, but is not reflected for maize. Even though discrepancies with observations exist (2000 and 2003), soybean sowing dates are reproduced with higher accuracy, and LAI appears less negatively biased. A more detailed analysis of the quality of modelled sowing dates is not possible, as scale differences between model data (sub-county) and observations (census districts, Figure 5.1) are prohibitively large. More steps need to be taken to move from a qualitative to a more quantitative validation of satellite-derived sowing dates (Wardlow *et al.*, 2006). Note however that the Bondville site data suggest that modelled estimates of sowing dates are close to observations for soybeans (within 4 days), and delayed for maize ($\sim$12 days, except

for 2001). Bondville observations support the notion that modelled sowing progress appears plausible (reported sowing dates are (except for 2003) generally within the 40% to 80% range of modelled sowing progress, Figure 5.4).

The general applicability of MODIS data for sowing date assessment has been successfully demonstrated in several studies. Using MODIS NDVI and rainfall data, Brown and de Beurs (2008) were able to produce high relationships between derived sowing dates and observations for West Africa (R^2 = 0.89). MODIS-derived sowing dates were consistent with the relative order of sowing of major crops in Kansas (U.S., Wardlow *et al.* (2006)). Despite deficiencies, MODIS data bear sufficient informational content for increasingly improved estimates of crop phenology. Progress in this respect is probably most hindered by the lack of reliable, spatially resolved observational constraints.

Even though we expect mixed-pixel effects on retrieved MODIS time series for Bondville, there is clear evidence that forward model runs with derived sowing dates reproduce, if not improve, FWrep model agreement with two independently measured data types (NEE and LAI). These findings suggest that modelled sowing dates themselves, despite discrepancies with observed patterns, are suitable constraints for agroecosystem C cycling and biomass growth at the point-scale. MODIS-derived sowing dates allow for highly accurate simulations of agroecosystem C cycling at locations for which land management information is not available.

Model improvement through MODIS DA

We found that MODIS DA improves our forward estimate of growing season C cycling by reducing a negative bias in model LAI (FWrep: R^2 = 0.55, mean error = -0.45 m^2 m^{-2}; DArep: R^2 = 0.58, mean error = -0.41 m^2 m^{-2}, Figure 5.6). Model improvements result from DA updates in model LAI (and a subsequent increase in GPP) and, to a lesser extent, from a reduction of growing season litter mineralization, as fallow season weed growth is suppressed. This statistical fit improvement is of similar magnitude

for both DA experiments (an R^2 increase of ∼0.04 compared to forward runs, i.e. improvement of reproducing observed variability by 4%). Out of all experiments, we find the highest growing season fit score and bias reduction for DAmod ($R^2 = 0.63$; mean error reduced from -0.57 m^2 m^{-2} (FWmod) to -0.40 m^2 m^{-2}). The quality of model results is comparable to predicted Bondville C fluxes (1996-2003) from SiBcrop (mean $R^2 = 0.58$, but derived under consideration of *reported* sowing dates, Lokupitiya *et al.* (2009)).

Both DA experiments independently confirm that MODIS data generally improve the estimation of growing season C fluxes. However, understanding to what extent this improvement is caused by an increase in GPP or a decrease in weed litter mineralization is complicated by the lack of observational constraints. We qualitatively compared model to EC-derived GPP, and found clear indications that forward model GPP is an underestimate, and DA brought GPP closer to observations through increasing LAI (data not shown). FW model growing season data are affected by litter mineralization. This C flux could be overestimated (either due to erroneous initial conditions in litter C content, or due to an overestimate in litter mineralization rate), and thus could explain part of the mismatch between modelled and observed NEE. However, as field data show (Buyanovsky *et al.*, 1987), this mineralisation flux during the growing period is rather small (∼15 gC m^{-2} growing $period^{-1}$ assuming a litter C input of ∼200 gC m^{-2} before sowing) compared to GPP and autotrophic respiration, and thus of second order importance.

We further acknowledge that our current model-DA-scheme is not exploiting the full potential of MODIS VI data for constraining agroecosystem C cycling. One deficiency in our model scheme is the representation of crop senescence. Here, we adopted a simple approach (van Laar *et al.*, 1997) where leaf senescence rate increases with developmental stage in the reproductive phase, until reaching its maximum potential rate shortly before maturity. Simulated crop senescence appears premature for soybean (Figure 5.5, Figure 5.6), and thus reduces MODIS DA potential during this developmental phase. Consequently, an improved senescence model is necessary that provides a better forward model agreement with observations. We tested a DA run

without simulated crop senescence, and found that C uptake was clearly overestimated. MODIS data uncertainty and temporal resolution are the main reasons why a smooth senescence curve could not be reproduced, and LAI at maturity (when it should be zero due to senescence) was about half its peak value. We expect considerable benefits from improvements in modelled senescence, and assimilation of MODIS data with higher temporal resolution (e.g. MOD09GQ). Scaling from MODIS RDVI to LAI using an empirical relationship is a considerable source of uncertainty in this study. However, we expect the influence on derived seasonality metrics to be comparably small, as timing of Bondville observed biomass growth and decay are clearly reproduced. Nonetheless, the application of a canopy reflectance model could provide improved estimates of C_{stor} (Doraiswamy *et al.*, 2004). It also has been shown that the simultaneous assimilation of the MODIS LAI product and EVI or NDVI data resulted in improved model agreement with NASS reported maize yields (Fang *et al.*, 2011).

We conclude that Bondville model data serve as a sound proof of our DA concept. MODIS data allow for spatio-temporal applications of SPAc without a priori knowledge on sowing dates. Even though certain model deficiencies remain unresolved after DA (such as fallow weed C uptake), we are confident that our methodology provides a representative upscaled estimate of agroecosystem C cycling (in particular of its seasonality). Our conclusions confirm previous findings that MODIS data contain enough useful information for correcting some deficiencies in a global BGCM (∼40% reduction of *RMSE* in modelled agricultural C fluxes and improved estimated GSL, Demarty *et al.* (2007)). The benefits of MODIS DA are particularly considerable during years of abnormal sowing patterns (as observed here in 2002), as their influence on crop establishment and growth are still rather poorly represented within SPAc. MODIS temporal and spatial resolution are sufficient to derive important information on land management and crop condition on scales for which ground observations are not readily available (see also Dorigo *et al.* (2007)). RS DA is also a suitable tool for mitigating uncertainties due to model parameters and weak understanding of phenological processes (Stöckli *et al.*, 2008). We encourage researchers to make us of MODIS' full spatiotemporal richness when addressing current key uncertainties of upscaled crop modelling. The applicability

of our DA approach is limited by the availability of crop type classification data outside of the U.S. However, MODIS seasonality has been used to provide such classification data in the U.S (Wardlow and Egbert, 2010) and the Ukraine (Becker-Reshef *et al.*, 2010), and is applicable to all agricultural regions with sufficient ground element (i.e. field patch) sizes given appropriate training data.

5.4.2 How large is the upscaled variability and seasonality in simulated C fluxes and biometry?

The consideration of pixel-specific sowing dates and MODIS DA allow for the quantification of variability in study area C cycling and biometry. Here we assume that all field sites within the study area are under no-till management as at Bondville (∼40% of U.S. croplands are no-till, Kucharik and Twine (2007)). Average relative spatial variability for C_{stor}, LAI, and NEE for both crops ranges from ∼7% to ∼10%. Variability of NBP though is considerably larger: ∼32% for soybean (536 ± 175 gC m^{-2} for study period), and ∼24% for maize (1064 ± 252 gC m^{-2}). These results show that, next to local meteorology, regional patterns of land management are important drivers of agricultural C cycling and major sources of uncertainty if not appropriately accounted for. Observing C cycling at one single field with its individual sowing pattern is not sufficient to constrain large-scale agroecosystem behaviour.

We find that the upscaled estimate of C flux seasonality is largely different from Bondville observations (i.e. mean GSL 20 days longer than observed, largely through earlier estimated SoS, Table 5.4), which nonetheless appear representative of the growing season C budget (Figure 5.8 c)). Whereas EC data appear representative for field patches with the same succession of crop types as at Bondville (i.e. soybean grown in even years, Figure 5.10), there are large differences in SoS and GSL values for modelled MS rotations (i.e. maize grown in even years). These in turn considerably affect mean study area NEE fluxes as they probably would be observed by a tall tower EC system with a footprint area covering a multitude of field patches. EoS metrics, which are strongly constrained by model senescence, are considerably closer

to observations throughout. Most likely, the developmental advantage of early sown crops is too little to cause considerable NEE variability around maturity. High summer temperatures accelerate crop development and result in a rather simultaneous decay in leaf biomass of all field patches. It is plausible that mean GSL increases when cropland NEE is averaged over several field locations: few "premature" sites will decrease mean NEE considerably, as their quickly increasing sink strength is soon larger than the rather small C losses of fallow sites (and vice-versa around maturity). That is partly why modelled SM rotations show little NEE phase shifts compared to observations (Figure 5.10 a)), even though growing season metrics differ (Table 5.4). Average GSL is within the range as observed for maize (102 to 112) by Verma *et al.* (2005), but they found measured soybean GSL to be ∼4 weeks shorter. The accurate quantification of GSL in itself is an important research aim. Important microclimatic variables such as atmospheric and soil temperature and humidity are strongly affected by vegetation cover (de Noblet-Ducoudré *et al.*, 2004; Kucharik and Twine, 2007). Trends in increasing GSL are indicative of farmers adopting longer season cultivars, which are known to provide more yield under a gradually warming climate (Sacks and Kucharik, 2011; Craufurd and Wheeler, 2009). GSL affects seasonal atmospheric CO_2 amplitudes (Keeling *et al.*, 1996) and possibly the terrestrial C balance (Piao *et al.*, 2007).

Differences between Bondville and upscaled NEE are especially large in years with non-optimal climatic sowing conditions (here in 2002). When intense spring precipitation delays field work, NASS reports suggest that farmers use (at times relatively short) time windows with drier weather conditions for crop sowing. This can lead to potentially large differences in maize and soybean sowing progress, as their usual time windows for sowing do not overlap. Thus, weather conditions during typical sowing phases can be considerably different for the two crops. The impact of excessive precipitation on crop sowing progress has been previously observed in the U.S. Midwest (a delay of several weeks in 1990, Changnon and Kunkel (1991)). Cool and wet conditions are favourable for pest development, and potentially affect the timing of major phenological events of rainfed crops (irrigated crops are relatively more phenologically stable, Reed *et al.* (1994)). DAmod data suggest that this was the case in 2002, when maize sowing and

establishment was about normal, but soybean progress was negatively affected by strong precipitation. If this modelled difference in NEE seasonality between the two crops was merely an artefact due to weaknesses in MODIS-derived sowing dates for maize (which appear to be premature compared to NASS data, Figure 5.4), early maize growth and C uptake would have been restricted through the assimilation of low MODIS RDVI data. Instead, model results suggest that the 2002 NEE seasonality shift (Figure 5.10) is realistic and supported by empirical evidence (NASS).

As the seasonality and regional variability of agroecosystem C cycling is considerably sensitive to sowing dates, the timing of this land management action needs particular attention in large-scale simulation runs. Models driven with sowing dates that are either static (e.g. soybean within LPJml, Bondeau *et al.* (2007)) or estimated through temperature thresholds (e.g. 10 °C for maize in ORCHIDEE-STICS, de Noblet-Ducoudré *et al.* (2004)) would not be able to reproduce the observed NEE phase shift and its consequence on C budgeting and biometry in 2002. Large-scale applications of cropland BGCMs certainly necessitate these simplifications, but associated uncertainties are large. In contrast to natural ecosystems whose C cycling primarily responds to climatic constraints and disturbances, croplands carry an additional "disturbance" signal provided by human management. Sowing progress is clearly linked to atmospheric variables, but their relationship is poorly quantified and difficult to predict from time series analysis of climatic data alone. The DA scheme developed and tested here appears highly suitable for accounting for human intervention and its knock-on effects on ecosystem services (such as fluxes of C, water, and energy). Our approach is a promising step forward in improving large-scale applications of BGCMs, within which the spatial extent of major crop types and temporally varying management schemes are major sources of uncertainty if not explicitly accounted for (McGuire *et al.*, 2001).

Through MODIS DA, we are able to improve simulated timing and duration of the crop residue layer. Crop residues were found to have an overwhelming influence on energy partitioning at the surface, and thus are important controls of biogeophysical feedbacks in coupled crop-climate models (Kucharik and Twine, 2007). Future larger scale applications (e.g. conterminous U.S.) could provide a thorough assessment of

the current state of agroecosystem C cycling and an improved quantification of the relationship between climate variables and sowing dates. As sowing delay and yield reductions are related (Andrade, 1995), a quasi operational application of this DA scheme could also be used as an early warning indicator of a decline in food production in less self-sufficient regions (e.g. West Sahel, Brown and de Beurs (2008)). Further, our DA scheme could allow for a detailed assessment of the "yield gap" (i.e. climatic potential yield - actual yield, Licker *et al.* (2010)), or possibly the "C sequestration gap" (modelled GSL might correlate with terrestrial C uptake, Piao *et al.* (2007)) of major agricultural areas. DA-derived "observed" GSL metrics could be compared with maximum potential GSL to see whether farmers exploit the full time period allowing for crop cultivation. This maximum GSL should be calculated with a well-calibrated crop model, which realistically simulates early season (e.g. frost damage, light limitation, precipitation) and late season (e.g. drought stress) environmental controls on crop sowing and growth. Further, developmental parameters could be varied to reflect the adoption of longer season cultivars (Sacks and Kucharik, 2011; Chmielewski *et al.*, 2004). Yield gaps are especially high in African countries and Eastern Europe, but also for wheat in the U.S and eastern Canadian plains (Licker *et al.*, 2010).

5.4.3 Does MODIS DA improve modelled C_{stor}?

Both Bondville and upscaled model results suggest that MODIS DA provides only moderate additional improvement in simulated C_{stor}. Observed seasonal variability is already well captured by forward model runs, and biases (e.g. study area maize C_{stor} overestimation, Figure 5.9) are only partly compensated for through DA. Residuals could be reduced, but correlation metrics improve only slightly (soybean) or deteriorate (maize). Mass balance breaches in C_{stor} are problematic during senescence if LAI is overestimated (maize 2003, Figure 5.5). In this case, the RS signal is interpreted as a reduction in aboveground biomass ($\approx C_{\mathrm{stor}}$ in the reproductive phase). Interconnection of LAI and C_{stor} poses a conceptual problem during reproductive growth, as C_{stor} is the only plant organ that does not senesce. A better yield estimate could presumably be achieved if C_{stor} was not part of the state vector, as mass balance breaches in

the reproductive phase potentially produce an unrealistic reduction in yield formation. However, a time series analysis of Bondville model data shows that considerable C_{stor} mass balance adjustments are rare (not obvious in other years than 2003).

Nonetheless, simulated soybean C_{stor} is improved after DA in 2002 (Figure 5.9). As already discussed, observed crop establishment soon after sowing could not be reproduced by FWmod. DA is a useful tool for improving LAI estimation during abnormal years (here late sowing) when the model fails to simulate observations (Viña *et al.*, 2004). The increased estimate of photosynthetic leaf area fostered C uptake and subsequent partitioning to the growing storage organ. Through DA, relative soybean *RMSE* was about halved (from ∼89% of the observed mean to ∼46%), but gains are lower for maize (from ∼18% to ∼16%). It has been shown that variational assimilation of MODIS 250 m data into a crop yield model provided good agreement of simulated crop yields in Iowa (U.S.) with NASS statistics (maize 3% underestimated, soybean 7% overestimated, Doraiswamy *et al.* (2004)). Variational assimilation of satellite data resulted in improvements in simulated yield of wheat in Italy (from a ∼14% overestimation in the forward run reduced to a ∼11% underestimation, Dente *et al.* (2008)) and sugar beet in northern France (*RMSE* reduced from 20% to 10%, Launay and Guerif (2005)). In comparison to these studies, the strength of our methodology however lies in the combination of variational and sequential DA techniques. Deficiencies in estimated sowing dates (in fact determined through simple variational DA) and model weaknesses can be sequentially compensated for by LAI updates at each individual time step for which a MODIS observation is available.

Next to model shortcomings in simulating C_{stor}, observational data are relatively uncertain. Unfortunately, no information on confidence intervals of measurements is available. Moreover, there are considerable differences in field site reported values (DM sampling vs. farmer reports, Figure 5.7), and NASS observations were converted to appropriate units based on a range of uncertain assumptions (e.g. yield fraction of C_{stor}, moisture and C content). Due to the lack of more reliable observational evidence (especially at the study area scale), our assessment of DA constraints on modelled C_{stor}

remains rather qualitative and necessitates further more detailed investigation in future studies.

5.4.4 Why are modelled NEE and NBP considerably larger than observed?

Our results indicate that growing season C cycling is well simulated: DAmod data yield high correlation scores with observed NEE (Figure 5.6, 5.10) and GPP (data not shown), and growing season cumulative NEE is almost identical to observations after the 7 study years (Figure 5.8 c), the contribution of weed grass mineralization to observed growing season NEE is rather small, probably <15 gC m^{-2} y^{-1}). This is a considerable improvement compared to a previous study, where SPAc reproduced daily cropland C fluxes observed at six different European flux tower sites with high accuracy, but growing season cumulative NEE was clearly overestimated (by ∼123 gC m^{-2} on average, Sus *et al.* (2010)). However, given that growing season C cycling is simulated with relatively high accuracy (in terms of both seasonality and magnitude), why are all-season NEE and NBP model data considerably larger than observed (by ∼650 gC m^{-2} on average, Figure 5.8)? The answer to this question primarily lies in model-observation discrepancies in fallow season processes, i.e. heterotrophic respiration rates and weed grass C cycling.

Based on field observations of corresponding parameters (Buyanovsky *et al.*, 1987; Verma *et al.*, 2005), residue mineralization and decomposition rates were carefully assessed. Applying these, C_{lit} (litter C mass) is continually turned over, fluctuating between maxima of 400 gC m^{-2} after and minima of <50 gC m^{-2} before harvest. Following Verma *et al.* (2005), the initial estimate in C_{lit} and its interannual dynamics (i.e. gains during maize and losses during soybean years) appear realistic. For fallow periods not considerably affected by weed growth, measured heterotrophic respiration fluxes appear well reproduced (Figure 5.6, 5.10). Thus, the dynamics of C_{lit} decomposition and mineralization are unlikely to be a major cause for model-observation disagreement in NEE and NBP.

However, observations suggest quite considerable weed grass C uptake during most autumn and spring months (Figure 5.6, 5.10, see also Aubinet *et al.* (2009)). The 2002 soybean sink was due to large fallow weed growth in spring (Hollinger *et al.*, 2004). Especially before sowing in 2003 (Jan to mid-Apr), fallow season C uptake was quite substantial (cumulated ∼280 gC m^{-2}). Based on humification rates for tallgrass prairie residue from Buyanovsky *et al.* (1987), ∼20% of that uptake in 2003 will add to C_{SOM} (soil organic matter C mass) in form of decomposed litter after one year (here ∼60 gC m^{-2}). This weed-derived gain in C_{SOM} is largely absent in experiment DAmod, as fallow weed growth and subsequent C sequestration are largely restricted trough assimilation of low RDVI. As MODIS DA suppresses weed grass growth, differences in cumulative NEE between forward and DA experiments suggest a potential weed C sequestration of ∼20 gC m^{-2} y^{-1} (data not shown). However, a more detailed assessment of fallow weed C sequestration is necessary to estimate its overall magnitude during the study period, and we assume that it probably explains only a rather small fraction of the gap between modelled and observed C budgets.

Moreover, initial C_{SOM} was calibrated in order to ensure that cropland soils were in rough equilibrium. However, C_{SOM} still lost on average ∼470 gC m^{-2} (or ∼70 gC m^{-2} y^{-1}) throughout the study period (experiment DAmod). This mineralization flux explains ∼70% of the difference between observed and simulated cumulative NEE by end-2006 (Figure 5.8), when assuming that soil C is balanced in reality. Agricultural C_{SOM} is expected to be in equilibrium after decadal C losses following land-use conversion (Luo *et al.*, 2010; Lal, 2004). Mature no-till cropland soils might even be gaining C, but current evidence remains contradictory (West and Marland, 2002; Verma *et al.*, 2005; Hollinger *et al.*, 2004). The need for further investigating soil C losses and their relationship with land-management remains large (Dawson and Smith, 2007).

Overall, the comparison between modelled and observed NEE and NBP is mainly confounded by steady-state assumptions on C_{SOM} and fallow weed grass C cycling, and less so by uncertainties in aboveground and belowground residue decomposition and mineralization rates. Model C_{SOM} is not in equilibrium, explaining ∼70% of the

disagreement on NEE. Furthermore, the contribution of weed grass litter decomposition to C sequestration was not negligible during some seasons (e.g. ∼60 gC m^{-2} in 2003), and is roughly estimated to ∼20 gC m^{-2} y^{-1}. Weed grass C sequestration corresponds to ∼22% of the observation-model gap in cumulative NEE. Hollinger *et al.* (2004) (but see also Hollinger *et al.* (2005)) assessed the regional C sequestration potential of no-till MSCR based on the Bondville flux data (1997-2002). Their analysis showed that the annual C sink strength is rather small (NBP ∼-30 gC m^{-2} y^{-1}). Cumulated over the 5 study years for which C_{stor} observations are available (Table 5.3), this estimate is comparable to the observed NBP data presented here (∼-200 gC m^{-2} after 7 years). However, their published estimate of cumulative NEE for years 2000-2002 is considerably lower (by ∼266 gC m^{-2}) than what we derived from the FLUXNET database. Hollinger *et al.* (2004) also accounted for fossil-fuel C emission of agricultural machinery, but its contribution is comparably small (∼1% of growing season C uptake). Magnitude and sign of the Bondville agroecosystem C budget are rather uncertain, as observational evidence and associated EC uncertainties (Anthoni *et al.*, 2004; Falge *et al.*, 2001) do not allow for significant conclusions. EC studies of other maize and/or soybean agroecosystems indicate C neutrality at best: a maize-fennel crop rotation in Italy was found to lose ∼417 gC m^{-2} y^{-1} even though organic manure was regularly applied (Kutsch *et al.*, 2010), and rainfed no-till MSCRs were found to be approximately C neutral (Verma *et al.*, 2005) or net sources of C (40 to 80 gC m^{-2} y^{-1}, Grant *et al.* (2007); Baker and Griffis (2005)).

A final assessment of NBP is further complicated by uncertainties in observed and modelled C_{stor}. Observed C_{stor} data show temporal discontinuities and, in some seasons, disagree with farmer reported values (Figure 5.7). Note that Hollinger *et al.* (2004) only accounted for the export and post-harvest consumption of grain C, but entire storage organs (∼120% to ∼130% of grain C) are harvested. Model data are affected by mass balance breaches following DA analysis (2003 only). Thus, the observations analysed provide no clear constraints on the sign of NBP, and the role of fallow season C sequestration necessitates more detailed analysis. While model data indicate a clear source of C after the seven study years, this estimate is probably an

overestimate when assuming that C_{SOM} should be in equilibrium, and when considering that fallow season C uptake could not be reproduced. Regarding these uncertainties, we are not able to firmly establish whether MSCR agroecosystems of the study area are net sources or sinks of C from model data alone.

5.5 Conclusions

In this study, we successfully developed and tested a model-DA-framework for accurate simulation of spatio-temporally resolved cropland C fluxes and biometry. This framework explicitly considers important constraints on land management (in particular on sowing dates) and disturbance events not captured by forward (i.e. no DA) model simulations. MODIS RDVI data were assimilated both variationally (for sowing date estimation) and sequentially (for improved model state estimation, using the EnKF), and the strength of our methodology lies in this combination of both DA techniques. Deficiencies in estimated sowing dates, model structure, or parameterisation can be sequentially compensated for by LAI updates at each individual time step for which a MODIS observation is available, keeping the model "on-track".

The study consists of two components: 1) proof of concept of the developed model-DA-framework by comparison of point-scale simulations with observations made at the Bondville Ameriflux site for five years (2001-2005), and 2) upscaled estimation of regional C cycling and biometry through the assimilation of MODIS RDVI time series of 104 field patches within the wider area for seven years (2000-2006). All field patches were simulated as under no-till, maize-soybean crop rotation management.

5.5.1 Proof of concept at the point-scale

We generally find that all model experiments (i.e. forward or DA model runs, driven with reported or modelled sowing dates) are largely able to reproduce the seasonality of C fluxes as observed at the Bondville EC site, but deficiencies in simulating

magnitude and fallow season processes are evident. However, SPAc runs forced with modelled sowing dates do not only reproduce observed C flux seasonality, but the fit to observed data (NEE and LAI) is even better when compared to model runs driven with reported sowing dates. We used an independent constraint on crop LAI (MODIS RDVI) for finding the model sowing date which best reproduces observed seasonality in green aboveground biomass. As this procedure clearly constrains the seasonality of cropland NEE, MODIS-derived sowing dates allow for highly accurate simulations of agroecosystem C cycling at locations for which ground-truth sowing dates are not available. Moreover, sequential MODIS DA improves model performance in anomalous growing seasons by reducing a negative bias in forward model LAI. The EnKF analysis also informs about seasonality of C fluxes and biometry through MODIS constraints on crop establishment and senescence. We further expect that important land management practices (fertilisation, irrigation, cultivar selection, double cropping) and disturbance events (frosts and droughts) are indirectly resolved in assimilated temporal RDVI profiles. This framework is readily applicable for accurately simulating current (i.e. last 10 years) C cycling of major agricultural regions of the U.S., but also elsewhere as long as crop type classification data are available and minimum requirements on field patch size are satisfied.

5.5.2 Upscaled estimation of agroecosystem C cycling

Averaged over the 104 field patches analysed, the relative spatial variability for C_{stor}, LAI, and NEE for both crops ranges from ∼7% to ∼10%. Variability of NBP though is considerably larger: ∼32% for soybean (536 ± 175 gC m^{-2} for study period), and ∼24% for maize (1064 ± 252 gC m^{-2}). These results show that, next to local meteorology, regional patterns of land management are important drivers of agricultural C cycling and major sources of uncertainty if not appropriately accounted for.

Observing C cycling at one single field with its individual sowing pattern is not sufficient to constrain large-scale agroecosystem behaviour. Whereas EC data appear representative for field patches with the same succession of crop types as at Bondville

(i.e. soybean grown in even years), there are large differences in SoS and GSL values for rotations where maize was grown in even years. Differences between Bondville and upscaled NEE are especially large in years with non-optimal weather conditions for sowing. When averaged over all field patches, mean GSL is 20 days longer than observed, primarily because of earlier estimated SoS. Thus, the DA scheme developed and tested here appears highly suitable for accounting for human intervention and its knock-on effects on ecosystem services (such as fluxes of C, water, and energy). Our approach is a promising step forward in improving large-scale applications of BGCMs.

The comparison between modelled and observed NEE and NBP is mainly confounded by fallow weed grass C cycling and steady-state assumptions on C_{SOM}, and (to a lower extent) by uncertainties in aboveground and belowground residue decomposition and mineralization rates. The contribution of weed grass litter decomposition to C sequestration is not negligible during some seasons (e.g. $\sim$60 gC m^{-2} in 2003), and is roughly estimated to $\sim$20 gC m^{-2} y^{-1}. Model results do not allow for firm conclusions on whether the agroecosystems of the study area are net sources or sinks of C. Reproducing multiannual C budgeting is not achieved even when temporally highly resolved local meteorological driver data, sowing dates, soil conditions, and satellite-derived observations of vegetation greenness are considered. Multiannual cropland C budget simulation runs are highly sensitive to initial conditions in belowground and crop residue C mass and corresponding decomposition and mineralization parameters. As MODIS data can not provide such constraints, additional information on cropland management and belowground C cycling still needs to be considered. Nonetheless, growing season C cycling is well simulated through MODIS DA, which is a considerable improvement compared to previous SPAc agroecosystem simulations where cumulative NEE was clearly overestimated.

Chapter 6

Discussion

6.1 Assessment of SPAc as a generalised crop C budget model

6.1.1 SPAc provides strong constraints on cropland C flux seasonality

SPAc reproduces observed growing season agroecosystem C fluxes of six Western European cropland sites (three in France, two in Germany, and one in Switzerland) with high accuracy (mean $R^2 = 0.83$, chapter 2). Even though flux seasonality is well reproduced, simulated cumulative NEE is clearly lower than observed ($\sim$123 gC m^{-2} y^{-1} on average) and correlates rather poorly with measurements ($R^2 = 0.27$). The cross-site comparison study showed that SPAc and ORDCHIDEE-STICS (Gervois *et al.*, 2008) were found to show highest accuracy metrics in simulating daily NEE and latent heat (chapter 3). The relative success of these two models is probably owed to their relatively high degree of process resolution and the half-hourly model time step, allowing for capturing diurnal variability in key processes (such as mid-day depression of canopy photosynthesis due to stomatal closure, Wang *et al.* (2007)). The simulation of water exchange is particularly strong, as latent heat fluxes are represented in a more process oriented way.

These results show that an agroecosystem BGCM can reproduce flux seasonality reasonably well, but derived C budgeting might not necessarily be simulated with equal fidelity. Models closest to observed daily NEE (SPAc and ORCHIDEE-STICS) show deficiencies in reproducing cumulative NEE due to weaknesses in simulating peak, senescence, and post-harvest fluxes (chapter 3). These point scale simulations are driven with site-specific information on sowing dates and local meteorology, so upscaled estimates (for which this detailed information is not readily available) might show even larger deviations and are thus considerably uncertain. A visual analysis of model values shows that cumulative NEE is generally underestimated for two different reasons: 1) difficulties in reproducing the seasonality of observed daily NEE and 2) underestimation of R_e after sowing and before harvest. Weaknesses in simulating the timing of senescence and the beginning of the growing season are evident for Gebesee a) and Klingenberg, respectively (chapter 2). Considerably large observed R_e fluxes after sowing and around harvest are underestimated for many site years, but most obviously at Gebesee b). Reasons for discrepancies in reproducing seasonality are largely related to simulated development, but especially senescence (see below for a more detailed discussion). The comparably late beginning of the Klingenberg growing season is probably related to local climate. A much better agreement with observations is found when restricting photosynthesis in cases where any soil layers are frozen (chapter 4). Further, the influence of land management and local climate on crop residue decomposition and mineralization needs to be established in more detail. Post-harvest R_h was largely overestimated for Auradé when all crop residue was added to C_{lit} (as reported by site PIs), probably because environmental effects (drying out of residue layer) on mineralization rate were not respected (Sus *et al.*, 2010).

6.1.2 Crop development - a key model constraint

A detailed sensitivity analysis was used to identify key parameters constraining model behaviour. In general, these key parameters can be classified into two groups: parameters affecting plant physiology, and parameters controlling plant development. Sensitivity was found to be largest for physiology parameters constraining plant

respiration (f_{a}, fraction of autotrophic respiration) and leaf thickness (C_{la}, C per leaf area), followed by developmental parameters constraining potential developmental rate ($r_{\max}$), temperature ($T_{\min}$, T_{opt}, $T_{\max}$, cardinal temperatures for development), and photoperiod (PH_{cr}) response. This analysis shows that the amplitude of NEE fluxes is largely influenced by crop physiological parameters (in particular f_{a} and C_{la}). The implemented developmental module is an important driver of NEE seasonality, as it determines the duration and timing of biomass growth and senescence phases.

For single growing seasons, model sensitivity to parameters constraining $\mathrm{R_h}$ is rather low. This is expected, as the relative contribution of $\mathrm{R_h}$ to cumulative NEE (the metric used in the sensitivity analysis) is small compared to the considerably larger fluxes of GPP and $\mathrm{R_a}$. However, $\mathrm{R_h}$ is a continuously occurring flux that needs thorough assessment for multiannual applications (as in chapter 5), for which it gains in importance (Prescher *et al.*, 2010). If the simulation of agroecosystem C flux seasonality is of primary importance (as in chapter 2), impacts of model weaknesses in $\mathrm{R_h}$ are negligible. However, decomposition and mineralization of crop residue and SOM are crucial constraints in any cropland C budget analysis. In chapter 2, SPAc was initialised with reported values for C_{SOM}, whilst C_{lit} was assumed to be zero. However, empirical C_{SOM} estimates need to be carefully assessed. I defined C_{SOM} as the C content of a reactive soil horizon affected by human management (i.e. the ploughing layer, 0 cm to 40 cm), but this simplification probably undermines a more realistic reflection of mineralization processes of various soil components and layers as affected by management. The mineralization rate of C_{SOM} is dependent on soil depth, and further affected by ploughing (Gervois *et al.*, 2008) and environmental conditions (Buyanovsky and Wagner, 1987). As SPAc does not account for these processes, its simulation of belowground C cycling is still rather simplified. If SPAc is to be used for assessments on cropland C sequestration potential, process detail of soil C dynamics needs to be improved. In addition, more information on crop residue decomposition and mineralization is needed, and especially how these are affected by local climate and management. The following research questions necessitate further attention: are rate constants different for above- and belowground components? Is

crop residue mineralization delayed by drought conditions (as suggested for Auradé in chapter 2)? How are these processes regulated by soil and residue moisture, as well as by pesticides/herbicides/fungicides?

The calculation of autotrophic respiration is uncertain, and is generally either described through two-component-simulations (i.e. divided in growth and maintenance respiration, Amthor (2000)) or through an a priori defined fraction of GPP. SPAc adopted the more simplistic (i.e. fraction-based) approach, as both concepts appear equally plausible (Gifford, 2003). The lack of detailed data constraints complicates the justification of a more detailed simulation of plant respiration, so SPAc autotrophic respiration remains rather empirically represented. Thus, f_{a} is a highly uncertain and sensitive model parameter. Model sensitivity to leaf thickness (i.e. parameter C_{la}) is also large, as the evolution of LAI is not prescribed within SPAc (e.g. in contrast to DNDC (Wattenbach *et al.*, 2010) or LPJmL (Bondeau *et al.*, 2007)), but estimated from C mass balancing. Scaling from leaf mass to area is empirically approximated and adopted in a simplified fashion, as presumed developmental (or in fact canopy layer) variability in C_{la} (Birch *et al.*, 1999; Penning de Vries *et al.*, 1989) are not represented.

Considering that the model exhibits high sensitivity to development and especially senescence, the underlying physiological processes and their representation within crop model concepts appear understudied (Kucharik and Twine, 2007; Suyker *et al.*, 2005). Poor simulation of crop development results in a premature timing of senescence (Grignon 2006) in DNDC (chapter 3). Based on a GDD approach, the model largely overestimated winter developmental progress as it failed to account for requirements on vernalization and daylength. The developmental module embedded in DNDC appears structurally incomplete, explaining the comparably poor performance of the model. Because crop development is a key constraint on NEE seasonality, and its estimation is the primary goal of this thesis, I will discuss it in more detail in the following paragraph.

Observational constraints on developmental parameters are variable, and are rather empirical surrogates for complex biochemical processes (Setiyono *et al.*, 2007). Developmental models apply specific parameter values for several sub-phases not considered

within SPAc (Porter and Semenov, 2005; Streck *et al.*, 2003). Thus, cardinal temperatures for development are expected to be temporally variable rather than constant (as currently represented) throughout a cereal crop's life cycle. For winter cereals, local climate constrains the beginning of the growing season in spring primarily through rises in temperature and irradiation. Sowing date is a crucial constraint on early C cycling and biometry for spring cereals. However, late-season C fluxes are determined by crop senescence, which is less linearly related to changing meteorology and often only poorly reproduced by crop models (Adiku *et al.*, 2006). Crop development is generally understood as a gradual process of crop ageing and finally death, and its timing depends on the cumulative effect of climate variables throughout the crop's life cycle. This is why senescence is comparably difficult to simulate: the response of crop development to ambient conditions is not as instantaneous as of growth. Further, it is not a passive and unregulated degeneration process (Lim *et al.*, 2007). In a more process-based representation, leaf senescence can be coupled to leaf N content. Accordingly, leaves will be shed when N content drops below a predefined threshold value (Yin *et al.*, 2000). However, the underlying processes of crop development and senescence, which may be a complicated mix of external (e.g. nutrient limitation, drought, shading, UV-B or ozone) and internal (hormones and reproduction) factors (Lim *et al.*, 2007), are still rather understudied and not well incorporated in crop models (Craufurd and Wheeler, 2009). Senescence is an important element of agricultural studies, as it may limit yield by limiting the growth phase (and thus constraining NEE seasonality) and may cause post-harvest spoilage in vegetable crops (Lim *et al.*, 2007). As long as our physiological understanding of crop senescence remains as simplified, associated uncertainties can be considerably large in upscaled estimates. Reproducing point-scale observations of C fluxes and biometry is already challenging. In this respect, much information can probably be drawn from satellite observations of aboveground green crop biomass. These data replace time and labour intensive ground measurements of crop biometry, and, given the appropriate spatio-temporal sensor resolution, provide strong constraints on agroecosystem seasonality in biomass (and in particular its senescence) and C cycling. Croplands might be especially suitable for such studies, as they are model ecosystems of

a "single species, bare soil to vegetation scenario for studying greenup" (Wardlow *et al.*, 2006).

6.1.3 Discrepancies in modelled biometry suggest weaknesses in model structure and C allocation

I identified deficiencies in the agreement of LAI and C_{f} with corresponding observations. LAI appeared to be overestimated, but C_{f} model values were rather close to measurements. While uncertainties in measurements (based on methodology and accuracy) are probably large, this discrepancy is nonetheless indicative that green surfaces of non-leaf crop organs (i.e. stems and ears) need to be considered in model simulations (Hoyaux *et al.*, 2008). To date, LAI might be overestimated in SPAc due to weaknesses in crop development (i.e. duration and fraction of leaf allocation overestimated, senescence rate due to mutual shading or ageing too low), C partitioning fractions, canopy architecture (i.e. C_{la} underestimated), or model structure (photosynthesis of non-leaf green surfaces not accounted for). Weaknesses in model structure are partly compensated by parameter calibration to observations (i.e. getting the right answers for the wrong reasons). Simulating LAI is further complicated by cultivar dependence of parameters and the potential effects of fertilization, irrigation, and pest or weed management. As these controls are currently not simulated, model LAI is rather representative of optimal growth conditions.

Model yield was found to be generally underestimated ($\sim$28%), even though C uptake has been overestimated. Again, deficiencies in the underlying C partitioning pattern, and/or its dynamics in response to crop development are possible causes for model shortcomings. However, yield is largely dependent on the availability of remobilizable C in other crop organs (especially leaves and stems). Yield growth occurs in the reproductive phase, and thus coincides with leaf senescence. Continually less newly assimilated C is available for growth as the crop ages, so receiving remobilized C from decaying plant organs becomes increasingly important (Birch *et al.*, 1999). The growth of the storage organ thus also indirectly profits from vegetative C assimilation,

a fraction of which is subsequently reallocated to yield (∼20% to 50% of C_s and C_f, Penning de Vries *et al.* (1989); Birch *et al.* (1999)). Accordingly, photosynthesis is not the only source of yield growth, and this GPP source looses importance as development progresses. In general, SPAc would benefit from a mechanistic representation of C partitioning (but regulation of C allocation at the whole-plant level is still poorly understood, Marcelis and Heuvelink (2007)), as underlying fractions might be unrealistic and do not allow for simulating changing strategies in C allocation in response to non-optimal environmental conditions for growth (e.g. availability of water and nutrients). In reality, C partitioning is the expression of crop growth but not its driver (Marcelis and Heuvelink, 2007).

6.1.4 Regional applicability is limited by land management

SPAc appears well calibrated and equipped for simulating C flux seasonality of European winter cereals, but their C budget as derived from model values remains rather elusive. More efforts are needed to improve point-scale estimates of C budgeting, but gains in accuracy should not be traded for applicability at larger scales (Adiku *et al.*, 2006).

In chapter 2 and chapter 3, SPAc simulations were limited to the growing season and following fallow periods not affected by land management, as no post-harvest activities such as regrowth of weeds and crop volunteers were simulated. Post-harvest activities that need to be included in multiannual applications are the cultivation of catch/cover crops, and land management types such as tillage practices. In comparison to DNDC and CERES-EGC (Lehuger *et al.*, 2010), SPAc is limited due to the low number of crops parameterised. Nonetheless, SPAc captures ∼43% of the EU27 cropland area with its parameterization for wheat and barley (chapter 2, maize and soybean were included in chapter 5). Model performance is additionally affected by carry-over effects of previously simulated crop rotations and their effects on C_{SOM} and C_{lit} in multi-seasonal simulations. For DNDC, these cumulative uncertainties partly explain the comparably poor fit of model data to observations. Without the representation

of further agricultural practices (irrigation, fertilization, ploughing, crop rotation, pest/weed management), annual cumulative NEE cannot be simulated accurately (Wattenbach *et al.*, 2010). Model results are extremely dependent on assumptions about past and present management options employed (Ciais *et al.*, 2010).

Next to the parameterisation of additional CFTs and land management options, a framework is needed that independently allows for improved growing season C budgeting and extrapolation in space and time. Data assimilation appears as a promising tool to overcome some of the difficulties mentioned. Its application seems warranted for agricultural simulations, as classical challenges in biogeochemical modelling of non-managed lands are further complicated by human interference with ecosystem functioning.

6.2 Assimilation of C flux and stock data as a useful a tool for model diagnosis

6.2.1 NEE constraints on biometry

The assimilation of C flux data improves the simulation of biometry. NEE data largely constrain aboveground green biomass and the timing and magnitude of growth and decay. Results suggest that leaf C and area probably form a broad plateau during peak season rather than a narrow peak (as in Gervois *et al.* (2004)). Moreover, assimilated NEE data suggest that senescence might be triggered too early. These findings generally confirm conclusions drawn from point-scale application of SPAc for several European sites (chapter 2 and chapter 3, see also above). C_{s} and C_{stor} are not strongly constrained, as they still need to be physiologically integrated within SPAc. Nonetheless, their estimation improved indirectly through NEE DA: the C flux data constrained the amount of C available for growth. Its subsequent partitioning to C_{s} and C_{stor} brought their end-season estimates closer to observations.

NEE DA constraints on belowground partitioning resulted in a lowered shoot:root ratio

at maturity. As C_r was considerably larger after DA, this suggests that belowground partitioning might be underestimated. However, the effects of root C exudation and sloughing off are not considered within SPAc. This DA derived estimate on C_r appears more realistic when considering that up to ∼45% of allocated C_r is lost through the two aforementioned processes (Buyanovsky and Wagner, 1987). A physiological interpretation of this C_r increase could be that plant drought stress, and in particular root resistivity to water transport, are overestimated. C_r might have increased in order to improve plant water status, but also might have acted as a noise sink (as in Williams *et al.* (2005)). Qualitative interpretation of model outputs suggests that stomatal conductance was indeed increased during the driest study period (i.e. July) after NEE DA compared to the forward run. However, belowground C pools showed high sensitivity to changes in a priori model uncertainty (data not shown), so noise sink behaviour was observed. As no parameters directly related to plant water hydraulics were part of this model diagnosis study, they should be diagnosed and analysed in future DA applications. Even though no belowground biometry data are available for the Ameriflux Bondville site, NEE flux data for maize and soybean were observed from 1997-present. These data could be used in a more detailed, multiannual, multiple constraints DA analysis for model diagnosis, parameterization, and interpretation of observed cumulative fluxes (Baldocchi, 2003).

6.2.2 Biometry constraints on NEE

When biometric data were assimilated into SPAc, C uptake was considerably underestimated. The explanation for this underestimation is threefold: 1) a reduction in C_r magnified the impact of drought stress on stomatal opening; 2) as a result of state vector interconnections between C_r, C_f and LAI, the reduction in C_r after DA resulted in simultaneous reductions in the other two state variables. Accordingly, photosynthetic potential decreased. 3) C uptake was underestimated given a realistic value for LAI. This confirms the previous assumption that SPAc is deficient in not accounting for photosynthesis of green stems and storage organs. Their relative contribution to GPP increases substantially during senescence, as green leaf area was found to senesce

first (stems represent up to ∼25% of total green area of winter wheat before heading, and this fraction continually increases until maturity, Broge and Mortensen (2002)). Photosynthesis of green stems and storage organs could easily be implemented within SPAc, but both plant organs would need to be linked with a well calibrated senescence model. Senescence triggers and rates are possibly different for leaves, stems, and ears, as observations suggest.

This DA study was largely dominated by NEE flux data when all observations were assimilated. The time resolution of biometric data samples is simply too low to inform about key model processes, but could be artificially increased through interpolation between data samples. Crop biometry follows rather gradual, smooth seasonal changes. An interpolation method would need to be well justified and analysed in detail. Resulting time series data could provide strong constraints on model C allocation fractions and their temporal variability. One way forward with real observational data would be the assimilation of remotely sensed VI signatures. These data are available at high spatial (250 m; 1 km data are probably too coarse to provide a sufficient number of non-mixed pixel VIs, Adiku *et al.* (2006)) and temporal (daily) resolution from MODIS. Certainly, data gaps after initial filtering (e.g. for cloud contamination, aerosol contamination, viewing geometry) reduce this temporal resolution. However, the density of high quality MODIS observations is probably especially large during the peak growing season of temperate zone croplands (increased frequency of anticyclones in summer). MODIS data can potentially constrain any aboveground variables and parameters crucial for the calculation of crop biomass, LAI, and NPP (Running *et al.*, 1999; Adiku *et al.*, 2006).

6.2.3 NEE and biometry constraints on parameter behaviour

NEE DA provides strong constraints for parameters controlling photosynthetic potential, namely plant respiration and leaf thickness. I found evidence that leaf thickness varies in time, with the growth of thinner young leaves promoting early plant establishment. This temporal variability in C_{la} confirms a presumed model deficiency in not

accounting for changing leaf growth strategies as the crop ages (Penning de Vries *et al.*, 1989; Birch *et al.*, 1999). The interesting finding here is that NEE DA is in fact able to expose this shortcoming, and thus appears as a suitable tool for detailed diagnosis of key model processes. In fact, the greatest value of current FLUXNET data is their representation of processes, rather than providing an unbiased estimate of C exchange (Friend *et al.*, 2006).

I further found strong indications that the prior value of f_{a} (0.44) was overestimated. The posterior value is below the typical range of published values (but likewise possibly overestimated a priori, see e.g. $f_{\mathrm{a}} = 0.35$ in Gifford (1995)), thus indicating that SPAc is deficient in reproducing observed productivity. This is most evident in a forward model run with posterior parameterisation, where cumulative NEE is considerably underestimated. Frost damage might have affected crop growth and development in mid- to late spring (see also chapter 2). In general, temporal parameter variability in C_{la} and f_{a} plausibly indicates expected model deficiencies. Late-season effects of senescence and yield formation on $\mathrm{R_a}$ (Aubinet *et al.*, 2009) and temporal (or in fact canopy layer) variability in leaf thickness are regarded as potential causes. Even though f_{a} appears to be rather constant throughout peak growth for experiment $\mathrm{NEE}_{Biometry}$, it is resolved as time variable when only NEE data are assimilated (with an increasing value of f_{a} as development progresses, data not shown). In theory, direct constraints on belowground and aboveground C allocation fractions and their temporal variability should be inferable from C flux data. To do so, a crop model has to be well calibrated, so that model deficiencies in simulating key processes (such as fraction of autotrophic respiration or drought stress) are not swept into the free parameters (Gove and Hollinger, 2006).

Developmental parameters are generally determined through empirical studies of crop development under controlled environmental conditions. Here, I aimed for providing an independent estimate of these parameters through DA. It is expectable that NEE data are impacted by crop development (Baldocchi, 1994), but it remains to be established if this link also holds for key developmental parameter values. Results show that NEE DA constraints on developmental parameters are generally less reliable,

as posterior residual variability (experiment NEE_{post} in chapter 4) is considerable. Overall, parameter trends shorten the vegetative phase, and support the idea that the duration of C partitioning to leaves and roots is overestimated. The timing of senescence is clearly improved with posterior parameters. In theory, DA might be less successful in constraining developmental parameters as crop development is the cumulative sum of daily developmental rates. DS is an abstract (i.e. non-tangible) cumulative state variable that gradually increases (except for sugar cane, it is not possible that DS reverts to lower values, Penning de Vries *et al.* (1989)). Consequently, temporal changes in C partitioning cannot be reversed, and respond rather gradually and non-linearly related to environmental conditions. However, sequential DA can only respond to instantaneous observations. Whereas crop physiological parameters are implicitly constrained by NEE data, developmental parameters are rather explicitly related (as for MODIS data in Stöckli *et al.* (2008)). DS itself is an empirically determined estimate and needs to be physiologically integrated in current crop models (Weixing *et al.*, 2002). Moreover, DS seasonality governs shifts in C partitioning coefficients, but these coefficients themselves are empirical parameters (Penning de Vries *et al.*, 1989). They are highly uncertain and do not reflect potential breeding effects of the last decades.

In summary, the lack of detailed process understanding of crop development hampers the extraction of solid parameter constraints from NEE data. Nonetheless, a future study could analyse the merits of satellite observations to constrain timing and rate of crop senescence parameters. Even though model senescence is still far from being mechanistically simulated, RS VI directly observes biometry seasonality and could thus help to calibrate empirical parameters. Recently, RS data have been used to parameterise a generic phenology model embedded within a C cycle DA system (Knorr *et al.*, 2010).

6.2.4 Deficiencies in simulating heterotrophic respiration remain unresolved

Weaknesses in reproducing respiration fluxes appear to be a common phenomenon of current agroecosystem BGCMs (Kucharik and Twine, 2007; Wattenbach *et al.*, 2010). In chapter 3, the four crop models have in common that they poorly simulate low C fluxes (i.e. within ± 2 gC m^{-2} d^{-1}). This discrepancy with measurements can be explained in two different ways: model mechanics are inadequate to simulate underlying processes (model conceptual deficiencies), and/or measured fluxes are unrealistic due to inherent uncertainties in EC data (observational deficiencies). Low C fluxes are generally observable during the early growth stages of a crop (i.e. throughout the "dormancy" phase from late autumn to early spring) or post-harvest fallow periods when crop or fallow weed photosynthesis is low to absent. During these phases, R_h fluxes gain in relative magnitude of the diurnal mean and now considerably constrain daily average C exchange. Whilst temperature defines seasonal and diurnal variability in modelled R_h (mineralization and decomposition rates ~double with every 10 °C increase in temperature), initial conditions in C_{SOM} and C_{lit} are key uncertainties and probably crucial variables that can largely explain low model performance for days when heterotrophic respiration processes dominate. Rate constants of decomposition and mineralization are further strong constraints of R_h and need to be properly assessed. In SPAc, reproduction of early season low C fluxes was clearly improved when initial C_{lit} was increased from 0 to 200 gC m^{-2} (chapter 2). In terms of observational constraints, daily averages of fallow season C fluxes (which are dominated by R_e if no weed or volunteer crop are present) are more uncertain. If photosynthesis is low to absent, night fluxes, with potentially insufficient turbulent mixing, become important, as they are also used to determine the (supposedly comparably large) daytime R_e component (Wattenbach *et al.*, 2010). Nonetheless, it is likely that model shortcomings in initial conditions and R_h-process parameterisation primarily explain model-data disagreement in night-time respiration fluxes.

Results show that night-time fluxes (R_a + R_h during the growing season, R_h during

"dormancy" or fallow periods) are not considerably improved through NEE DA (chapter 4). The mineralization of C_{lit} and C_{SOM} are clearly deficient in their mechanistic representation and parameterisation. R_e is generally underestimated, even though an initial C_{lit} of 200 gC m^{-2} was assumed (which was absent in all model runs in chapter 2). This mismatch in reproducing R_e remains elusive and necessitates further more detailed analysis. NEE data hold some informational content on night-time respiration, but nocturnal model values were weighted more than observations due to methodological constraints. Moreover, key controlling parameters (decomposition and mineralization rates) were not part of the DA assessment, and effects of land management on controlling processes remain to be conceptually integrated (e.g. effects of ploughing and herbicides/fungicides on soil microbiology).

Overall, this DA study showed that expected constraints on key crop processes are resolved in NEE data. They serve as a diagnostic tool for model analysis, which is brought about by DA. SPAc was diagnosed by observational constraints on (1) state variables and (2) parameters. For (1), external control of state estimation through assimilated measurements reveals model behaviour under realistic conditions, whilst respecting confidence limits on simulated and observed data. DA of biometry clearly showed that SPAc is deficient in reproducing flux data when biomass and LAI meet external constraints. NEE DA resulted in an increased "C flow" into the agroecosystem available for growth, and independent biometry constraints of aboveground biometry were more closely met. However, belowground C pools exhibited noise sink behaviour. Independent data on fine root dynamics are required to provide further constraint (Richardson *et al.*, 2010). For (2), temporal parameter variability is indicative of ecosystem processes that are resolved within NEE data (biometric measurements are too temporally sparse and thus provide few process constraints) but are not captured within SPAc. Rather than providing defendable, calibrated, posterior parameter values (which is nonetheless possible if a model is well calibrated and analysed parameters are carefully selected), DA reasonably confirmed model deficiencies, as indicated through a qualitative model-observation comparison in chapter 2 and chapter 3. The time richness of EC flux data is an important commodity for detailed model testing. These data

clearly provided important, quantitatively determined insights into model shortcomings, and potential solutions were highlighted chapter 4.

6.3 Improving and testing the applicability of SPAc for upscaling

6.3.1 MODIS DA strongly constrains C flux seasonality

I found that sowing dates as estimated from MODIS VI time series are well suitable for realistically simulating NEE seasonality of soybean-maize rotations. In fact, a comparison to Bondville flux data showed that model results are of even higher quality compared to runs that were driven with reported sowing dates. However, seasonality was improved at the expense of an increasingly underestimated crop C uptake. Observational evidence suggests deficiencies in simulated sowing dates, so that improvements in seasonality might have been gained for the wrong reasons (e.g. premature estimation of sowing dates in order to compensate for weaknesses in simulating early growth or for overestimating drought effects on C assimilation). However, direct (i.e. sequential) assimilation of MODIS VI data further improved fit scores between model and observations, with this improvement being most considerable during years of anomalous sowing patterns when crop growth is underestimated by the forward model. These results clearly suggest that the developed model-DA-framework allows for upscaling model cropland C fluxes and biometry without necessitating a priori knowledge about sowing dates and possibly further land management activities and non-captured disturbance events (e.g. frosts, droughts). Model results for Bondville NEE (mean $R^2 = 0.63$) are comparable to SiBcrop estimates (0.58), but it is noted that Lokupitiya *et al.* (2009) derived these under consideration of *reported* sowing dates. The findings in this thesis are in line with results of Inoue and Olioso (2006) (there based on variational DA of ground-truth RS signatures) and Demarty *et al.* (2007) (sequential DA of the MODIS LAI product), who found that the combined use of RS

and (agro)ecosystem modelling is an effective means for estimating key state variables such as biometry and C fluxes.

6.3.2 Are key model deficiencies resolved?

The model-DA framework is able to compensate for some key model deficiencies as identified beforehand. LAI, which is directly related to assimilated MODIS data, is the key state variable within SPAc, as it is used to calculate GPP (the "C gate" of the model). However, the quality of predicted LAI largely depends on uncertain model parameters (C_{la}, f_{a}, sowing date) and on further processes affecting the growth of aboveground biomass (the C allocation pattern, crop development and senescence, drought stress effects). I found that corresponding model sensitivity is substantial, and large uncertainties regarding parameter values and conceptual formulation remain. Through DA, these uncertainties are largely addressed: the estimation of sowing dates (here through simple variational DA) is a strong constraint on NEE seasonality and the sequential assimilation of MODIS RDVI data is useful to keep the model "on track" when simulated LAI considerably differs from observational constraints. This is an advantage in comparison to other crop model-RS fusion studies (e.g. Becker-Reshef *et al.* (2010); Fang *et al.* (2008); Launay and Guerif (2005); Dente *et al.* (2008); Inoue and Olioso (2006); Doraiswamy *et al.* (2004, 2005); Guerif and Duke (2000)): that deficiencies in estimated sowing dates (in fact determined through simple variational DA) and model weaknesses can be sequentially compensated for by LAI updates at each individual time step for which a MODIS observation is available (as in Demarty *et al.* (2007)).

6.3.3 MODIS provides strong constraints on spatio-temporally resolved growing season NEE

Forward model outputs driven with modelled sowing dates proved to be deficient in simulating LAI and the timing and rate of senescence during some years, but interannual

variability was reasonably captured nonetheless. Consequently, the variational DA estimation of sowing dates allows for a first assessment of upscaled cropland NEE under the consideration of spatio-temporally resolved, field patch-specific observational constraints. I explicitly accounted for rotational succession (between soybean, fallow weed growth, and maize), and crop residue dynamics and management (a considerable improvement compared to chapter 2). This study is a major advancement in improving and testing the applicability of SPAc at regional scales, which was cardinally restricted by the lack of reliable sowing dates.

SPAc results are considerably improved through sequential MODIS DA compared to previous model estimates for European winter cereals, where I found growing season cumulative NEE to be largely underestimated (by ∼123 gC m^{-2} per growing season, chapter 2). For Bondville, observed and modelled cumulative NEE are within <100 gC m^{-2} after seven growing seasons. Nonetheless, the representation of crop senescence needs to be further improved so that MODIS constraints on late season biomass are more effective. Additionally, potential improvements of this framework would be the assimilation of MODIS data with higher temporal resolution (such as the MOD09GQ 250 m daily reflectance product; MOD09CMG 0.05° daily reflectance data have been used for winter wheat yield estimation in Kansas (U.S.) and the Ukraine by Becker-Reshef *et al.* (2010)), or the simultaneous assimilation of various satellite products (Fang *et al.*, 2011). The empirical relationship between LAI and RDVI allows for valuable constraints on crop seasonality, but a canopy reflectance model could be implemented for improving the accuracy of simulated LAI and GPP (and thus the C uptake potential, Doraiswamy *et al.* (2004)). Especially at high biomass values (Haboudane *et al.*, 2004), a canopy reflectance model is probably more sensitive to rather small changes in reflectance values. Overall, this framework can be seen as a promising way of enabling modellers to account for the intensity of human management when crop models are used across larger spatial scales (which was previously identified as a critical challenge for agroecosystem modelling, Kucharik and Twine (2007)).

6.3.4 Is cropland C budgeting reliably estimated?

Results further show that all season cumulative NEE (i.e. including fallow periods between harvest and sowing) and NBP are considerably larger than observed. This shows that SPAc and MODIS constraints serve as a highly accurate tool for estimating growing season C flux seasonality and cycling, but reproducing multiannual C budgeting is not achieved even when temporally highly resolved local meteorological driver data, sowing dates, soil conditions, and satellite-derived observations of vegetation greenness are considered. Fallow season processes appear to be poorly reproduced, with particular model weaknesses in simulating R_h and weed grass C cycling. This is in line with the findings in previous chapters, where I found that low C fluxes (presumably dominated by R_h fluxes) are comparably uncertain (chapter 2), are poorly reproduced by various crop models (chapter 3), and are only weakly constrained by NEE DA (chapter 4). For simplification, most croplands can be assumed to be in equilibrium after decadal agricultural use, but large-scale scenarios or assumptions on crop residue management need to be developed or derived from state or district level management statistics (Smith *et al.*, 2010). The effects of fallow weed grass and crop volunteer growth need to be approximated. In chapter 5, their relative contribution to total C balance are probably comparably small (here ∼22% of the gap between observed and modelled data, which was explained by ∼70% through C_{SOM} mineralization). Nonetheless, model data suggest a fallow weed/crop volunteer C sequestration potential of ∼20 gC m^{-2} y^{-1}, and Lehuger *et al.* (2010) estimate significant C uptake through catch crops and volunteers.

In theory, each cropland field is associated with an "individual" C_{SOM} value for which soil C losses through mineralization are balanced by soil C uptake through decomposing crop residue. Cropland soils are known to lose ∼50% to ∼60% of C following land-use change, and will regain equilibrium at this lower level after several decades under cropland cultivation (Luo *et al.*, 2010; Lal, 2004). Best-practice management is recommended for replenishing a certain fraction of this lost belowground C pool (Dawson and Smith, 2007; West and Marland, 2002). The equilibrium value is primarily dependent on local site history, climate, and current crop residue management, but

also on ploughing intensity, type (i.e. organic manure) and frequency of fertilization, application of herbicides/pesticides/fungicides (in particular their effects on soil microbiology), crop succession, and fallow season vegetation growth (Luo *et al.*, 2010; Lal, 2004; Dawson and Smith, 2007; Arevalo *et al.*, 2010). Some of these variables in turn influence rate constants of decomposition and mineralization of crop residues and belowground organic matter (Ciais *et al.* (2010), assimilation of soil respiration flux data into a crop model could provide a parameterization). For a thorough assessment of heterotrophic respiration fluxes through EC measurements or agroecosystem BGCMs (and thus of upscaled cropland C budgeting), these unknowns have to be determined or at least carefully approximated (Anthoni *et al.*, 2004). The spatial, temporal, and spectral resolution of MODIS has been shown to be sufficient for providing information on some of the relevant management practices in this context, such as double cropping, fallow, and irrigation (Wardlow *et al.*, 2007). Still, the main hurdle in large-scale applications of agroecosystem BGCMs is data limitation, even though RS products have already greatly improved datasets on land use and land cover (Smith *et al.*, 2010).

However, it is virtually impossible that a regional cropland C simulation can realistically accommodate all of the processes mentioned above and changes in agricultural practices over time, so simplifications and assumptions are unavoidable. Modelling alone cannot provide a reliable absolute estimate of a field specific C_{SOM} equilibrium level and the associated current degree of soil C "saturation" (i.e. C storage potential - actual C_{SOM}, Luo *et al.* (2010); Bondeau *et al.* (2007)), and should be supported by evidence from cropland inventories (such as shown in Ciais *et al.* (2010)). Climate may be the primary control of the annual C balance, but management characteristics become increasingly important in multiannual studies (Prescher *et al.*, 2010). In this thesis, I did not attempt to define assumptions for above variables or to develop scenarios for spatio-temporal extrapolation. Instead, I focussed on aboveground C cycling as the primary control of cropland NEE seasonality and amplitude. I found that a more detailed representation of near surface and belowground processes operating on available organic C is necessary for realistically simulating cropland C budgeting (Fang *et al.*, 2005; Lehuger *et al.*, 2010). SPAc is devoid of such process detail, and thus provides

strong constraints on NEE seasonality and amplitude rather than on its cumulative estimate.

6.3.5 The influence of land management on agroecosystem C flux seasonality and biometry is substantial

Results suggest that the upscaled variability in aboveground biomass and growing season NEE ranges from ±7% to ±10% of the average value, but this variability is considerably larger for NBP (±24% to ±32%). Model results indicate that croplands within the study area are net sources of C (by ∼80 gC m^{-2} y^{-1}) after accounting for emissions from post-harvest C_{stor} consumption. These estimates are derived from a relatively small study area (32 km x 25 km), assuming uniform patterns in local climate, land-use, and soil conditions. These findings show that land management is an important driver of agricultural C cycling, and constitutes a major uncertainty source if not explicitly accounted for (see also McGuire *et al.* (2001)). Likewise, Lobell and Field (2007) found that only ∼30% of interannual global yield variability can be attributed to climate variables.

The Bondville EC flux data appear highly representative of the regional growing season C budget, but model values show considerable differences in derived seasonality metrics. Even though phase shifts in soybean-maize rotation NEE are largely absent, model GSL is on average ∼14 days longer than observed (∼20 days longer for all pixels). Study area averages of NEE fluxes (i.e. also including pixels with a different crop succession than Bondville) are likely to reflect measurements as they would have been obtained from a tall tower EC system or atmospheric CO_2 flasks. Deviations in model from Bondville site observed GSL are largest in "anomalous" years (here 2002), when spring precipitation caused a considerable delay in soybean sowing progress. Quantifying the interplay between local meteorological variables and farmer decisions on optimal sowing dates remains elusive, and is difficult to determine accurately (i.e. <1 month deviation from observations) based on climate data alone (Sacks *et al.*, 2010; Waha *et al.*, 2011). A crop model driven without observed or realistically estimated constraints on sowing

dates would not be able to reproduce the obvious phase shifts in NEE seasonality as seen in both the Bondville data and the SPAc DA outputs for 2002. The sensitivity of crop models to sowing date estimates is large (Twine and Kucharik, 2008), posing major problems for regional (Huang *et al.*, 2009b), but also interannual applications. The DA scheme specifically accounts for this "human signal" in agroecosystem C cycling, and for its variability in space and time. Future applications at larger spatial scales (e.g. the conterminous U.S.) not only provide a highly accurate state assessment of modern agriculture, but potentially valuable insights into the relationship between climate variables and sowing dates. If applied to less self-sufficient agricultural regions (e.g. West Sahel, Brown and de Beurs (2008)), operationally estimated sowing dates could serve as an early warning indicator of food supply.

DA constraints on simulated C_{stor} on the other hand were found to be rather moderate. The interannual variability is already well captured by the forward data. DA helps to reduce residuals (e.g. a $\sim$50% reduction in RMSE for soybean), but correlation metrics were largely unaltered. As residuals for soybean were considerably larger than for maize (89% of mean for soybean, 18% maize), DA improvements were generally larger for this crop type. Through methodological adjustments (e.g. removing C_{stor} from the model state vector) improved estimates on spatiotemporally crop yield are expected. Nonetheless, results indicate that the developed model-DA framework holds large potential in not only realistically reproducing NEE seasonality and growing season C cycling, but also for crop yield simulations. Accordingly, the methodology can be seen as a tool for integrated studies of two key agroecosystem services: C sequestration potential and food supply.

6.3.6 Future applications of the SPAc model

In this thesis, I have developed a crop module for SPAc that accounts for four generic crop functional types, which are amongst the top six crops in terms of global area harvested (2009): wheat (1. position, 15.6% of global croplands), maize (3., 11.0%), soybean (4., 6.8%), and barley (6., 3.7%). This corresponds to more than a third

of global croplands (37.1%). In terms of total production, maize and wheat are the top two staple crops for human consumption. SPAc should be further parameterized for simulations of rice, the 3rd most important staple crop in terms of production and the 2nd most important in terms of acreage (11.2%). Taken together, these five crops constitute about half of global croplands (48.3%, FAOSTAT [Rome, Italy]: FAO, http://faostat.fao.org/). Further, SPAc was run on multiannual scales (here seven years) accounting for long-term processes in C_{SOM} mineralization, crop residue management, and their decomposition and mineralization. Rotational succession was explicitely accounted for, i.e. current simulations where affected by the legacy of previously cultivated crops on C_{lit} and C_{SOM}. In chapter 5, crop rotations were assumed to be under no-till management, so ploughing effects on surface litter and belowground C cycling did not need to be considered but should be represented for upscaling.

After relatively minor modifications, SPAc is readily applicable to cropland NEE seasonality simulations of the continental U.S.; however further research efforts are necessary in order to extend this applicability to countries for which crop type classification data (here CDL) are not at hand. MODIS data themselves have been shown to provide valuable information that allows for crop type discrimination, such as for soybean, maize (Wardlow *et al.*, 2007), and winter wheat (Becker-Reshef *et al.*, 2010). In Europe, the commonly cultivated wheat and barley crops might not be distinguishable based on their temporal VI profiles, but the identification of and discrimination between winter and spring cereals might be broadly possible based on differences in temporal VI profiles. The classification of rice croplands is facilitated by commonly practised temporal flooding of field patches, which leads to characteristic features in VI data (Boschetti *et al.*, 2009; Motohka *et al.*, 2009). For areas with typically small field patch sizes, the joint utilization of frequent coarse-resolution observations and temporally sparse fine-resolution measurements is a promising solution (Li *et al.*, 2008; Hill *et al.*, 2011a; Lobell and Asner, 2004). However, its feasibility for large-scale applications still needs to be examined. The importance of RS data for detecting cropland phenology and constraining relevant models will increase with

future progress in sensor resolution: hyperspectral data is suitable for providing more detailed information on crop phenology (such as the timing of maize tassel appearance, Viña *et al.* (2004)), residue cover, and soil tillage (based on the cellulose absorption index, Daughtry *et al.* (2006)). Moreover, long-term RS data sets (e.g. NDVI from AVHRR for >30 years at 1 km pixel resolution) could provide important decadal ecosystem constraints (Williams *et al.*, 2005) on management, C flux seasonality, and yield. However, these can only be reliably derived from field patches of sufficient size. The NASS CDL provide ideal information for detecting these fields (which are particularly large in the U.S.) and the subsequent extraction of RS time series data.

The improved quantification of cropland GSL has implications for the effects of crop residue on microclimatic variables (e.g. soil moisture, energy balance, de Noblet-Ducoudré *et al.* (2004); Kucharik and Twine (2007)). Moreover, model results could allow for conclusions on cultivar type selection by local farmers and their degree of yield adaptation to local climate, comparing "actual" with "potential" GSL. Finally, GSL is related to seasonal CO_2 amplitude (Keeling *et al.*, 1996), and possibly the terrestrial C balance (Piao *et al.*, 2007). A better exploitation of potential GSL might not necessarily lead to enhanced ecosystem C sequestration (White and Nemani, 2003). However, climate change mitigation strategies could be applied that foster belowground C allocation. In this context, the adoption of C fixing vegetation (by means of double-cropping or fallow season cultivation (Lehuger *et al.*, 2010), and preferably with large belowground C allocation) and appropriate residue management might be suitable options. I showed that the growth of fallow season weed grasses or crop volunteers has positive implications for C sequestration (see also Aubinet *et al.* (2009)). However, associated costs need to be quantified (e.g. for pest/weed control) and detrimental effects on cash crop growth and agroecosystem services (e.g. the effects of enhanced application of pesticides/herbicides on soil biology, water quality, see also Foley *et al.* (2005)) should be minimized. Given realistic assumptions on land management investments in labour and capital (see in Smith *et al.* (2005b) how successful C sequestration depends on appropriate incentives), a so-called "C sequestration gap" could be quantified. This metric would indicate the currently unexploited potential of modern agriculture

to serve as a tool in climate change mitigation strategies. Finally, SPAc could provide an independent estimate of cropland HANPP in large-scale application (Haberl *et al.*, 2007).

Probably the key finding of this thesis is that the model-DA scheme provides solid constraints on upscaled cropland C flux seasonality. Phenological variability, here expressed through GSL, is seen as an excellent barometer of short- and long-term climatic variability (White and Nemani, 2003), but large-scale observations are "contaminated" by land management signals. DA methodology applied in this thesis helps to isolate an anthropogenic signal in atmospheric CO_2 concentration time series from natural variability. Future, more upscaled studies applying this model-DA framework will prove to be useful in quantifying interannual fluctuations of cropland-specific growing season metrics. Predictions of future atmospheric CO_2 concentrations as simulated by state-of-the-art DGVMs are highly uncertain (e.g. for terrestrial biospheric uptake equivalent to >50 years of anthropogenic CO_2 emissions at current levels, Sitch *et al.* (2008)), which is associated with uncertainties in the terrestrial biosphere response to changing climate conditions. In Sitch *et al.* (2008), DGVMs did not consider C cycling of cropland areas (but efforts have been made to include these, Bondeau *et al.* (2007); Kucharik and Twine (2007); de Noblet-Ducoudré *et al.* (2004)), which correspond to ∼12% of the Earth's ice-free land surface (Ramankutty *et al.*, 2008). Atmospheric CO_2 concentrations as modelled by a DGVM were found to be out of phase with Northern Hemisphere observations. Modelled start of season was premature, and the amplitude of summer CO_2 drawdown was overestimated (Sitch *et al.*, 2003). But what would results look like if current and/or future land-use (not only land-use change) were represented? If the model-DA framework were adopted in a DGVM, testing its ability to respond to changing climate conditions by comparing modelled with observed atmospheric CO_2 concentration time series would provide more crucial insights. This would allow to quantify how observed seasonality is constrained by land management, and to examine if a DGVM realistically reproduces the intrinsic "natural" component of measurements. The model-DA cropland scheme is a promising tool for testing and improving state-of-the-art DGVMs in their representation of cropland C fluxes, and

consequently of observed atmospheric CO_2 seasonality and amplitude. Finally, the key methodological developments and findings of this thesis could help to better quantify the so-called "missing sink" of anthropogenic CO_2 emissions (Gifford, 1994). Future applications of the framework presented here could improve our still limited understanding of how terrestrial and global C cycling respond to changes in climate and atmospheric CO_2 concentrations (Meir *et al.*, 2006; Reay *et al.*, 2007), and key questions on present and future food security could be answered within a coupled climate-C-cycle model.

Chapter 7

Conclusions

Model development and testing

I developed and tested an agroecosystem BGCM (SPAc) simulating C fluxes and biometry for several major crop types. Model structure and parameterisation were kept rather generic to facilitate applicability over a range of temperate climates and major cropping areas. I found that SPAc reproduces observed growing season agroecosystem C fluxes of six Western European cropland sites with high accuracy. In a cross-site model comparison study, SPAc was found to show highest accuracy metrics in simulating daily NEE and latent heat, and this relative success is probably owed to the high temporal resolution of model time steps and a comparably high degree in process resolution. However, even though flux seasonality is well reproduced, simulated cumulative NEE is clearly lower than observed and correlates rather poorly with measurements. These results indicate that an agroecosystem BGCM can reproduce flux seasonality reasonably well, but derived C budgeting might not necessarily be simulated with equal fidelity.

I further identified model shortcomings in simulating development (in particular senescence) and ecosystem respiration. More study is necessary in determining how senescence is influenced by crop developmental stage or local meteorology. Uncertainties in initial conditions of decomposing/mineralizing organic C pools and in corresponding

rate constants are primary causes of deficiencies in reproducing heterotrophic respiration fluxes. These point scale shortcomings in simulated C budgeting probably propagate considerable uncertainty into large scale applications, which are further complicated by uncertainties in land management patterns and climate.

A detailed sensitivity analysis revealed that model sensitivity is largest for physiology parameters constraining plant respiration and leaf thickness, followed by developmental parameters. The amplitude of NEE fluxes is largely influenced by crop physiological parameters, whereas the developmental module is an important driver of NEE seasonality. The underlying processes of crop development and senescence are still rather understudied and not well incorporated in crop models.

Moreover, deficiencies in the agreement of LAI and C_{f} with corresponding observations were evident. A key conclusion in this context is that green surfaces of non-leaf crop organs (i.e. stems and ears) need to be considered in model simulations. LAI might be overestimated due to weaknesses in crop development, C partitioning fractions, canopy architecture, or model structure. In general, SPAc would benefit from a mechanistic representation of C partitioning, as underlying fractions might be unrealistic and do not allow for simulating changing strategies in C allocation in response to non-optimal environmental conditions for growth.

To conclude, SPAc appears well calibrated and equipped for simulating C flux seasonality of European winter cereals, but their C budget as derived from model values remains rather elusive. More efforts are needed to improve point-scale estimates of C budgeting (such as key management practices, number of crops parameterised, improved estimation of belowground and crop residue C content and corresponding rates of decomposition/mineralization as affected by management), but gains in accuracy should not be traded for applicability at larger scales. Model results are highly dependent on assumptions about past and present management options employed.

Model diagnosis

I showed that constraints on key crop processes are resolved in assimilated NEE data, providing quantitatively determined insights into model shortcomings. Due to their richness in time, C flux data serve as a powerful diagnostic tool for model analysis, which is brought about by DA. SPAc was diagnosed by observational constraints on state variables and parameters. Moreover, I tested model behaviour under realistic conditions by DA of biometry. Experiments showed throughout that SPAc is deficient in reproducing flux data when biomass and LAI meet external constraints.

Assimilation of C flux data improves the simulation of biometry. NEE data largely constrain aboveground green biomass and the timing and magnitude of growth and decay. NEE DA constraints on belowground partitioning resulted in a lowered shoot:root ratio at maturity, suggesting that belowground partitioning might be underestimated. Longer time series of flux data (such as available at Bondville) could be used in a more detailed, multiannual, multiple constraints DA analysis for model diagnosis, parameterisation, and interpretation of observed cumulative fluxes.

When biometric data were assimilated into SPAc, C uptake was considerably underestimated. This confirms our previous assumption that the crop model is deficient in not accounting for photosynthesis of green stems and storage organs, and further suggests that drought stress and aboveground C partitioning are overestimated. DA experiments were clearly dominated by high temporal density of NEE flux data when all observations were assimilated. The time resolution of biometric data samples is too low to inform about key model processes, but temporal resolution could be improved in future studies through interpolation techniques or satellite observations.

NEE DA provides strong constraints for parameters controlling photosynthetic potential, namely plant respiration and leaf thickness. The interesting finding is that NEE DA is in fact able to expose those model shortcomings previously (chapter 2, chapter 3) identified, and thus appears as a suitable tool for detailed diagnosis of key model processes. Temporal parameter variability is indicative of ecosystem processes that are

resolved within NEE data but are not captured by SPAc. Crop physiological parameters are implicitly constrained by NEE data, but developmental parameters are rather explicitly related. The lack of detailed process understanding of crop development hampers the extraction of more solid parameter constraints from NEE data. Nonetheless, RS VI data are presumably strong constraints on biometry seasonality and could thus help to calibrate empirical senescence parameters.

Finally, weaknesses in reproducing respiration fluxes (a common phenomenon of current agroecosystem BGCMs) are not considerably ameliorated through NEE DA. Mineralization of C_{lit} and C_{SOM} is clearly deficient in its mechanistic representation and parameterisation. The mismatch in reproducing $\mathrm{R_e}$ remains elusive and necessitates further more detailed analysis. NEE data hold some informational content on nighttime respiration, but nocturnal model values were weighted more than observations due to methodological constraints, and key controlling parameters were not part of the DA assessment.

Model upscaling

I demonstrated that sowing dates as estimated from MODIS VI time series are well suitable for realistically simulating NEE seasonality of MSCR, but seasonality was improved at the expense of crop C uptake underestimation. Especially for years of considerable delay in sowing progress, direct (i.e. sequential) assimilation of MODIS VI data proved successful in reducing this negative bias. These results clearly suggest that this model-DA-framework allows for upscaling model cropland C fluxes and biometry without necessitating a priori knowledge about sowing dates and possibly further land management activities (crop cultivar selection, irrigation, fertilization) and non-captured disturbance events (e.g. frosts, droughts). Sowing dates (here determined through simple variational DA) are a strong constraint on NEE seasonality, and the sequential assimilation of MODIS RDVI data is useful to keep the model "on track". Another considerable advancement compared to previous chapters is the

explicit consideration of rotational succession (between soybean, fallow weed growth, and maize), as well as of crop residue dynamics and their management.

Simulated cumulative NEE of crop growing seasons is considerably improved through sequential MODIS DA (deviations from observations are within <100 gC m^{-2} after seven growing seasons). Again, this is a major improvement compared to model estimates for European winter cereals as outlined above. Nonetheless, the representation of crop senescence needs to be refined so that MODIS constraints on late season biomass are more effective. Potential improvements would be the assimilation of MODIS data with higher temporal resolution, the simultaneous assimilation of various satellite products, or the implementation of a canopy reflectance model. In its current setup however, this framework can already be seen as a promising way of enabling modellers to accurately account for the intensity of human management when crop models are used across larger spatial scales.

SPAc and MODIS constraints serve as highly accurate tools for estimating growing season C flux seasonality and cycling, but reproducing multiannual C budgeting is not achieved even when temporally highly resolved local meteorological driver data, sowing dates, soil conditions, and satellite-derived observations of vegetation greenness are considered. Modelling alone cannot provide a reliable absolute estimate of a field specific C_{SOM} equilibrium level and the associated current degree of soil C "saturation", and should be supported by evidence from cropland inventories. SPAc is devoid of a detailed representation of near surface and belowground processes operating on available organic C, and thus provides strong constraints on NEE seasonality and amplitude rather than on its cumulative estimate.

Nonetheless, results clearly show that land management is an important driver of agricultural C cycling, and constitutes a major uncertainty source if not explicitly accounted for (i.e. ±7% to ±10% for aboveground biomass and growing season NEE, ±24% to ±32% for NBP). The Bondville EC flux data appear highly representative of the regional growing season C budget, but our model values show considerable differences in derived seasonality metrics. Study area model GSL is on average ∼20

days longer than observed. Deviations in model from the Bondville site observed GSL are largest in "anomalous" years, when spring precipitation caused a considerable delay in soybean sowing progress. A crop model driven without observed or realistically estimated constraints on sowing dates would not be able to reproduce the obvious phase shifts in NEE seasonality as seen in both the Bondville data and the SPAc DA outputs. Our DA scheme specifically accounts for this "human signal" in agroecosystem C cycling, and for its variability in space and time. Future applications at larger spatial scales (after relatively minor modifications, SPAc is readily applicable to cropland NEE seasonality simulations of the continental U.S.) not only provide a highly accurate state assessment of modern agriculture, but also potentially valuable insights into the relationship between climate variables and sowing dates.

In this thesis, I parameterised SPAc for four generic CFTs: wheat, barley, maize, and soybean. These CFTs are amongst the top six crops in terms of global area harvested and correspond to more than a third of global croplands. Thus, the model is readily applicable for simulating major crop types on continental scales, and crucial management information can be provided by assimilated satellite observations. For areas with typically small field patch sizes, the joint utilization of frequent coarse-resolution observations and temporally sparse fine-resolution measurements is a promising solution. The importance of RS data for detecting cropland phenology and constraining relevant models will increase with future progress in sensor resolution. Long-term RS data sets (e.g. AVHRR) could provide important decadal ecosystem constraints on management, C flux seasonality, and yield.

The precise quantification of cropland GSL has implications for simulating seasonal CO_2 amplitude and maybe even the terrestrial C balance. Probably the key finding of this thesis is that the model-DA scheme provides solid constraints on upscaled cropland C flux seasonality. Phenological variability, here expressed through GSL, is seen as an excellent barometer of short- and long-term climatic variability, but large-scale observations are "contaminated" by land management signals. DA methodology applied in this thesis helps to isolate an anthropogenic signal from natural variability in atmospheric CO_2 concentration time series. Future, more upscaled studies applying this

model-DA framework will prove to be useful in quantifying interannual fluctuations of cropland-specific growing season metrics. If this framework were adopted in a DGVM, testing its ability to respond to changing climate conditions by comparing modelled with observed atmospheric CO_2 concentration time series would provide more crucial insights. This would allow to quantify how observed seasonality is constrained by land management, and to examine if a DGVM realistically reproduces the intrinsic "natural" component of measurements. Key methodological developments and findings of this thesis could help to better quantify the so-called "missing sink" of anthropogenic CO_2 emissions.

Appendix A

Tables

Table A.1: List of model parameters, units, nominal values, and corresponding sources. For V_{cmax}, J_{max}, and C_{la}, values are given for winter wheat/winter barley. New parameters (SPAc vs. SPA) are marked (*), and all parameter values but *I* and *tar* have been altered.

Parameter symbol	Name	Unit	Nominal value	Source
N_{frac}	leaf nitrogen distribution through canopy layers	fraction	0.33, 0.27, 0.22, 0.18	Hirose and Werger (1987)
g_{plant}	stem conductance	mmol m^{-2} s^{-1} MPa^{-1}	5	adjusted to match leaf specific conductance from Liu *et al.* (2005)
Ψ_{l}	minimum leaf water potential	MPa	-1.9	Johnson *et al.* (1987)
I	stomatal efficiency	-/-	1.007	adjusted to maintain max. g_{s} <400 mmol m^{-2} s^{-1} (Ye and Yu, 2008)
C	leaf capacitance	mmol m^{-2} MPa^{-1}	2000	estimated (Williams *et al.*, 1996)
R_{r}	root resistivity	MPa s g $mmol^{-1}$	10	adjusted to match leaf specific conductance from Liu *et al.* (2005)
V_{cmax}	maximum carboxylation capacity	μmol m^{-2} s^{-1}	64/79	Wullschleger (1993),Tambussi *et al.* (2005)
J_{max}	maximum electron transport rate	μmol m^{-2} s^{-1}	137/157	Wullschleger (1993),Tambussi *et al.* (2005)
C_{la}	carbon per leaf area	gC m^{-2}	19.5/15	Penning de Vries *et al.* (1989, p 100)
r_{dc}	decomposition rate	h^{-1}	2.3×10^{-5}	Buyanovsky and Wagner (1987)
f_a	fraction of GPP respired	fraction	0.44	Monje and Bugbee (1998)
t_{root}	turnover rate of roots	h^{-1}	6.25×10^{-3}	Penning de Vries *et al.* (1989, p 210)
m_{lit}	mineralization rate of litter	h^{-1}	2.8×10^{-4}	Buyanovsky and Wagner (1987)
m_{SOM}	mineralisation rate of SOM/CWD	h^{-1}	2.28×10^{-6}	Buyanovsky and Wagner (1987)
t_{lab}	turnover rate of labile pool	h^{-1}	6.25×10^{-3}	Penning de Vries *et al.* (1989, p 47/48)
r_{tr}	respiratory cost of labile transfers	fraction	0.2133	Goudriaan and van Laar (1994, p 52)
t_{ar}	turnover rate of autotrophic respiration pool	h^{-1}	0.07	adjusted to give ∼daily turnover of pool
GDD_{em}*	temperature sum at emergence	degree days	125	Wang and Engel (1998)

trl_{stem}*	rate of translocation of remobilisable carbon from stems	h^{-1}	8.3×10^{-3}	Penning de Vries *et al.* (1989, p 47)
$r_{\mathrm{max,v}}$*	maximum development rate in vegetative phase	d^{-1}	0.04	Yan and Wallace (1998); Li *et al.* (2008)
$r_{\mathrm{max,r}}$*	maximum development rate in reproductive phase	d^{-1}	0.035	Streck *et al.* (2003)
T_{min}*	minimum temperature for development	°C	0	Li *et al.* (2008)
T_{opt}*	optimum temperature for development	°C	24	Li *et al.* (2008)
T_{max}*	maximum temperature for development	°C	35	Li *et al.* (2008)
$T_{\mathrm{min,vn}}$*	minimum temperature for vernalization	°C	-1.3	Porter and Gawith (1999)
$T_{\mathrm{opt,vn}}$*	optimum temperature for vernalization	°C	4.9	Porter and Gawith (1999)
$T_{\mathrm{max,vn}}$*	maximum temperature for vernalization	°C	15.7	Porter and Gawith (1999)
VD_{h}*	effective vernalization days when plants are 50% vernalized	VD	22.5	Streck *et al.* (2003)
LAI_{cr}*	critical leaf area index beyond which leaf senescence due to self-shading occurs	$m^2\ m^{-2}$	4	van Laar *et al.* (1997)
dsh_{max}*	maximum value of relative death rate due to shading	h^{-1}	1.25×10^{-3}	van Laar *et al.* (1997)
PH_{cr}*	minimum (or critical) photoperiod for development	h	8.25	Streck *et al.* (2003)
PH_{sc}*	photoperiod sensitivity coefficient	-/-	0.25	Streck *et al.* (2003)

Table A.2: Performance criteria of the models across sites and models. E: Nash Sutcliffe efficiency (Nash and Sutcliffe, 1970), r: Kendall correlation coefficient, Δx: NEE absolute error [gC m^{-2}].

Site	Flux	Model												
		DNDC			CERES-EGC			ORCHIDEE-STICS			SPAc			Site mean	
		E	r	Δx	E	r	Δx	E	r	Δx	E	r	Δx	E	r
Oensingen 2007	NEE	0.33	0.45	-127	NA	NA	NA	0.56	0.54	125	0.7	0.56	22	0.53	0.52
	GPP	0.62	0.57		NA	NA		0.58	0.43		0.52	0.54		0.57	0.51
	R_e	0.1	0.5		NA	NA		0.14	0.66		-0.06	0.64		0.06	0.60
	Eta	-0.13	0.41		NA	NA		0.27	0.68		0.2	0.65		0.11	0.58
Grignon 2005	NEE	0.25	0.28	-207	0.85	0.4	185	0.29	0.59	-189	NA	NA	NA	0.46	0.42
	GPP	0.76	0.51		NA	NA		0.53	0.54		NA	NA		0.65	0.53
	R_e	-2.0	0.61		NA	NA		0.38	0.71		NA	NA		-0.81	0.66
	Eta	0.08	0.4		0.72	0.37		0.52	0.57		NA	NA		0.44	0.45
Grignon 2006	NEE	-0.15	0.32	-204	0.84	0.6	109	0.82	0.72	22	0.87	0.71	46	0.51	0.58
	GPP	0.31	0.49		NA	NA		0.83	0.59		0.87	0.51		0.67	0.53
	R_e	-1.79	0.29		NA	NA		0.64	0.71		0.43	0.65		-0.24	0.55
	Eta	-0.04	0.42		-0.75	0.32		0.78	0.61		0.69	0.68		0.48	0.57
Auradé 2006	NEE	0.62	0.68	-67	0.64	0.57	40	0.56	0.63	-8	0.86	0.63	82	0.68	0.65
	GPP	0.47	0.59		NA	NA		0.68	0.51		0.77	0.64		0.64	0.58
	R_e	-2.91	0.38		NA	NA		0.35	0.71		0.22	0.62		-0.78	0.57
	Eta	-0.04	0.43		-0.47	0.46		0.59	0.6		0.5	0.68		0.35	0.57
Klingenberg 2006	NEE	0.47	0.59	-97	NA	NA	NA	0.39	0.55	217	0.62	0.69	179	0.49	0.61
	GPP	0.68	0.59		NA	NA		0.67	0.46		0.45	0.8		0.60	0.62
	R_e	-0.27	0.63		NA	NA		0.69	0.79		0.66	0.51		0.36	0.64
	Eta	0.23	0.58		NA	NA		0.49	0.54		0.68	0.76		0.47	0.63
Gebesee 2007	NEE	0.35	0.5	-67	0.67	0.74	110	NA	NA	NA	0.76	0.81	126	0.59	0.68

	GPP	0.67	0.67		NA	NA		NA	NA		0.84	0.74		0.76	0.71
	R_e	0.73	0.62		NA	NA		NA	NA		0.41	0.72		0.57	0.67
	Eta	-0.35	0.48		-0.29	0.38		NA	NA		0.61	0.66		-0.01	0.51
Model mean	NEE	0.31	0.47	-128	0.75	0.58	111	0.52	0.61	27	0.76	0.68	91	0.55	0.58
	GPP	0.59	0.57		NA	NA		0.66	0.51		0.69	0.65		0.65	0.58
	R_e	-1.02	0.51		NA	NA		0.44	0.72		0.33	0.63		-0.14	0.62
	Eta	-0.04	0.45		-0.20	0.38		0.53	0.60		0.54	0.69		0.31	0.55

Table A.3: Overview of estimated model uncertainty per time step (also shown per day for pools), the number of observations available, and the initial C content of labile (i.e. seed), litter, and SOM C together with their initial uncertainty. Further, the estimated uncertainty for each observation type is shown, followed by a description of fluxes and pools listed.

Symbol	Model uncertainty ts^{-1} (d^{-1}) [%]	Number of observations	Initial value [gC m^{-2}]	Initial uncertainty [%]	Observation error	Pool/flux description
C_f	0.1 (4.8)	5	N/A	N/A	13–31% (mean=20%)	Foliar C mass
C_d	0.1 (4.8)	N/A	N/A	N/A	N/A	Dead foliar C mass
C_s	0.1 (4.8)	4	N/A	N/A	8–26% (mean=14%)	Stem C mass
C_r	0.1 (4.8)	6	N/A	N/A	11–90% (mean=36%)	Fine root C mass
C_{stor}	0.1 (4.8)	2	N/A	N/A	15–25% (mean= 20%)	Storage organ C mass
C_{lab}	0.1 (4.8)	N/A	9	50%	N/A	Labile C mass
C_{lit}	0.1 (4.8)	N/A	200	10%	N/A	Fresh litter C mass
C_{som}	0.01 (0.48)	N/A	7200	1%	N/A	Soil organic matter C mass
C_{aresp}	0.1 (4.8)	N/A	N/A	N/A	N/A	Autotrophic respiration pool C mass
LAI	0.1 (4.8)	5	N/A	N/A	11–28% (mean=18%)	Leaf area index
A_f	10	N/A	N/A	N/A	N/A	Foliage allocation rate
A_s	10	N/A	N/A	N/A	N/A	Stem allocation rate
A_r	10	N/A	N/A	N/A	N/A	Fine root allocation rate
A_{stor}	10	N/A	N/A	N/A	N/A	Storage organ allocation rate
$A_{fromlab}$	10	N/A	N/A	N/A	N/A	Allocation rate from labile C pool
L_f	10	N/A	N/A	N/A	N/A	Remobilization rate of foliar C mass
L_r	10	N/A	N/A	N/A	N/A	Fine root litter production rate
L_s	10	N/A	N/A	N/A	N/A	Remobilization rate of stem C mass
D	10	N/A	N/A	N/A	N/A	Decomposition rate of litter
G	10	N/A	N/A	N/A	N/A	Gross primary production
R_a	10	N/A	N/A	N/A	N/A	Autotrophic respiration rate

R_{h1}	10	N/A	N/A	N/A	N/A	Heterotrophic respiration rate of fresh litter
R_{h2}	10	N/A	N/A	N/A	N/A	Heterotrophic respiration rate of SOM
NEE	N/A	7292	N/A	N/A	0.035 gC m^{-2} ts^{-1} (1.68 gC m^{-2} d^{-1})	Net ecosystem exchange rate of C

Table A.4: SPAc model parameters for maize (m), soybean (s), and generic C_3 grass (g) vegetation (shown as m/s/g if parameter values differ between plant functional types). Only those parameters are shown that we changed from Sus *et al.* (2010).

Parameter symbol	Name	Unit	Nominal Value m/s/g	Source m/s/g
ψ_{l}	Minimum leaf water potential	MPa	-2.0/-2.3/-1.9	Reicosky and Lambert (1978)/Boyer (1970)/unchanged from Sus *et al.* (2010)
R_{r}	Root resistivity	MPa s g mmol^{-1}	05/05/2005	Adjusted from Sus *et al.* (2010)
V_{cmax}	Maximum carboxylation capacity	μmol m^{-2} s^{-1}	32/93/66	Massad *et al.* (2007)/Wullschleger (1993)/ Wullschleger (1993)
J_{max}	Maximum electron transport rate	μmol m^{-2} s^{-1}	191/164/149	Massad *et al.* (2007)/Wullschleger (1993)/ Wullschleger (1993)
C_{la}	Carbon per leaf area	gC m^{-2}	25/28/33	Penning de Vries *et al.* (1989); Chun *et al.* (2011)/Hesketh *et al.* (1981)/Foley *et al.* (1996)
f_{a}	Fraction of GPP respired	Fraction	0.3/0.28/0.41	Louwerse *et al.* (1990)/Bunce (1989)/Gilmanov *et al.* (2003)
r_{dc}	Decomposition rate	h^{-1}	1.8 x 10^{-5}	Buyanovsky *et al.* (1987)
m_{lit}	Mineralization rate of litter	h^{-1}	7.2 x 10^{-5}	Buyanovsky *et al.* (1987)
m_{SOM}	Mineralization rate of SOM/CWD	h^{-1}	1.83 x 10^{-6}	Buyanovsky *et al.* (1987)
T_{min}	Minimum temperature for development	°C	8/7/-	Streck *et al.* (2009)/Setiyono *et al.* (2007)/-
T_{opt}	Optimum temperature for development	°C	28/30/-	Streck *et al.* (2009)/ Setiyono *et al.* (2007)/-
T_{max}	Maximum temperature for development	°C	36/41.9/-	Streck *et al.* (2009)/ Setiyono *et al.* (2007)/-
P_{opt}	Daylength below which developmental rate is optimum	h	-/12/-	-/Setiyono *et al.* (2007)/-

P_{crt}	Daylength above which development rate is 0	h	-/18/-	-/Setiyono *et al.* (2007)/-
$r_{\mathrm{max,v}}$	Maximum development rate in vegetative phase	d^{-1}	0.025/0.025/-	Penning de Vries *et al.* (1989)/ Penning de Vries *et al.* (1989)/-
$r_{\mathrm{max,r}}$	Maximum development rate in reproductive phase	d^{-1}	0.029/0.027/-	Streck *et al.* (2009)/ Penning de Vries *et al.* (1989)/-

References

Abdalla, M., Wattenbach, M., Smith, P., Ambus, P., Jones, M. and Williams, M. (2009). Application of the DNDC model to predict emissions of N_2O from Irish agriculture. *Geoderma*, **151**, 327 – 337.

Aber, J.D. and Federer, C.A. (1992). A generalized, lumped-parameter model of photosynthesis, evapotranspiration and net primary production in temperate and boreal forest ecosystems. *Oecologia*, **92**, 463–474.

Adiku, S.G.K., Reichstein, M., Lohila, A. and Dinh, N.Q. (2006). PIXGRO: A Model for Simulating the Ecosystem CO_2 Exchange and Growth of Spring Barley. *Ecological Modelling*, **190**, 260–276.

Aksoy, A., Zhang, F., John and Nielsen-gammon, W. (2005). Ensemble-Based Simultaneous State and Parameter Estimation in a Two-Dimensional Sea-Breeze Model. *Monthly Weather Review*, **134**, 2951.

Amatya, D.M., Skaggs, R.W. and Gregory, J.D. (1995). Comparison of Methods for Estimating REF-ET. *J. Irrig. and Drain. Engrg*, **121**, 427–436.

Amos, B. and Walters, D.T. (2006). Maize Root Biomass and Net Rhizodeposited Carbon: An Analysis of the Literature. *Soil Science Society of America Journal*, **70**, 1489–1503.

Amthor, J.S. (2000). The McCree-de Wit-Penning de Vries-Thornley Respiration Paradigms: 30 Years Later. *Ann Bot*, **86**, 1–20.

Andrade, F.H. (1995). Analysis of growth and yield of maize, sunflower and soybean grown at Balcarce, Argentina. *Field Crops Research*, **41**, 1 – 12.

Anthoni, P.M., Freibauer, A., Kolle, O. and Schulze, E.D. (2004). Winter wheat carbon exchange in Thuringia, Germany. *Agricultural and Forest Meteorology*, **121**, 55–67.

Arevalo, C.B.M., Bhatti, J.S., Chang, S.X., Jassal, R.S. and Sidders, D. (2010). Soil respiration in four different land use systems in north central Alberta, Canada. *Journal of Geophysical Research*, **115**, 1–12.

Arora, V.K. (2003). Simulating Energy and Carbon Fluxes Over Winter Wheat Using Coupled Land Surface and Terrestrial Ecosystem Models. *Agricultural and Forest Meteorology*, **118**, 21–47.

Aubinet, M. (2008). Eddy covariance CO_2 flux measurements in nocturnal conditions: an analysis of the problem. *Ecological Applications*, **18**, 1368–1378.

Aubinet, M., Grelle, A., Ibrom, A., Rannik, U., Moncrieff, J., Foken, T., Kowalski, A., Martin, P., Berbigier, P., Bernhofer, C., Clement, R., Elbers, J., Granier, A., Grünwald, T., Morgenstern, K., Pilegaard, K., Rebmann, C., Snijders, W., Valentini, R. and Vesala, T. (1999). Estimates of the Annual Net Carbon and Water Exchange of Forests: The EUROFLUX Methodology. In A. Fitter and D. Raffaelli, eds., *Advances in Ecological Research*, vol. 30, 113 – 175, Academic Press.

Aubinet, M., Moureaux, C., Bodson, B., Dufranne, D., Heinesch, B., Suleau, M., Vancutsem, F. and Vilret, A. (2009). Carbon sequestration by a crop over a 4-year sugar beet/winter wheat/seed potato/winter wheat rotation cycle. *Agricultural and Forest Meteorology*, **149**, 407–418.

Baker, J. and Griffis, T. (2005). Examining strategies to improve the carbon balance of corn/soybean agriculture using eddy covariance and mass balance techniques. *Agricultural and Forest Meteorology*, **128**, 163 – 177.

Baldocchi, D. (1994). A comparative study of mass and energy exchange rates over a closed C_3 (wheat) and an open C_4 (corn) crop: II. CO_2 exchange and water use efficiency. *Agricultural and Forest Meteorology*, **67**, 291 – 321.

Baldocchi, D., Valentini, R., Running, S., Oechel, W. and Dahlman, R. (1996). Strategies for measuring and modelling carbon dioxide and water vapour fluxes over terrestrial ecosystems. *Global Change Biology*, **2**, 159–168.

Baldocchi, D., Falge, E., Gu, L., Olson, R., Hollinger, D., Running, S., Anthoni, P., Bernhofer, C., Davis, K. and Evans, R. (2001). FLUXNET: A New Tool to Study the Temporal and Spatial Variability of Ecosystem-Scale Carbon Dioxide, Water Vapor, and Energy Flux Densities. *Bulletin of the American Meteorological Society*, **82**, 2415–2434.

Baldocchi, D.D. (2003). Assessing the Eddy Covariance Technique for Evaluating Carbon Dioxide Exchange Rates of Ecosystems: Past, Present and Future. *Global Change Biology*, **9**, 479–492.

Baret, F., Olioso, A. and Luciani, J.L. (1992). Root biomass fraction as a function of growth degree days in wheat. *Plant and Soil*, **140**, 137–144.

Becker-Reshef, I., Vermote, E., Lindeman, M. and Justice, C. (2010). A generalized regression-based model for forecasting winter wheat yields in Kansas and Ukraine using MODIS data. *Remote Sensing of Environment*, **114**, 1312 – 1323.

Beer, C., Reichstein, M., Ciais, P., Farquhar, G.D. and Papale, D. (2007). Mean annual GPP of Europe derived from its water balance. *Geophys. Res. Lett.*, **34**, L05401.

Bellamy, P.H., Loveland, P.J., Bradley, R.I., Lark, R.M. and Kirk, G.J.D. (2005). Carbon losses from all soils across England and Wales 1978-2003. *Nature*, **437**, 245–248.

Bernacchi, C.J., Hollinger, S.E. and Meyers, T. (2005). The conversion of the corn/soybean ecosystem to no-till agriculture may result in a carbon sink. *Global Change Biology*, **11**, 1867–1872.

Best, D.J. and Gipps, P.G. (1974). An Improved Gamma Approximation to the Negative Binomial. *Technometrics*, **16**, 621–624.

Béziat, P., Céschia, E. and Dedieu, G. (2009). Carbon balance of a three crop succession over two cropland sites in South West Franc. *Agricultural and Forest Meteorology*, **149**, 1628 – 1645.

Birch, C.J., Hammer, G.L. and Rickert, K.G. (1999). Dry matter accumulation and distribution in five cultivars of maize (*Zea mays*): relationships and procedures for use in crop modelling. *Aust. J. Agric. Res.*, **50**, 513–528.

Black, T.A., Den Hartog, G., Neumann, H.H., Blanken, P., Yang, P., Russell, C., Nesic, Z., Lee, X., Chen, S.G., Staebler, R. and Novak, M.D. (1996). Annual cycles of water vapour and carbon dioxide fluxes in and above a boreal aspen forest. *Global Change Biology*, **2**, 219–229.

Bondeau, A., Smith, P.C., Zaehle, S., Schaphoff, S., Lucht, W., Cramer, W., Gerten, D., Lotze-Campen, H., Muller, C., Reichstein, M. and Smith, B. (2007). Modelling the role of agriculture for the 20th century global terrestrial carbon balance. *Global Change Biology*, **13**, 679–706.

Boryan, C., Yang, Z., Mueller, R. and Craig, M. (2011). Monitoring US agriculture: the US Department of Agriculture, National Agricultural Statistics Service, Cropland Data Layer Program. *Geocarto International*, in press.

Bosch, J. and Hewlett, J. (1982). A review of catchment experiments to determine the effect of vegetation changes on water yield and evapotranspiration. *Journal of Hydrology*, **55**, 3 – 23.

Boschetti, M., Stroppiana, D., Brivio, P.A. and Bocchi, S. (2009). Multi-year monitoring of rice crop phenology through time series analysis of MODIS images. *International Journal of Remote Sensing*, **30**, 4643–4662.

Boyer, J.S. (1970). Leaf Enlargement and Metabolic Rates in Corn, Soybean, and Sunflower at Various Leaf Water Potentials. *Plant Physiology*, **46**, 233–235.

Brisson, N., Mary, B., Ripoche, D., Jeuffroy, M.H., Ruget, F., Nicoullaud, B., Gate, P., Devienne-Barret, F., Antonioletti, R., Durr, C., Richard, G., Beaudoin, N., Recous, S., Tayot, X., Plenet, D., Cellier, P., Machet, J.M., Meynard, J.M. and Delécolle, R. (1998). STICS: a generic model for the simulation of crops and their water and nitrogen balances. I. Theory and parameterization applied to wheat and corn. *Agronomie*, **18**, 311–346.

Brisson, N., Ruget, F., Gate, P., Lorgeou, J., Nicoullaud, B., Tayot, X., Plenet, D., Jeuffroy, M.H., Bouthier, A., Ripoche, D., Mary, B. and Justes, E. (2002). STICS: a generic model for simulating crops and their water and nitrogen balances. II. Model validation for wheat and maize. *Agronomie*, **22**, 69–92.

Brisson, N., Gary, C., Justes, E., Roche, R., Mary, B., Ripoche, D., Zimmer, D., Sierra, J., Bertuzzi, P., Burger, P., Bussiere, F., Cabidoche, Y., Cellier, P., Debaeke, P., Gaudillere, J.P., Hanault, C., Maraux, F., Seguin, B. and Sinoquet, H. (2003). An overview of the crop model STICS. *European journal of agronomy*, **18**, 309–332.

Broge, N.H. and Mortensen, J.V. (2002). Deriving green crop area index and canopy chlorophyll density of winter wheat from spectral reflectance data. *Remote Sensing of Environment*, **81**, 45 – 57.

Brown, L., Syed, B., Jarvis, S.C., Sneath, R.W., Phillips, V.R., Goulding, K.W.T. and Li, C. (2002). Development and application of a mechanistic model to estimate emission of nitrous oxide from UK agriculture. *Atmospheric Environment*, **36**, 917 – 928.

Brown, M.E. and de Beurs, K.M. (2008). Evaluation of multi-sensor semi-arid crop season parameters based on NDVI and rainfall. *Remote Sensing of Environment*, **112**, 2261 – 2271.

Bunce, J.A. (1989). Growth Rate, Photosynthesis and Respiration in Relation to Leaf Area Index. *Annals of Botany*, **63**, 459–463.

Buyanovsky, G.A. and Wagner, G.H. (1987). Carbon transfer in a winter wheat (*Triticum aestivum*) ecosystem. *Biology and Fertility of Soils*, **5**, 76–82.

Buyanovsky, G.A., Kucera, C.L. and Wagner, G.H. (1987). Comparative Analyses of Carbon Dynamics in Native and Cultivated Ecosystems. *Ecology*, **68**, pp. 2023–2031.

Carvalhais, N., Reichstein, M., Seixas, J., Collatz, G.J., Pereira, J.S., Berbigier, P., Carrara, A., Granier, A., Montagnani, L., Papale, D., Rambal, S., Sanz, M.J. and Valentini, R. (2008). Implications of the carbon cycle steady state assumption for biogeochemical modeling performance and inverse parameter retrieval. *Global Biogeochem. Cycles*, **22**, 16pp.

Ceglar, A., Crepinsek, Z., Kajfez-Bogataj, L. and Pogacar, T. (2011). The simulation of phenological development in dynamic crop model: The Bayesian comparison of different methods. *Agricultural and Forest Meteorology*, **151**, 101 – 115.

Changnon, S. and Kunkel, K. (1991). Assessing impacts of a climatologically unique year (1990) in the Midwest. *Physical Geography*, **13**, 180–190.

Chen, M., Liu, S., Tieszen, L. and Hollinger, D. (2008). An improved state-parameter analysis of ecosystem models using data assimilation. *Ecological Modelling*, **219**, 317 – 326.

Chen, P.Y., Fedosejevs, G., Tiscareno-López, M. and Arnold, J. (2006). Assessment of MODIS-EVI, MODIS-NDVI and VEGETATION-NDVI Composite Data Using Agricultural Measurements: An Example at Corn Fields in Western Mexico. *Environmental Monitoring and Assessment*, **119**, 69–82.

Chmielewski, F.M., Muller, A. and Bruns, E. (2004). Climate changes and trends in phenology of fruit trees and field crops in Germany, 1961-2000. *Agricultural and Forest Meteorology*, **121**, 69 – 78.

Chouard, P. (1960). Vernalization and its Relations to Dormancy. *Annual Review of Plant Physiology*, **11**, 191–238.

Chun, J.A., Wang, Q., Timlin, D., Fleisher, D. and Reddy, V.R. (2011). Effect of elevated carbon dioxide and water stress on gas exchange and water use efficiency in corn. *Agricultural and Forest Meteorology*, **151**, 378 – 384.

Ciais, P., Wattenbach, M., Vuichard, N., Smith, P., Piao, S.L., Don, A., Luyssaert, S., Janssens, I.A., Bondeau, A., Dechow, R., Leip, A., Smith, P.C., Beer, C., van Der Werf, G.R., Gervois, S., van Oost, K., Tomelleri, E., Freibauer, A., Schulze, E.D. and Team, C.S. (2010). The European carbon balance. Part 2: croplands. *Global Change Biology*, **16**, 1409–1428.

Cleveland, W.S. (1979). Robust Locally Weighted Regression and Smoothing Scatterplots. *Journal of the American Statistical Association*, **74**, pp. 829–836.

Cleveland, W.S. (1981). LOWESS: A Program for Smoothing Scatterplots by Robust Locally Weighted Regression. *The American Statistician*, **35**.

Collatz, G.J., Ribas-Carbo, M. and Berry, J.A. (1992). Coupled Photosynthesis-Stomata1 Conductance Model for Leaves of C_4 Plants. *Aust. J. Plant Physiol*, **19**, 519–538.

Craufurd, P.Q. and Wheeler, T.R. (2009). Climate change and the flowering time of annual crops. *Journal of Experimental Botany*, **60**, 2529–2539.

Crutzen, P.J. and Steffen, W. (2003). How Long Have We Been in the Anthropocene Era? *Climatic Change*, **61**, 251–257.

Céschia, E., Béziat, P., Dejoux, J., Aubinet, M., Bernhofer, C., Bodson, B., Buchmann, N., Carrara, A., Cellier, P., Tommasi, P.D., Elbers, J., Eugster, W., Grünwald, T., Jacobs, C., Jans, W., Jones, M., Kutsch, W., Lanigan, G., Magliulo, E., Marloie, O., Moors, E., Moureaux, C., Olioso, A., Osborne, B., Sanz, M., Saunders, M., Smith, P., Soegaard, H. and Wattenbach, M. (2010). Management effects on net ecosystem carbon and GHG budgets at European crop sites. *Agriculture, Ecosystems & Environment*, **139**, 363 – 383.

Daughtry, C., Doraiswamy, P., Hunt, E., Jr., Stern, A., McMurtrey, J. and Prueger, J. (2006). Remote sensing of crop residue cover and soil tillage intensity. *Soil and Tillage Research*, **91**, 101 – 108.

David, M., Del Grosso, S., Hu, X., Marshall, E., McIsaac, G., Parton, W., Tonitto, C. and Youssef, M. (2009). Modeling denitrification in a tile-drained, corn and soybean agroecosystem of Illinois, USA. *Biogeochemistry*, **93**, 7–30.

Davidson, E.A., Janssens, I.A. and Luo, Y. (2006). On the variability of respiration in terrestrial ecosystems: moving beyond Q_{10}. *Global Change Biology*, **12**, 154–164.

Dawson, J.J. and Smith, P. (2007). Carbon losses from soil and its consequences for land-use management. *Science of The Total Environment*, **382**, 165 – 190.

de Noblet-Ducoudré, N., Gervois, S., Ciais, P., Viovy, N., Brisson, N., Seguin, B. and Perrier, A. (2004). Coupling the soil-vegetation-atmosphere-transfer scheme ORCHIDEE to the agronomy model STICS to study the influence of croplands on the European carbon and water budgets. *Agronomie*, **24**, 397–407.

de Wit, A. and van Diepen, C. (2007). Crop model data assimilation with the Ensemble Kalman filter for improving regional crop yield forecasts. *Agricultural and Forest Meteorology*, **146**, 38 – 56.

Demarty, J., Chevallier, F., Friend, A.D. and Viovy, N. (2007). Assimilation of Global MODIS Leaf Area Index Retrievals Within a Terrestrial Biosphere Model. *Geophysical Research Letters*, **34**, 1–6.

Denman, K.L., Brasseur, G., Chidthaisong, A., Clais, P., Cox, P.M., Dickinson, R., Hauglustaine, D., Heinze, C., Holland, E., Jacob, D., Lohmann, U., Ramachandran, S., da Silva Dias, P., Wofsy, S. and Zhang, X. (2007). *Climate Change 2007: The Physical Science Basis. Contribution of Working Group I to the Fourth Assessment Report of the Intergovernmental Panel on Climate Change*, chap. Couplings Between Changes in the Climate System and Biogeochemistry. Cambridge University Press, Cambridge, New York.

Dente, L., Satalino, G., Mattia, F. and Rinaldi, M. (2008). Assimilation of leaf area index derived from ASAR and MERIS data into CERES-Wheat model to map wheat yield. *Remote Sensing of Environment*, **112**, 1395 – 1407.

Dietiker, D., Buchmann, N. and Eugster, W. (2010). Testing the ability of the DNDC model to predict CO_2 and water vapour fluxes of a Swiss cropland site. *Agriculture, Ecosystems & Environment*, **139**, 396 – 401.

Doraiswamy, P.C., Hatfield, J.L., Jackson, T.J., Akhmedov, B., Prueger, J. and Stern, A. (2004). Crop condition and yield simulations using Landsat and MODIS. *Remote Sensing of Environment*, **92**, 548 – 559.

Doraiswamy, P.C., Sinclair, T.R., Hollinger, S., Akhmedov, B., Stern, A. and Prueger, J. (2005). Application of MODIS derived parameters for regional crop yield assessment. *Remote Sensing of Environment*, **97**, 192 – 202.

Dorigo, W.A., Zurita-Milla, R., de Wit, A.J.W., Brazile, J., Singh, R. and Schaepman, M.E. (2007). A Review on Reflective Remote Sensing and Data Assimilation Techniques for Enhanced Agroecosystem Modeling. *International Journal of Applied Earth Observation and Geoinformation*, **9**, 165–193.

Eknes, M. and Evensen, G. (2002). An Ensemble Kalman filter with a 1-D marine ecosystem model. *Journal of Marine Systems*, **36**, 75 – 100.

Eugster, W., Moffat, A.M., Céschia, E., Aubinet, M., Ammann, C., Osborne, B., Davis, P.A., Smith, P., Jacobs, C., Moors, E., Dantec, V.L., Béziat, P., Saunders, M., Jans, W., Grünwald, T., Rebmann, C., Kutsch, W.L., Czerny, R., Janous, D., Moureaux, C., Dufranne, D., Carrara, A., Magliulo, V., Tommasi, P.D., Olesen, J.E., Schelde, K., Olioso, A., Bernhofer, C., Cellier, P., Larmanou, E., Loubet, B., Wattenbach,

M., Marloie, O., Sanz, M.J., Sagaard, H. and Buchmann, N. (2010). Management effects on European cropland respiration. *Agriculture, Ecosystems & Environment*, **139**, 346 – 362.

Eurostat (2008). Agricultural statistics. Main results — 2006–2007. eurostat Pocketbooks, Luxembourg.

Evensen, G. (2003). The Ensemble Kalman Filter: theoretical formulation and practical implementation. *Ocean Dynamics*, **53**, 343–367.

Evensen, G. (2009). The ensemble kalman filter for combined state and parameter estimation. *Control Systems, IEEE*, **29**, 83 –104.

Falge, E., Baldocchi, D., Olson, R., Anthoni, P., Aubinet, M., Bernhofer, C., Burba, G., Ceulemans, R., Clement, R., Dolman, H., Granier, A., Gross, P., Grünwald, T., Hollinger, D., Jensen, N.O., Katul, G., Keronen, P., Kowalski, A., Lai, C.T., Law, B.E., Meyers, T., Moncrieff, J., Moors, E., Munger, J.W., Pilegaard, K., Rannik, Ü., Rebmann, C., Suyker, A., Tenhunen, J., Tu, K., Verma, S., Vesala, T., Wilson, K. and Wofsy, S. (2001). Gap filling strategies for defensible annual sums of net ecosystem exchange. *Agricultural and Forest Meteorology*, **107**, 43–69.

Falge, E., Reth, S., Braggemann, N., Butterbach-Bahl, K., Goldberg, V., Oltchev, A., Schaaf, S., Spindler, G., Stiller, B., Queck, R., Kastner, B. and Bernhofer, C. (2005). Comparison of surface energy exchange models with eddy flux data in forest and grassland ecosystems of Germany. *Ecological Modelling*, **188**, 174 – 216.

Falloon, P. and Betts, R. (2010). Climate impacts on European agriculture and water management in the context of adaptation and mitigation — The importance of an integrated approach. *Science of The Total Environment*, **408**, 5667 – 5687.

Fang, C., Smith, P. and Smith, J.U. (2005). A simple equation for simulating C decomposition in a multi-component pool of soil organic matter. *European Journal of Soil Science*, **56**, 815–820.

Fang, H., Liang, S., Hoogenboom, G., Teasdale, J. and Cavigelli, M. (2008). Corn-yield estimation through assimilation of remotely sensed data into the CSM-CERES-Maize model. *Int. J. Remote Sens.*, **29**, 3011–3032.

Fang, H., Liang, S. and Hoogenboom, G. (2011). Integration of MODIS LAI and vegetation index products with the CSM-CERES-Maize model for corn yield estimation. *Int. J. Remote Sens.*, **32**, 1039–1065.

Farley, K.A., Jobbagy, E.G. and Jackson, R.B. (2005). Effects of afforestation on water yield: a global synthesis with implications for policy. *Global Change Biology*, **11**, 1565–1576.

Farquhar, G.D. and von Caemmerer, S. (1982). Modelling of photosynthetic response to the environment. In O.L. Lange, P.S. Nobel, C.B. Osmond and H. Ziegler, eds., *Physiological Plant Ecology II. Encyclopedia of plant physiology, New Series*, vol. 12B, 549–587, Springer, Berlin.

Foley, J.A., Prentice, I.C., Ramankutty, N., Levis, S., Pollard, D., Sitch, S. and Haxeltine, A. (1996). An integrated biosphere model of land surface processes, terrestrial carbon balance, and vegetation dynamics. *Global Biogeochemical Cycles*, **10**, 603–628.

Foley, J.A., DeFries, R., Asner, G.P. and Barford, C. (2005). Global Consequences of Land Use. *Science*, **309**, 570–574.

Friend, A.D., Arneth, A., Kiang, N.Y. and Lomas, M. (2006). FLUXNET and Modelling the Global Carbon Cycle. *Global Change Biology*, **12**, 1–24.

Frolking, S., Mosier, A., Ojima, D., Li, C., Parton, W., Potter, C., Priesack, E., Stenger, R., Haberbosch, C., Darsch, P., Flessa, H. and Smith, K. (1998). Comparison of N_2O emissions from soils at three temperate agricultural sites: simulations of year-round measurements by four models. *Nutrient Cycling in Agroecosystems*, **52**, 77–105.

Gabrielle, B., Laville, P., Duval, O., Nicoullaud, B., Germon, J.C. and Henault, C. (2006). Process-based modeling of nitrous oxide emissions from wheat-cropped soils at the subregional scale. *Global Biogeochem. Cycles*, **20**, GB4018.

Galloway, J.N., Cowling, E.B., Seitzinger, S.P. and Socolow, R.H. (2002). Reactive Nitrogen: Too Much of a Good Thing? *Ambio*, **31**, pp. 60–63.

Galloway, J.N., Townsend, A.R., Erisman, J.W., Bekunda, M., Cai, Z., Freney, J.R., Martinelli, L.A., Seitzinger, S.P. and Sutton, M.A. (2008). Transformation of the Nitrogen Cycle: Recent Trends, Questions, and Potential Solutions. *Science*, **320**, 889–892.

Gelb, A., Kasper, J.F., Nash, R.A., Price, C.F. and Sutherland, A.A. (2001). *Applied optimal estimation*, vol. 16. M.I.T. Press, Cambridge, MA and London, GB.

Gent, M.P.N. (1983). Rate of Increase in Size and Dry Weight of Individual Pods of Field Grown Soya Bean Plants. *Annals of Botany*, **51**, 317–329.

Gervois, S., de Noblet-Ducoudré, N., Viovy, N., Ciais, P., Brisson, N., Seguin, B. and Perrier, A. (2004). Including Croplands in a Global Biosphere Model: Methodology and Evaluation at Specific Sites. *Earth Interactions*, **8**, 1–25.

Gervois, S., Ciais, P., de Noblet-Ducoudré, N., Brisson, N., Vuichard, N. and Viovy, N. (2008). Carbon and water balance of European croplands throughout the 20th century. *Global Biogeochem. Cycles*, **22**, GB2022.

Gifford, R.M. (1994). The Global Carbon-Cycle — a Viewpoint on the Missing Sink. *Australian Journal of Plant Physiology*, **21**, 1–15.

Gifford, R.M. (1995). Whole plant respiration and photosynthesis of wheat under increased CO_2 concentration and temperature: long-term vs. short-term distinctions for modelling. *Global Change Biology*, **1**, 385–396.

Gifford, R.M. (2003). Plant respiration in productivity models: conceptualisation, representation and issues for global terrestrial carbon-cycle research. *Functional Plant Biology*, **30**, 171 – 186.

Gilmanov, T., Verma, S., Sims, P., Meyers, T., Bradford, J., Burba, G. and Suyker, A. (2003). Gross primary production and light response parameters of four Southern Plains ecosystems estimated using long term CO_2-flux tower measurements. *Global Biogeochem. Cycles*, **17**.

Goldberg, V., Baums, A. and Häntzschel, J. (2002). Klima, Boden und Landnutzung. In C. Bernhofer, ed., *Exkursions und Praktikumsführer Tharandter Wald. Material zum Hydrologisch-Meteorologischen Feldpaktikum*, vol. 6, Technische Universität Dresden, Dresden, GE.

Goudriaan, J. and van Laar, H. (1994). *Modelling Potential Crop Growth Processes — Textbook with Exercises*, vol. 2 of *Current Issues in Production Ecology*. Kluwer Academic Publishers, Dordrecht.

Gove, J.H. and Hollinger, D.Y. (2006). Application of a dual unscented Kalman filter for simultaneous state and parameter estimation in problems of surface-atmosphere exchange. *Journal of Geophysical Research*, **111**, 1–21.

Grant, R.F., Arkebauer, T.J., Dobermann, A., Hubbard, K.G., Schimelfenig, T.T., Suyker, A.E., Verma, S.B. and Walters, D.T. (2007). Net Biome Productivity of Irrigated and Rainfed Maize–Soybean Rotations: Modeling vs. Measurements. *Agronomy Journal*, **99**, 1404–1423.

Grayston, S.J., Vaughan, D. and Jones, D. (1997). Rhizosphere carbon flow in trees, in comparison with annual plants: the importance of root exudation and its impact on microbial activity and nutrient availability. *Applied Soil Ecology*, **5**, 29 – 56.

Grünwald, T. and Bernhofer, C. (2007). A decade of carbon, water and energy flux measurements of an old spruce forest at the Anchor Station Tharandt. *Tellus B*, **59**, 387–396.

Guerif, M. and Duke, C.L. (2000). Adjustment procedures of a crop model to the site specific characteristics of soil and crop using remote sensing data assimilation. *Agriculture, Ecosystems & Environment*, **81**, 57 – 69.

Guindin-Garcia, N. (2011). *Estimating maize grain yield from crop biophysical parameters using remote sensing*. Ph.D. thesis, University of Nebraska, Lincoln.

Haberl, H., Erb, H.K., Krausmann, F., Gaube, V., Bondeau, A., Plutzar, C., Gingrich, S., Lucht, W. and Fischer-Kowalski, M. (2007). Quantifying and Mapping the Human Appropriation of Net Primary Production in Earth's Terrestrial Ecosystems. *PNAS*, **104**, 12942–12947.

Haboudane, D., Millera, J.R., Pattey, E., Zarco-Tejada, P.J. and Strachan, I.B. (2004). Hyperspectral vegetation indices and novel algorithms for predicting green LAI of crop canopies: Modeling and validation in the context of precision agriculture. *Remote Sensing of Environment*, **90**, 337–352.

Halley, R.J. and Soffe, R.J., eds. (1988). *The Agricultural Notebook*. Blackwell, London, 18th edn.

Hesketh, J., Ogren, W., Hageman, M. and Peters, D. (1981). Correlations among leaf CO_2-exchange rates, areas and enzyme activities among soybean cultivars. *Photosynthesis Research*, **2**, 21–30.

Hill, T.C., Quaife, T. and Williams, M. (2011a). A data assimilation method for using low-resolution Earth observation data in heterogeneous ecosystems. *J. Geophys. Res.*, **116**, D08117.

Hill, T.C., Ryan, E. and Williams, M. (2011b). The use of CO_2 flux time series for parameter and carbon stock estimation in carbon cycle research. *Global Change Biology*.

Hirose, T. and Werger, M.J.A. (1987). Maximizing daily canopy photosynthesis with respect to the leaf nitrogen allocation pattern in the canopy. *Oecologia*, **72**, 520–526.

Hollinger, D.Y. and Richardson, A.D. (2005). Uncertainty in eddy covariance measurements and its application to physiological models. *Tree Physiology*, **25**, 873–885.

Hollinger, S.E., Bernacchi, C.J. and Meyers, T.P. (2004). Carbon Budget of Mature No-till Ecosystems in North Central Region of the United States. *Agricultural and Forest Meteorology*, **130**, 59–69.

Hollinger, S.E., Bernacchi, C.J. and Meyers, T.P. (2005). Corrigendum to "Carbon budget of Mature No-till Ecosystem in North Central Region of the United States [Agric. For. Meteorol. 130 (2005) 59-69]". *Agricultural and Forest Meteorology*, **136**, 88–89.

Houghton, R.A. (1999). The annual net flux of carbon to the atmosphere from changes in land use 1850–1990. *Tellus B*, **51**, 298–313.

Hoyaux, J., Moureaux, C., Tourneur, D., Bodson, B. and Aubinet, M. (2008). Extrapolating gross primary productivity from leaf to canopy scale in a winter wheat crop. *Agricultural and Forest Meteorology*, **148**, 668–679.

Hu, X.M., Zhang, F. and Nielsen-Gammon, J.W. (2010). Ensemble-based simultaneous state and parameter estimation for treatment of mesoscale model error: A real-data study. *Geophys. Res. Lett.*, **37**, 7 PP.

Huang, Y., Yu, Y., Zhang, W., Sun, W., Liu, S., Jiang, J., Wu, J., Yu, W., Wang, Y. and Yang, Z. (2009a). Agro-C: A biogeophysical model for simulating the carbon budget of agroecosystems. *Agricultural and Forest Meteorology*, **149**, 106–129.

Huang, Y., Yu, Y., Zhang, W., Sun, W., Liu, S., Jiang, J., Wu, J., Yu, W., Wang, Y. and Yang, Z. (2009b). Agro-C: A biogeophysical model for simulating the carbon budget of agroecosystems. *Agricultural and Forest Meteorology*, **149**, 106 – 129.

Huete, A., Justice, C. and van Leeuwen, W. (1999). MODIS vegetation index (MOD13) algorithm theoretical document — Version 3. Tech. rep., University of Arizona, University of Virginia.

Huete, A., Didan, K., Miura, T., Rodriguez, E., Gao, X. and Ferreira, L. (2002). Overview of the radiometric and biophysical performance of the MODIS vegetation indices. *Remote Sensing of Environment*, **83**, 195–213.

Ines, A.V. and Honda, K. (2005). On quantifying agricultural and water management practices from low spatial resolution RS data using genetic algorithms: A numerical study for mixed-pixel environment. *Advances in Water Resources*, **28**, 856 – 870.

Inoue, Y. and Olioso, A. (2006). Estimating the dynamics of ecosystem CO_2 flux and biomass production in agricultural fields on the basis of synergy between process models and remotely sensed signatures. *Journal of Geophysical Research (Atmospheres)*, **111**, D24S91.

Jamieson, P.D., Semenov, M.A., Brooking, I.R. and Francis, G.S. (1998). Sirius: a mechanistic model of wheat response to environmental variation. *European Journal of Agronomy*, **8**, 161–179.

Janssens, I.A., Freibauer, A., Ciais, P., Smith, P., Nabuurs, G.J., Folberth, G., Schlamadinger, B., Hutjes, R.W.A., Ceulemans, R., Schulze, E.D., Valentini, R. and Dolman, A.J. (2003). Europe's Terrestrial Biosphere Absorbs 7 to 12% of European Anthropogenic CO_2 Emissions. *Science*, **300**, 1538–1542.

Janssens, I.A., Freibauer, A., Schlamadinger, B., Ceulemans, R., Ciais, P., Dolman, A.J., Heimann, M., Nabuurs, G.J., Smith, P., Valentini, R. and Schulze, E.D. (2005). The carbon budget of terrestrial ecosystems at country-scale — a European case study. *Biogeosciences*, **2**, 15–26.

Johnson, R.C., Mornhinweg, D.W., Ferris, D.M. and Heitholt, J.J. (1987). Leaf Photosynthesis and Conductance of Selected *Triticum* Species at Different Water Potentials. *Plant Physiol.*, **83**, 1014–1017.

Jones, C. and Kiniry, J. (1986). *CERES-Maize: A Simulation Model of Maize Growth and Development*. Texas A&M University Press, Temple, TX.

Jones, H.G. (1992). *Plants and Microclimate*. Cambridge University Press, Cambridge.

Juskiw, P.E., Jame, Y.W. and Kryzanowski, L. (2001). Phenological Development of Spring Barley in a Short-Season Growing Area. *Agronomy Journal*, **93**, 370–379.

Justice, C., Townshend, J., Vermote, E., Masuoka, E., Wolfe, R., Saleous, N., Roy, D. and Morisette, J. (2002). An overview of MODIS Land data processing and product status. *Remote Sensing of Environment*, **83**, 3–15.

Karkee, M., Steward, B.L., Tang, L. and Aziz, S.A. (2009). Quantifying sub-pixel signature of paddy rice field using an artificial neural network. *Computers and Electronics in Agriculture*, **65**, 65 – 76.

Keating, B.A., Carberry, P.S., Hammer, G.L., Probert, M.E., Robertson, M.J., Holzworth, D., Huth, N.I., Hargreaves, J.N.G., Meinke, H., Hochman, Z., McLean, G., Verburg, K., Snow, V., Dimes, J.P., Silburn, M., Wang, E., Brown, S., Bristow, K.L., Asseng, S., Chapman, S., McCown, R.L., Freebairn, D.M. and Smith, C.J.

(2003). An overview of APSIM, a model designed for farming systems simulation. *European Journal of Agronomy*, **18**, 267 – 288.

Keeling, C.D., Chin, J.F.S. and Whorf, T.P. (1996). Increased activity of northern vegetation inferred from atmospheric CO_2 measurements. *Nature*, **382**.

Keenan, T., Carbone, M., Reichstein, M. and Richardson, A. (2011). The model–data fusion pitfall: assuming certainty in an uncertain world. *Oecologia*, 1–11.

Klein Tank, A.M.G., Wijngaard, J.B., Kannen, G.P., Bohm, R., Demarie, G., Gocheva, A., Mileta, M., Pashiardis, S., Hejkrlik, L., Kern-Hansen, C., Heino, R., Bessemoulin, P., Mueller-Westermeier, G., Tzanakou, M., Szalai, S., Palsdottir, T., Fitzgerald, D., Rubin, S., Capaldo, M., Maugeri, M., Leitass, A., Bukantis, A., Aberfeld, R., van Engelen, A.F.V., Forland, E., Mietus, M., Coelho, F., Mares, C., Razuvaev, V., Nieplova, E., Cegnar, T., Antonio López, J., Dahlstrom, B., Moberg, A., Kirchhofer, W., Ceylan, A., Pachaliuk, O., Alexander, L.V. and Petrovic, P. (2002). Daily dataset of 20th-century surface air temperature and precipitation series for the European Climate Assessment. *International Journal of Climatology*, **22**, 1441–1453.

Knorr, W., Kaminski, T., Scholze, M., Gobron, N., Pinty, B., Giering, R. and Mathieu, P.P. (2010). Carbon cycle data assimilation with a generic phenology model. *J. Geophys. Res.*, **115**, G04017.

Kramer, K., Leinonen, I., Bartelink, H.H., Berbigier, P., Borghetti, M., Bernhofer, C., Cienciala, E., Dolman, A.J., Froer, O., Gracia, C.A., Granier, A., Grünwald, T., Hari, P., Jans, W., Kellomaki, S., Loustau, D., Magnani, F., Markkanen, T., Matteucci, G., Mohren, G.M.J., Moors, E., Nissinen, A., Peltola, H., Sabate, S., Sanchez, A., Sontag, M., Valentini, R. and Vesala, T. (2002). Evaluation of six process-based forest growth models using eddy-covariance measurements of CO_2 and H_2O fluxes at six forest sites in Europe. *Global Change Biology*, **8**, 213–230.

Krinner, G., Viovy, N., de Noblet-Ducoudré, N., Ogee, J., Polcher, J., Friedlingstein, P., Ciais, P., Sitch, S. and Prentice, I.C. (2005). A dynamic global vegetation model for studies of the coupled atmosphere-biosphere system. *Global Biogeochemical Cycles*, **19**, GB1015+.

Kucharik, C.J. and Twine, T.E. (2007). Residue, Respiration, and Residuals: Evaluation of a Dynamic Agroecosystem Model Using Eddy Flux Measurements and Biometric Data. *Agricultural and Forest Meteorology*, **146**, 134–158.

Kutsch, W., Aubinet, M., Buchmann, N., Smith, P., Osborne, B., Eugster, W., Wattenbach, M., Schrumpf, M., Schulze, E., Tomelleri, E., Céschia, E., Bernhofer, C., Béziat, P., Carrara, A., Tommasi, P.D., Grünwald, T., Jones, M., Magliulo, V., Marloie, O., Moureaux, C., Olioso, A., Sanz, M., Saunders, M., Sogaard, H. and Ziegler, W. (2010). The net biome production of full crop rotations in Europe. *Agriculture, Ecosystems & Environment*, **139**, 336 – 345.

Kätterer, T., Eckersten, H., Andren, O. and Pettersson, R. (1997). Winter wheat biomass and nitrogen dynamics under different fertilization and water regimes: application of a crop growth model. *Ecological Modelling*, **102**, 301 – 314.

Lal, R. (2004). Soil Carbon Sequestration Impacts on Global Climate Change and Food Security. *Science*, **304**, 1623–1627.

Lambers, H., Van Den Boogaard, R., Veneklaas, E.J. and Villar, R. (1995). Effects of global environmental change on carbon partitioning in vegetative plants of *Triticum aestivum* and closely related Aegilops species. *Global Change Biology*, **1**, 397–406.

Lasslop, G., Reichstein, M., Kattge, J. and Papale, D. (2008). Influences of observation errors in eddy flux data on inverse model parameter estimation. *Biogeosciences Discussions*, **5**, 751–785.

Launay, M. and Guerif, M. (2005). Assimilating remote sensing data into a crop model to improve predictive performance for spatial applications. *Agriculture, Ecosystems & Environment*, **111**, 321 – 339.

Law, B.E., Williams, M., Anthoni, P.M., Baldocchi, D.D. and Unsworth, M.H. (2000). Measuring and modelling seasonal variation of carbon dioxide and water vapour exchange of a Pinus ponderosa forest subject to soil water deficit. *Global Change Biology*, **6**, 613–630.

Lee, H., Fok, L. and Zhang, D. (2008). Climatic change and Chinese population growth dynamics over the last millennium. *Climatic Change*, **88**, 131–156.

Leff, B., Ramankutty, N. and Foley, J.A. (2004). Geographic Distribution of Major Crops Across the World. *Global Biogeochemical Cycles*, **18**, 1–27.

Lehuger, S., Gabrielle, B., Larmanou, E., Laville, P., Cellier, P. and Loubet, B. (2007). Predicting the global warming potential of agro-ecosystems. *Biogeosciences Discussions*, **4**, 1059–1092.

Lehuger, S., Gabrielle, B., van Oijen, M., Makowski, D., Germon, J.C., Morvan, T. and Hinault, C. (2009). Bayesian calibration of the nitrous oxide emission module of an agro-ecosystem model. *Agriculture, Ecosystems & Environment*, **133**, 208 – 222.

Lehuger, S., Gabrielle, B., Cellier, P., Loubet, B., Roche, R., Béziat, P., Céschia, E. and Wattenbach, M. (2010). Predicting the net carbon exchanges of crop rotations in Europe with an agro-ecosystem model. *Agriculture, Ecosystems & Environment*, **139**, 384 – 395.

Leip, A., Marchi, G., Koeble, R., Kempen, M., Britz, W. and Li, C. (2008). Linking an economic model for European agriculture with a mechanistic model to estimate nitrogen and carbon losses from arable soils in Europe. *Biogeosciences*, **5**, 73–94.

Li, C., Frolking, S. and Frolking, T.A. (1992). A Model of Nitrous Oxide Evolution From Soil Driven by Rainfall Events: 1. Model Structure and Sensitivity. *J. Geophys. Res.*, **97**, 9759–9767.

Li, C., Frolking, S.E., Harriss, R.C. and Terry, R.E. (1994). Modeling nitrous oxide emissions from agriculture: A Florida case study. *Chemosphere*, **28**, 1401 – 1415.

Li, C., Frolking, S., Crocker, G.J., Grace, P.R., Klar, J., Karchens, M. and Poulton, P.R. (1997). Simulating trends in soil organic carbon in long-term experiments using the DNDC model. *Geoderma*, **81**, 45 – 60.

Li, C., Frolking, S., Xiao, X., Moore, B., Boles, S., Qiu, J., Huang, Y., Salas, W. and Sass, R. (2005). Modeling impacts of farming management alternatives on CO_2, CH_4, and N_2O emissions: A case study for water management of rice agriculture of China. *Global Biogeochem. Cycles*, **19**, GB3010.

Li, C., Farahbakhshazad, N., Jaynes, D.B., Dinnes, D.L., Salas, W. and McLaughlin, D. (2006). Modeling nitrate leaching with a biogeochemical model modified based on observations in a row-crop field in Iowa. *Ecological Modelling*, **196**, 116 – 130.

Li, L., McMaster, G.S., Yu, Q. and Du, J. (2008). Simulating winter wheat development response to temperature: Modifying Malo's exponential sine equation. *Comput. Electron. Agric.*, **63**, 274–281.

Licker, R., Johnston, M., Foley, J.A., Barford, C., Kucharik, C.J., Monfreda, C. and Ramankutty, N. (2010). Mind the gap: how do climate and agricultural management explain the yield gap of croplands around the world? *Global Ecology and Biogeography*, **19**, 769–782.

Lim, P.O., Kim, H.J. and Nam, H.G. (2007). Leaf Senescence. *Annual Review of Plant Biology*, **58**, 115–136.

Liu, L., Kon, H., Matsuoka, N. and Kobayashi, T. (2005). Coordination between Stomatal Conductance and Leaf-specific Hydraulic Conductance in Maize (*Zea mays* L.). *Journal of Agricultural Meteorology*, **61**, 143–152.

Lobell, D.B. and Asner, G.P. (2004). Cropland distributions from temporal unmixing of MODIS data. *Remote Sensing of Environment*, **93**, 412 – 422.

Lobell, D.B. and Field, C.B. (2007). Global scale climate–crop yield relationships and the impacts of recent warming. *Environmental Research Letters*, **2**.

Lohila, A., Aurela, M., Regina, K. and Laurila, T. (2003). Soil and total ecosystem respiration in agricultural fields: effect of soil and crop type. *Plant and Soil*, **251**, 303–317.

Lokupitiya, E., Denning, S., Paustian, K., Baker, I., Schaefer, K., Verma, S., Meyers, T., Bernacchi, C., Suyker, A. and Fischer, M. (2009). Incorporation of crop phenology in Simple Biosphere Model (SiBcrop) to improve land-atmosphere carbon exchanges from croplands. *Biogeosciences Discussions*, **6**, 1903–1944.

Louwerse, W., Sibma, L. and van Kleef, J. (1990). Crop photosynthesis, respiration and dry matter production of maize. *Netherlands Journal of Agricultural Science*, **38**, 95–108.

Luo, Y., Weng, E., Wu, X., Gao, C., Zhou, X. and Zhang, L. (2009). Parameter identifiability, constraint, and equifinality in data assimilation with ecosystem models. *Ecological Applications*, **19**, 571–574.

Luo, Z., Wang, E. and Sun, O.J. (2010). Soil carbon change and its responses to agricultural practices in Australian agro-ecosystems: A review and synthesis. *Geoderma*, **155**, 211 – 223.

Luyssaert, S., Inglima, I., Jung, M., Richardson, A.D., Reichstein, M., Papale, D., Piao, S.L., Shulze, E.D., Wingate, L., Matteucci, G., Aragao, L., Aubinet, M., Beer, C., Bernhofer, C., Black, K.G., Bonal, D., Bonnefond, J.M., Chambers, J., Ciais, P., Cook, B., Davis, K.J., Dolman, A.J., Gielen, B., Goulden, M., Grace, J., Granier, A., Grelle, A., Griffis, T., Grünwald, T., Guidolotti, G., Hanson, P.J., Harding, R., Hollinger, D.Y., Hutyra, L.R., Kolari, P., Kruijt, B., Kutsch, W., Lagergren, F., Laurila, T., Law, B.E., Le Maire, G., Lindroth, A., Loustau, D., Malhi, Y., Mateus, J., Migliavacca, M., Misson, L., Montagnani, L., Moncrieff, J., Moors, E., Munger, J.W., Nikinmaa, E., Ollinger, S.V., Pita, G., Rebmann, C., Roupsard, O., Saigusa, N., Sanz, M.J., Seufert, G., Sierra, C., Smith, M.L., Tang, J., Valentini, R., Vesala, T. and Janssens, I.A. (2007). CO_2 balance of boreal, temperate, and tropical forests derived from a global database. *Global Change Biology*, **13**, 2509–2537.

López, M.V. and Arrue, J.L. (1997). Growth, yield and water use efficiency of winter barley in response to conservation tillage in a semi-arid region of Spain. *Soil and Tillage Research*, **44**, 35 – 54.

Marcelis, L. and Heuvelink, E. (2007). *Proceedings of the Frontis Workshop on Functional-Structural Plant Modelling in Crop Production*, chap. Concepts of modelling carbon allocation among plant organs. Springer, Wageningen, NL.

Massad, R.S., Tuzet, A. and Bethenod, O. (2007). The effect of temperature on C_4-type leaf photosynthesis parameters. *Plant, Cell & Environment*, **30**, 1191–1204.

Mathieu, P.P. and O'Neill, A. (2008). Data assimilation: From photon counts to Earth System forecasts. *Remote Sensing of Environment*, **112**, 1258 – 1267.

McGuire, A.D., Sitch, S., Clein, J.S., Dargaville, R., Esser, G. and Foley, J. (2001). Carbon Balance of the Terrestrial Biosphere in the Twentieth Century: Analyses of CO_2, Climate and Land Use Effects with Four Process-based Ecosystem Models. *Global Biogeochemical Cycles*, **15**, 183–206.

McKenney, M.S. and Rosenberg, N.J. (1993). Sensitivity of some potential evapotranspiration estimation methods to climate change. *Agricultural and Forest Meteorology*, **64**, 81 – 110.

McMaster, G.S. and Wilhelm, W.W. (2003). Phenological responses of wheat and barley to water and temperature: improving simulation models. *The Journal of Agricultural Science*, **141**, 129–147.

Mearns, L.O., Mavromatis, T., Tsvetsinskaya, E., Hays, C. and Easterling, W. (1999). Comparative responses of EPIC and CERES crop models to high and low spatial resolution climate change scenarios. *J. Geophys. Res.*, **104**, 6623–6646.

Meir, P., Cox, P. and Grace, J. (2006). The influence of terrestrial ecosystems on climate. *Trends in Ecology & Evolution*, **21**, 254 – 260.

Meyers, T.P. and Hollinger, S.E. (2004). An assessment of storage terms in the surface energy balance of maize and soybean. *Agricultural and Forest Meteorology*, **125**, 105 – 115.

Minchin, P.E.H. (2007). *Proceedings of the Frontis Workshop on Functional-Structural Plant Modelling in Crop Production*, chap. Mechanistic modelling of carbon partitioning. Springer, Wageningen, NL.

Moffat, A.M., Papale, D., Reichstein, M., Hollinger, D.Y., Richardson, A.D., Barr, A.G., Beckstein, C., Braswell, B.H., Churkina, G., Desai, A.R., Falge, E., Gove, J.H., Heimann, M., Hui, D., Jarvis, A.J., Kattge, J., Noormets, A. and Stauch, V.J. (2007). Comprehensive comparison of gap-filling techniques for eddy covariance net carbon fluxes. *Agricultural and Forest Meteorology*, **147**, 209 – 232.

Moncrieff, J., Massheder, J., de Bruin, H., Elbers, J., Friborg, T., Heusinkveld, B., Kabat, P., Scott, S., Soegaard, H. and Verhoef, A. (1997). A system to measure surface fluxes of momentum, sensible heat, water vapour and carbon dioxide. *Journal of Hydrology*, **188-189**, 589 – 611.

Monje, O. and Bugbee, B. (1998). Adaptation to high CO_2 concentration in an optimal environment: radiation capture, canopy quantum yield and carbon use efficiency. *Plant, Cell & Environment*, **21**, 315–324.

Monteith, J. (1965). Evaporation and environment. In G. Fogg, ed., *The State and Movement of Water in Living Organisms*, 205–234, Academic Press, London.

Monteith, J.L. and Moss, C.J. (1977). Climate and the Efficiency of Crop Production in Britain. *Philosophical Transactions of the Royal Society of London*, **281**, 277–294.

Moradkhani, H., Sorooshian, S., Gupta, H.V. and Houser, P.R. (2005). Dual state-parameter estimation of hydrological models using ensemble Kalman filter. *Advances in Water Resources*, **28**, 135 – 147.

Morales, P., Sykes, M.T., Prentice, I.C., Smith, P., Smith, B., Bugmann, H., Zierl, B., Friedlingstein, P., Viovy, N., Sabate, S., Sanchez, A., Pla, E., Gracia, C.A., Sitch, S., Arneth, A. and Ogee, J. (2005). Comparing and evaluating process-based ecosystem model predictions of carbon and water fluxes in major European forest biomes. *Global Change Biology*, **11**, 2211–2233.

Motohka, T., Nasahara, K.N., Miyata, A., Mano, M. and Tsuchida, S. (2009). Evaluation of optical satellite remote sensing for rice paddy phenology in monsoon Asia using a continuous in situ dataset. *International Journal of Remote Sensing*, **30**, 4343–4357.

Moulin, S., Bondeau, A. and Delecolle, R. (1998). Combining agricultural crop models and satellite observations: From field to regional scales. *International Journal of Remote Sensing*, **19**, 1021 – 1036.

Moureaux, C., Debacq, A., Hoyaux, J., Suleau, M., Tourneur, D., Vancutsem, F., Bodson, B. and Aubinet, M. (2008). Carbon Balance Assessment of a Belgian Winter Wheat Crop (*Triticum aestivum* L.). *Global Change Biology*, **14**, 1353–1366.

Mueller, L., Behrendt, A., Schalitz, G. and Schindler, U. (2005). Above ground biomass and water use efficiency of crops at shallow water tables in a temperate climate. *Agricultural Water Management*, **75**, 117 – 136.

Nash, J. and Sutcliffe, J. (1970). River flow forecasting through conceptual models part I – A discussion of principles. *Journal of Hydrology*, **10**, 282 – 290.

Ogle, S.M., Breidt, F.J., Easter, M., Williams, S., Killian, K. and Paustian, K. (2010). Scale and uncertainty in modeled soil organic carbon stock changes for US croplands using a process-based model. *Global Change Biology*, **16**, 810–822.

ORNL (2010). MODIS subsetted land products, Collection 5. Available online [http://daac.ornl.gov/MODIS/modis.html] from ORNL DAAC, Oak Ridge, Tennessee, U.S.A. Accessed November 26, 2010.

Osborne, B., Saunders, M., Walmsley, D., Jones, M. and Smith, P. (2010). Key questions and uncertainties associated with the assessment of the cropland greenhouse gas balance. *Agriculture, Ecosystems & Environment*, **139**, 293 – 301, the carbon balance of European croplands.

Osborne, T.M., Lawrence, D.M., Challinor, A.J., Slingo, J.M. and Wheeler, T.R. (2007). Development and Assessment of a Coupled Crop-Climate Model. *Global Change Biology*, **13**, 169–183.

Pan, G., Xu, X., Smith, P., Pan, W. and Lal, R. (2010). An increase in topsoil SOC stock of China's croplands between 1985 and 2006 revealed by soil monitoring. *Agriculture, Ecosystems & Environment*, **136**, 133 – 138.

Papale, D., Reichstein, M., Aubinet, M., Canfora, E., Bernhofer, C., Kutsch, W., Longdoz, B., Rambal, S., Valentini, R., Vesala, T. and Yakir, D. (2006a). Towards a standardized processing of Net Ecosystem Exchange measured with eddy covariance technique: algorithms and uncertainty estimation. *Biogeosciences*, **3**, 571–583.

Papale, D., Reichstein, M., Canfora, E., Aubinet, M., Bernhofer, C., Longdoz, B., Kutsch, W., Rambal, S., Valentini, R., Vesala, T. and Yakir, D. (2006b). Towards a more harmonized processing of eddy covariance CO_2 fluxes: algorithms and uncertainty estimation. *Biogeosciences Discussions*, **3**, 961–992.

Parton, W. and Rasmussen, P. (1994). Long-term effects of crop management in wheat-fallow: II. CENTURY model simulations. *Soil Science Society of America Journal*, **58**, 530–536.

Pastor, J. and Post, W. (1986). Influence of climate, soil moisture, and succession on forest carbon and nitrogen cycles. *Biogeochemistry*, **2**, 3–27.

Penman, H.L. (1948). Natural Evaporation from Open Water, Bare Soil and Grass. *Proceedings of the Royal Society of London. Series A. Mathematical and Physical Sciences*, **193**, 120–145.

Penning de Vries, F.W.T., Jansen, D.M., ten Berge, H.F.M. and Bakema, A. (1989). *Simulation of Ecophysiological Processes of Growth in Several Annual Crops*, vol. 29 of *Simulation Monographs*. Pudoc, Wageningen.

Piao, S., Friedlingstein, P., Ciais, P., Viovy, N. and Demarty, J. (2007). Growing season extension and its impact on terrestrial carbon cycle in the Northern Hemisphere over the past 2 decades. *Global Biogeochemical Cycles*, **21**, 1–11.

Porter, J.R. and Gawith, M. (1999). Temperatures and the growth and development of wheat: a review. *European Journal of Agronomy*, **10**, 23–36.

Porter, J.R. and Semenov, M.A. (2005). Crop responses to climatic variation. *Philos Trans R Soc Lond B Biol Sci*, **360**, 2021–2035.

Porter, J.R., Bragg, P.L., Rayner, J.H., Weir, A.H. and Landsberg, J.J. (1983). The ARC wheat simulation model-principles and progress. In *Opportunities for manipulation of cereal productivity*, vol. 7 of *British Plant Growth Regulator Group Monograph*, 97–108.

Prescher, A.K., Grünwald, T. and Bernhofer, C. (2010). Land use regulates carbon budgets in eastern Germany: From NEE to NBP. *Agricultural and Forest Meteorology*, **150**, 1016 – 1025.

Qiu, J., Li, C., Wang, L., Tang, H., Li, H. and Van Ranst, E. (2009). Modeling impacts of carbon sequestration on net greenhouse gas emissions from agricultural soils in China. *Global Biogeochem. Cycles*, **23**, GB1007.

Quaife, T., Lewis, P., Kauwe, M.D., Williams, M., Law, B.E., Disney, M. and Bowyer, P. (2008). Assimilating canopy reflectance data into an ecosystem model with an Ensemble Kalman Filter. *Remote Sensing of Environment*, **112**, 1347 – 1364.

Ramankutty, N., Evan, A.T., Monfreda, C. and Foley, J.A. (2008). Farming the planet: 1. Geographic distribution of global agricultural lands in the year 2000. *Global Biogeochemical Cycles*, **22**, GB1003+.

Raupach, M.R., Rayner, P.J., Barrett, D.J., DeFries, R.S., Heimann, M., Ojima, D.S., Quegan, S. and Schmullius, C.C. (2005). Model–data synthesis in terrestrial carbon observation: methods, data requirements and data uncertainty specifications. *Global Change Biology*, **11**, 378–397.

Reay, D.S., Smith, P., Hymus, G. and Sabine, C. (2007). New Directions: The changing role of the terrestrial carbon sink in determining atmospheric CO_2 concentrations. *Atmospheric Environment*, **41**, 5813 – 5815.

Reed, B.C., Brown, J.F., VanderZee, D., Loveland, T.R., Merchant, J.W. and Ohlen, D.O. (1994). Measuring Phenological Variability from Satellite Imagery. *Journal of Vegetation Science*, **5**, pp. 703–714.

Reeves, M., Zhao, M. and Running, S. (2005). Usefulness and limits of MODIS GPP for estimating wheat yield. *International Journal of Remote Sensing*, **26**, 1403–1421.

Reichle, R.H., McLaughlin, D.B. and Entekhabi, D. (2002). Hydrologic Data Assimilation with the Ensemble Kalman Filter. *Monthly Weather Review*, **130**, 103–114.

Reichstein, M., Falge, E., Baldocchi, D., Papale, D., Aubinet, M., Berbigier, P., Bernhofer, C., Buchmann, N., Gilmanov, T., Granier, A., Grünwald, T., Havrankova, K., Ilvesniemi, H., Janous, D., Knohl, A., Laurila, T., Lohila, A., Loustau, D., Matteucci, G., Meyers, T., Miglietta, F., Ourcival, J.M., Pumpanen, J., Rambal, S., Rotenberg, E., Sanz, M., Tenhunen, J., Seufert, G., Vaccari, F., Vesala, T., Yakir, D. and Valentini, R. (2005). On the separation of net ecosystem exchange into assimilation and ecosystem respiration: review and improved algorithm. *Global Change Biology*, **11**, 1424–1439.

Reicosky, D. and Lambert, J. (1978). Field measured and simulated corn leaf water potential. *Soil Science Society of America journal*, **42**, 221–228.

Richardson, A., Williams, M., Hollinger, D., Moore, D., Dail, D., Davidson, E., Scott, N., Evans, R., Hughes, H., Lee, J., Rodrigues, C. and Savage, K. (2010). Estimating parameters of a forest ecosystem C model with measurements of stocks and fluxes as joint constraints. *Oecologia*, **164**, 25–40.

Richardson, A.D. and Hollinger, D.Y. (2005). Statistical modeling of ecosystem respiration using eddy covariance data: Maximum likelihood parameter estimation, and Monte Carlo simulation of model and parameter uncertainty, applied to three simple models. *Agricultural and Forest Meteorology*, **131**, 191 – 208.

Roujean, J.L. and Breon, F.M. (1995). Estimating PAR absorbed by vegetation from bidirectional reflectance measurements. *Remote Sensing of Environment*, **51**, 375 – 384.

Royston, P. (1992). Approximating the Shapiro-Wilk W-test for non-normality. *Statistics and Computing*, **2**, 117–119.

Ruddiman, W.F. (2003). The Anthropogenic Greenhouse Era Began Thousands of Years Ago. *Climatic Change*, **61**, 261–293.

Running, S.W., Baldocchi, D.D., Turner, D.P. and Gower, S.T. (1999). A Global Terrestrial Monitoring Network Integrating Tower Fluxes, Flask Sampling, Ecosystem Modeling and EOS Satellite Data. *Remote Sensing of Environment*, **70**, 108–127.

Sacks, W.J. and Kucharik, C.J. (2011). Crop management and phenology trends in the U.S. Corn Belt: Impacts on yields, evapotranspiration and energy balance. *Agricultural and Forest Meteorology*, **151**, 882 – 894.

Sacks, W.J., Deryng, D., Foley, J.A. and Ramankutty, N. (2010). Crop planting dates: an analysis of global patterns. *Global Ecology and Biogeography*, **19**, 607–620.

Sakamoto, T., Yokozawa, M., Toritani, H., Shibayama, M., Ishitsuaka, N. and Ohno, H. (2005). A Crop Phenology Detection Method Using Time-Series MODIS Data. *Remote Sensing of Environment*, **96**, 366–374.

Salinger, M.J. (2005). Climate Variability and Change: Past, Present and Future — An Overview. *Climatic Change*, **70**, 9–29.

Schulze, E.D., Luyssaert, S., Ciais, P., Freibauer, A. and Janssens, I.A. (2009). Importance of methane and nitrous oxide for Europe's terrestrial greenhouse-gas balance. *Nature*, **2**, 842–850.

Schwalm, C.R., Williams, C.A., Schaefer, K., Anderson, R., Arain, M.A., Baker, I., Barr, A., Black, T.A., Chen, G., Chen, J.M., Ciais, P., Davis, K.J., Desai, A., Dietze, M., Dragoni, D., Fischer, M.L., Flanagan, L.B., Grant, R., Gu, L., Hollinger, D., Izaurralde, R.C., Kucharik, C., Lafleur, P., Law, B.E., Li, L., Li, Z., Liu, S., Lokupitiya, E., Luo, Y., Ma, S., Margolis, H., Matamala, R., McCaughey, H., Monson, R.K., Oechel, W.C., Peng, C., Poulter, B., Price, D.T., Riciutto, D.M., Riley, W., Sahoo, A.K., Sprintsin, M., Sun, J., Tian, H., Tonitto, C., Verbeeck, H. and Verma, S.B. (2010). A model–data intercomparison of CO_2 exchange across North America: Results from the North American Carbon Program site synthesis. *Journal of Geophysical Research*, **115**.

Seneviratne, S.I., Pal, J.S., Eltahir, E.A.B. and Schär, C. (2002). Summer Dryness in a Warmer Climate: A Process Study with a Regional Climate Model. *Climate Dynamics*, **20**.

Setiyono, T., Weiss, A., Specht, J., Bastidas, A., Cassman, K. and Dobermann, A. (2007). Understanding and modeling the effect of temperature and daylength on soybean phenology under high-yield conditions. *Field Crops Research*, **100**, 257 – 271.

Siebert, S., Hoogeveen, J. and Frenken, K. (2006). Irrigation in Africa, Europe and Latin America - Update of the Digital Global Map of Irrigation Areas to Version 4. *Frankfurt Hydrology Paper*, **5**.

Sitch, S., Smith, B., Prentice, I.C., Arneth, A., Bondeau, A., Cramer, W., Kaplan, J.O., Levis, S., Lucht, W., Sykes, M.T. and et al. (2003). Evaluation of ecosystem dynamics, plant geography and terrestrial carbon cycling in the LPJ dynamic global vegetation model. *Global Change Biology*, **9**, 161–185.

Sitch, S., Huntingford, C., Gedney, N., Levy, P.E., Lomas, M., Piao, S.L., Betts, R., Ciais, P., Cox, P., Friedlingstein, P., Jones, C.D., Prentice, I.C. and Woodward, F.I. (2008). Evaluation of the terrestrial carbon cycle, future plant geography and climate-carbon cycle feedbacks using five Dynamic Global Vegetation Models (DGVMs). *Global Change Biology*, **14**, 2015–2039.

Slafer, G.A. and Rawson, H.M. (1994). Sensitivity of wheat phasic development to major environmental factors: a re-examination of some assumptions made by physiologists and modellers. *Australian journal of plant physiology*, **21**, 393–426.

Smith, J., Smith, P., Wattenbach, M., Zaehle, S., Hiederer, R., Jones, R.J., Montanarella, L., Rounsevell, M.D., Reginster, I. and Ewert, F. (2005a). Projected changes in mineral soil carbon of European croplands and grasslands, 1990–2080. *Global Change Biology*, **11**, 2141–2152.

Smith, P. (2004). Carbon Sequestration in Croplands: the Potential in Europe and the Global Context. *European Journal of Agronomy*, **20**, 229–236.

Smith, P. (2008). Land use change and soil organic carbon dynamics. *Nutrient Cycling in Agroecosystems*, **81**, 169–178.

Smith, P., Smith, J.U., Powlson, D.S., McGill, W.B., Arah, J.R.M., Chertov, O.G., Coleman, K., Franko, U., Frolking, S., Jenkinson, D.S., Jensen, L.S., Kelly, R.H., Klein-Gunnewiek, H., Komarov, A.S., Li, C., Molina, J.A.E., Mueller, T., Parton, W.J., Thornley, J.H.M. and Whitmore, A.P. (1997). A comparison of the performance of nine soil organic matter models using datasets from seven long-term experiments. *Geoderma*, **81**, 153 – 225.

Smith, P., Andrén, O., Karlsson, T., Perälä, P., Regina, K., Rounsevell, M. and Van Wesemael, B. (2005b). Carbon sequestration potential in European croplands has been overestimated. *Global Change Biology*, **11**.

Smith, P., Martino, D., Cai, Z., Gwary, D., Janzen, H., Kumar, P., McCarl, B., Ogle, S., O'Mara, F., Rice, C., Scholes, B., Sirotenko, O., Howden, M., McAllister, T., Pan, G., Romanenkov, V., Schneider, U., Towprayoon, S., Wattenbach, M. and Smith, J. (2008). Greenhouse gas mitigation in agriculture. *Philosophical Transactions of the Royal Society B: Biological Sciences*, **363**, 789–813.

Smith, P., Lanigan, G., Kutsch, W.L., Buchmann, N., Eugster, W., Aubinet, M., Céschia, E., Béziat, P., Yeluripati, J.B., Osborne, B., Moors, E.J., Brut, A., Wattenbach, M., Saunders, M. and Jones, M. (2010). Measurements necessary for assessing the net ecosystem carbon budget of croplands. *Agriculture, Ecosystems & Environment*, **139**, 302 – 315.

Soegaard, H., Jensen, N.O., Boegh, E., Hasager, C.B., Schelde, K. and Thomsen, A. (2003). Carbon dioxide exchange over agricultural landscape using eddy correlation and footprint modelling. *Agricultural and Forest Meteorology*, **114**, 153 – 173.

Solano, R., Didan, K., Jacobson, A. and Huete, A. (2010). MODIS Vegetation Indices (MOD13) C5 User's Guide. Tech. rep., Terrestrial Biophysics and Remote Sensing Lab, The University of Arizona.

Stone, P.J., Sorensen, I.B. and Jamieson, P.D. (1999). Effect of soil temperature on phenology, canopy development, biomass and yield of maize in a cool-temperate climate. *Field Crops Research*, **63**, 169 – 178.

Streck, N.A., Weiss, A., Xue, Q. and Baenziger, P.S. (2003). Improving Predictions of Developmental Stages in Winter Wheat: a Modified Wang and Engel Model. *Agricultural and Forest Meteorology*, **115**, 139–150.

Streck, N.A., Lago, I., Gabriel, L.F. and Samboranha, F.K. (2008). Simulating maize phenology as a function of air temperature with a linear and a nonlinear model. *Pesquisa Agropecuaria Brasileira*, **43**, 449 – 455.

Streck, N.A., Gabriel, L.F., Samboranha, F.K., Lago, I., Schwantes, A.P. and Schons, A. (2009). Comparing two versions of a non-linear model for simulating leaf number and developmental stages in maize based on air temperature. *Ciencia Rural*, **39**, 642–648.

Stöckle, C.O., Martin, S.A. and Campbell, G.S. (1994). CropSyst, a cropping systems simulation model: Water/nitrogen budgets and crop yield. *Agricultural Systems*, **46**, 335–359.

Stöckli, R., Rutishauser, T., Dragoni, D., O'Keefe, J., Thornton, P.E., Jolly, M., Lu, L. and Denning, A.S. (2008). Remote sensing data assimilation for a prognostic phenology model. *Journal of Geophysical Research*, **113**.

Suleau, M., Moureaux, C., Dufranne, D., Buysse, P., Bodson, B., Destain, J.P., Heinesch, B., Debacq, A. and Aubinet, M. (2011). Respiration of three Belgian crops: Partitioning of total ecosystem respiration in its heterotrophic, above- and below-ground autotrophic components. *Agricultural and Forest Meteorology*, **151**, 633 – 643.

Sus, O., Williams, M., Bernhofer, C., Béziat, P., Buchmann, N., Céschia, E., Doherty, R., Eugster, W., Grünwald, T., Kutsch, W., Smith, P. and Wattenbach, M. (2010). A linked carbon cycle and crop developmental model: Description and evaluation against measurements of carbon fluxes and carbon stocks at several European agricultural sites. *Agriculture, Ecosystems & Environment*, **139**, 402 – 418.

Suyker, A.E., Verma, S.B., Burba, G.G., Arkebauer, T.J., Walters, D.T. and Hubbard, K.G. (2004). Growing season carbon dioxide exchange in irrigated and rainfed maize. *Agricultural and Forest Meteorology*, **124**, 1 – 13.

Suyker, A.E., Verma, S.B., Burba, G.G. and Arkebauer, T.J. (2005). Gross primary production and ecosystem respiration of irrigated maize and irrigated soybean during a growing season. *Agricultural and Forest Meteorology*, **131**, 180 – 190.

Tambussi, E., Nogués, S., Ferrio, P., Voltas, J. and Araus, J. (2005). Does higher yield potential improve barley performance in Mediterranean conditions?: A case study. *Field Crops Research*, **91**, 149–160.

Tang, J. and Zhuang, Q. (2008). Equifinality in parameterization of process-based biogeochemistry models: A significant uncertainty source to the estimation of regional carbon dynamics. *J. Geophys. Res.*, **113**, 13pp.

Thornley, J.H.M. (2011). Plant growth and respiration re-visited: maintenance respiration defined — it is an emergent property of, not a separate process within, the system — and why the respiration : photosynthesis ratio is conservative. *Annals of Botany*.

Thornthwaite, C. and Hare, F. (1965). The loss of water to the air. *Meteorological Monographs*, 163–180.

Tilman, D., Fargione, J., Wolff, B., D'Antonio, C., Dobson, A., Howarth, R., Schindler, D., Schlesinger, W.H., Simberloff, D. and Swackhamer, D. (2001). Forecasting Agriculturally Driven Global Environmental Change. *Science*, **292**, 281–284.

Tonitto, C., David, M., Drinkwater, L. and Li, C. (2007a). Application of the DNDC model to tile-drained Illinois agroecosystems: model calibration, validation, and uncertainty analysis. *Nutrient Cycling in Agroecosystems*, **78**, 51–63.

Tonitto, C., David, M., Li, C. and Drinkwater, L. (2007b). Application of the DNDC model to tile-drained Illinois agroecosystems: model comparison of conventional and diversified rotations. *Nutrient Cycling in Agroecosystems*, **78**, 65–81.

Tucker, C., Jr., J.E., III, J.M. and Fan, C. (1979). Monitoring corn and soybean crop development with hand-held radiometer spectral data. *Remote Sensing of Environment*, **8**, 237 – 248.

Turner, M., Walker, J. and Oke, P. (2008). Ensemble member generation for sequential data assimilation. *Remote Sensing of Environment*, **112**, 1421 – 1433.

Twine, T.E. and Kucharik, C.J. (2008). Evaluating a terrestrial ecosystem model with satellite information of greenness. *J. Geophys. Res.*, **113**, G03027.

USDA (1992). *Weights, Measures, and Conversion Factors for Agricultural Commodities and Their Products*. Agricultural Handbook No. 697, U. S. Department of Agriculture, Washington, DC.

USDA (1997). *Usual Planting and Harvesting Dates for U.S. Field Crops*. Agricultural Handbook No. 628, U. S. Department of Agriculture, Washington, DC.

van den Boogaard, R., Alewijnse, D., Veneklaas, E.J. and Lambers, H. (1997). Growth and water-use efficiency of 10 *Triticum aestivum* cultivars at different water availability in relation to allocation of biomass. *Plant, Cell & Environment*, **20**, 200–210.

van Groenigen, K.J., Hastings, A., Forristal, D., Roth, B., Jones, M. and Smith, P. (2011). Soil C storage as affected by tillage and straw management: An assessment using field measurements and model predictions. *Agriculture, Ecosystems & Environment*, **140**, 218 – 225.

van Laar, H.H., Goudriaan, J. and van Keulen, H. (1997). SUCROS97: Simulation of crop growth for potential and water-limited production situations. In *Quantitative Approaches in Systems Analysis*, 14, DLO Research Institute for Agrobiology and Soil Fertility, The C.T. de Wit Graduate School for Production Ecology, Wageningen.

Verma, S.B., Dobermann, A., Cassman, K.G., Walters, D.T., Knops, J.M., Arkebauer, T.J., Suyker, A.E., Burba, G.G., Amos, B., Yang, H., Ginting, D., Hubbard, K.G., Gitelson, A.A. and Walter-Shea, E.A. (2005). Annual carbon dioxide exchange in irrigated and rainfed maize-based agroecosystems. *Agricultural and Forest Meteorology*, **131**, 77 – 96.

Viña, A., Gitelson, A.A., Rundquist, D.C., Keydan, G., Leavitt, B. and Schepers, J. (2004). Monitoring Maize (*Zea mays* L.) Phenology with Remote Sensing. *Agronomy Journal*, **96**, 1139–1147.

Vitale, L., Di Tommasi, P., Arena, C. and Fierro, A. (2007). Effects of Water Stress on Gas Exchange of Field Grown *Zea Mays* L. in Southern Italy: an Analysis at Canopy and Leaf Level. *Acta Physiologiae Plantarum*, **29**, 317–326.

Vitousek, P.M., Mooney, H.A., Lubchenco, J. and Melillo, J.M. (1997). Human Domination of Earth's Ecosystems. *Science*, **277**, 494–499.

Vleeshouwers, L.M. and Verhagen, A. (2002). Carbon emission and sequestration by agricultural land use: a model study for Europe. *Global Change Biology*, **8**, 519–530.

Vuichard, N., Ciais, P., Belelli, L., Smith, P. and Valentini, R. (2008). Carbon sequestration due to the abandonment of agriculture in the former USSR since 1990. *Global Biogeochem. Cycles*, **22**, GB4018.

Waha, K., van Bussel, L.G.J., Muller, C. and Bondeau, A. (2011). Climate-driven simulation of global crop sowing dates. *Global Ecology and Biogeography*.

Wang, E. and Engel, T. (1998). Simulation of Phenological Development of Wheat Crops. *Agricultural Systems*, **58**, 1–24.

Wang, J., Yu, Q. and Lee, X. (2007). Simulation of Crop Growth and Energy and Carbon Dioxide Fluxes at Different Time Steps From Hourly to Daily. *Hydrological Processes*, **21**, 2474–2492.

Wang, Q., Watanabe, M. and Ouyang, Z. (2005). Simulation of water and carbon fluxes using BIOME-BGC model over crops in China. *Agricultural and Forest Meteorology*, **131**, 209–224.

Wardlow, B.D. and Egbert, S.L. (2008). Large-area crop mapping using time-series MODIS 250 m NDVI data: An assessment for the U.S. Central Great Plains. *Remote Sensing of Environment*, **112**, 1096 – 1116.

Wardlow, B.D. and Egbert, S.L. (2010). A comparison of MODIS 250-m EVI and NDVI data for crop mapping: a case study for southwest Kansas. *International Journal of Remote Sensing*, **31**.

Wardlow, B.D., Kastens, J.H. and Egbert, S.L. (2006). Using USDA Crop Progress Data for the Evaluation of Greenup Onset Date Calculated from MODIS 250-Meter Data. *Photogrammetric Engineering & Remote Sensing*, **72**, 1225–1234.

Wardlow, B.D., Egbert, S.L. and Kastens, J.H. (2007). Analysis of time-series MODIS 250 m vegetation index data for crop classification in the U.S. Central Great Plains. *Remote Sensing of Environment*, **108**, 290 – 310.

Waring, R.H., Landsberg, J.J. and Williams, M. (1998). Net primary production of forests: a constant fraction of gross primary production? *Tree Physiol*, **18**, 129–134.

Wattenbach, M., Sus, O., Vuichard, N., Lehuger, S., Gottschalk, P., Li, L., Leip, A., Williams, M., Tomelleri, E., Kutsch, W.L., Buchmann, N., Eugster, W., Dietiker, D., Aubinet, M., Céschia, E., Béziat, P., Grünwald, T., Hastings, A., Osborne, B., Ciais, P., Cellier, P. and Smith, P. (2010). The carbon balance of European croplands: A cross-site comparison of simulation models. *Agriculture, Ecosystems & Environment*, **139**, 419 – 453.

Weixing, C., Tiemei, L., Weihong, L., Shaohua, W., Jie, P. and Wenshang, G. (2002). Simulating Organ Growth in Wheat Based on the Organ-Weight Fraction Concept. *Plant production science*, **5**, 248–256.

West, T.O. and Marland, G. (2002). A synthesis of carbon sequestration, carbon emissions, and net carbon flux in agriculture: comparing tillage practices in the United States. *Agriculture, Ecosystems & Environment*, **91**, 217 – 232.

West, T.O., Brandt, C.C., Baskaran, L.M., Hellwinckel, C.M., Mueller, R., Bernacchi, C.J., Bandaru, V., Yang, B., Wilson, B.S., Marland, G., Nelson, R.G., De La Torre Ugarte, D.G. and Post, W.M. (2010). Cropland carbon fluxes in the United States: increasing geospatial resolution of inventory-based carbon accounting. *Ecological Applications*, **20**, 1074–1086.

White, M.A. and Nemani, R.R. (2003). Canopy duration has little influence on annual carbon storage in the deciduous broad leaf forest. *Global Change Biology*, **9**, 967–972.

Williams, J.R., Jones, C.A., Kiniry, J.R. and Spanel, D.A. (1989). The EPIC crop growth model. In *Transactions of the ASABE*, vol. 32, 497–511.

Williams, M. and Rastetter, E.B. (1999). Vegetation characteristics and primary productivity along an arctic transect: implications for scaling-up. *Journal of Ecology*, **87**, 885–898.

Williams, M., Rastetter, E.B., Fernandes, D.N., Goulden, M.L., Wofsy, S.C., Shaver, G.R., Melillo, J.M., Munger, J.W., Fan, S.M. and Nadelhoffer, K.J. (1996). Modelling the Soil-Plant-Atmosphere Continuum in a Quercus-Acer Stand at Harvard, Forest: the Regulation of Stomatal Conductance by Light, Nitrogen and Soil/Plant Hydraulic Properties. *Plant, Cell and Environment*, **19**, 911–927.

Williams, M., Malhi, Y., Nobre, A.D., Rastetter, E.B., Grace, J. and Pereira, M.G.P. (1998). Seasonal variation in net carbon exchange and evapotranspiration in a Brazilian rain forest: a modelling analysis. *Plant, Cell and Environment*, **21**, 953–968.

Williams, M., Eugster, W., Rastetter, E.B., Mcfadden, J.P. and Chapin, F.S. (2000). The controls on net ecosystem productivity along an Arctic transect: a model comparison with flux measurements. *Global Change Biology*, **6**, 116–126.

Williams, M., Law, B.E., Anthoni, P.M. and Unsworth, M.H. (2001a). Use of a simulation model and ecosystem flux data to examine carbon-water interactions in ponderosa pine. *Tree Physiol*, **21**, 287–298.

Williams, M., Rastetter, E.B., Shaver, G.R., Hobbie, J.E., Carpino, E. and Kwiatkowski, B.L. (2001b). Primary production of an Arctic watershed: an uncertainty analysis. *Ecological Applications*, **11**, 1800–1816.

Williams, M., Schwarz, P.A., Law, B.E. and Irvine, J. (2005). An Improved Analysis of Forest Carbon Dynamics Using Data Assimilation. *Global Change Biology*, **11**, 89–105.

Williams, M., Richardson, A.D., Reichstein, M., Stoy, P.C., Peylin, P., Verbeeck, H., Carvalhais, N., Jung, M., Hollinger, D.Y., Kattge, J., Leuning, R., Luo, Y., Tomelleri, E., Trudinger, C. and Wang, Y.P. (2009). Improving land surface models with FLUXNET data. *Biogeosciences Discussions*, **6**.

Wilson, T. and Meyers, T. (2007). Determining vegetation indices from solar and photosynthetically active radiation fluxes. *Agricultural and Forest Meteorology*, **144**, 160 – 179.

Wolfe, R., Nishihama, M., Fleig, A. and Roy, D. (1999). The MODIS operational geolocation error analysis and reduction methodology. In *Geoscience and Remote Sensing Symposium, 1999. IGARSS '99 Proceedings. IEEE 1999 International*, vol. 1, 449 –451 vol.1.

Wolfe, R.E., Roy, D.P. and Vermote, E. (1998). MODIS Land Data Storage, Gridding, and Compositing Methodology: Level 2 Grid. *IEEE transactions on geoscience and remote sensing*, **36**, 1324–1338.

Wullschleger, S.D. (1993). Biochemical Limitations to Carbon Assimilation in C_3 Plants — A Retrospective Analysis of the A/C_i Curves from 109 Species. *J. Exp. Bot.*, **44**, 907–920.

Xue, Q., Weiss, A. and Baenziger, P. (2004). Predicting phenological development in winter wheat. *Climate Research*, **25**, 243–252.

Yan, W. and Hunt, L.A. (1999). An Equation for Modelling the Temperature Response of Plants using only the Cardinal Temperatures. *Annals of Botany*, **84**, 607–614.

Yan, W. and Wallace, D.H. (1998). Simulation and Prediction of Plant Phenology for Five Crops Based on Photoperiod x Temperature Interaction. *Annals of Botany*, **81**, 705–716.

Yang, H.S., Dobermann, A., Lindquist, J.L., Walters, D.T., Arkebauer, T.J. and Cassman, K.G. (2004). Hybrid-maize — a maize simulation model that combines two crop modeling approaches. *Field Crops Research*, **87**, 131–154.

Ye, Z.P. and Yu, Q. (2008). A coupled model of stomatal conductance and photosynthesis for winter wheat. *Photosynthetica*, **46**, 637–640.

Yin, X., Kropff, M.J., McLaren, G. and Visperas, R.M. (1995). A nonlinear model for crop development as a function of temperature. *Agricultural and Forest Meteorology*, **77**, 1 – 16.

Yin, X., Schapendonk, A.H.C.M., Kropff, M.J., van Oijen, M. and Bindraban, P.S. (2000). A Generic Equation for Nitrogen-limited Leaf Area Index and its Application in Crop Growth Models for Predicting Leaf Senescence. *Annals of Botany*, **85**, 579 – 585.

Zhang, D.D., Lee, H.F., Wang, C., Li, B., Zhang, J., Pei, Q. and Chen, J. (2011). Climate change and large-scale human population collapses in the pre-industrial era. *Global Ecology and Biogeography*, in press.

Zhang, F., Li, C., Wang, Z. and Wu, H. (2006). Modeling impacts of management alternatives on soil carbon storage of farmland in Northwest China. *Biogeosciences*, **3**, 451–466.

Zhang, L., Dawes, W.R. and Walker, G.R. (2001). Response of mean annual evapotranspiration to vegetation changes at catchment scale. *Water Resour. Res.*, **37**, 701–708.